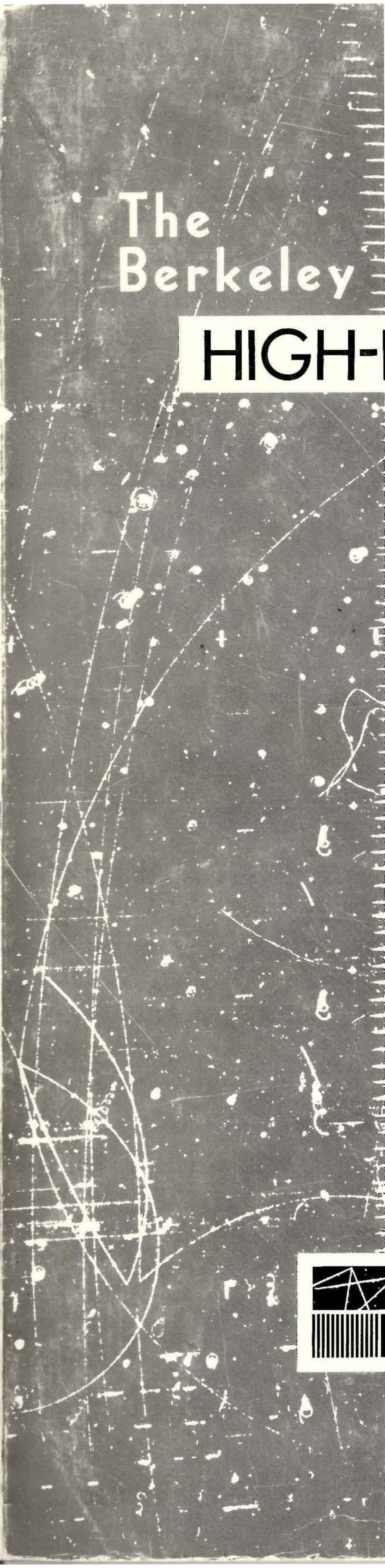

The Berkeley HIGH-ENERGY PHYSICS STUDY

Summer 1961

LRL

University of California
LAWRENCE RADIATION LABORATORY
Berkeley, California

UCRL-10022
UC-34 Physics
TID-4500 (17th Ed.)

THE BERKELEY HIGH-ENERGY PHYSICS STUDY

at the

ERNEST O. LAWRENCE RADIATION LABORATORY

Berkeley, California

June 15 through August 15, 1961

University of California
Berkeley

Printed in USA. Price $3.50. Available from the
Office of Technical Services
U.S. Department of Commerce
Washington 25, D. C.

FOREWORD

Lloyd Smith

Over the past few years, high-energy physicists have become aware of the real possibility of achieving much higher energies than presently available by a straightforward extrapolation of the alternating-gradient synchrotron (AGS). The interest in this possibility has been stimulated considerably by the successful completion of the 25- and 30-Gev machines at CERN and Brookhaven. Several independently conducted preliminary studies indicate that a machine could be constructed to accelerate protons to at least 1000 Gev, but we still have no precise picture of the necessary commitment in manpower, time, experimental facilities, and money. A decision to build one or more very large accelerators, whether in the United States, Western Europe, or the Soviet Union, must be based, as in the past, on a conviction that exciting and important discoveries will be made by using very large accelerators. Unfortunately, it remains true that discoveries that significantly alter the course of physics are almost by definition unpredictable; it is probably fruitless to attempt to "justify" such a large commitment by listing possible experiments pertaining to questions of current interest. Nevertheless, one cannot hope to form a responsible judgment without a thorough knowledge of present trends in theory and experiment concerning high-energy phenomena.

In the summer of 1961, there were three separate gatherings for the purpose of bringing together physicists interested in high-energy phenomena to review and discuss the present status of this branch of physics and to consider future developments, with particular reference to the utilization of accelerators in the range of several hundred Gev. In June, the first was a symposium at CERN,[1] and took the form of an intensive series of lectures and discussions over a relatively short time. The second was a study group that assembled at Berkeley for about two months to work on special problems. During the month of August the third group, at Brookhaven,[2] worked on a design study for a possible joint US-USSR project. The Berkeley and Brookhaven studies were correlated with respect to timing to avoid undue conflict. It also was agreed that the Berkeley study group would emphasize theoretical aspects of the subject whereas the Brookhaven study group would emphasize experimental aspects and the accelerator itself.

This report is a compilation of seminar talks and special reports arising from the Berkeley summer study. The seminar program, consisting of about four meetings per week, was the only formal activity during the study period; most of the time was spent in work on particular

---

1. International Conference on Theoretical Aspects of Very High Energy Phenomena, June 5-9, 1961. CERN 61-22, August 11, 1961.

2. Design Study for a 300–1000-Gev Accelerator, J. P. Blewett et al., August 28, 1961; Experimental Program Requirements for a 300 to 1000-Gev Accelerator, L. C. L. Yuan et al., August 28, 1961.

problems by individuals and small groups, with interruptions for frequent spontaneous discussion periods involving larger numbers of people. This report includes also a summary of the theoretical situation, written later by Geoffrey F. Chew, and some remarks by Sulamith Goldhaber on experimental aspects of the study.

The Radiation Laboratory wishes to express its gratitude to the visiting participants for their diligent efforts in pursuing these elusive questions. We hope that they found the summer as profitable for themselves as it was for us.

HIGH-ENERGY PHYSICS STUDY

---

* Oral report only

† Material presented in this seminar is contained in the report by K. L. Brown et al. , Linear Accelerator Progress at Stanford University, in Proceedings of the 1961 International Conference on High-Energy Accelerators, Brookhaven.

REPORTS

Related to the Summer Study

Participants, Speakers, and Contributors With Key To Contributions

	Reference
Daniele Amati CERN Geneva, Switzerland	S5, S13, [S18], R1
Hans Bichsel University of Southern California Los Angeles, California	
John P. Blewett Brookhaven National Laboratory Upton, New York	
Sidney A. Bludman Lawrence Radiation Laboratory Berkeley, California	S17
Kenneth M. Case University of Michigan Ann Arbor, Michigan	S13, S27
Geoffrey F. Chew Lawrence Radiation Laboratory Berkeley, California	S1, S13, R1
Giuseppe Cocconi Cornell University Ithaca, New York	S3, S4, S28(II)
Ernest D. Courant Brookhaven National Laboratory Upton, New York	
Norman Dombey California Institute of Technology Pasadena, California	S7, S13
Steven G. Frautschi University of California Berkeley, California	S2, S13, S15(II), R1
William Frazer University of California San Diego, California	[S19]
William B. Fretter University of California Berkeley, California	S14
Stephen G. Gasiorowicz University of Minnesota Minneapolis, Minnesota	S13
Murray Gell-Mann California Institute of Technology Pasadena, California	[S21, S22]
Charles J. Goebel University of Wisconsin Madison, Wisconsin	S6, S13, [S18], R1
Gerson Goldhaber Lawrence Radiation Laboratory Berkeley, California	R2
Sulamith Goldhaber Lawrence Radiation Laboratory Berkeley, California	S16, R2
Kjell Johnsen CERN Geneva, Switzerland	R3
Lawrence W. Jones University of Michigan Ann Arbor, Michigan	R4
Denis Keefe Lawrence Radiation Laboratory Berkeley, California	S9(II)
Leroy T. Kerth Lawrence Radiation Laboratory Berkeley, California	S9(I), S23(II)
Louis J. Koester University of Illinois Urbana, Illinois	S23(I), S28(II)
Gerald R. Lynch Lawrence Radiation Laboratory Berkeley, California	R5
George F. Masek University of Washington Seattle, Washington	S15(I)

Participants, Speakers, and Contributors (Continued)

Robert Mozley [S25]
Stanford University
Stanford, California

Gerald K. O'Neill S12
Princeton University
Princeton, New Jersey

W. K. H. Panofsky [S24]
Stanford University
Stanford, California

Donald H. Perkins S10&S11, S28(II), R6, R7
University of Bristol
Bristol, England

Matthew Sands
California Institute of Technology
Pasadena, California

Fred H. Schmidt R8
University of Washington
Seattle, Washington

Lloyd Smith
Lawrence Radiation Laboratory
Berkeley, California

Jack Steinberger S26
Columbia University
Irvington, New York

Harold Ticho S8
University of California
Los Angeles, California

Alvin V. Tollestrup
California Institute of Technology
Pasadena, California

George H. Trilling R9
Lawrence Radiation Laboratory
Berkeley, California

Robert L. Walker
California Institute of Technology
Pasadena, California

William Walkinshaw R10
Rutherford High Energy Laboratory
Harwell, England

David Y. Wong S13
University of California
La Jolla, California

James A. Young S17
General Electric Company
Pleasanton, California

Luke C. L. Yuan S20
Brookhaven National Laboratory
Upton, New York

Frederick Zachariasen S28(I)
California Institute of Technology
Pasadena, California

SUMMARY OF THEORETICAL CONCLUSIONS FROM 1961 BERKELEY SUMMER STUDY

Geoffrey F. Chew

To prophesy the state of particle physics ten years hence is impossible. Looking back ten years, one realizes that questions discussed now will in all likelihood be settled within three or four years and entirely new questions will have arisen in the meantime. Nevertheless, we were asked to do our best in predicting the impact on particle physics of a 300-Gev proton synchrotron that would require a decade for its design and construction.

Our clearest conclusion was that there is no reason to expect the present theoretical split between strong interactions, weak interactions, and electromagnetic interactions to be resolved through a step-up in laboratory energy by a factor of 10 or even 30. This picture might be changed for electromagnetic interactions if energies of the order of e^{137} Mev could be achieved, while weak interactions conceivably might become strong at energies of 200 to 300 Gev in the center-of-mass system. We do not approach such energies with the proposed accelerator, so this summary will deal with the three interactions separately. Most of the emphasis is on strong interactions because the majority of the participants in our theoretical study were particularly interested in this area.

Strong Interactions

From the current point of view, one can imagine at least three different possible circumstances to be faced if we go into this new energy region. The most exciting possibility is that we may discover new symmetries and new conservation laws. In particular, there may be new particles, stable with respect to strong interactions (i. e., with lifetimes $\gtrsim 10^{-20}$ sec), which have eluded observation because of their large mass. There has been no call made by theory for such particles, but then, there was no theoretical call for the strange particles, either. Experimenters will have to explore this area without help from the theorists.

A second possibility for strong interactions is that there may be "hidden" symmetries. This notion has been circulating for a number of years, the basic presumption being that the fundamental strong interaction may be more symmetrical than it appears at low energies, where the existence of nonzero rest masses is important. There is a host of theories of this type which are frustrating to deal with; as yet, it is not known how to test them experimentally. Some of these theories predict the existence of new unstable particles with lives of the order of 10^{-22} second, but how to distinguish such particles from dynamical resonances is not known. Some believe that at high energies we shall find a region where the influence of the rest masses becomes small and the symmetry is revealed. For example, suppose that, if their outer shells were stripped away, the π and K mesons had equivalent "cores." Then, by scattering π and K mesons off the same target, one might find similarities in the way they behave in high-momentum-transfer scattering experiments.

Unfortunately, only vague proposals for experiments of this kind have been made thus far. This point will be touched on again below.

The existence of no further symmetries at all appears, at first, to be the least interesting possibility. But even if this be the case, there remain vital questions within the framework of S-matrix theory to be answered experimentally. Until recently, the standard approach to high-energy collisions has been through semiclassical "optical" and "statistical" models, which avoid a detailed specification of particle structure, so that their verification, or lack of verification, has not been relevant to the development of particle theory. Within the past year, however, a potentially quantitative framework for describing strong interactions at high as well as at low energies has begun to emerge from the combined properties of unitarity and analyticity of the S matrix. It is too soon to say how detailed and how reliable will be the high-energy theoretical predictions based on the S matrix, but it appears at the moment that the region of laboratory-system energies $\gtrsim 100$ Gev will be of major interest to the new theory.

It is to be expected that during the next few years detailed and quantitative calculations will be based on S-matrix theory, predicting total and elastic cross sections as well as the multiplicity and distribution of produced particles. The verification of such predictions will obviously be important, and it is expected that the most clear-cut predictions will apply to the "asymptotic" region, where low-energy irregularities have disappeared. The asymptotic region is, of course, not well defined and develops gradually, but an increase over existing accelerator energies by a factor of ten will be clearly useful, since current CERN measurements show a substantial energy variation in some total cross sections as well as differences between particle and antiparticle cross sections. Such effects are expected to die out "asymptotically." Although no reliable calculations on the basis of the analytically continued S matrix have yet been completed, we mention here a special class of relatively simple predictions to illustrate the kind of experiments that may be desirable.

An exciting experimental possibility emerges from a conjectured connection between forward high-energy peaks (and between backward peaks) in collisions of the type

$$a + b \to c + d, \tag{1}$$

and the elementary or nonelementary character of particles that have the quantum numbers of the "crossed" reactions

$$a + \overline{c} \to d + \overline{b} \tag{2}$$

and

$$a + \overline{d} \to c + \overline{b}\,. \tag{3}$$

If we define the forward direction as that in which particle c maintains the direction of particle a , then the forward peak should be controlled by systems with the quantum numbers of reaction (2), and should have the form

$$\frac{d\sigma}{d\Delta^2} \xrightarrow[E \to \infty]{} F(\Delta^2) E^{2\left[\alpha(\Delta^2) - 1\right]} , \tag{4}$$

where Δ is the (invariant) momentum transfer and E the lab energy. If there exists an elementary particle with the quantum numbers of reaction (2) and spin S, then one sets $\alpha(\Delta^2)$ equal to S, a constant, in Formula (4). By contrast, composite particles lead to $\alpha(\Delta^2) < S$, with $d\alpha/d\Delta^2 < 0$. Thus, the elementary character of a particle can be identified through two properties of the peak that it produces: (a) the magnitude of the peak should vary approximately as $E^{(2S-1)}$; (b) the shape of the peak should become, at sufficiently high energy, independent of E. By contrast, the height of the peak due to a composite particle should decrease more rapidly with increasing E and the width of the peak should also decrease. Similar remarks apply to backward peaks produced by particles with the quantum numbers of reaction (3).

High energies are needed to suppress background terms in the cross section that vary with lower powers of E than in Formula (4). An estimate of the experimental requirements on the energy is achieved by considering the forward diffraction peak, associated with the quantum numbers of the vacuum, which corresponds theoretically to $\alpha(0) = 1$ if high-energy total cross sections approach constants as expected. Experimentally, the CERN data on π^+-p and π^--p scattering between 5 and 10 Gev indicate $\alpha(0) = 0.93$ if a pure power law is assumed. It appears, therefore, that already at these energies the background is relatively weak, but there will no doubt be situations in which the background requires further suppression in order to establish the point at issue. An extra factor of ten in lab energy should then be of great assistance. If one wishes to establish the narrowing of a forward or backward peak, such a factor will be essential, since narrowing varies logarithmically with energy.

Attempts to discover hidden symmetries by experiment would require a detailed investigation of the tails of high-energy elementary particle peaks, and would be extremely difficult. If all the strongly interacting particles turn out to be composite, the notion of hidden symmetry loses its apparent significance.

Electromagnetic Interactions

The proposed accelerator is of some interest in the field of electromagnetic interactions because of the two secondary beams:

a. photons from the decay of the π^0 mesons, and

b. muons from the decay of charged π mesons.

It is unlikely that one can investigate quantum electrodynamics itself with these tools, owing to the presence of strong interactions. For example, a photon can produce a pair of pions, either real or virtual, and then $\pi - \pi$ interactions come in through the back door. However, the muon beam might be useful to measure the form factor of the nucleon to higher momentum transfers than will be possible with electron scattering using the two-mile Stanford linear accelerator. The Stanford accelerator will produce a maximum electron momentum of about 20 Gev, whereas the proton accelerator should produce secondary muons up to about 100 Gev.

The photon beam also would go up to energies of approximately 100 Gev, but would be less intense than the 20-Gev Stanford beam and contain a high neutron contamination. A possible, if unlikely, use of this photon beam would be to pair-produce the intermediate vector bosons of weak coupling theory, which, if they exist, might otherwise escape detection because of a mass beyond the range of either present accelerators or the new Stanford accelerator.

Weak Interactions

In the field of weak interactions, currently considered neutrino experiments would almost certainly benefit from higher energies, particularly if the mass of an eventual intermediate vector boson is large. The qualitative question of the existence of two types of neutrinos, (ν_e and ν_μ), will be answered, we hope, before a 300-Gev accelerator is ready. However, the determination of weak-interaction form factors and other quantitative measurements will probably require substantially higher counting rates than present accelerators can produce. Unfortunately, lepton-lepton collisions will still be out of reach, as will most other exotic weak reactions. One must remember that the contemplated increase in center-of-mass energy is only moderate.

To summarize, in the field of strong interactions the proposed accelerator might play a crucial role in determining whether any baryons or mesons are "elementary" and whether further symmetries, manifest or hidden, exist. In the field of electromagnetic interactions it is difficult to see how the existence of this accelerator could be significant in altering the current (successful) theory. In the field of weak interactions the higher counting rates should make possible quantitative neutrino experiments that are out of the range of present accelerators; the theory, which at present is both incomplete and inconsistent, might thereby be decisively influenced.

SOME COMMENTS ON EXPERIMENTAL QUESTIONS

Sulamith Goldhaber

The work in this area was divided into a number of distinguishable categories, of which the four principal ones are secondary beams, beam transport, particle detection, and particle separation.

Secondary Beams

The character of the secondary beams was considered to be of primary importance, since it determines the way in which experiments can be carried out. An empirical approach was used, without reference to a specific model, by constructing expressions for angular and energy distributions consistent with the results of cosmic ray experiments, and then determining a free parameter from data obtained by the CERN and Brookhaven groups. The agreement obtained with existing data was sufficiently good that we have considerable confidence that the main features of secondary beams are predictable; rare events are another matter.

Beam Transport

On the assumption that the accelerator would have the recently suggested long straight sections, an effort was made to lay out beam-transport systems for the types of secondary beams expected. A possible solution may be the insertion of bending magnets in the straight sections, as suggested by Kerth. The problem might be simplified by the development of superconducting analyzing and focusing magnets to achieve high field strengths.

Particle Detection

Detection by present means, such as combinations of Cerenkov counters, appears possible, though cumbersome, for energies up to 100 Gev, and can be used if better methods are not available. Xenon scintillators to distinguish particles of different masses by the relativistic rise in ionization loss may be useful. Preliminary tests at Brookhaven are encouraging.

Particle Separation

The extension of the present crossed-field separators to energies of 50 Gev looks unpromising, though other means, such as rf separators, are not to be excluded from consideration. This difficult problem might be solved by exploiting the difference in character between the interactions of different particle types with nuclear matter. In particular, a scheme to enrich antinucleon beams by utilizing the difference in angular distribution of scattering between pions and antinucleons seems feasible.

Conclusion

Commonly encountered differences in individual approaches to unknown situations were evident in this study. Some prefer to examine a particular technique in detail, while others prefer to design hypothetical experiments and meet the problematical situations as they arise. It is difficult to generalize the results of the latter approach; the reader is referred to the examples discussed in the main text.

One general remark may be in order. It appears that, even with techniques now available or in the course of development, meaningful work can be done. The inventions that are sure to come in the next decade will facilitate significant experiments at much higher energies than presently available.

SEMINARS

1. REPORT ON THE LA JOLLA CONFERENCE ON THEORY OF WEAK AND STRONG INTERACTIONS

Geoffrey F. Chew

June 22, 1961

This is not a complete report because many topics covered at La Jolla (e. g. , gravitation) are not relevant to our study. Also several speakers will report directly to us (Salam, Gell-Mann, Amati).

Symmetries

Gell-Mann, Salam, Sakurai, Nambu, and Okubo — all use relatively conventional field theory but postulate a variety of symmetries which are broken by the existence of nonzero masses. Except for Sakurai, the underlying idea seems to be an attempt to unify weak and strong interactions, keeping in mind those simple properties of the former that have been observed (e.g., V-A coupling). Tests of the various theories are difficult because the symmetries are broken so severely. It is often conjectured that "hidden symmetries," if they exist, may be seen in experiments at very high energies (and momentum transfers) in which masses are unimportant. However, no concrete specification of the required experimental conditions has been given.

S-Matrix Theory of Strong Interactions

In addition to the survey of the general philosophy of the S-matrix approach, a number of special topics were discussed.

Froissart's paper was of great importance.[1] He proves, among other things, that the combined requirements of unitarity and analyticity prevent total cross sections from increasing faster than $\ln^2 E$, and uses this result to limit the number of independent subtractions in the Mandelstam representation. Froissart also demonstrated, very elegantly, the flaw in Gribov's argument that total cross sections must decrease faster than $1/\ln E$.

Frazer's paper on inelastic resonances was interesting, but probably is not relevant to our study, since it deals with intermediate energies.

For the expression

$$A_\ell(q^2) = \frac{e^{2i\delta_\ell} - 1}{2i} ,$$

where

$$\delta_\ell = \delta_R + i\delta_I ,$$

the quantity δ_ℓ/q is a real analytic function of q^2 with branch point at q^2_{inel} . There is also an unphysical cut (associated with "forces") which is temporarily neglected. Then,

$$\frac{\delta_R}{q} = \frac{P}{\pi} \int_{q^2_{inel}}^{\infty} dq'^2 \; \frac{\delta_I\left(q'^2\right)}{q'\left(q'^2 - q^2\right)} ,$$

and, if δ_I increases rapidly in some region, it is possible to get a strong sharp peak in $\left[A_\ell\left(q^2\right)\right]^2$. The phenomenon appears more closely related to a cusp than to a resonance. Frazer described preliminary calculations to show how this mechanism could explain the peaks in π-N scattering above 500 Mev as well as the K^--p peak near 1 Gev.

Amati and Cini described new S-matrix calculations of low-energy N-N and π-N

1. M. Froissart, Asymptotic Behavior in the Mandelstam Representation (The La Jolla Conference, June 16, 1961)

scattering, respectively. The main interest, here, has been the extent to which these involve the $I = 1$, $J = 1$ π-π resonance; the current indication is that at low energies this π-π interaction is of less quantitative significance than once believed. However, the role of an $I = 0$, $J = 0$ state near $2m_\pi$ or an $I = 0$, $J = 1(3\pi)$ state has not yet been evaluated.

2. REPORT ON THE CERN CONFERENCE: "THEORETICAL ASPECTS OF VERY-HIGH-ENERGY PHENOMENA"

Steven Frautschi

June 23, 1961

Recently CERN began operating its 28-Gev proton accelerator. This accelerator took some 6 to 7 years to complete; therefore, if an even larger accelerator is to be completed by 1970, planning must begin now. The purpose of the recent CERN conference was to survey what is known or conjectured about the very-high-energy region in which such an accelerator would operate, and to determine what questions can be asked at these very high energies.

The conference included a few talks on accelerator and cosmic ray data, and many talks (at a fairly lowbrow level) on theory.

Discussion concerning this energy region was necessarily tentative and speculative for the most part. Many of the ideas and data discussed here were developed within the past two years, and further developments are expected to occur rapidly.

I shall discuss what is expected or interesting to look for, and then what machines have been considered to do the looking. I shall largely follow Van Hove's excellent conference summary.

Weak Interactions

Present theory works well in many respects at low energies, but is clearly unsatisfactory at high energies.

Experiments in weak interactions are difficult, but if they can be done, many theoretical questions will be answered in unambiguous fashion.

Qualitative Questions

a. Are there one or two types of ν ? Can ν from $\pi \to \mu + \nu$ produce reaction $\nu + N \to e + p$?

b. Is there an intermediate boson W with low mass? If so, the cross sections for reaction $\nu + Z \to W^+ + \mu^- + Z\,(Z^*)$ should be quite large.

Quantitative Questions

a. A study of the reactions

$$\nu + n \to p + \mu^- (e^-)$$

and

$$\bar{\nu} + p \to n + \mu^+ (e^+)$$

as a function of energy would provide weak-interaction form factors. In some cases these form factors may be difficult-to-obtain manifestations of strong interactions, but the term analogous to the electromagnetic anomalous moment tests the concept of conserved vector current. If this conservation law holds, the anomalous-moment term is relatively large. Nevertheless, it is difficult to see at low energies, but increases with an increase of energy and leads to a large difference between $\sigma(\nu + N)$ and $\sigma(\bar{\nu} + N)$ at approximately 500 Mev (Lee and Yang).

To give an increased counting rate, the experiment should be done with heavy nuclei. The Pauli effect inhibits the final nucleon; Berman and others estimate that σ_{tot} is reduced 15% by this effect.

b. Attempts could be made to observe the reactions $\nu + e \to \nu + e$ (which could be seen only at very small angles) and $\nu + p \to \nu + p$.

c. Does the ratio $\frac{\Delta S}{\Delta Q}$ equal - 1 (e.g., in the reaction $\nu + n \to \Sigma^+ + e^-$) ?

d. Since muons from π decay have about four times the energy of neutrinos from π decay, it might be profitable to study the inverse reactions initiated by muons.

Higher-Order Weak Interactions

Baryons

Marshak et al. calculate $K_1 - K_2$ mass difference in second-order perturbation theory with cutoff Λ. For an acceptable mass difference, Λ must be less than 1 Gev. This gives a crude estimate of where conventional theory must be changed. Low-energy "structure" is expected for weak interactions of baryons because pions, etc., can be exchanged.

Leptons

From similar estimates (e.g., $\mu \to e + \gamma$), the cutoff Λ of second-order perturbation theory must be not more than about 50 Gev to make various unseen processes sufficiently small. No important low-energy corrections are anticipated, except for possible intermediate bosons, because the biggest known corrections are electromagnetic.

It would also be interesting to look for evidence of the reaction $\mu^+ + e^- \to e^+ + \mu^-$.

Parity Nonconservation at High Energies

If weak interactions become strong at high energies, would parity nonconservation occur at high energies in p-p and other reactions?

Pursuit of the qualitative and quantitative questions seems practical; the others, less practical (e.g., 50 Gev in the center-of-mass system is at the limit of proposed accelerator energies).

Quantum Electrodynamics (QED)

In this field, precise calculation is possible; therefore, basic principles can be tested quite directly by experiment. We wish to test the principles at small distances. A limited number of tests are available from high-precision low-energy experiments (e.g., Lamb shift). At high energies, one can find more tests, such as the reaction $e^- + e^- \to e^- + e^-$. Within 6 months, Stanford hopes to try this with 500-Mev colliding beams, thus testing QED in the realm of 10^{-14} cm.

The order of magnitude of π, K, $\cdots$ contributions to QED is approximately 1% at high energies. Thus at a given energy there is a limit to testing in the realm of pure QED, and, if one exceeds that limit, one is in the realm of meson physics. This brings us to the second use of QED.

Not-So-Pure QED

Here one uses the accuracy of QED to give a clean probe of specialized strong-interaction amplitudes, such as in

$$e^+ + e^- \to 2\pi \ ,$$

$$e^- + p \to e^- + p \ .$$

Strong Interactions

Considerable data exist on the gross features of strong interactions.

Perkins reviewed the cosmic-ray data, which give an impressively smooth extrapolation upwards from lab energies. No spectacular structure is found at high energies (one possible exception is discussed below). Experimental quantities vary slowly compared with the resonance region. We consider first the dominant processes,

- pionization (many pions produced, mostly at small angles),
- elastic scattering of diffraction type;

and then the exceptional processes,

- production of strange particles and antibaryons (rare compared with statistical theory),
- processes with low multiplicity and high momentum transfer,
- specialized "peripheral collisions."

Dominant Processes

a. Roughly speaking, $\sigma_{tot} \approx$ const. For p+p and $\pi + p$, accelerator data merge into cosmic-ray data, which give constant σ_{tot} up to 10^4-Gev lab energy (errors less than a factor of 2).

b. The differential cross section $\frac{d\sigma_{el}}{d\Omega}$ shows a diffraction peak (accelerator data). The shape corresponds to a cloudy disk, not a black disk. As energy increases, the disk seems to enlarge slowly, and become less black.

c. The ratio $\frac{\sigma_{inel}}{\sigma_{el}}$ is greater than 1. For example, in 24-Gev p-p collisions at CERN, $\sigma_{tot} = 43 \pm 3$ mb, and $\sigma_{el} = 9 \pm 1.3$ mb.

Points b and c are mutually consistent; if the disk were black with a sharp edge, we would find $\sigma_{inel} = \sigma_{el}$.

Several qualitative arguments indicate that these results are not unreasonable. Inelastic scattering can occur by one-pion exchange, therefore the range is approximately m_π^{-1}. Elastic scattering occurs by exchange of two or more pions (one-pion exchange is either nonexistent, as in π-π scattering or π-N scattering, or negligible at high energy, as in N-N scattering), and therefore has a shorter range. A second argument proceeds on grounds of continuity; one doesn't expect the absorbing region to have a sharp edge, and, in fact, dispersion relations suggest a diffuse edge.

d. Pomeranchuk has observed that an elastic amplitude T of diffraction type should satisfy Im T >> Re T. From the forward dispersion relation for T, he shows that, if

$$\sigma_{AB}^{tot} \to \text{constant at high energies,}$$

then

$$\sigma_{AB}^{tot} \to \sigma_{\bar{A}B}^{tot}$$

is required to ensure Im T >> Re T.

The data are inconclusive:

σ_{pp}^{tot} is flat from 5 to 25 Gev,

$\sigma_{p\bar{p}}^{tot}$ decreases towards σ_{pp}^{tot} (up to 10 Gev),

$\sigma_{\pi^- p}^{tot}$ and $\sigma_{\pi^+ p}^{tot}$ both decrease slowly up to 10 Gev, with constant separation, and

$\sigma_{K^- p}^{tot}$ and $\sigma_{K^+ p}^{tot}$ appear to approach each other up to 10 Gev.

e. Pomeranchuk has also observed that exchange scattering is a form of inelastic scattering. As the energy increases, an increasing number of inelastic processes compete for the constant total cross section, so the cross section for each particular inelastic process may be expected to approach zero.

The CERN data for $\pi^- + p \to \pi^0 + n$ at 16 Gev give $\sigma_{exch}/\sigma_{el} < .05$ (the smallness of σ_{exch} happens to be implied by either Pomeranchuk relation in this case). In another CERN experiment (which tests only the Pomeranchuk relation on exchange scattering), 25-Gev protons hit an internal target; the forward beam beyond the target is swept clean of charged particles, leaving neutrons and other neutral particles; this beam hits an external target; and the protons that emerge in the forward direction from the second target are momentum-analyzed. In other words, double forward charge exchange occurs. The result is

$$\frac{d\sigma(0°)_{exch}}{d\Omega} \leqslant .03 \, \frac{d\sigma(0°)_{el}}{d\Omega} .$$

f. In inelastic scattering, pions are always strongly peaked forward and backward in the center-of-mass system. In cosmic rays, there are events known as "fireballs," which can be described as two "centers" emerging back to back in the center-of-mass system, each "center" emitting pions isotropically in its own rest frame.

To find fireballs one makes a considerable selection of events — one tries to exclude collisions of cosmic rays with complex nuclei, and then one further restricts the selection to the more strongly peaked events. The average transverse momentum of secondaries, $\langle p_\perp \rangle$, is approximately 500 Mev, both in accelerators and at higher cosmic-ray energies, reflecting a rather sharp peak in the momentum distribution.

In most collisions, a couple of particles retain about 50% of the primary energy. This is usually interpreted as evidence that the primary particle retains a substantial part of its energy. In cosmic rays, the "interaction length" is 80 g/cm^2, whereas the "attenuation length," within which the average primary energy is reduced to e^{-1} of its initial value, is 120 g/cm^2. The last figure seems constant up to 10^6-Gev primary lab energies.

The average number of secondaries N_s varies as $E^{1/4}_{\text{primary}}$ (lab), up to 10^6 Gev. The number of secondaries fluctuates considerably.

g. There is one fairly well-established anomaly in cosmic rays. It may be seen in the energy spectrum of γ rays initiated in cosmic-ray collisions. Since the main source of energetic γ rays is $\pi^0 \to 2\gamma$, the γ rays inform us about the energy spectrum of secondary π^0. Above about 2×10^4 Gev (lab) the spectrum changes in a way corresponding to higher pion multiplicities and the leveling off of average pion energies. The center-of-mass energy of this phenomenon is approximately 100 Gev. The only known interaction that could produce this effect is the weak interaction, which may become strong at about this energy. Unfortunately, 100 Gev (c.m.) is beyond the range of proposed accelerators.

Exceptional Processes

In general, exceptional processes are sufficiently exceptional that high intensity will be required to study them quantitatively.

a. Both from accelerators and cosmic rays, one knows that particles heavier than pions are rarely produced. In cosmic rays, pions are estimated to form about 80% of all secondaries. There is also some weaker evidence from cosmic rays that strange particles receive only a small fraction of the energy of the primary cosmic ray.

b. At large momentum transfers, few data are available. According to some theories, such as the "hidden symmetry" approach, large momentum transfers yield important information on the structure of the underlying interactions. On the other hand, this region does not seem of fundamental importance to many partisans of the S-matrix approach.

c. The specialized "peripheral collisions" received much attention at the conference. They include the one-pion-exchange mechanisms suggested by Drell and Salzman, as well as diffraction dissociation (discussed by Good). In the latter process, an incident particle hits a target, undergoes a small momentum transfer without exchange of quantum numbers, and thus scatters coherently from different parts of the target. A diffraction peak may be produced even if the incident particle dissociates into several particles.

One has to specify restricted conditions to get any of these peripheral collisions: that is, small angles and high energies (when a cluster of secondaries is created at each vertex of a one-pion exchange the clusters must clearly move in opposite directions in the center-of-mass system). Since the conditions are about the same for each mechanism, it is not easy to find experimental situations that clearly illustrate one isolated mechanism. For example, considerable confusion arose in the discussion of the "quasi-elastic peaks" discovered by Cocconi et al. at CERN. These peaks occur in the process $p + p \to p + ?$, plotted as intensity versus momentum of the final proton, at about 1 Gev/c below the elastic peak. One-pion exchange, diffraction dissociation, isobar models — all were advanced as explanations, but no reliable calculations could be made for any of the models. Furthermore, one-pion exchange is a possible mechanism for producing diffraction dissociation.

In a study more relevant to lower energies, Selleri found a one-pion exchange with a built-in control which allows one to check whether this mechanism is really dominant. He proposes that we study $N + N \to N + N + \pi$ at the 3-3 resonance peak. If exchanges of several pions are important one will not be able to fit the data to the functional form predicted on the basis of one-pion exchange.

I shall leave applications of the Mandelstam representation to other speakers on our schedule. Suffice it to say that the Mandelstam representation offers promise of explaining many of the experimental features I have described. In this approach, it is of great importance to know the behavior of low-energy pion-pion scattering, as one might expect from the experimental circumstance that secondary pions tend to emerge with rather low relative energies even when the primary energy is high.

Possible future machines were discussed, and the following points were brought out:

a. Everyone agreed that high-intensity colliding electron beams of 1 Gev or more are highly desirable.

b. Very-high-energy electron accelerators such as the Stanford Monster were not discussed. Nevertheless, we should remember the Drell mechanism for producing a collimated pion beam in γ, p collisions by one-pion exchange. With this mechanism, Drell estimated that a 40-Gev electron accelerator can produce a pion beam comparable to that from a 25-Gev proton accelerator.

c. A study group at CERN established technically feasible parameters for

(i) colliding 25-Gev proton beams, fed by the present CERN accelerator;

(ii) a 300- to 500-Gev proton accelerator;

(iii) a high-intensity accelerator (10^{13} to 10^{14} particles per sec) at 25 Gev (the present CERN accelerator, but with injection at 2 Gev).

Items (i) and (ii) would give comparable center-of-mass energies. Item (ii) would be more expensive than (i) — it would also be more versatile, because a storage ring can store only stable particles, not π or K ; and it is difficult to know the intensities, and therefore the total cross section, in a colliding-beam experiment.

The high intensity suggested for (iii) would be advantageous in studying weak interactions or the "rare events" in strong interactions and, of course, might be useful as a source for colliding beams.

The question of possible cooperation among the U. S., Russia, and Europe was not discussed explicitly, but, from the standpoint of physics, the consensus was that more than one accelerator might be desirable.

3. EXPERIMENTAL RESULTS FROM THE CERN PROTON SYNCHROTRON. PART I.

Giuseppe Cocconi

June 26, 1961

Discussion in the first part of this talk centers on the results obtained from the analysis of interactions of 16-Gev π^- and of 24-Gev protons with H_2, observed in the CERN 30-cm H_2 bubble chamber (Peyrou, Filthood, et al.).

About one year ago, approximately 35,000 pictures were taken in each case.

The analysis has been carried out mostly at CERN by the Bubble-Chamber and the IEP groups, and by the Oxford-Birmingham group in England. The information that I will discuss was given to me personally by Drs. D. R. O. Morrison and C. Peyrou (CERN) and by Dr. B. French (Oxford-Birmingham).

In these analyses one must bear in mind that momenta above about 10 Gev/c are not easily measured (the chamber is too small) and that the distinction between heavy particles (protons) and light particles (π mesons) is possible only if the momentum (lab) is less than about 1.5 Gev. This limitation means that only secondaries emitted backward in the c.m. system can usually be identified with certainty.

16-Gev $\pi^- + H_2$

General Characteristics

a. Total energy available in c.m. system is $W_0 = 5.4$ Gev.

b. Average number of charged secondaries produced in each interaction (elastic scatterings excluded) is $\langle n_s \rangle = 4.2$.

c. Average momentum of the secondaries (c.m.) is $\langle P_s \rangle = 0.6$ Gev/c ; the average momentum of two-prong events is greater than that of the four-prong events, etc.; the actual distributions extend to momenta approximately 2.6 Gev/c.

d. Average transverse momentum, $\langle P_\perp \rangle = 0.37$ Gev, is independent of the number of prongs; the actual distribution extends up to momenta approximately 1.1 Gev/c.

From points c and d , it follows that, in the c.m. system, the angular distribution of the secondaries is more peaked forward and backward for low-multiplicity events.

e. Total cross section is $\sigma_{tot} = 25$ mb; elastic cross section $\sigma_{el} \approx 4$ mb. The angular distribution for elastic scattering is that characteristic of a diffraction by a body of about 1 fermi radius — a rather transparent body, however, since $\sigma_{el}/\pi R^2 \approx 15\%$.

f. In 25,000 pictures 38 cases were found in which the π^- disappeared in the middle of the chamber with no charged secondaries. For these there are three possibilities:

(i) charge exchange,

(ii) a neutral star of the kind $n + i\,\pi^0$,

(iii) a neutral star of the kind $\Lambda^0 + K^0 + i\,\pi^0$.

Seven cases were found to belong to category (iii), since a neutral strange particle was observed to decay in the chamber. An estimate of the cases missed, always of category (iii), is approximately 25.

It appears that no more than a few of the 38 stoppings observed can belong to category (i), and, since each event corresponds to approximately 0.01 mb,

$$\sigma_{c.e.} < 0.2 \text{ mb}, \quad \text{i.e.}, \quad \sigma_{c.e.}/\sigma_{el} < 5\% \;;$$

a value close to zero is probable.

Inelastic Events with Two Visible Prongs (+ and -)

This selection, of course, includes all the events with any number of neutral secondaries. Results are summarized in Fig. S3-1.

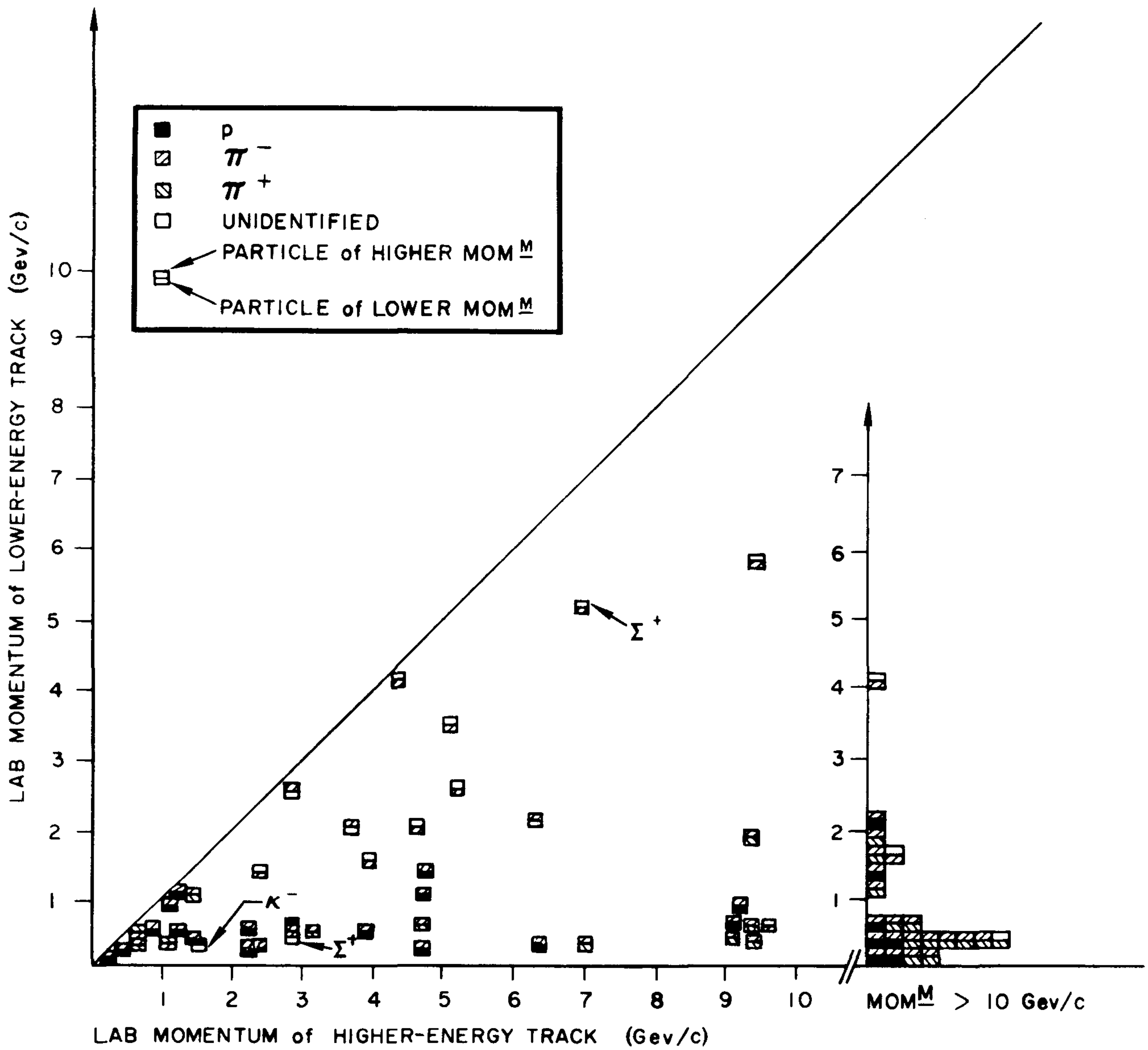

Fig. S3-1. Lab momentum of inelastic two-prong events for 16-Gev π^- on protons.

A characteristic of these π^- - p interactions is that the second particle has low momentum. This must be true also for the invisible ones, of which there should be many, when the missing energy is an appreciable fraction of the 16 Gev.

Several cases of quasi-elastic charge exchange are observed (left corner), and many quasi-elastic ones (right corner).

In Fig. S3-2 forward and backward peaks for π^- and protons (c.m.) are pronounced;

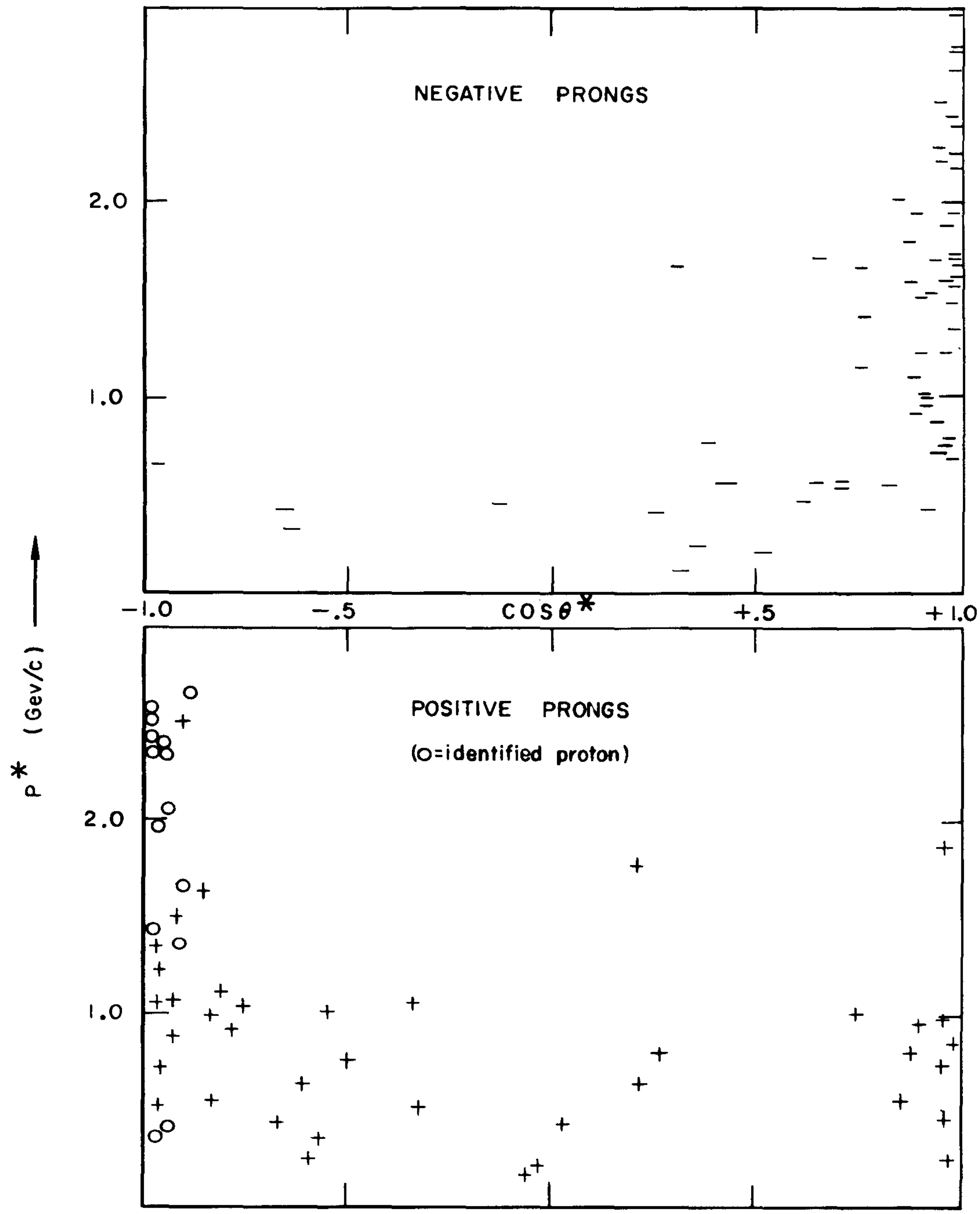

Fig. S3-2. Two-prong stars from 16-Gev π^- on H_2 .

it is also clear that, in many cases, most of the momentum remains in the original particles.

The scattering diagram for the positive particles (Fig. S3-3) shows that the protons are often quasi-elastic, while the π^+ are emitted (in the c. m. system) with low momentum.

Pionization seems the right word for describing this behavior of the strong interactions at these energies. The transverse momentum distributions are amazingly independent of the longitudinal ones.

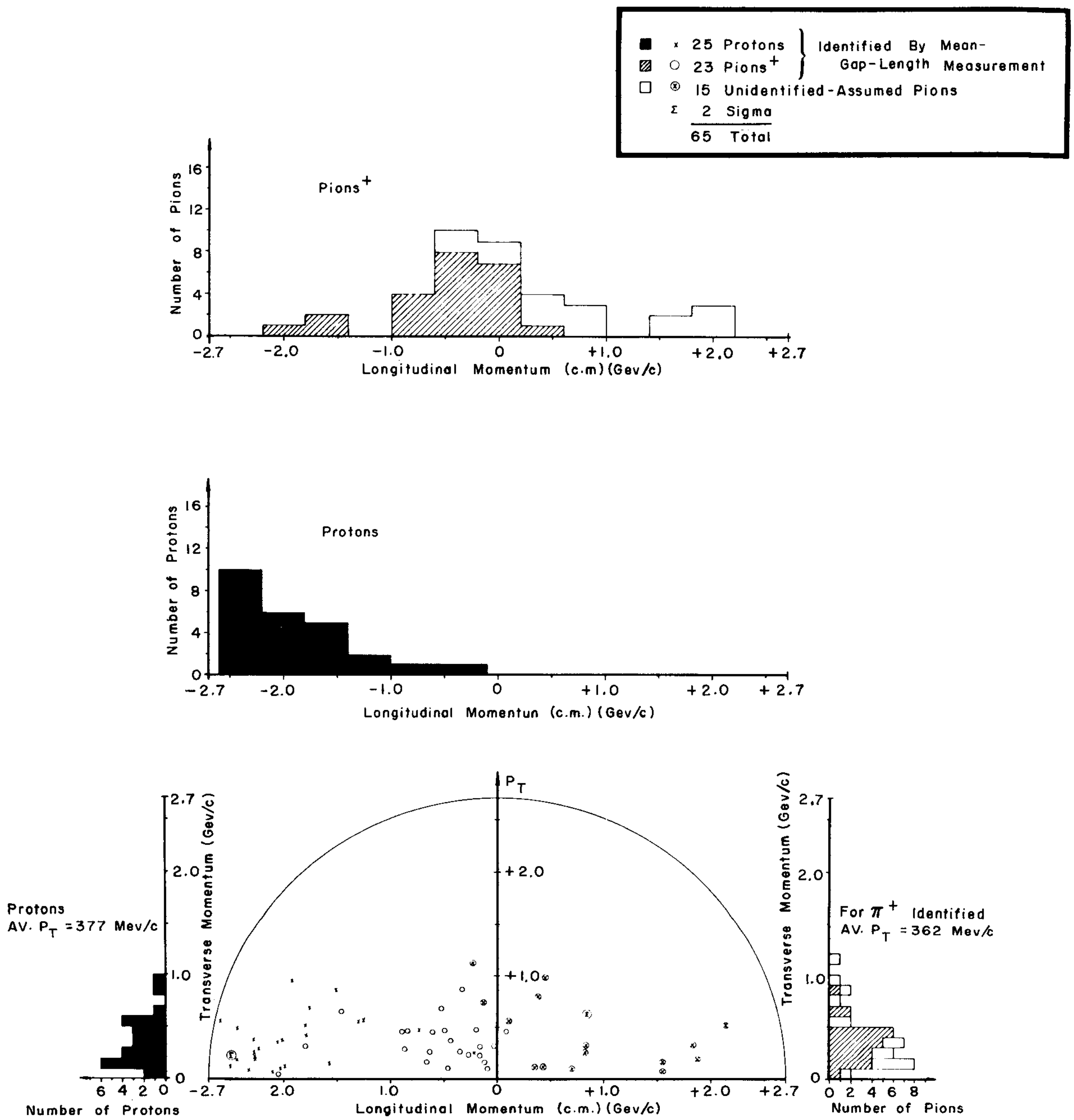

Fig. S3-3. Momentum distributions (c. m.) of inelastic two-prong events in 16-Gev/c π^- -p interactions: positive prongs.

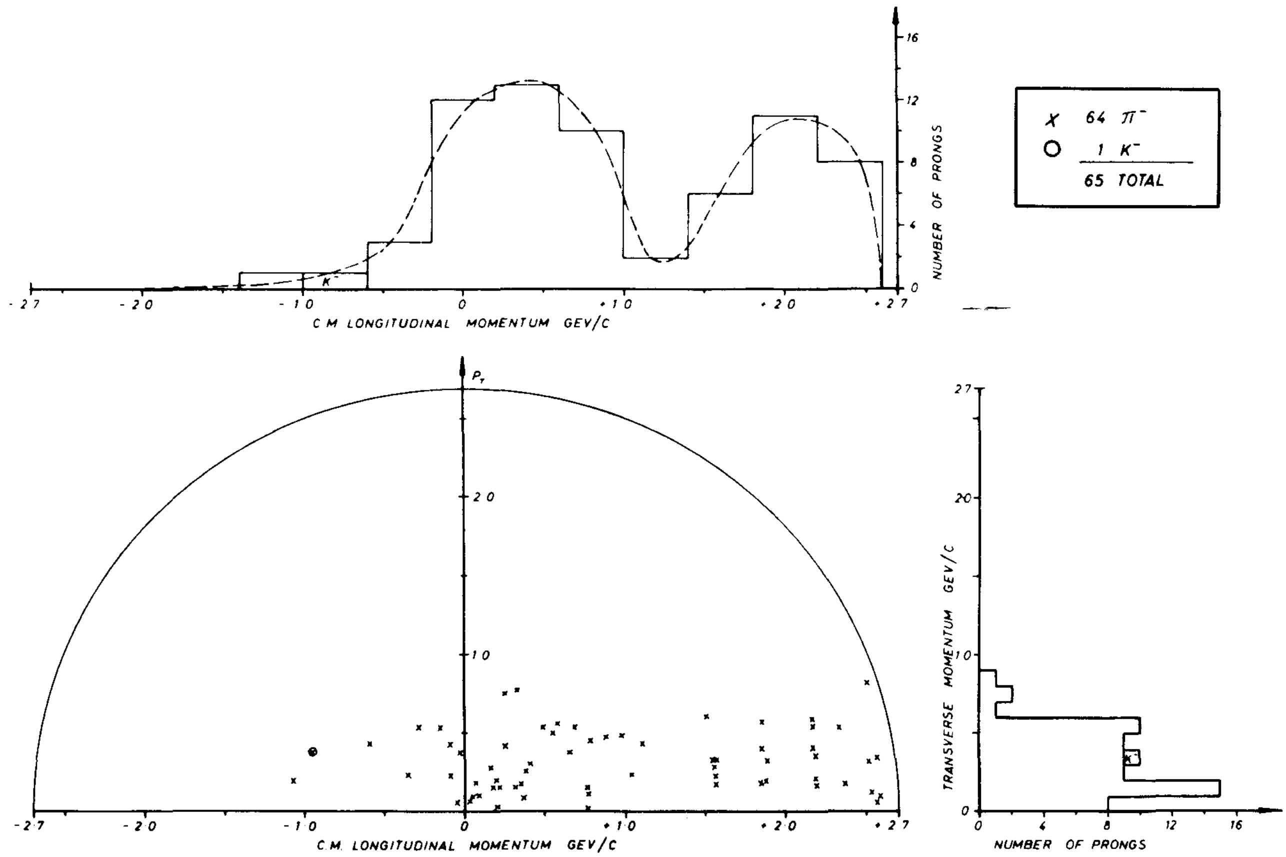

Fig. S3-4. Momentum distributions (c. m.) of inelastic two-prong events in 16-Gev/c π^- - p interactions: negative prongs.

The scattering diagram for the negative particles shown in Fig. S3-4 emphasizes even more the importance of pionization. The high-momentum track is readily interpreted as being due to the original π^-, which remains a π^- and continues to move at close to the original momentum.

It is worth noticing that, both for protons and for π^- (Figs. S3-3 and S3-4), no cases are observed in which the momentum loss is less than approximately 0.1 Gev/c.

The plot in Fig. S3-5 shows the result of an attempt to find correlations between all pairs of pions observed (all events with four, six, and eight prongs are also included). The plot of the Q's of all possible pairs of pions with equal charge and with different charges do not show any peculiar trend. (Q = mass of the body that, by decay, produces the pairs of pions.)

A trend in the Q distribution is found in- instead in Fig. S3-6, where only the pairs $p\pi$ are considered, which are emitted backwards in the c.m. system (and can thus be identified from the mean gap density) in four-prong events. There is strong suggestion that the 3/2, 3/2 state makes its presence felt in the $p\pi^+$ pair formation.

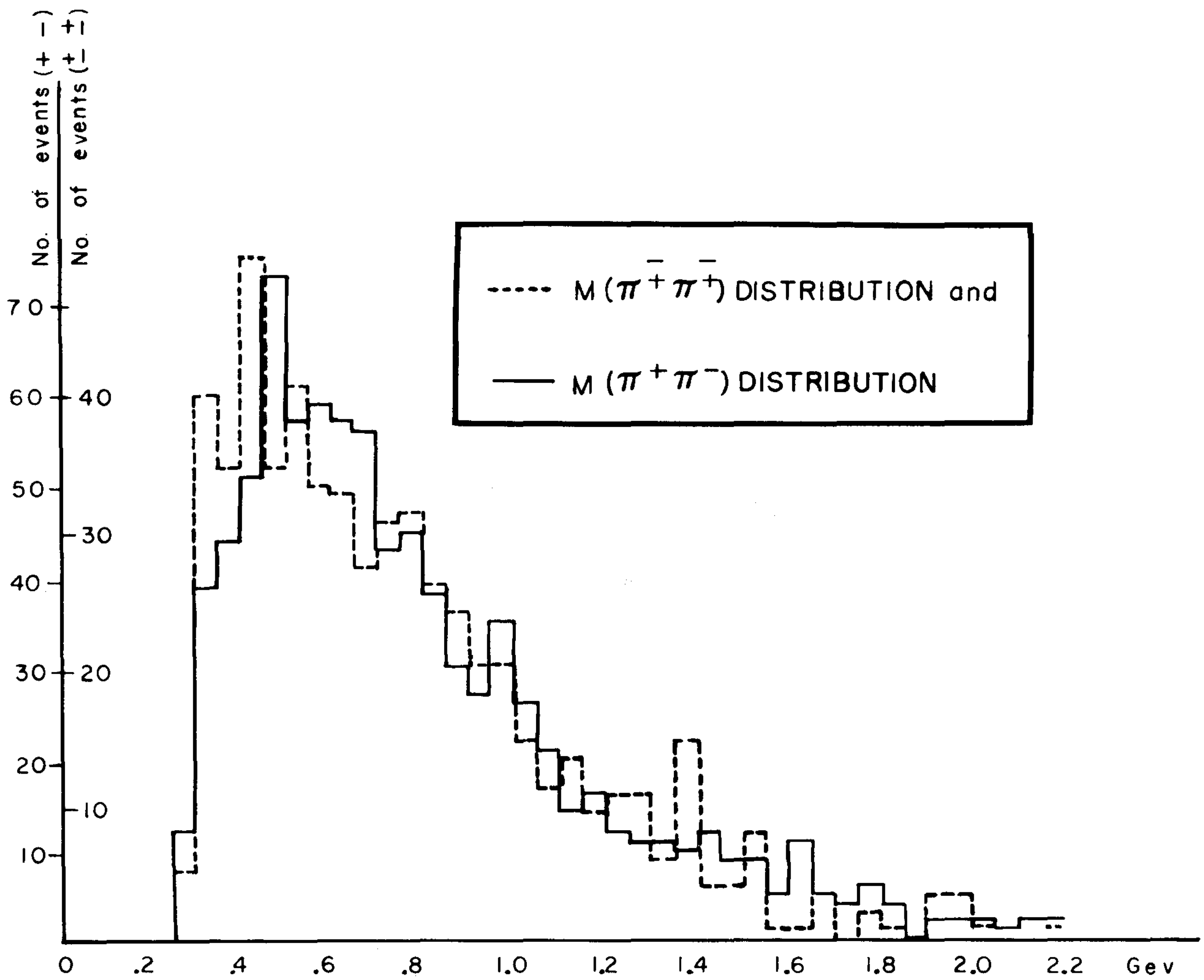

Fig. S3-5. Distributions of M ($\pi^{\pm}\ \pi^{\pm}$) and M ($\pi^{+}\ \pi^{-}$) for two-, four-, six-, and eight-prong events.

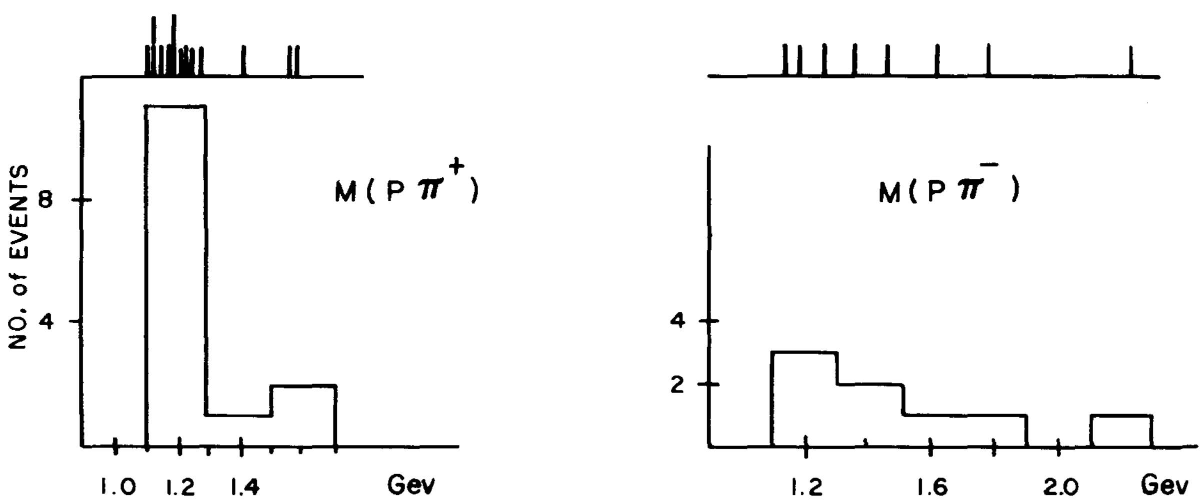

Fig. S3-6. M (pπ) for four-prong events: p with associated π in back c.m. system.

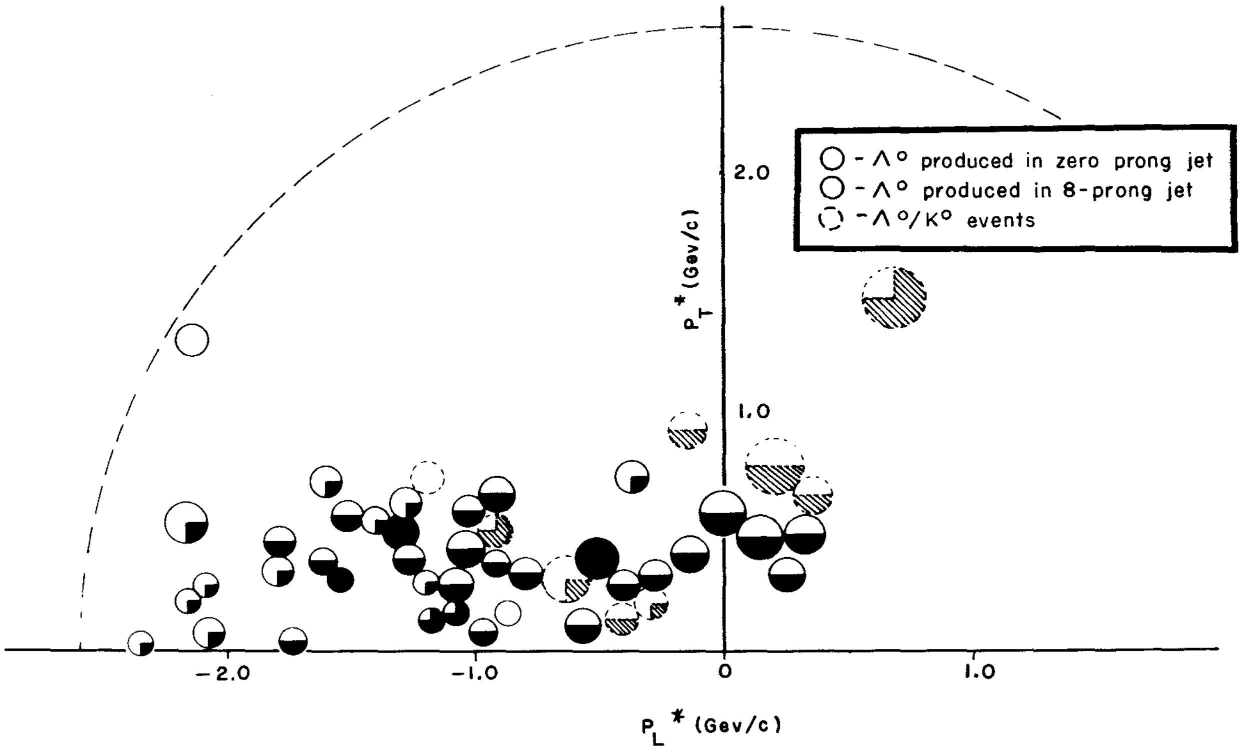

Fig. S3-7. $P_L^* - P_T^*$ distribution of Λ^0 produced in H_2 by 16-Gev/c π^-.

Strange Particles

The CERN groups have analyzed 34,000 pictures, looking for strange particles produced and decaying in the chamber. (See also Bartke et al., Phys. Rev. Letters 6, 303, 1961.) They found $28\Sigma^+$, $18\Sigma^-$, approximately $40\Lambda^0$, and approximately $60 K^0$ (mostly K_2^0). Production cross sections were deduced as follows:

Particle	σ(mb)
Σ^+	0.35
Σ^-	0.14
$\Lambda^0 + \Sigma^0$	0.48
K^0	2.9 ± .4

They found the average transverse momentum to be $\langle P_\perp \rangle = 0.45$ Gev/c .

The scattering diagram for Λ^0 is shown in Fig. S3-7.

In Fig. S3-8, each circle represents one event, and the surface of the circle, the a priori probability of actually observing the particle decaying in the chamber. The blackness of the circle is proportional to the number of charged secondaries accompanying the hyperon.

The following points become evident: First, it seems that the momentum of the original proton is remembered by the hyperon; second, $P_\perp$ is always rather small; and third, hyperons closer to the elastic shell are produced in small-multiplicity events.

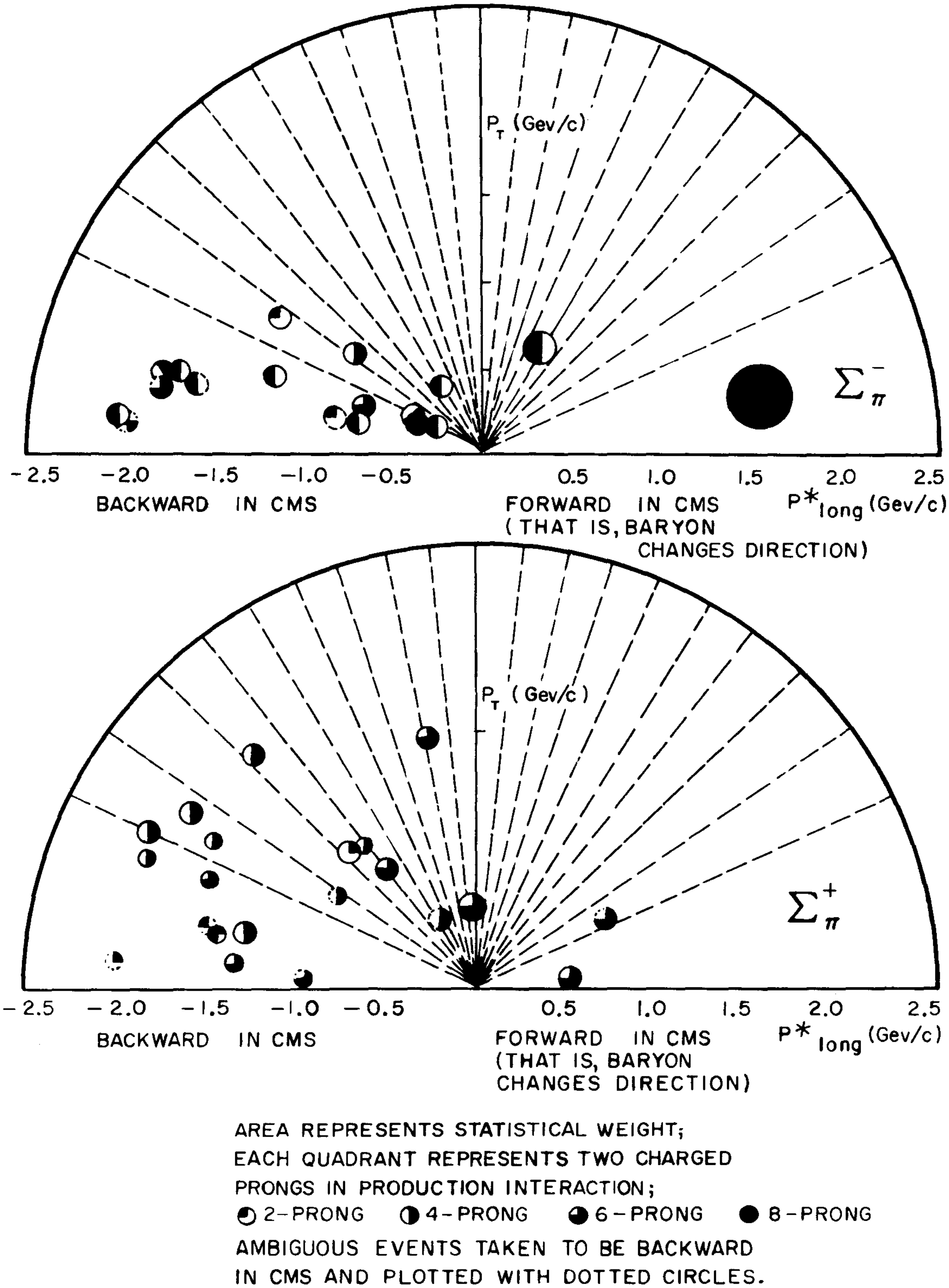

Fig. S3-8. Scattering diagrams of Σ^+ and Σ^-.

Everything suggests the exchange of a single particle. Is it a π or a K ?

For

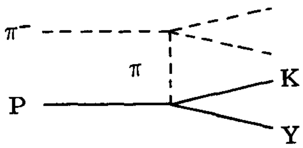

the kaon and hyperon go preferentially backward in the c. m. system;

for

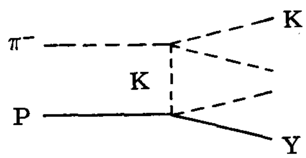

the kaon and hyperon go preferentially forward and backward;

and so on.

The few cases in which two strange particles were observed to decay in the same picture give this still rather inconclusive table:

	Λ	K
6	b	f
2	f	b
1	f	b

	$\Sigma^{\pm}$	K
2	b	f
1	f	b
3	b	b
1	f	f

	K	K
7	b	f
2	f	f

24-Gev Protons + H_2

(analysis far from being complete)

General Characteristics

a. total energy available in c.m. $W_0 = 6.7$ Gev.

b. $\langle n_s \rangle = 4.3$ with dispersion practically equal to that observed for 16-Gev π^- .

c. $\sigma_{tot} \approx 40$ mb,

$\sigma_{el} = 9 \pm 1.3$ mb.

Inelastic Events with Two Visible Prongs (+ and +)

This selection (Fig. S3-9), of course, includes all the events with any number of neutral secondaries.

The second particle always has small momentum in the lab system.

Many quasi-elastic collisions and several quasi-elastic charge exchanges occur.

The forward-backward peaks (c.m.) are due to the protons (Fig. S3-10). Pions are more isotropic.

Figure S3-11 includes the scattering diagram for the backward particles only (always identifiable). The forward particles should give a mirror image. This condition represents pionization at its best.

Note that protons are present with momentum losses nearly equal to zero (at variance, it seems, with the characteristic momentum losses for pions). Is this a manifestation of one-pion exchange?

Elastic Charge Exchange

A counter experiment by M. Fidecaro, Gatti, Giacomelli, Love, Middelkoop, and Yamagata gives some preliminary information about the differential charge-exchange cross section at 0° .

The experimental setup is

P $\longrightarrow$ Be $\longrightarrow$

Int. beam — Int. target

n $\longrightarrow$ Be $\longrightarrow$ P $\longrightarrow$

0°, cleaned with magnet and absorber — Ext. target — 0°, magnet. Momentum analysis $\Delta p = \pm 1$ Gev

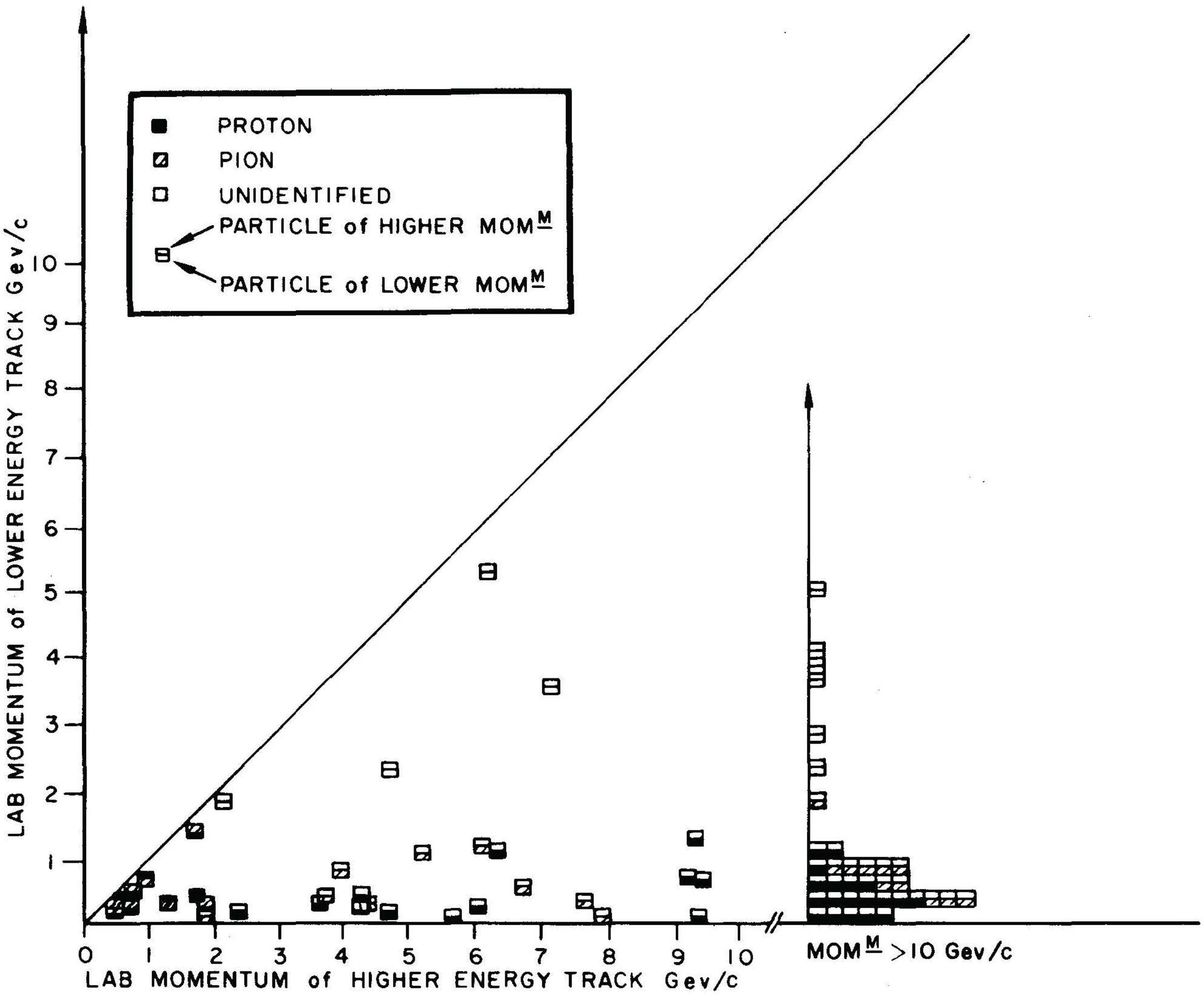

Fig. S3-9. Lab momentum of inelastic two-prong events in proton-proton interactions at 24 Gev.

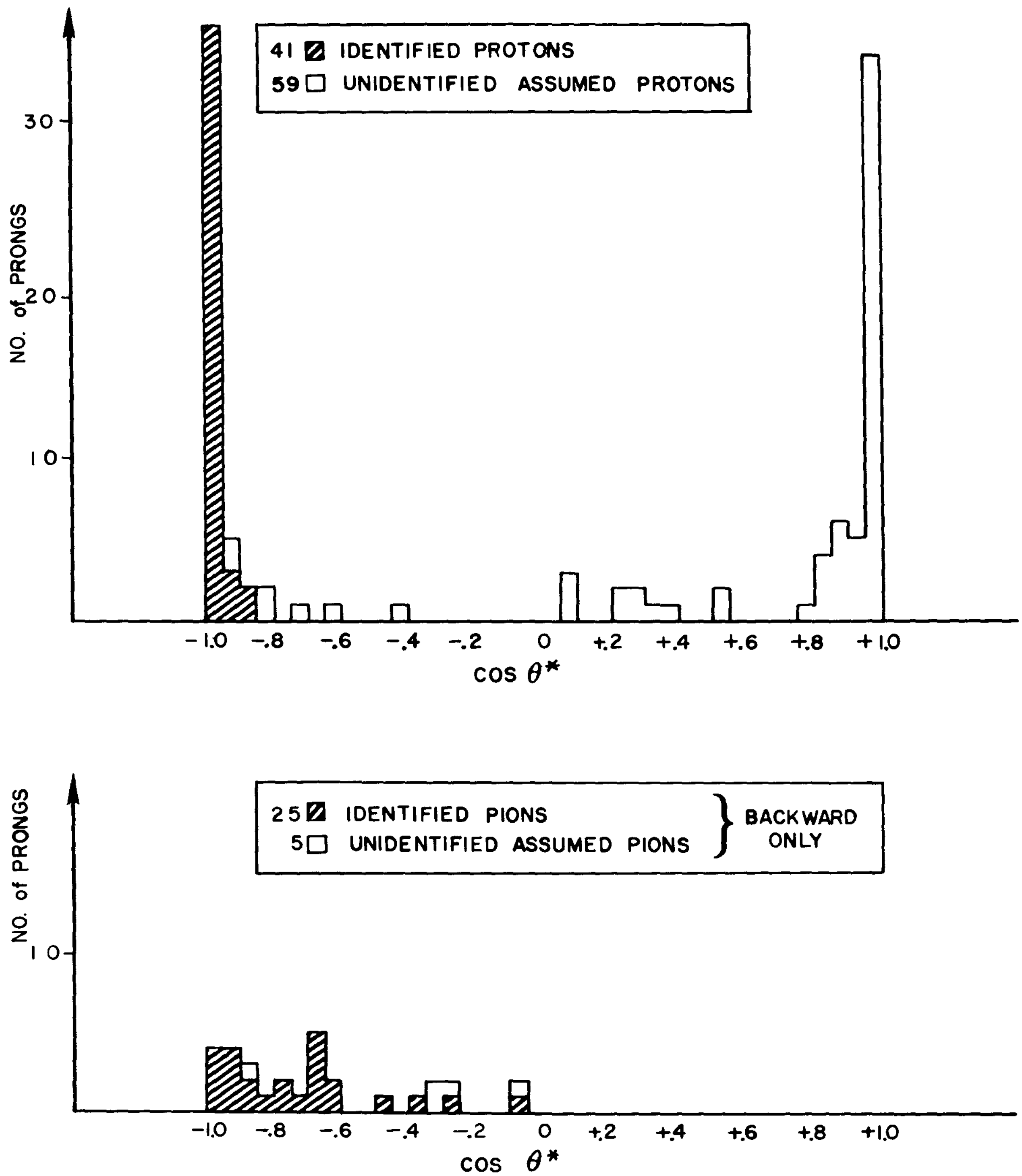

Fig. S3-10. Center-of-mass angular distribution of two-prong inelastic events in 24-Gev proton-proton interactions.

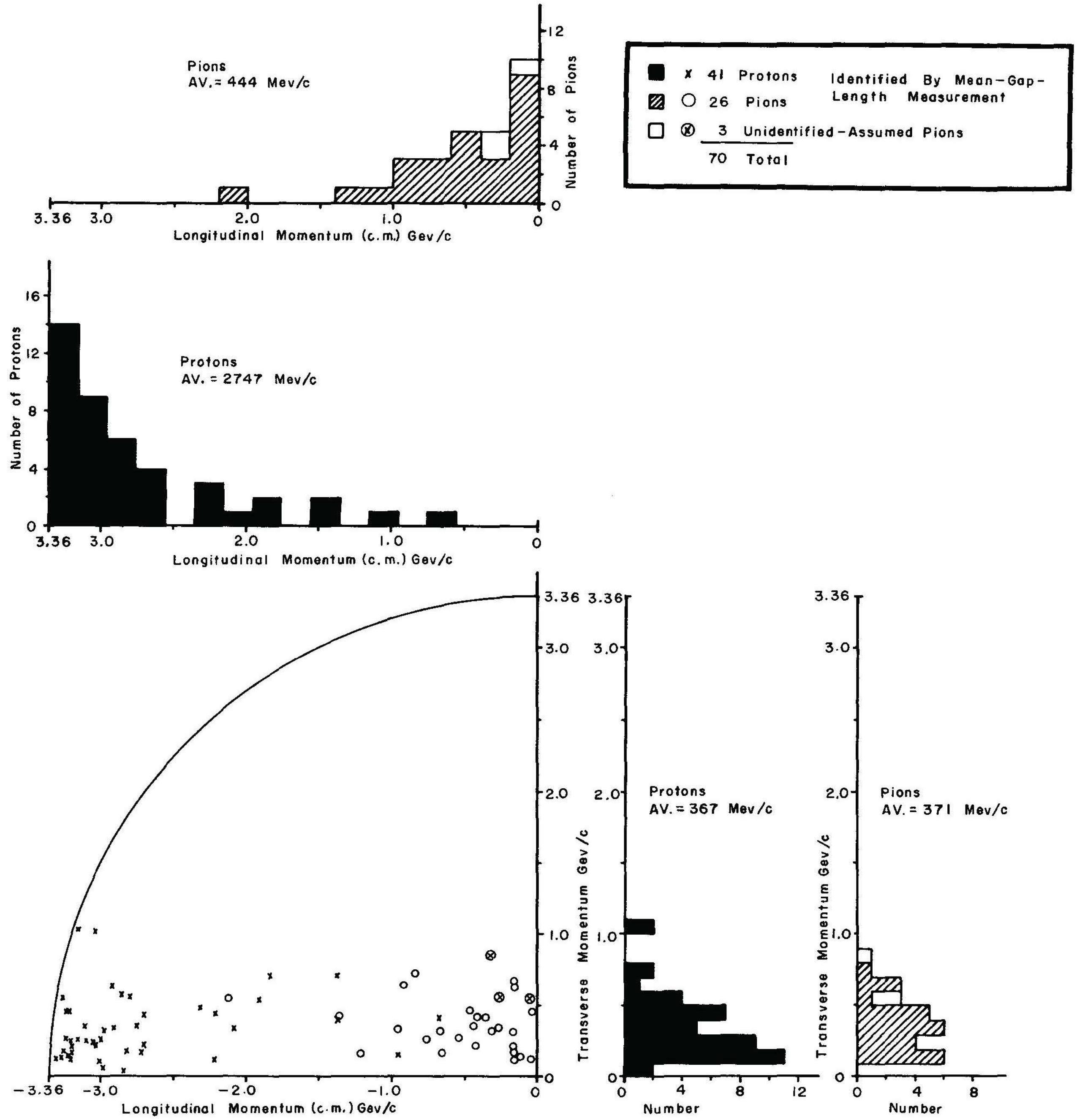

Fig. S3-11. Momentum distributions (c.m.) of inelastic two-prong events in 24-Gev proton-proton interactions.

Figure S3-12 gives the momentum spectrum of the doubly charge-exchanged protons.

The absence of a peak around 28 Gev/c means that

$$\left[\frac{d\sigma(0°)}{d\,\Omega}\right] < .05 \text{ b/sr.}$$

and that

$$\frac{d\sigma(0°)_{c.e.}}{d\sigma(0°)_{el}} < 3\%$$

The quasi-elastic charge exchange, of the order of 0.2 b/sr Gev at $\Delta p \approx 3$ Gev, is not in disagreement with that predicted by Drell's evaluation of the effect of one-pion exchange.

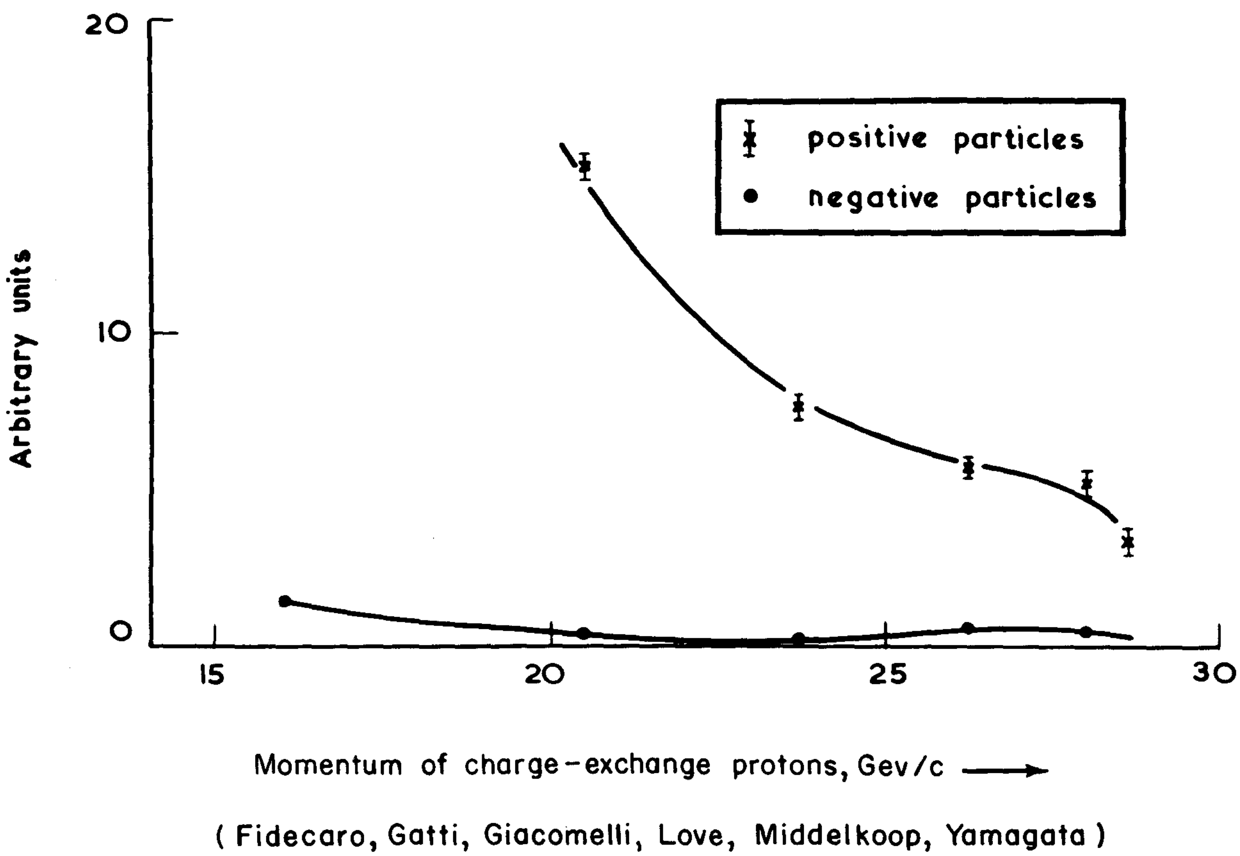

Fig. S3-12. Double charge exchange of 28-Gev protons at 0°.

4. EXPERIMENTAL RESULTS FROM THE CERN PROTON SYNCHROTRON. PART II.

Giuseppe Cocconi

June 27, 1961

In this part, I describe the measurements on the elastic and the quasi-elastic scattering of protons on protons done by the group to which I belonged (Diddens, Lillethun, Manning, Taylor, Walker, and Wetherell). The results of a first series of measurements with the internal beryllium target were published some months ago (Phys. Rev. Letters 6, 231, 1961).

Since February, however, we have been operating with two internal targets: one of CH_2 (polyethylene) and the other of carbon. They are put alternately into the accelerator every 3 seconds, and, at the end of each run, the absolute measurement of the activity of Be^7 produced by spallation of C^{12} (approximately 0.5-Mev γ, $T \approx 60$ d) allows one to determine the total number of protons that hit each target. (We assumed that the spallation cross section, 11 mb, which is constant for protons of incident energy ranging from 0.5 to 6 Gev, remains nearly constant up to 25 Gev.)

The protons of the internal beam, scattered by these targets at an angle (lab) of 56 mr, were collimated, 25 m away from the target, by an iron collimator 6 mm wide, 8 cm high, and 1.5 m long, deflected 90 mr by 4 m of magnetic field (max. field ≈ 18 kgauss), and counted by five pairs of scintillators 6 mm wide, 1 cm thick, and 8 cm high. The double coincidences of each pair were recorded in separate channels, depending on whether the polyethylene or the carbon target was flipped into the beam. With vacuum pipes and helium bags to reduce scattering, the momentum resolution of the system was

$$\frac{\Delta p}{p} \approx 0.5\% \text{ ; i.e., } \pm \text{ approximately 60 Mev at 20 Gev.}$$

Special care was taken by the CERN accelerator experts to keep the radial and longitudinal positions of the two targets constant to within 1 mm, and also to maintain the maximum energy delivered by the accelerator at a constant level. Eventually, a system was found that restricted fluctuations of the maximum energy to less than 0.1% (± approximately 10 Mev at 25 Gev). (See H. Fischer, CERN Report PS-2562, June 1961.)

Before discussing the subtraction method, I shall give the final results obtained for the elastic cross section of protons on protons (CH_2 - C). We remember that a black disk of radius R gives the diffraction pattern

$$\frac{d\sigma_{el}}{d\Omega} = R^2 \left[\frac{J_1(KR \sin \Theta)}{\sin \Theta}\right]^2 = K^2 \left[\frac{\sigma_{tot}}{2\pi} \times \frac{J_1(KR \sin \Theta)}{KR \sin \Theta}\right]^2,$$

where Θ is the scattering angle and $K = p/\hbar$.

Hence, if σ_{tot} is constant (and this is the case for protons of energy greater than a few Gev), the quantity

$$\frac{1}{K^2} \times \frac{d\sigma_{el}}{d\Omega} = \left[\frac{\sigma_{tot}}{2\pi} \times \frac{J_1(KR \sin \Theta)}{KR \sin \Theta}\right]^2$$

is relativistically invariant, since $K \sin\Theta$ is the transverse momentum.

When $\Theta \to 0$, we have

$$\frac{1}{K^2} \times \frac{d\sigma_{el}}{d\Omega} = \left(\frac{\sigma_{tot}}{4\pi}\right)^2,$$

a particular case of the optical theorem.

For these reasons, the experimental results are plotted in these coordinates (Fig. S4-1), though it is known that protons are not black disks. (The actual values of the cross sections are given in Table S4-I.)

The dotted line of Fig. S4-1 represents the central region of the band resulting from the elastic-scattering measurements made by Cork, Wentzel, and Causey (Phys. Rev. 107, 859, 1957), at a few Gev (measurements made by others in the same energy range also fall in the same region).

It is clear that, at energies around 20 Gev and with transverse momenta around 1.5 Gev/c, the elastic-differential cross section is substantially smaller than that measured at a few Gev. Classically, this means that, when the energy increases, the nucleon becomes more extended geometrically and, at the same time, more transparent, since both the total and the elastic cross sections remain nearly unchanged.

Figure S4-2 gives the momentum spectra of the scattered protons (always CH_2 - C).

At all energies the following features are recognizable.

First, the elastic peak, at a momentum p_1 which satisfies rather well the equation of the recoil energy loss,

$$\frac{\Delta p_1}{M} = \frac{p_0 - p_1}{M} = \frac{1}{2} \gamma^2 \Theta^2 ,$$

where $\gamma = p_0/M$ is the Lorentz factor of the incoming proton. (See also Table S4-I.) The areas of the elastic peaks give the elastic cross sections discussed above.

Second, the quasi-elastic peak, occurring at a momentum p_2 for which $\Delta p_2 = p_2 - p_1 \approx$ 0.9 Gev/c. There is some evidence that the quasi-elastic peak consists of two peaks approximately 300 Mev apart.

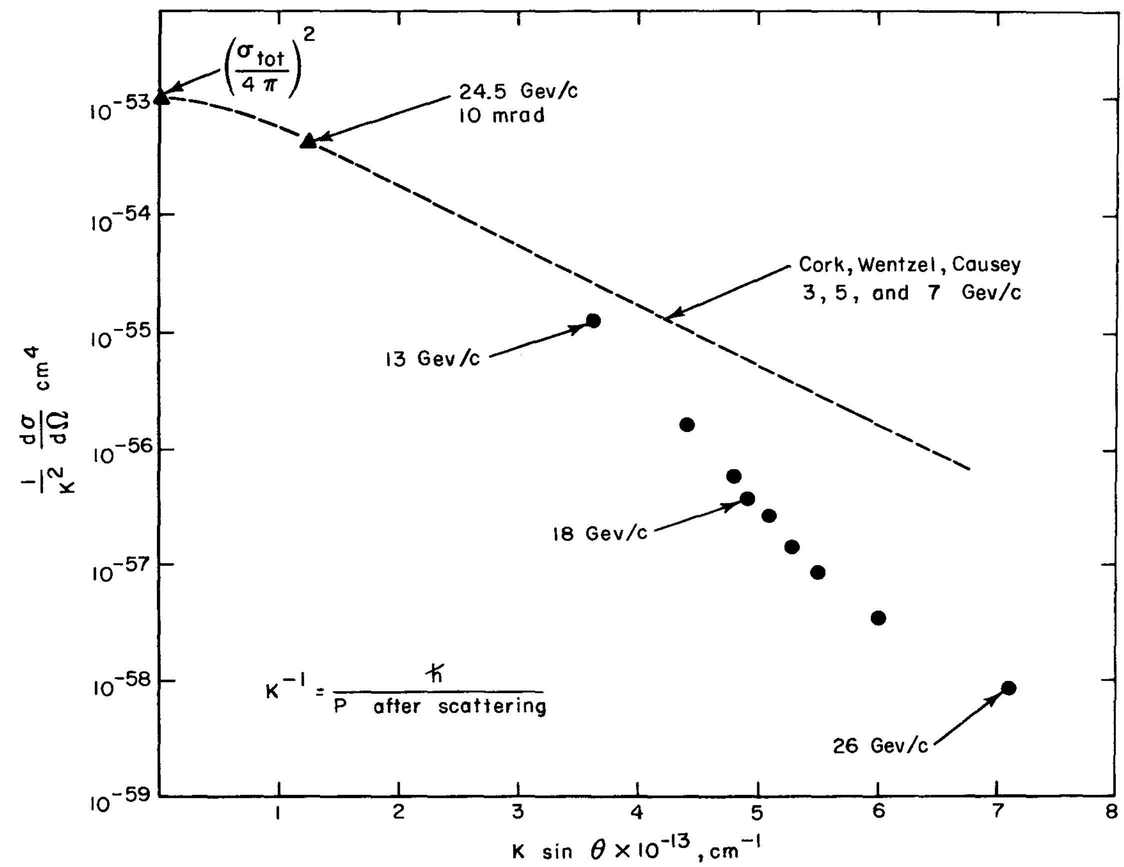

Fig. S4-1. p-p elastic scattering at Θ_{lab} = 56 mrad.

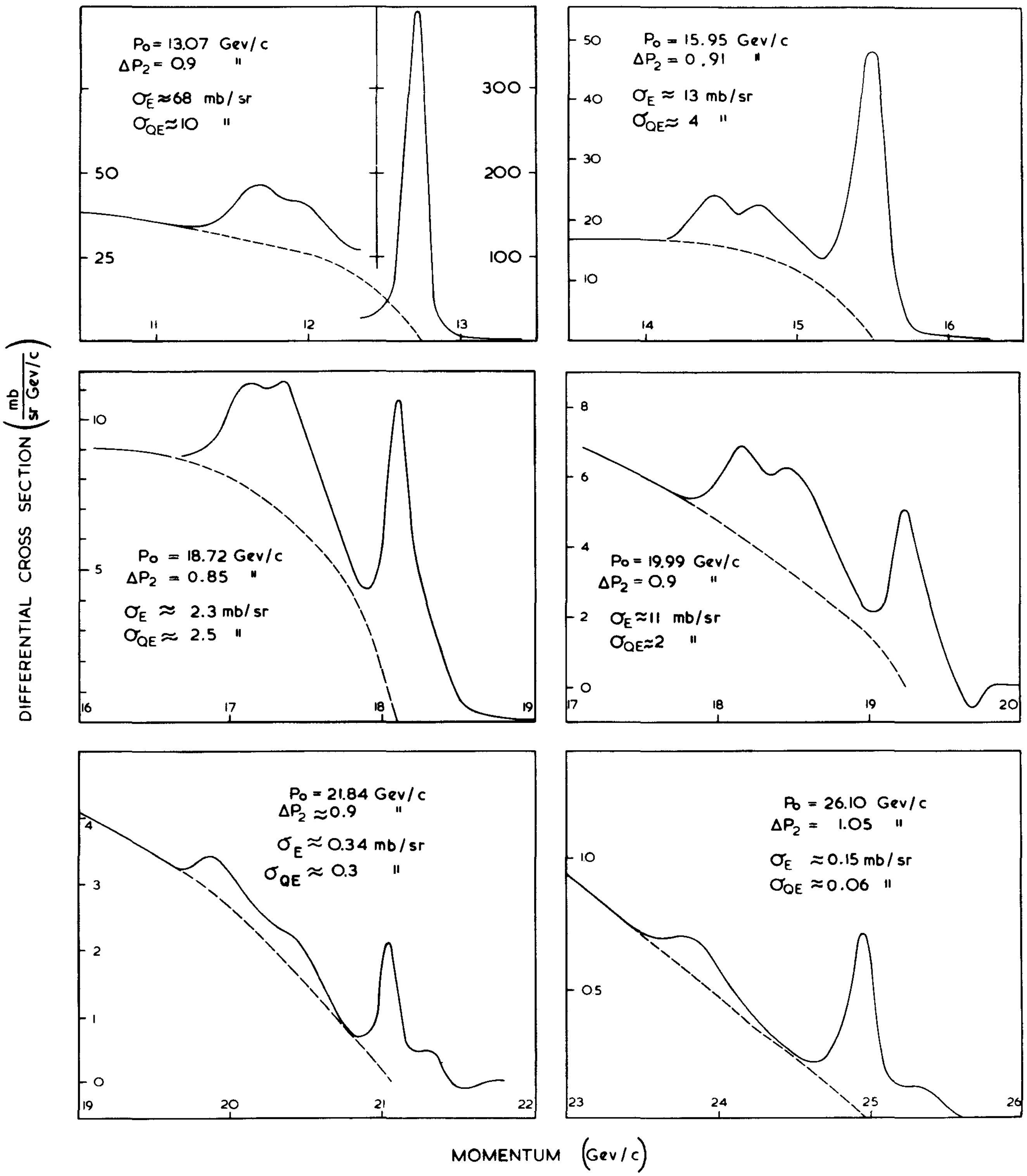

Fig. S4-2. p-p scattering at Θ_{lab} = 56 mrad.

Third, the quasi-elastic continuum (dotted line, under the quasi-elastic peak), could be due to a single-pion exchange (Drell), though 56 mr is an angle much greater than that for which Drell's calculations apply:

$$\Theta \lessapprox \frac{\mu}{p_0} \approx 10 \text{ mr} \quad .$$

A rough approximation to Drell's equation (Phys. Rev. Letters 5, 343, 1960) is

$$\frac{d^2\sigma}{d\Omega dp} \propto \frac{\Delta p}{\Theta^2 p_0^2} \sigma_{\pi-p}(\Delta p) \quad ;$$

it predicts

$$\frac{d^2\sigma}{d\Omega dp} \times \frac{p_0^2}{\Delta p} \approx \text{constant} \approx 3 \times 10^{-24} \text{ cm}^2/\text{sr}$$

at $\Theta = 56$ mr. The corresponding experimental values (see Table S4-I) range from 3 to 1 b/sr, in agreement with the predictions.

The experimental points are plotted in Figs. S4-3 and S4-4.

The width of the quasi-elastic peak (approximately 0.7 Gev) is much greater than that coming from the experimental resolution (approximately 0.12 Gev).

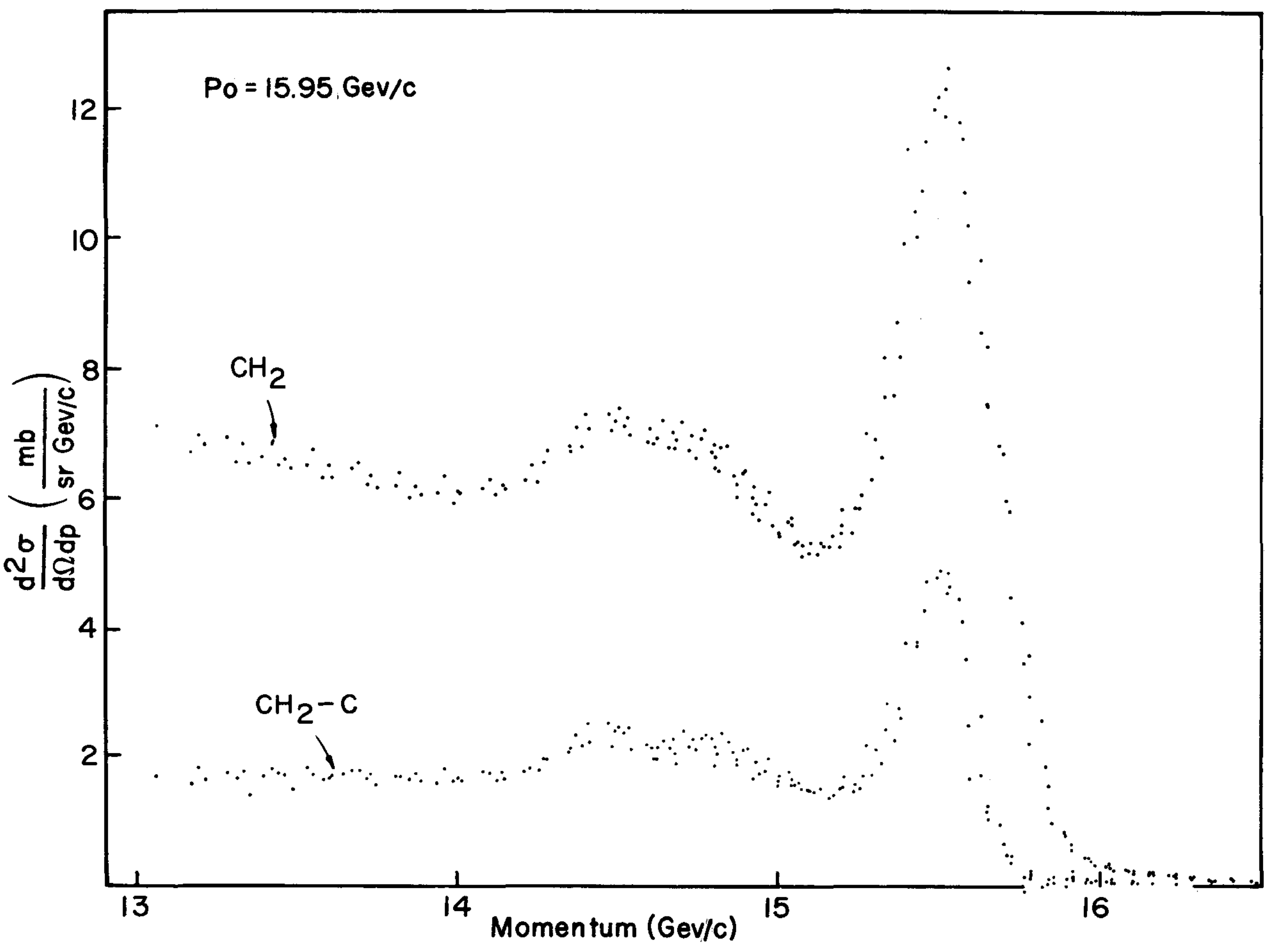

Fig. S4-3. p-p scattering at $\Theta_{lab} = 56$ mrad.

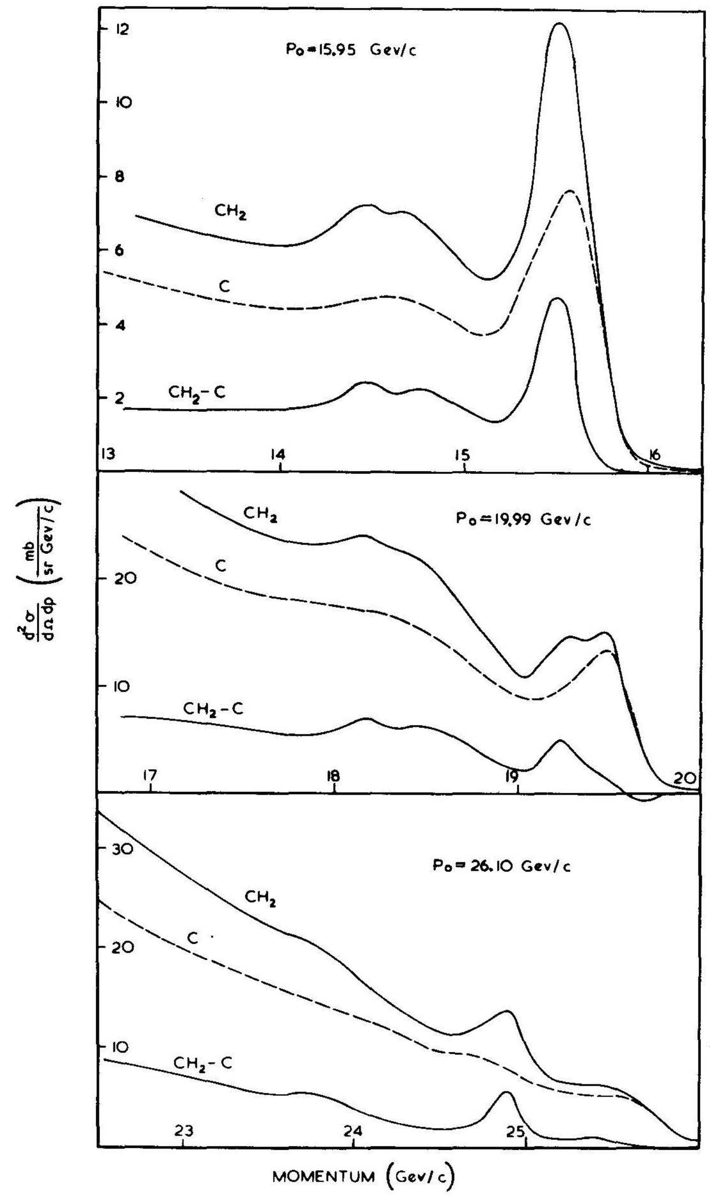

Fig. S4-4. p-p scattering at Θ_{lab} = 56 mrad.

If the two humps exist, they fall, with respect to the elastic peak, where the third and fourth π-p resonances are expected to be.

Thus far, three models have been proposed for explaining the quasi-elastic peak.

First, Drell-like single-pion exchange (Selleri); in which case, all the π-p excited states, and especially the 3/2, 3/2 state, occurring at $\Delta p_2 \approx 0.3$ Gev, should be present. Our measurements exclude any 3/2, 3/2 peak greater than about 10% of the elastic peak.

Second, diffraction excitation analogous to the nuclear excitation observed with α particles: this should occur in any order, hence an optical-model treatment is possible (B. Feld). Also, in this case, the 3/2, 3/2 excited level is expected to be present.

Table S4-I

p - p scattering at Θ_{lab} = 56 mrad

Beam Momentum p_0 (Gev/c)	$\Delta p_1 =$ $p_0 - p_{eH}$ experim. (theor.) (Gev/c)	σ_e (mb/sr)	$\Delta p_2 =$ $p_{eH} - p_{qe}$ (Gev/c)	Γ_{qe} (Gev/c)	σ_{qe} (mb/sr)	$\frac{d^2\sigma}{dp d\Omega} \frac{p_0^2}{\Delta p}$ (b/sr)	$p_{eC} - p_{eH}$ (Gev/c)
13.07	0.35 (0.27)	68.00	0.90	0.6	≈ 10.00	≈ 3.4	0.00
15.95	0.45 (0.42)	13.00	0.91	0.7	≈ 4.00	≈ 3.2	0.07
17.39	0.56 (0.51)	4.50					0.10
17.78	0.53 (0.52)	3.00	0.97	0.5			0.11
18.72	0.62 (0.59)	2.30	0.85	0.6	≈ 2.50	≈ 2.2	0.19
19.43	0.58 (0.67)	1.40					0.16
19.79	0.75 (0.66)	0.83	0.94	0.6			0.24
19.99	0.74 (0.68)	1.01	0.90	0.7	≈ 2.00	≈ 0.8	0.23
21.84	0.79 (0.82)	0.34	≈ 0.90	≈ 0.7	≈ 0.30	≈ 1.1	0.30
22.77	0.92 (0.87)	0.31	0.98	≈ 0.7			0.35
26.10	1.25 (1.20)	0.15	≈ 1.00		≈ 0.06	≈ 1.0	≈ 0.50

Third, diffraction scattering by the virtual pions (Amati, Drell); this occurs for the same reason that the (virtual) nucleons in a nucleus give nucleon-nucleon diffraction scattering when our protons hit the target nucleus. Also, the virtual pions present in the nucleon cloud should give a diffraction elastic peak, displaced even more, since the mass of the virtual pion is smaller than that of the nucleon. Amati and Drell state that this mechanism can be brought forward to explain $\Delta p_2 \approx 0.9$ Gev, independent of primary energy and angle.

The subtraction method, polyethylene - carbon, showed the existence of a nuclear effect, not foreseen (at least, not by us). The peak produced by the protons elastically scattered by the nucleons bound in the carbon nucleus shifts toward larger momenta than the peak produced by the free nucleons (see Fig. S4-4). This shift is due to the strong angular dependence of the elastic scattering coupled with the Fermi motion of the nucleons in the nucleus. At 25 Gev it amounts to more than 0.3 Gev.

A provisional summary of our results is tabulated in the last column of Table S4-I. At the beginning of our experimenting with the subtraction method this splitting of the elastic peak in CH_2 complicated and confused the interpretation of the experimental data.

Finally, I shall mention an application of quasi-elastic nucleon collisions to radiochemistry.

Previously, we considered only the case in which the relatively small energy loss is suffered by the nucleons of the beam. The same process, however, is expected to take place for the target nucleons, also with charge exchange, if a single-pion exchange is responsible for it.

In this case, what before represented an energy loss — e.g., of $\epsilon = 10\%$ (2 Gev at $p_0 = 20$ Gev) — now corresponds to a gain of energy by the target nucleon, initially at rest, of

$$\frac{KE}{Mc^2} \times \frac{\epsilon^2}{2} \quad ,$$

i.e., of some 5 Mev (rather independent of p_0).

Reactions of the kind

$$X_Z^A (p, p\pi^+)\, Y_{Z-1}^A$$

etc., should thus be expected, and, in fact, Rudstam in CERN has shown that the reaction

$$Cu_{29}^{65} (p, p\pi^+)\, Ni_{28}^{65} \quad (\beta^-, 2.7\,h)$$

takes place with a cross section, extrapolated to zero target thickness, of 0.11 mb ($p_0 = 25$ Gev). This number compares well with the still incomplete calculation by Ericson, Selleri, and Van de Walle, who, using Drell's formulas, have evaluated the probability that the nucleon, after the charge exchange, remains in the original nucleus.

5. A THEORETICAL APPROACH TO HIGH-ENERGY SCATTERING

Daniele Amati

June 29, 1961

I shall sketch in a qualitative way a line of research in which I am working — together with Fubini, Stanghellini, and Tonin — in order that we may understand some features of high-energy scattering. Let us analyze some general experimental information available. First, we note that, even though the energy region below the Gev region is rich in characteristics peculiar to the different processes (i. e., resonances, in particular isospin states, for different partial waves in π-N ; flatness of K^+-p cross section in energy, and angular distribution over a wide region of energy; bumps, peaks, and threshold behavior for different phenomena), as soon as the Gev region is surpassed, these peculiarities disappear; the cross sections are smooth and the angular distribution is peaked in the forward direction. There are still many features that can distinguish different processes at these high energies, but I wish to stress the qualitative behavior that all processes share, at least up to the energies at which present accelerators can provide us with accurate information. Let us try to list such "regularities."

a. All elastic cross sections show the characteristic diffraction pattern consisting of a peak in the forward direction. The width of such a peak when plotted as a function of the transfer momentum is nearly independent of the process and of the energy, and it is of the order of magnitude of the pion mass. Another general indication is that, aside from the diffraction peak, elastic scattering is substantially small.

b. Total cross sections tend to reach energy-independent behavior approximately satisfying "Pomeranchuk's theorems."

c. If the energy is not too great, it seems that peripheral formulae work rather well for total cross sections (for which point, refer to Drell's review paper to be published in Reviews of Modern Physics) as well as for many inelastic processes (mainly those for which there is a clear distinction between forward and backward "cones" in the c.m. system — processes that are rather dominant, however).

It is fortunate that regularities are present in elastic angular distributions and total cross section. Both features are related to the elastic scattering amplitudes by the optical theorem; and, because we know some general theoretical properties for elastic amplitudes (i. e., the location of singularities through the Mandelstam representation), we may hope to understand the regularities from a general theoretical standpoint.

Let us consider any elastic process (Fig. S5-1) in which p_1 and p_2 , and q_1 and q_2 , are the four momenta of the incident and scattered particles, respectively; and let us define, as usual,

$$s = \left(p_1 + p_2\right)^2 \ ,$$

$$t = \left(p_1 - q_1\right)^2 = -2p_c^2\left(1 - \cos\Theta_c\right)$$

$$u = \left(p_1 - q_2\right)^2 \ , \quad \text{and}$$

$$s + t + u = 2m_A^2 + 2m_B^2 \ ,$$

where p_c is the momentum and $\cos\Theta_c$ is the scattering angle in the c.m. system. In the physical region for our scattering process, s is positive, and equal to or greater than

$$\left(m_A + m_B\right)^2 ,$$

while t is smaller than or equal to zero. In our scattering process, the absorptive part A(s,t) of

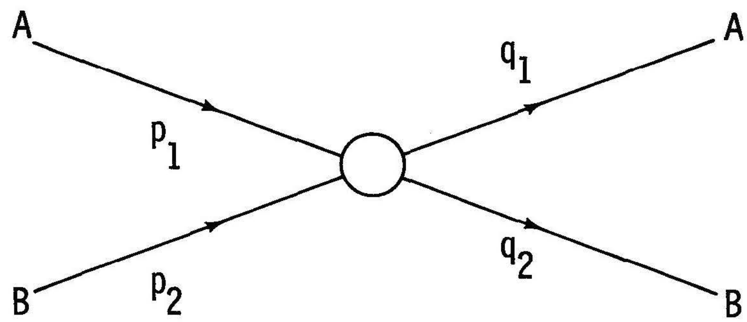

Fig. S5-1

the scattering amplitude $T(s,t)$ satisfies, by virtue of the Mandelstam representation,

$$\begin{aligned} \operatorname{Im} T(s,t) &= A_{AB}(s,t) \\ &= \frac{1}{\pi} \int_{4\mu^2} \frac{\rho(s,t')}{t'-t} dt' \\ &+ \frac{1}{\pi} \int_{4\mu^2} \frac{\rho(s,u')}{u'-u} du' , \qquad (1) \end{aligned}$$

where μ is the pion mass.

The second integral in the right-hand side of Eq. (1) contributes, if it does at all, only to the backward scattering, so we shall not deal with it here.

The integration over t' in Eq. (1) starts at $4\mu^2$, as seen in Fig. S5-2.

Now let us observe that the first empirical "regularity" (refer to point a) implies that the bulk of the contribution to the integral over t' in Eq. (1) must come from small values of t'. This means that $\rho(s,t')$ must contribute up to a certain value t'_{max}, and, then either ρ becomes very small or there is a mechanism (such as that provided by an oscillating function) for which its contribution to the integral in Eq. (1) is small.

The value of t'_{max} is given roughly by $t'_{max} - 4\mu^2 \approx \Gamma$, where Γ is the width of the diffraction peak when represented as a function of t. This means, by the way, that the value of t'_{max} is nearly independent of the energy s. This is the physical meaning of the strip approximation; i. e., the idea that the main contribution of $\rho(s,t')$ to the scattering amplitude must come from values of the variables lying in a narrow strip in the s-t' plane, as soon as s leaves the low-energy region. (See Fig. S5-3.)

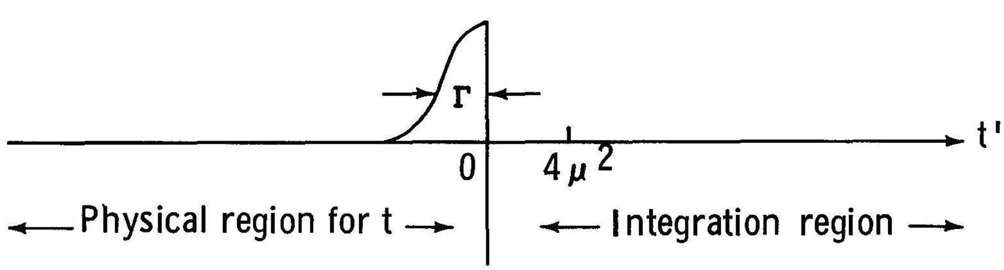

Fig. S5-2

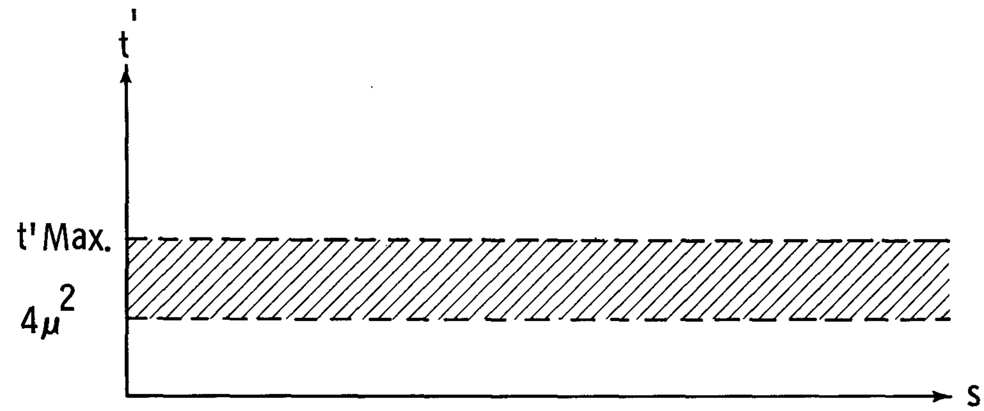

Fig. S5-3

In the future, we shall restrict our integrations to the strip, and we shall see that this procedure will allow us to construct a solution for the scattering amplitude and, therefore, for its spectral function ρ . At the end of this program, we must determine whether the solution we obtain is consistent with the strip approximation (i. e. , ρ outside the strip does not contribute to the integrals). If this is the case, we should obtain a physical solution for the scattering amplitude; if this is not the case, we shall be in conflict with both nature and ourselves. Since this is a program in progress more than an accomplished work, we are not yet able to prove the consistency, but we have good reason to hope for the best, because we already see in our preliminary solution the mechanism that will suppress the integrals outside the strip.

Let us now construct the solution. First of all, we note that, in the strip approximation, we have a definite expression for ρ , and, therefore, for $A(s,t)$ from Eq. (1), given by Mandelstam three years ago; i. e. ,

$$A_{AB}(s,t) = \int ds_1 \int ds_2 \int_{t_0(s,s_1,s_2)}^{t_{max}} dt' \times \frac{A^*_{\pi A}(s_1,t')\, A_{\pi B}(s_2,t')\, f(s,s_1,s_2)}{(t'-t)\sqrt{t'\left[t'-t_0(s,s_1,s_2)\right]}} , \quad (2)$$

where $f(s,s_1,s_2)$ and $t_0(s,s_1,s_2)$ are well-known functions for every definite process and

$$A_{\pi A}\left(s_1,t'\right) \quad , \quad A_{\pi B}\left(s_2,t'\right)$$

are themselves absorptive amplitudes for the $\pi A \rightarrow \pi A$ and $\pi B \rightarrow \pi B$ processes, respectively.

For example, in $\pi - \pi$ scattering (the simplest process) the A's inside the integral in Eq. (2) are again absorptive amplitudes for $\pi - \pi$ scattering (as A itself), and f and t_0 are given by

$$f(s,s_1,s_2) = \left[s^2 + s_1^2 + s_2^2 - 2\left(s\, s_1 + s\, s_2 + s_1\, s_2\right)\right]^{-1/2} , \quad (3)$$

$$t_0 = 4\mu^2 + 4\left(s\; s_1\; s_2\right) f^2(s,s_1,s_2) \quad . \quad (4)$$

For π-N , or N-N , f and t_0 would have slightly more complicated expressions.

We note immediately that we cannot consider Eq. (2) as a solution of our problem; in fact Eq. (2) gives us a scattering amplitude in terms of other scattering amplitudes, and would thus require a separate solution before it could be used for solving other problems. As is seen in the $\pi - \pi$ case, Eq. (2) is really a nonlinear and singular integral equation. The solution of such an integral equation (and therefore the solution of both low- and high-energy $\pi - \pi$ scattering) is a problem that Chew and Frautschi are dealing with. We shall not attempt here to solve Eq. (2), but shall try to use some physical knowledge for $A_{\pi A}$ and $A_{\pi B}$ in Eq. (2) so that we may obtain new physical information about A_{AB} . First let us ask: Can we take

$$A_{\pi A}\left(s_1, t'\right), \text{ or } A_{\pi B} ,$$

directly from experiments? The answer is clearly no, and the reason is that we need $t' > 4\mu^2$ whether or not the physical information is given for $t' \lesssim 0$. Therefore, we must try to extrapolate the physical information from negative t' up to $4\mu^2 \lesssim t' \lesssim t_{max}$. We may now ask ourselves if such an extrapolation can be done, and this time the answer is yes, provided s_1 and s_2 are rather small. We proceed by expanding A in Legendre polynomials of $\cos \Theta' = 1 + 2t'/s_1$ in the manner usual and familiar to experimentalists, and by using this expression for the values of t' we are interested in.

The theoretical reason why such a continuation breaks down when s_1 is too large is that singularities of

$$A_{\pi A}\left(s_1, t'\right)$$

(in t') enter at their turn in the strip so that the Legendre polynomial expansion fails to converge. Or, more physically, as soon as we have too many partial waves we begin to have the typical constructive interference in the forward direction and destructive interference in other directions, so that such a simple wave-by-wave reasoning is no longer valid. The Legendre polynomial continuation can be done in a straightforward manner: because the values of t' in which we are interested are very small, let us simplify, again, by taking only the value at $t' = 0$. Thus, for small s_1 and s_2 (some hundreds of Mev of kinetic energy) we shall take

$$A(s_1, t') \approx A(s_1, 0) \propto s_1 \, \sigma_{tot} (s_1) \ . \tag{5}$$

We still have not investigated what role $t_0 (s, s_1, s_2)$ has as a limit of integration in Eq. (2). It cuts out the contribution of large s_1 and s_2 ; it can be seen from Eqs. (4) and (5) that t_0 is nearly $4\mu^2$ for small s_1 and s_2 , and increases with increasing s_1 and s_2 . As soon as s_1 and s_2 are sufficiently large so that $t_0(s, s_1, s_2)$ reaches t_{max} , the integral in Eq. (2) becomes zero.

In N-N scattering, for instance, we see that, where $s = 16$ Gev^2 (4 Gev of kinetic energy in the lab system), $\sqrt{s_1}$ and $\sqrt{s_2}$, which are total energies for the π-N systems in their c.m. systems, are restricted to less than approximately 1.6 Gev — a rather small energy, some hundreds of Mev of kinetic energy of the pion. This fact is very fortunate, for it permits extrapolation of

$$A_{\pi A}\left(s_1, t'\right) \text{ and } A_{\pi B}\left(s_2, t'\right)$$

from the physical region. Thus, there is a region of energy s , going up to several Gev, for which

$$A_{\pi A}\left(s_1, t'\right) \text{ and } A_{\pi B}\left(s_2, t'\right)$$

in Eq. (2) can be approximated by Eq. (5). In such a case, the dependence on t' in Eq. (2) is explicit, and we obtain, for A(s,t), *

$$A(s,t) = \int ds_1 ds_2 \, s_1 \sigma(s_1) \, s_2 \sigma(s_2) \, f(s, s_1, s_2) \times F_1(t, t_0) \ , \tag{6}$$

where

$$F_1 = \frac{2}{\sqrt{t(t-t_0)}} \ln \left[1 + \frac{-t + \sqrt{t(t-t_0)}}{t_0/2} \right] . \tag{7}$$

Because s_1 and s_2 are limited to small values, as mentioned previously $t \simeq 4\mu^2$, in which case, F_1 can be written as

$$F_1 = \frac{1}{X\sqrt{(1+X^2)}} \ln \left(\sqrt{1+X^2} + X \right) , \tag{8}$$

* The integration over t' in such a case, being convergent, can be extended up to ∞ with almost no change in the result. The important thing to keep in mind is that the s_1 and s_2 integrations in (6) are restricted by the "strip."

where

$$X = \frac{p_c}{\mu} \sin \frac{\Theta}{2} \quad .$$

The whole angular dependence of A is in F ; this means that F^2 is our theoretical prediction for the diffraction pattern of every process in the region of several Gev (c.m.). The comparison with experiments is encouragingly good.

For $t = 0$,

$$A(s, 0) \propto s\, \sigma_{tot}(s) \quad , \tag{9}$$

so that Eq. (6) provides us with an expression for the total cross section. If the coefficients π , 2 , etc. , are properly inserted, it may be seen that such results coincide with the prediction of the peripheral formulae (which may be obtained from the work of the Salzmans, Phys. Rev. Letters 5, 377, 1960) for total cross sections.

This is in some way a Mandelstam-representation support to peripheralism, but we must remember that this is true only when the energy is not too high. When s increases too much (around 8 or 10 Gev c.m.), Eq. (5) breaks down and, therefore, so does the rest of the argument. In spite of this, can we still hope to say something about higher energies? Fortunately, yes, because the breaking down of Eq. (5) results from the appearance of diffraction in the π - A process and the consequent strong dependence of

$$A_{\pi A}\left(s_1, t'\right)$$

on t' . But the dependence of $A_{\pi A}\left(s_1, t'\right)$ on t' for energies (s_1) that are not very high, but for which diffraction is present, is simply given by our previous results in Eq. (6). Therefore, we may insert this first solution for

$$A_{\pi A}\left(s_1, t'\right)$$

in Eq. (2), obtain again an explicit t' dependence, and integrate over it. The result is roughly

$$\iiint s_1 \sigma(s_1)\, s_2\, \sigma(s_2)\, s_3\, \sigma(s_3)\, F_2(t) \quad , \tag{10}$$

where F_2 is a definite function slightly more complicated than F_1 .

The angular distribution of such a contribution is somewhat more forward peaked than in Eq. (6); it remains difficult to determine whether or not preliminary indication concerning elastic angular distribution at high energies shows such a shrinking of the diffraction peak.

For the contribution of Eq. (10) to the total cross section $(t = 0)$, we note that Eq. (10) contains three σ's in the integrand. As Eq. (6) is representable by the usual peripheral diagram (Fig. S5-4), Eq. (10) shall be represented by the diagram in Fig. S5-5. Following the indicated procedure, we see that as s increases we shall construct A(s, t) by iterating further and further our first solution. At present, we have reached only the second iteration; we are, however, pushing forward this program — hoping that, after a few iterations (energies of the order of some tens of Gev c. m.), we shall be able to visualized the qualitative asymptotic behavior.

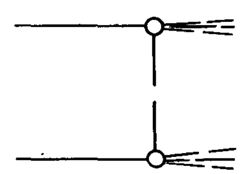

Fig. S5-4

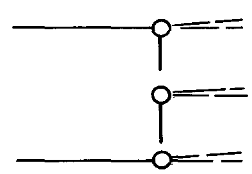

Fig. S5-5

Summary

Let us summarize which properties of high-energy scattering (among the "regularities") can be understood from this theoretical approach.

a. It is evident why the shape of the diffraction peak (including its width) is rather independent of the particular process involved; the shape is mainly controlled by

$$\sqrt{t' \left(t' - t_0\right)}$$

in Eq. (2) for small values of t'. This square root is similar to a phase-space quantity that roughly describes how two pions can share the transfer momentum, and is therefore nearly independent of the process, provided the particles that take part in the process interact strongly with pions (strong interactions).

b. For energies of some Gev (c.m.) the diffraction peak is predicted by Eq. (8); we note that such a formula contains no other parameter besides the pion mass. This formula could be checked further with more refined experimental data. It is expected that at higher energies the form of the diffraction peak will become somewhat narrower.

c. For total cross sections a simple one-boson exchange formula is justified, if the c.m. energy of each of the two bubbles is sufficiently low so that the processes in question will remain nondiffractive. If this is not the case, the bubble must be "split" in two, so that the one-boson exchange picture is still valid, but the picture would look like the diagram in Fig. S5-5. For higher energies this "splitting" will increase so that we find chains of bubbles (see Fig. S5-6).

d. The question arises: Can we hope that this simple peripheral picture we found for total cross sections will remain valid for partial inelastic cross sections? It would be tempting to answer "yes," even if there is not much theoretical justification for it. If one believed in such a "yes," one would have an opening for the investigation of inelastic processes. Investigations along this line are actually contemplated by us, and by other physicists as well. The first qualitative indications of such a model for the multiplicities and nature of secondary particles and their spectra seem promising. Therefore, we may expect that from such a description of inelastic processes it would be possible to understand some characteristic features observed in high-energy accelerators and cosmic rays; for instance, the large amount of pions among the secondaries, as compared with K mesons and baryons; their multiplicity as a function of the incident primary energy; the small and rather constant mean transverse momentum; as well as the spectra of secondary pions showing a reasonable high-energy tail.

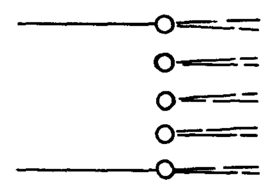

Fig. S5-6

6. MANDELSTAM PERIPHERALISM

Charles J. Goebel

June 30, 1961

I. I will assume your familiarity with the Williams-Weizsacker (W-W) one-meson-exchange "peripheral" formula, given in covariant form by the Salzmans and by Drell as

$$\sigma^{AB} = \frac{1}{4\pi^3 k^2 W^2} \int_{\Delta_{min}}^{\Delta_{max}} \frac{d\Delta^2}{\left(\mu^2 + \Delta^2\right)^2} \int dW_1 k_1 W_1^2 \sigma_\Delta^{\pi A}\left(W_1\right) \int dW_2 k_2 W_2^2 \sigma_\Delta^{\pi B}\left(W_2\right) , \tag{1}$$

and symbolized as in Fig. S6-1.

The limits $\Delta_{min,\,max}$ are kinematic as

$$\Delta_{min} \approx \frac{\sqrt{W_1^2 - m_A^2}\,\sqrt{W_2^2 - m_B^2}}{W} , \tag{2}$$

and

$$\Delta_{max} \approx W ,$$

if $W_{1,2} << W$.

The W-W formula certainly cannot be believed for large Δ (which are kinematically allowed at large W), particularly if the cross section is large there. For instance, suppose that $\sigma^{\pi A}$ and $\sigma^{\pi B}$ are constant at high energy, then, doing the $\iint dW_1\, dW_2$ integrations (note that these have upper limits imposed by $\Delta_{min}(W_1, W_2) < \Delta$), we find

$$\frac{d\sigma^{AB}}{d\Delta^2} \propto \frac{\Delta^4}{\left(\mu^2 + \Delta^2\right)^2} \ln\left(\frac{W_{1max}}{W_{1min}}\right) , \tag{3}$$

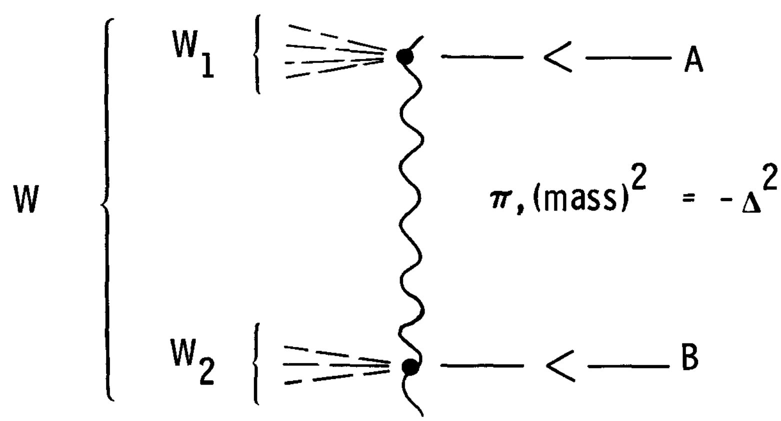

Fig. S6-1

which is roughly constant at large Δ. This is nonsense, because, roughly speaking, interactions with momentum transfer $> \Delta_0$ come from collisions at impact parameters $< \Delta_0^{-1}$, and, here, there is only an area (and, hence, cross section) of $\pi \Delta_0^{-2}$. That is, very roughly,

$$\frac{d\sigma^{AB}}{d\Delta^2} < \frac{\pi}{\Delta^4} \tag{4}$$

is a limit imposed by unitarity.

It is not even obvious that the W-W formula can be believed at small Δ, because our ignorance of the dependence of $\sigma_\Delta^{\pi A}$ on Δ forces us to use its value at $\Delta^2 = -\mu^2$ (real π), which is a finite distance from the least value of Δ^2 in the production process (namely, zero).

Now the Mandelstam relations in a peripheral approximation yield formulae with great similarity to the W-W formula, having, however, the advantages that (a) they are on the mass shell, so that the unphysical quantities occurring in the formula are better known than $\sigma_\Delta^{\pi A}$; (b) it is easy to express quantities (namely, the partial-wave amplitudes) for which the unitarity conditions are simply expressed, and thus we can clearly observe whether unitarity nonsense has crept in.

II. The Mandelstam formulae in the peripheral or "strip" approximation can be written

$$\sigma_{AB}(s,t) = \frac{1}{\pi}\int \frac{dt'}{t'-t-i\epsilon}\, \mathrm{Im}\, \sigma_{AB}(s,t') \ , \tag{5}$$

and

$$\left[\mathrm{Im}\ \sigma_{AB}(s,t)\right]_{2MX} = \iint ds_1\, ds_2\, K\left(s, s_1, s_2, t\right) \times 2k_1 W_1 \sigma^*_{\pi A}\left(s_1, t\right) \times 2k_2 W_2 \sigma_{\pi B}\left(s_2, t\right) \ , \tag{6}$$

where, for the case $m_A = m_B = m_\pi = \mu = 1$, we have

$$K = \frac{1}{16\pi^2 \sqrt{s^2 (s-4)\, t \left[\dfrac{\nu \Delta\left(s, s_1, s_2\right)}{s} - s_1 s_2\right]}} \ , \tag{7}$$

where

$$\Delta\left(s, s_1, s_2\right) = \left(s - s_1 - s_2\right)^2 - 4 s_1 s_2 \ ,$$

$$\nu = \frac{t-4}{4} \ ,$$

and K = zero when the argument of the radical is not positive; hence, $\mathrm{Im}\,\sigma = 0$ for $t < 4$. (When $s_1 + s_2 << s$, we see that the threshold for K is at $\nu \approx s_1 s_2 / s$.) As always, $s = W^2$ = (c.m. energy)^2, $t = -\Delta^2 = -$ (invariant momentum transfer)^2; the function $\sigma_{AB}(s,t)$ is the absorptive (imaginary) part of the elastic scattering amplitude of particles A and B, with a normalization chosen so that the optical theorem is simply $\sigma(s,0) = \sigma_{tot}(s)$. Thus, in the c.m. system,

$$\frac{d\sigma_{el}}{d\Omega} = \left(\frac{k}{4\pi}\right)^2 \left|\ \sigma(s,t)\ \right|^2$$

The second equation, for $\mathrm{Im}\ \sigma_{AB}$, the double spectral function, is exact for $t < 9\mu^2$ (or $< 16\mu^2$, if at least one of A or B is a π); for larger t, other terms contribute to $\mathrm{Im}\ \sigma$. By keeping only this term we have the two-meson-exchange (2 MX) approximation, symbolized by the Landau-Cutkosky diagrams of the type shown in Fig. S6-2.

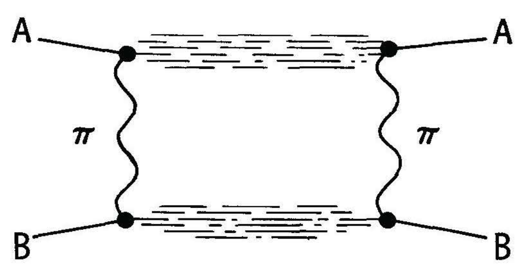

Fig. S6-2. Diagram for two-meson exchange.

The substitution of Eq. (6) in Eq. (5) yields a formula for σ_{AB} in terms of $\sigma_{\pi A}$ and $\sigma_{\pi B}$ which is formally equivalent to the W-W formula (1); that is, the formulae are the same if $\sigma_{\Delta}(s)$ and $\sigma(s,t)$ are suitably identified — e.g., if we neglect the Δ and t dependence and put $\sigma_{\Delta}(s) \approx \sigma(s,t) \approx \sigma_{tot}(s)$. Doing this in the M formulae [Eqs. (5) and (6)], and doing the $\int dt$ integration, we find

$$\sigma_{AB}(s,t) = \iint ds_1\, ds_2\, G\left(s,t,s_1,s_2\right) \times 2k_1 W_1 \sigma_{\pi A}\left(s_1\right) 2k_2 W_2 \sigma_{\pi B}\left(s_2\right), \quad (8)$$

where

$$G = \frac{1}{4\pi^3 \sqrt{\Delta\left(s,s_1,s_2\right)\, s\,(s-4)\, T}} \frac{i\pi - \Theta}{sh\Theta},$$

where

$$\Theta = ch^{-1}\left(\frac{2t}{T} - 1\right)$$

and

$$T = 4\left[1 + \frac{s\, s_1\, s_2}{\Delta\left(s,s_1,s_2\right)}\right].$$

For $t = 0$ the last factor reduces to 1. For $s_1 + s_2 << s$, we have a further simplification to

$$G\left(s,0,s_1,s_2\right) \approx \frac{1}{16\pi^3\, s\left(s + s_1 s_2\right)}. \quad (9)$$

Substituting this in Eq. (8), we see that we get the same result as from doing the $\int d\Delta^2$ integration in Eq. (1); thus,

$$\sigma_{AB}(s) \approx \quad (10)$$

$$\iint \frac{dW_1^2\, dW_2^2\, 2k_1 W_1 \sigma^{\pi A}\left(W_1\right) 2k_2 W_2 \sigma^{\pi B}\left(W_2\right)}{16\pi^3 W^4 \left(\mu^2 + \Delta^2_{min}\right)}.$$

It should be noted that the diffraction-elastic cross section is not included in the 2 MX approximation (it first appears in the 4MX diagrams as in Fig. S6-3) and so the $\sigma(s,0)$ calculated from Eqs. (5) and (6) (and likewise the σ from Eq. (1)) is an estimate of the absorptive, not the total, cross section.

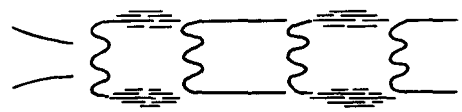

Fig. S6-3.

As we shall emphasize many times, at high energy the neglect of the t dependence of $\sigma_{\pi A}(s,t)$ is entirely wrong and, therefore, Eqs. (8), (9), and (10) are useless. Now the advantage of the M formulae becomes apparent, because something can be said about the t dependence of $\sigma(s,t)$ (see Section V below), in contrast to the Δ dependence of σ_{Δ}. In principle, $\sigma(s,t)$ may be determined by Eqs. (5) and (6) themselves; when A and B are pions, Eqs. (5) and (6) form an integral equation for $\sigma_{\pi\pi}(s,t)$, to which, however, an inhomogeneous term must be added; namely, $[\sigma(s,t)]_{>2MX}$. If the strip approximation is a valid one, then $\sigma_{>2MX}$ is in fact purely 2MX in the crossed channel, and hence is $\sigma_{el}(s,t)$, having spectral function diagrams of the form seen in Fig. S6-4.

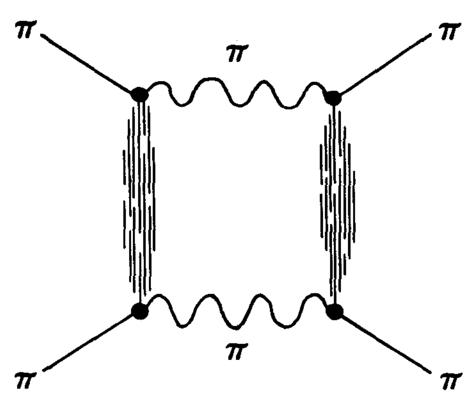

Fig. S6-4. Diagram for $\sigma_{>2MX}$.

Clearly,

$$\sigma^{el}_{\pi\pi}(s,t) = \left[\sigma^{abs}_{\pi\pi}(t,s)\right]_{2MX} \quad . \tag{11}$$

Thus, the equation to be solved for $\sigma_{\pi\pi}(s,t)$ is

$$\sigma(s,t) = \frac{1}{\pi}\iiint \frac{dt'\, ds_1\, ds_2}{(t'-t-i\epsilon)}\, K\left(s, s_1, s_2, t'\right)$$

$$2k_1 W_1 \sigma^*\left(s_1, t'\right)\, 2k_2 W_2\, \sigma\left(s_2, t'\right)$$

$$+ \left[s \leftrightarrow t\right] \quad , \tag{12}$$

the last term being $\sigma^{el}(s,t)$. This equation still lacks an inhomogeneous term, which is finally supplied by the fact that, for convergence, the s wave must be subtracted out and determined by a single partial-wave equation. Equations of the type represented by Eq. (12) have been proposed by several people (Chew, Frautschi, K. Wilson) and solutions are being attempted. Amati and Fubini have attempted to determine $\sigma(s,t)$ by an ansatz for the form of the inhomogeneous term. Another approach would be to find a form for $\sigma(s,t)$ which was asymptotically correct as $s \to \infty$, with $\sigma^{el}(s,t)$ determined approximately from $\sigma^{abs}(s,t)$ by unitarity (see below).

III. The decomposition of $\sigma(s,t)$, given by Eq. (5), into partial waves or into impact parameters is given, respectively, by

$$\sigma(s,t) = \frac{\pi}{k^2}\sum_{\ell=0}(2\ell+1)\, P_\ell\left(1+\frac{t}{2k^2}\right)\mathscr{A}_\ell \, , \tag{13}$$

where

$$\mathscr{A}_\ell = \frac{1}{2\pi^2}\int dt\, Q_\ell\left(1+\frac{t}{2k^2}\right)\, \mathrm{Im}\,\sigma(s,t) \quad ;$$

and by

$$\sigma(s,t) = \int_0 2\pi b\, db\, J_0\left(b\sqrt{-t}\right)\mathscr{S}(b,s) \quad , \tag{14}$$

where

$$\mathscr{S}(b,s) = \frac{1}{2\pi^2}\int dt\, K_0\left(b\sqrt{t}\right)\, \mathrm{Im}\,\sigma(s,t) \, .$$

If $k\ell >> 1$ and $t << s$ then $P_\ell \approx J_0$ and $Q_\ell \approx K_0$. Unitarity imposes the limits

$$0 < \mathscr{A}_\ell < 4 \, . \tag{15}$$

In more detail, if we define

$$\left\{\sigma_{tot}, \sigma^{el}, \sigma^{abs}\right\} = \pi/k^2\, \Sigma(2\ell+1)\left\{\mathscr{A}_\ell, e_\ell, a_\ell\right\}, \tag{16}$$

then unitarity imposes the limits

$$a_\ell < 2\sqrt{e_\ell} - e_\ell \quad , \tag{17}$$

or, inversely,

$$\left(1-\sqrt{1-a_\ell}\right)^2 < e_\ell < \left(1+\sqrt{1-a_\ell}\right)^2 ; \tag{17'}$$

that is, we have the well-known allowed region sketched in Fig. S6-5.

We can likewise define impact-parameter densities as

$$\left\{\sigma_{tot}, \sigma^{el}, \sigma^{abs}\right\} = \int_0 2\pi b\, db\left\{\mathscr{S}(b), \mathscr{E}(b), \mathscr{A}(b)\right\} , \tag{18}$$

which for $bk >> 1$ are nearly the same as the corresponding partial-wave amplitudes and so will obey the same unitarity limits.

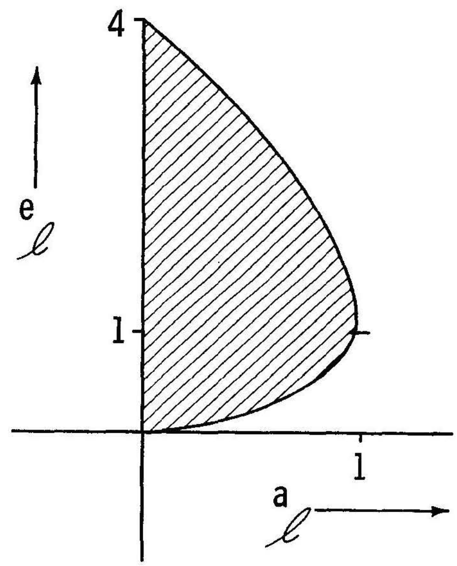

Fig. S6-5.

Equation (14) exhibits clearly the behavior of the amplitudes at large impact parameters.

Since

$$K_0\left(b\sqrt{t}\right) \approx \sqrt{\frac{\pi}{2b\sqrt{t}}}\; e^{-b\sqrt{t}} \quad ,$$

it follows that $\mathscr{A}(b)$ at large b is determined by $\operatorname{Im}\sigma$ at small t. In particular, if $\operatorname{Im}\sigma$ has the threshold behavior

$$\operatorname{Im}\,\sigma(s,t) \propto \left(t-t_0\right)^N \quad , \text{ as } \quad t \to t_0 \quad ,$$

then

$$\mathscr{A}\,(b) \propto \frac{\exp\left(-2b\sqrt{t_0}\right)}{b^{N+3/2}}, \text{ as } \quad b \to \infty \quad . \qquad (19)$$

From Eq. (17') it can then be deduced that

$$\operatorname{Im}\,\sigma^{el}(s,t) \geqslant O\left[\left(t - t_0\right)^{2N+3/2}\right] \text{as } t \to t_0 \quad .$$

IV. We now discuss the limitation on the spectral function imposed by unitarity [Eq. (15)]. To satisfy $\mathscr{A}_\ell > 0$, $\operatorname{Im}\sigma \geqslant 0$ would suffice; but we can easily show that the condition $\mathscr{A}_\ell < 4$ would then force $\operatorname{Im}\sigma$ to yield a $\sigma_{tot}(s)$ which is smaller than observed. Assuming $\operatorname{Im}\sigma \geqslant 0$, then $\mathscr{A}_0 > \mathscr{A}_1 > \mathscr{A}_2$; thus it suffices to consider the inequality $\mathscr{A}_0 < 4$. *

We now wish to find the form of $\operatorname{Im}\sigma$ which maximizes $\sigma_{tot}/\mathscr{A}_0$. Comparing

$$\mathscr{A}_0 = \frac{1}{4\pi^2}\int dt\, \ln\left(1 + \frac{s-4}{t}\right) \operatorname{Im}\,\sigma(s,t) \quad (20a)$$

with

$$\sigma(s) = \frac{1}{\pi}\int \frac{dt}{t}\, \operatorname{Im}\,\sigma(s,t) \quad , \qquad (20b)$$

we see clearly that $\sigma_{tot}/\ _0$ is largest for an $\operatorname{Im}\sigma$ which exists only at the smallest possible value of t ; i.e., $\operatorname{Im}\sigma \propto \delta(t-t_0)$, where

$$t_0 \xrightarrow{s\,\to\,\infty} 4\mu^2 \quad .$$

The use of this "best possible" positive-definite spectral function then leads to the result

$$\sigma(s) \leqslant \frac{4\pi}{\mu^2 \ln\left(s/4\mu^2\right)} \quad , \qquad (21)$$

where

$$s >> \mu^2 \quad .$$

By distinguishing the partial cross sections, this result can be sharpened to

$$\sigma_{abs}(s) \leqslant \frac{\pi}{\mu^2 \ln\left(s/4\mu^2\right)} \qquad (22a)$$

and

$$\sigma_{\text{diffraction el}}(s) \leqslant \frac{\pi}{\mu^2 \ln\left(s/16\mu^2\right)} \, . \qquad (22b)$$

Experimentally, the inequality [Eq. (22a)] is not observed for N-N and π-N scattering in the 10- to 20-Gev region, and so we conclude that the spectral function in those cases is not positive definite. This conclusion also follows from consideration of the shape of the diffraction pattern: Our "best possible" positive definite $\operatorname{Im}\sigma$, above, also yields the most steeply falling diffraction pattern; namely, from Eq. (5),

$$\operatorname{Im}\,\sigma \propto \frac{1}{\left[1 + (-t)/4\mu^2\right]^2} \quad .$$

Experimentally, diffraction patterns fall more steeply.

As an explicit example of an oscillating spectral function the form of which allows a constant cross section, we have

$$\operatorname{Im}\,\sigma = \text{const} \times \frac{\cos\left[\omega \ln\left(t/4\mu^2\right)\right]}{t} \qquad (23a)$$

for

$$t > 4\mu^2 \quad ,$$

---

* If the integrals Eq. (13) for $\mathscr{A}_0, \mathscr{A}_1, \ldots \mathscr{A}_N$ diverge, the inequality is replaced by $\mathscr{A}_{N+1} < 4$.

which, if

$$\omega >> \frac{1}{\ln\left(s/4\mu^2\right)} \ ,$$

yields

$$\sigma_{abs} = \frac{\omega^2}{\omega^2+1} \times \frac{\pi}{\mu^2} \times \mathcal{Q}(0). \qquad (23b)$$

The feature of Eq. (23a) that seemed to be the most critical in yielding a constant cross section is

$$\int dt \ \mathrm{Im}\ \sigma = 0 \ .$$

It might be noted that from Eq. (23a) we get the absorptive amplitude

$$\sigma\left(s, -\Delta^2\right) = \frac{\sin\left(2\omega \ln \frac{\Delta}{2}\right)}{\Delta^2} \times \frac{4\pi^2\ \omega^2 \mathcal{Q}(0)}{\sinh(\pi\omega)}$$

$$+ O\left(\frac{1}{\Delta^4}\right) \ , \qquad (23c)$$

which oscillates in the physical region; this is a general property of any $\mathrm{Im}\,\sigma$ which varies as $\mathrm{Re}\ t^{\alpha}$, α complex, for large t.

Chew and Frautschi, following Regge's work in potential scattering, have conjectured that

$$\sigma(s,t) \approx \alpha(t)\ s^{\nu(t)} \qquad (24)$$

for $s >> t$, where ν is complex for $t > 4\mu^2$. The conclusion above, that $\mathrm{Im}\,\sigma$ is an oscillating function of t, is implied by the conjecture [Eq. (24)] if $\mathrm{Im}\,\nu$ merely is not constant.

V. We now discuss qualitatively the effect of the t dependence of $\sigma_{\pi A}(s,t)$ on $\sigma_{AB}(s,t)$, calculated by Eqs. (5) [or Eqs. (13) or (14)] and (6). As remarked above, we know something about the t dependence of $\sigma_{\pi A}(s,t)$ [unlike the Δ dependence of $\sigma_{\Delta}^{\pi A}(s)$] because it is a physically observable quantity for $t < 0$. Further, since

$$P_{\ell}\left(1 + \frac{t}{2k^2}\right) = \sum_{n=0}^{\ell} a_n t^n$$

where all a_n are positive, and since in Eq. (13) the $\mathscr{A}_{\ell}$ are all positive, it follows that $\sigma(s,t)$ and all its derivatives with respect to t, are nondecreasing for $0 < t < t_0$, where t_0, the threshold of $\mathrm{Im}\ \sigma(s,t)$, is where the series [Eq. (13)] diverges. At t_0, $\sigma(s,t)$ is continuous if $\mathrm{Im}\,\sigma(s,t)$ is continuous, and this is guaranteed by Eq. (6). Thus, we may conclude that, in the region of t near t_0, $\sigma_{\pi A}(s,t)$ is certainly larger than $\sigma_{\pi A}(s,0) = \sigma_{\pi A}(s)$; hence, using Eqs. (6) and (14), $\mathscr{A}(b)$ at large b is certainly larger than would be calculated by using the approximation

$$\sigma_{\pi A}(s,t) \approx \sigma_{\pi A}(s) \ .$$

This result has a straightforward physical interpretation known as the "size effect": The slope of $\sigma_{\pi A}(s,t)$ with t is a measure of the size of the π-A interaction region; in particular, if π and A had only a near-point interaction, then $\sigma_{\pi A}(s,t)$ would vary only slowly with t. Thus, $\sigma_{\pi A}(s)$ would be a good approximation to use in calculating $\mathrm{Im}\ \sigma_{AB}$. Conversely, if π and A have a long-range interaction, $\sigma_{\pi A}(s,t)$ varies rapidly with t, and $\sigma_{\pi A}(s,t)$ at $t \approx t_0$ is much larger than $\sigma_{\pi A}(s)$.

By picturing the one-meson-exchange interaction in coordinate space, it becomes intuitively clear that the size effect should indeed increase $\mathscr{A}(b)$ at large b: If the π-A and π-B interactions occur at a point (Fig. S6-6a), the probability for A and B to interact when passing by at an impact parameter b is, roughly,

$$\mathcal{Q}(b) = \mathrm{const} \times \frac{e^{-2\mu b}}{b^N} \sigma_{\pi A}\ \sigma_{\pi B} \ . \qquad (25a)$$

But if the π-A and π-B interactions are spread out over a range comparable to μ^{-1} (Fig. S6-6b), we have, roughly,

$$\mathcal{Q}(b) = \mathrm{const} \times \iint db_1^2\ db_2^2\ \frac{e^{-2\mu b_{12}}}{\left(b_{12}\right)^N} \mathscr{A}_{\pi A}\left(b_1\right) \mathscr{A}_{\pi B}\left(b_2\right), \qquad (25b)$$

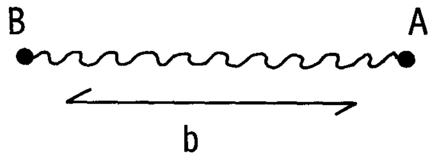

Fig. S6-6a.

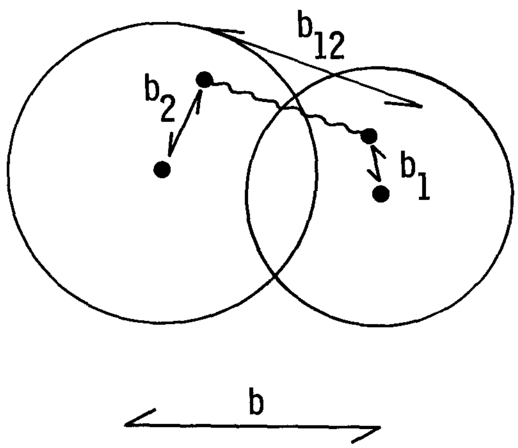

Fig. S6-6b.

where, as usual,

$$\int d\,b_1^2\,\mathcal{A}_{\pi A}\left(b_1\right) = \sigma_{\pi A} \quad .$$

For large b this result is larger than Eq. (25a) because

$$\frac{e^{-2\mu X}}{X^N}$$

is a concave function.

Another conclusion which can be drawn from Fig. S6-6b and Eq. (25b) is that, owing to the weighting of the factor

$$\frac{e^{-2\mu b_{12}}}{\left(b_{12}\right)^N} \quad ,$$

when b is large the virtual π-A and π-B collisions are more peripheral than free π-A and π-B collisions; that is, higher proportions occur at large b_1 and b_2, respectively. This "internal peripheral enhancement" can indeed be seen to be contained in the Mandelstam formulae. An example (Fig. S6-7) of its effect is to be found in the ratio of

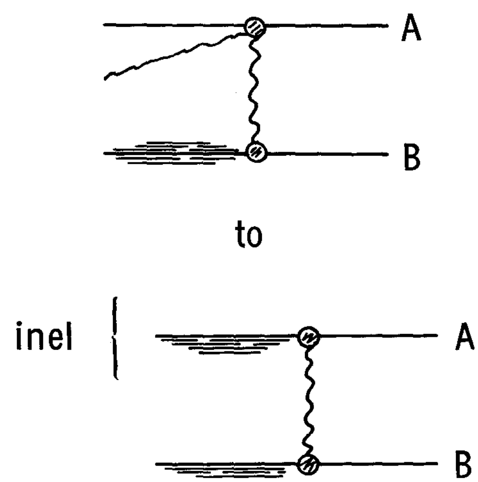

Fig. S6-7.

(where "inel" means all inelastic states), which at large b is smaller than the ratio $\sigma^{el}_{\pi A}/\sigma^{inel}_{\pi A}$ because σ^{el} is shorter-ranged than σ^{inel} .

The importance of the size effect in high-energy N-N collisions can be exhibited by the attempt to calculate $\mathcal{A}_{NN}(b)$ at large b by using the "point-interaction approximation" $\sigma_{\pi N}(s,t) \approx \sigma_{\pi N}(s)$; a rough calculation gives, on this basis, $\mathcal{A}_{NN}(0.8\,\mu^{-1}) \approx 0.02$. That this is far too small is demonstrated by the fact that the shape of the N-N diffraction pattern shows the range of interaction to be approximately $0.8\,\mu^{-1}$, i.e., out to at least this distance, $\mathcal{A}_{NN}(b)$ is not much smaller than 1 .

VI. I shall conclude by speculating about what can be deduced from the Mandelstam equations on peripheral inelastic collisions. First of all, it is clear that, in an A-B collision, partial cross sections for the production of specific numbers of specific particles can be obtained by using appropriate partial π-A and π-B production cross sections in Eq. (6). The justification for this is that individual Feynman diagrams of the type represented by Fig. S6-2 obey the Mandelstam representation. Further, it might be thought that, by not completing the $\iint ds_1 \, ds_2$ integrations in Eq. (6), one would obtain the differential cross section for the production of two particle clusters of masses $\sqrt{s_1}$ and $\sqrt{s_2}$, respectively. There is certainly identity in the form of this formula [Eqs. (8), (9), and (10) above] with the W-W formula, but the identity is suspect, since there are other terms of the same form as that in Fig. S6-2, which contribute to the production of the same particles, but in which the two clusters of particles are divided differently. These terms cannot be put into the desired form of a differential cross section in the masses $\sqrt{s_1}$, $\sqrt{s_2}$ of the original clusters.

As remarked above, the Mandelstam equations in the strip approximation can be used as an integral equation for $\sigma_{\pi\pi}(s,t)$, i. e. [e. g., Eq. (12)] with the s wave separated out. The process of iterating this equation can be described by the diagrams in Fig. S6-8,

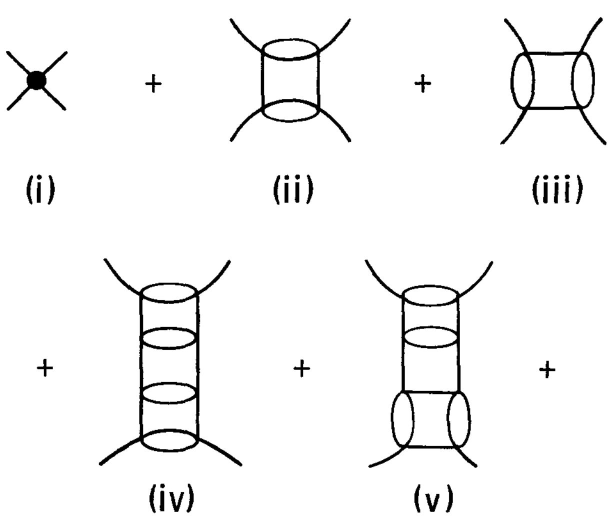

Fig. S6-8.

where each represents the complete s-wave amplitude, and the s-wave part is to be subtracted out from each diagram. The carrying out of the strip approximation thus leads to a $\sigma_N(s,t)$ for each multiplicity N, although it gives no useful information about the final-state distributions of these inelastic cross sections. It should be noted that in this approximation, collisions at arbitrarily high energies are ultimately described in terms of low-energy π-π collisions. The situation in this approximation is reminiscent of high-energy electrodynamics, in which, as is well known, the bulk of bremsstrahlung processes can be described in terms of a low-energy γ-e scattering and a low-energy γ-Z vertex. In strong interactions the difference is that there is no small coupling constant to suppress higher-order effects, which leads to the possibility of there being many internal collisions, as in Fig. S6-8 (iv).

At the moment, we have little idea how applicable the strip approximation is to high-energy collisions, and what proportion of the high-energy cross sections is peripheral. There are, however, several experimental results in high-energy N-N collisions which may lead one to hope that the proportion is large: (a) the long range ($0.8\,\mu^{-1}$) of the interaction, (b) the great predominance of π's over other produced particles, and (c) the small longitudinal momenta of the produced π's compared with the final nucleons. These would all be consequences of the interaction's proceeding through many low-energy collisions as in Fig. S6-9.

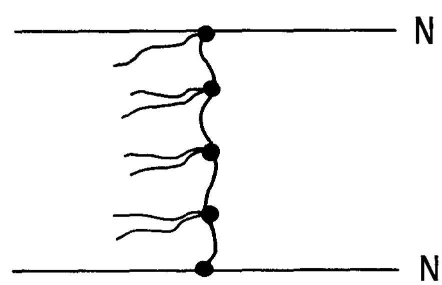

Fig. S6-9.

It is surely wishful thinking to imagine that the Mandelstam relations [Eqs. (5) and (6)] for the elastic-scattering amplitudes can lead to a complete understanding of very-high-energy interactions, but, also, it is surely remarkable how far they lead us toward it.

7. NEUTRINOS AND WEAK INTERACTIONS

Norman Dombey

July 3, 1961

This is a survey of existing and presently fashionable theories which have particular reference to high-energy neutrino reactions. Most of the results stated here have been reported before; notably, by Yamaguchi and by Lee and Yang.

Pure Weak Interaction-Leptons

Muon decay is the only known example of a pure weak interaction (tempered by electromagnetism). All available evidence supports the Lagrangian

$$L_{int} = \frac{G_\mu}{2}\left[\bar{\nu}\gamma_\alpha\left(1+\gamma_5\right)e\right]\left[\bar{\nu}'\gamma_\alpha\left(1+\gamma_5\right)\mu\right]^+$$

+ Hermitian conjugate,

where ν' is written for the neutrino associated with the muon, ν for that associated with the electron. The coupling constant has the value

$$G_\mu M_p^2 \approx 10^{-5} .$$

We infer the existence of

$$\bar{\nu} + e^- \rightarrow \mu^- + \bar{\nu}' \qquad (1)$$

and

$$\nu' + e^- \rightarrow \mu^- + \nu \quad . \qquad (2)$$

For the conjectured neutrino experiments one has only ν', $\bar{\nu}'$ from pion decay, so that Eq. (1) will hold only for $\nu = \nu'$.

The cross sections in the c.m. system are, for $p >> m_\mu$,

$$\sigma^{\nu' e^- \rightarrow \nu\mu^-} = 3\sigma^{\bar{\nu} e^- \rightarrow \bar{\nu}'\mu^-} \approx \frac{4}{\pi} G_\mu^2 p^2$$

$$= 0.6 \times 10^{-37} \left(p/M_p\right)^2 \mathrm{cm}^2 \quad ,$$

which must break down at sufficiently high energies; e.g., the wave mechanical limit, $\sigma \approx \pi/p^2$, is reached when

$$p \approx M/\sqrt{G_\mu M^2} = 300 \text{ Gev} -$$

an interesting figure, but one that corresponds to the lab energy

$$E_\nu = 3.6 \times 10^8 \text{ Gev.}$$

Even the threshold for $\nu e \rightarrow \nu\mu$ is 11 Gev (lab), whereas, for the proposed 300-Gev machine, the peak neutrino energy would be 5 Gev.

The simplest way to damp the cross section at high energies is to introduce a spin-1 boson $[W^\pm, W^0 (?)]$ with $M_W > M_K$. Small differences arise in the formulae for muon decay but they are consistent with experiment. The cross sections then have the form

$$\sigma^{\nu e \rightarrow \nu\mu} = \frac{G_\mu^2 M_W^2}{\pi} \cdot \frac{4p^2}{M_W^2 + 4p^2}$$

and

$$\sigma^{\bar{\nu} e \rightarrow \mu\bar{\nu}} = \frac{4G_\mu^2}{3\pi} \cdot \frac{M_W^4 p^2}{\left(M_W^2 - 4p^2\right)^2 + M_W^2\Gamma^2} ,$$

where Γ = rate of W decay, and the lifetime of W would be less than 10^{-17} sec. These expressions deviate from those derived from a point interaction for $p \approx M_W/2 > 250$ Mev, which corresponds to $E_\nu > 250$ Gev (lab).

Concerning elastic collisions, do the reactions

$$\nu + e^- \rightarrow \nu + e^-$$

and

$$\bar{\nu} + e^- \rightarrow \bar{\nu} + e^-$$

occur in first or second order in G ? If in first order, the cross sections are the same as before (neglecting particle masses), but, of course, no thresholds are involved. For $E_\nu = 5$ Gev, the magnitude is $\sigma \approx 10^{-40}\ \mathrm{cm}^2$.

An interesting way of possibly doing leptonic weak-interaction experiments has been suggested by Chou Kuang-chao. He suggests that they be done via the Coulomb field of a nucleus; e.g., $\nu + Z \rightarrow Z + \nu + e^+ + e^-$. The cross section for this process is

$$\sigma_\nu = \frac{G^2}{3\pi^3}\left(Ze^2\right)^2 \times E_\nu^2 \ln\frac{E_\nu}{m_e} \quad .$$

For $Z = 80$,

$$\sigma_\nu \approx 7 \times 10^{-40}\left(E_\nu/M\right)^2\ \mathrm{cm}^2 \ .$$

Strongly Interacting Particles

By analogy with leptons, the β-decay interaction is taken to be

$$L_{int} = \frac{G}{\sqrt{2}}\left(V_\alpha + P_\alpha\right)\left[\bar{\nu}\gamma_\alpha\left(1+\gamma_5\right) e + \bar{\nu}'\gamma_\alpha\left(1+\gamma_5\right)\mu\right]^+$$

$$+ \text{ Hermitian conjugate} \ ,$$

where V_α is the vector weak current of strongly interacting particles ($\Delta S = 0$) , and P_α the axial vector weak current. In the limit of zero momentum transfer,

$$G\left\langle p \middle| V_\alpha \middle| n\right\rangle \rightarrow G_V \bar{u}_f \gamma_\alpha \tau_+ u_i \ ,$$

and

$$G\left\langle p \middle| P_\alpha \middle| n\right\rangle \rightarrow -G_A \bar{u}_f \gamma_\alpha \gamma_5 \tau_+ u_i \ ,$$

where G_V and G_A are the Fermi and Gamow-Teller coupling constants of nuclear theory.

The setting of $G_V = G_\mu$ represents the assumption of the conserved vector current theory. In this case, V_α represents only the isotopic spin current, which is conserved in strong interactions. For finite momentum transfer,

$$G\left\langle p \middle| V_\alpha \middle| n\right\rangle = iG_V \bar{u}_f \gamma_\alpha \tau_+ u_i F_1^V(q^2)$$

$$- \frac{iG_V}{2M}\mu^V q_\nu \bar{u}_f \sigma_{\mu\nu} \tau_+ u_i F_2^V(q^2) \ ,$$

where $\mu^V = \mu_p - \mu_n = 3.69$, the difference between the anomalous nucleon magnetic moments, and where F_1^V and F_2^V are the electromagnetic form factors,

$$F_1^V \text{ and } F_2^V \approx \frac{1}{1+q^2/22.4\ m_\pi^2} \ ,$$

and $22.4\ m_\pi^2$ is the square of the energy of the $I = 1$, $J = 1$ $\pi - \pi$ resonance.

A low-energy nuclear physics experiment at CalTech by Barnes et al. produced findings consistent with $\mu^V = 3.69$ and not with $\mu^V = 0$. Lee suggests that $\sigma(\nu + N) - \sigma(\bar{\nu} + N)$ is critically dependent upon μ^V and would be noticeable at $E_\nu = 500$ Mev.

Concerning the axial vector P_α , Feynman, Gell-Mann, and Levy suggest the relations

$$\frac{-G_A}{G} = 1.25 \ ,$$

and

$$\partial_\alpha P_\alpha = \frac{ia}{\sqrt{2}}\Psi_{\pi^-} \ ,$$

where a is a constant. The correct rate of pion decay is obtained for

$$a = \frac{-2M}{g_1} m_\pi^2 \left(\frac{-G_A}{G}\right),$$

where g_1 is the pion-nucleon coupling constant. Now

$$G \left\langle p \left| P_\alpha \right| n \right\rangle = (-G_A)\Big[\bar{u}_f \tau_+ \gamma_\alpha \gamma_5 u_i \alpha(q^2) + iq_\alpha \bar{u}_f \tau_+ \gamma_5 u_i \beta(q^2)\Big],$$

where $\beta(q^2)$ is the induced pseudoscalar term of Goldberger and Treiman;

$$\beta(q^2) = \frac{ag_1}{m_\pi^2} \cdot \frac{1}{q^2 + m_\pi^2} + \cdots .$$

If $\alpha(q^2)$ has the same sort of dependence on q^2 as F_1^V and F_2^V, one should find a strong interaction (resonance) in the three-pion state for $I = 1$, $J = 1^+$; then,

$$\alpha\ (q^2) \approx \frac{1}{1 + q^2/M_R^2},$$

where M_R is the energy of the resonance.

The form factors F_1^V, F_2^V, α, β could be measured, in principle, by elastic neutrino-nucleon scattering as in

$$\nu + n \to p + e^- \quad \text{and}$$

$$\bar{\nu} + p \to n + e^+ ,$$

for which $\sigma \approx 10^{-38}$ cm^2 at high energies.

Intermediate Boson

A low-mass intermediate boson $W^\pm$ would enormously increase the cross section for neutrino scattering off nuclei. At high energies, the scattering is coherent, giving $\sigma \approx G^2\alpha^2Z^2$. For Fe, if $M_W = 500$ Mev, σ would reach 10^{-35} cm^2 for $E_\nu \approx 2$ to 3 Gev; there would also exist the incoherent reactions $\nu + Z \to W^+ + e^- + Z$ and $\nu + Z \to W^+ + e^- +$ star, for which $\sigma \approx G^2\alpha^2Z^2$. For the reaction $\pi^+ + p \to W^+ + p$,

$$\sigma \approx 10^{-32} \left\{ \left[F_1^V\left(-M_W^2\right)\right]^2 + \left[\alpha\left(-M_W^2\right)\right]^2 \right\} \text{cm}^2 .$$

If $M_W \approx \pi - \pi$ resonance energy, then

$$\left[F_1^V\left(-M_W^2\right)\right]^2 \approx 35 .$$

Similarly, if α is strongly peaked at M_R, $M_W \approx M_R$ would produce a large increase in cross section. However, pair production with high-energy photons remains the best way of producing W.

The characteristic decay modes of W would be

$$W^+ \to e^+ + \nu ,$$

$$\to \mu^+ + \nu , \text{ and}$$

$$\to \pi^+ + \pi^0 \text{ (lifetime} < 10^{-17} \text{ sec).}$$

Strange Particles

What we surmise about strange-particle decays can be summarized by

$$|\Delta S| = 0,\ 1 ; \quad |\Delta I| = \frac{1}{2}; \quad \Delta Q = \Delta S .$$

In neutrino-nucleon interactions, these rules can be tested by

$$\nu + n \to \Sigma^+ + e^- \quad \text{(No)} ,$$

$$\bar{\nu} + n \to \Sigma^- + e^+ \quad \text{(Yes)} ,$$

$$\to \Xi^- + e^+ \quad \text{(No)} ,$$

$$\bar{\nu} + p \to \Lambda^0 + e^+ \quad \text{(Yes)} ,$$

$$\to \Sigma^0 + e^+ \quad \text{(Yes)} ,$$

and

$$\to \Xi^0 + e^+ \quad \text{(No)} .$$

From the energy spectrum of the produced lepton, one could deduce the mass of the particle produced with it. In particular, if $\nu + n \rightarrow \Sigma^+ + e^-$ occurs, then the $\Delta S = \Delta Q, |\Delta I| = 1/2$ theories will have to be abandoned.

Experiments in progress at Padua, Wisconsin, and Berkeley already indicate that these theories are wrong. Starting with a beam of K^0, the ratio of (π^-, e^+) to (π^+, e^-) decays was plotted for various time intervals. By the above rules,

$$K^0 \rightarrow \pi^- + e^+ + \nu ,$$

but not

$$\rightarrow \pi^+ + e^- + \bar{\nu} .$$

However, $\bar{K}^0$ should decay to $\pi^+ + e^- + \bar{\nu}$, and not to $\pi^- + e^+ + \nu$. Since the rate of natural $\bar{K}^0$ production from K^0 can be found as a function of time by observing the process $\bar{K}^0 + p \rightarrow \Lambda^0 + \pi^+$, definite predictions are made by the above theory concerning the ratio

$$r = \frac{R(\pi^+, e^-)}{R(\pi^-, e^+)}$$

as a function of time; i. e., $r = 0$ at $t = 0$, etc. Instead, r seems to equal unity for all time intervals considered (about 18 events at present).

Total Cross Sections

Although it is clear that, for any particular neutrino-nucleon process, the cross sections are limited by the form factors for increasing energy, it is not clear what happens to the total cross sections. Clearly, the number of channels increases rapidly with energy, and once phase-space limitations are overcome, the processes are comparable in cross section. Thus, even with the present theories, the total cross section may still increase as a function of energy.

8. SECONDARY-BEAM INTENSITIES FROM A 300 Gev SYNCHROTRON

Harold K. Ticho

July 6, 1961

[The main content of this lecture, together with the figures, is contained in Technical Report No. 1, "Flux Estimates for a 300-Gev Proton Accelerator," by Harold Ticho, June 1961, University of California, Department of Physics, Los Angeles 24. Presented below is the discussion that followed the lecture.]

In reply to a question from the audience, Fretter and Perkins stated that only about 20% of the high-energy events observed in cosmic radiation display angular distributions that are clearly described in terms of the two-fireball model. Although transverse momentum is always definitely limited, the longitudinal momentum is smeared out in such a way that a fixed value of the fireball Lorentz factor Γ cannot apply to all collisions. Cocconi said that one must allow Γ to vary from near unity to large values in order to account for the Boltzmann-like distribution in the longitudinal momentum. Ticho agreed that the few events with large Γ are very important for estimates of the high-energy tails of the laboratory-system spectra of secondary particles; however, he used average Γ values, since he did not know of any experimental information regarding the Γ distribution function near 300 Gev.

9. PART I. SOME CONSIDERATIONS OF EXPERIMENTAL FACILITIES FOR A 300-Gev ACCELERATOR.

Leroy T. Kerth

July 7, 1961

It may seem premature to consider experimental facilities for a 300-Gev machine before one is even sure whether or not such a machine will be built. Certainly, so far as experimental physics is concerned, many things will change drastically in the next ten years. It is important, however, that we consider what form experiments may take and what experimental equipment may be used for the 300-Gev machine, even so early in the design stage as this. All high-energy physicists who have worked with existing machines can point to mistakes in design of the machine that make their life difficult. By careful planning of the experimental areas throughout the entire design process, rather than waiting until the machine is almost complete and then considering the experimental equipment and areas as an afterthought, we should be able to make a far more useful machine for experimental physics. This report lays a few important ground rules with respect to carrying on experiments with a high-energy accelerator, and points to some of the problems that should be solved during the designing of the machine.

Experimental Areas and Secondary-Particle Beams

One of the most important factors to be considered in design of a machine concerns the related experimental area and the efficiency with which experimental setups can be made. Even with present high-energy accelerators a great deal of machine time is lost in setting up an experiment. High-energy physics experiments have become enormously complicated, requiring from days to several weeks for the experimental setup alone. Much of this setup time requires the accelerator to be shut down. This is a clear loss of accelerator operating time. Every effort must be made to make this loss in experimental time as short as possible.

One very obvious solution is for the machine to provide simultaneously for a number of experimental setups. These experiments may then operate on a beam-sharing, a target-sharing, or an alternate-time basis, thereby utilizing the machine more efficiently. Having a number of experimental setups operable at one time allows for one or more experiments to run while yet another experiment is being put in place and debugged.

Another major problem in carrying on high-energy experiments at present accelerators is the difficulty with which particles produced at 0° may be brought from a target in the machine and captured in a secondary-beam focusing system. With today's weak-focusing machines, some secondary-particle beams can be drawn into the beam-transport system rather easily, by using the field of the accelerator itself. However, it is impossible to use a positive secondary beam except by working inward from the accelerator ring, usually an undesirable feature owing to space limitation and rather high background in this area. With the strong-focusing machines of today, the problem is even more severe, owing to the rather short straight sections available in the machine and the bad focusing fields that exist when a particle traverses the fringing fields of the machine magnet. Recently, Tom Collins demonstrated that it is possible to have straight sections much longer than the usual ones, by using quadrupole magnets at each end to match the focusing properties of the rest of the machine. In the proposed 300-Gev machine under study, it will be possible to have a straight section with a clear space of approximately 90 feet between quadrupole

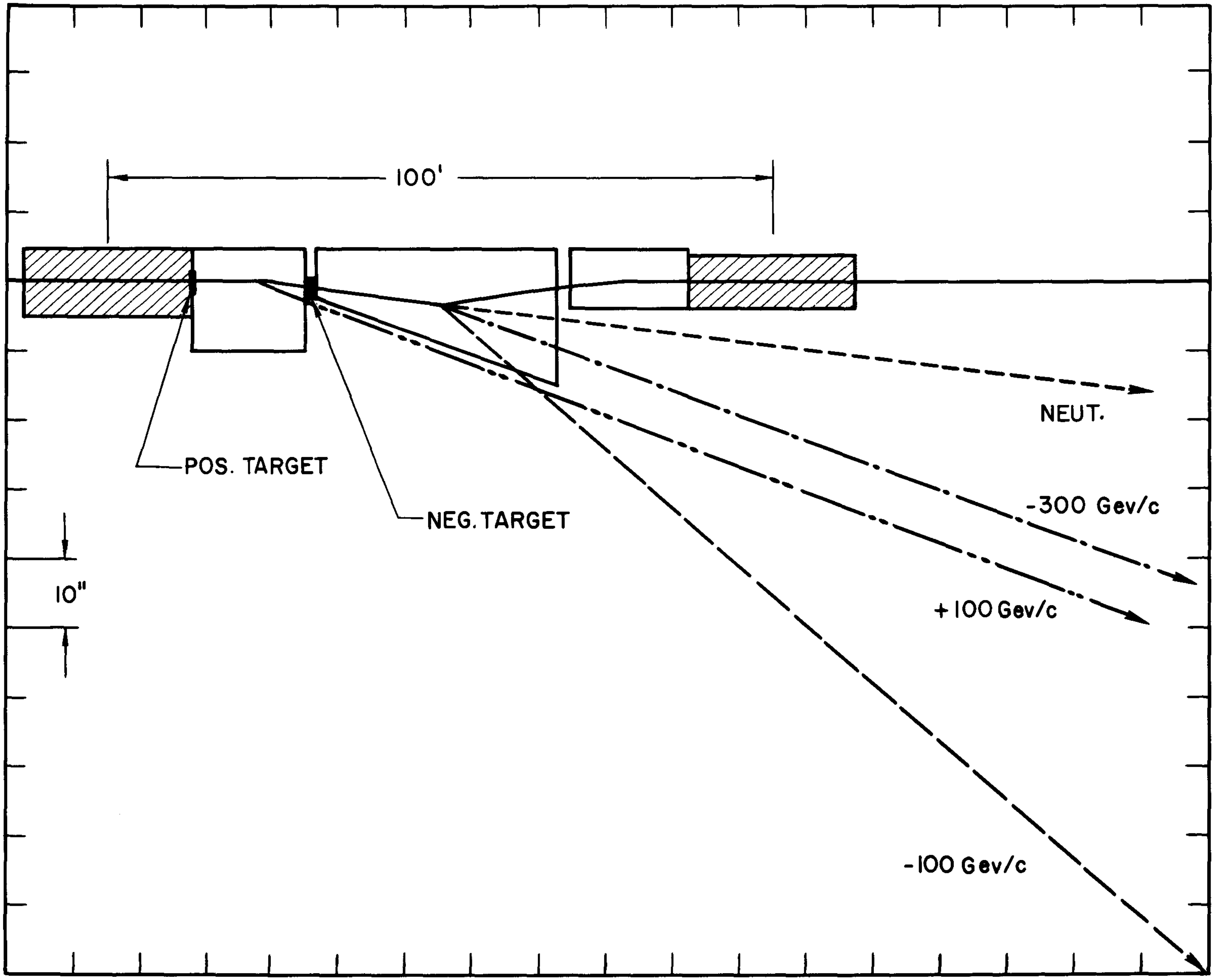

Fig. S9-1.

magnets. The upstream quadrupole in this long straight section would allow one to deflect secondary particles from a target and have them miss the machine at the downstream end. An improvement can be made over this by placing an achromatic set of three magnets in the long straight section (see Fig. S9-1). Such magnets will not affect the operation of the machine at all. As can be seen from Fig. S9-1, however, even neutral particles produced at 0° to the target can be easily extracted from the machine. Negative particles up to 300 Gev/c will clear the machine, and positive particles up to about 100 Gev/c will also be available. The magnets that have been considered for use in this achromatic set are standard nonsuperconducting magnets, using a 20,000-gauss field and filling the complete space between the two quadrupoles. Another advantage of this achromatic set is that fields of these magnets can be under control of the experimenter. He can set the field at any desired value without disturbing the operation of the machine, provided that the magnets are not turned on until after injection or until a high enough energy has been reached so that the first magnet in the achromatic set does not deflect the beam completely out of the machine. This means that it is possible for the experimenter to use the field in these magnets as well as the magnets in his beam-transport system as parameters that may be adjusted to produce his secondary beam. Figure S9-2 shows a portion of a 300-Gev machine and straight section. Several secondary beams produced at 0° to the target and emerging from the long straight section are shown. The experiment shown on Fig. S9-2 is described in a later report (Seminar 23).

External Beams

An external proton beam extracted from the machine gives an experimental facility that will allow a great number of experiments to be set up at one time, and, in addition, will give a number of places (for example, the backstop where the beam is stopped) in which parasitic experiments can be carried out for the testing of equipment. In addition, the nature of the experiments set up along the external beam is such that probably more setup work could be done while the beam is still in operation, thus greatly increasing the efficiency in preparing experiments. A problem appears with the external beam of AGS-type machines. As yet, the only extraction system that appears feasible is the so-called one-turn extraction system. For the 300-Gev machine under consideration here, this would give a 26-μsec beam every 3 seconds; this is a duty cycle of 8×10^{-6}. For all but bubble-chamber-type experiments, this would be a very severe limitation on the use of the external beam. Considerable thought should be given the problem of extracting the beam from the machine with a better duty cycle.

Variable-Energy Variable-Repetition-Rate Machine

There is one final machine facility that seems important to consider at this point. It is conceivable that some of the experimental physics done with a 300-Gev machine would be carried out at energies less than the full energy of the machine. With a machine using a linear accelerator for the injector, and a nominal period of 3 sec for full energy, it is possible to operate at a reduced energy and higher repetition rate, since the injector would be capable of injecting more current than is required by the once-every-3-sec cycle. If, for example, the 300-Gev machine should be operated at 60 Gev, then an increase by at least a factor of 5 in pulse rate could be realized. This is a direct increase by a factor of 5 in beam intensity or protons accelerated per second. This seems to be a very useful feature of the machine and should be considered in its design. Such a feature combines, to some extent, a moderate-energy high-intensity machine with the high-energy machine.

Before more detailed plans can be made for experimental areas, we believe it is important to consider the exact form that experiments might take. In this vein, we considered one experiment specifically, and this will be described in a later paper.

Considerable thought should now be given by experimental physicists to experiments that might be carried out with such a machine, before concrete and final proposals for experimental areas and facilities are made. One thing is clear: a great deal of space should be allowed for the experimental areas. For example, several experiments already considered for the machine use

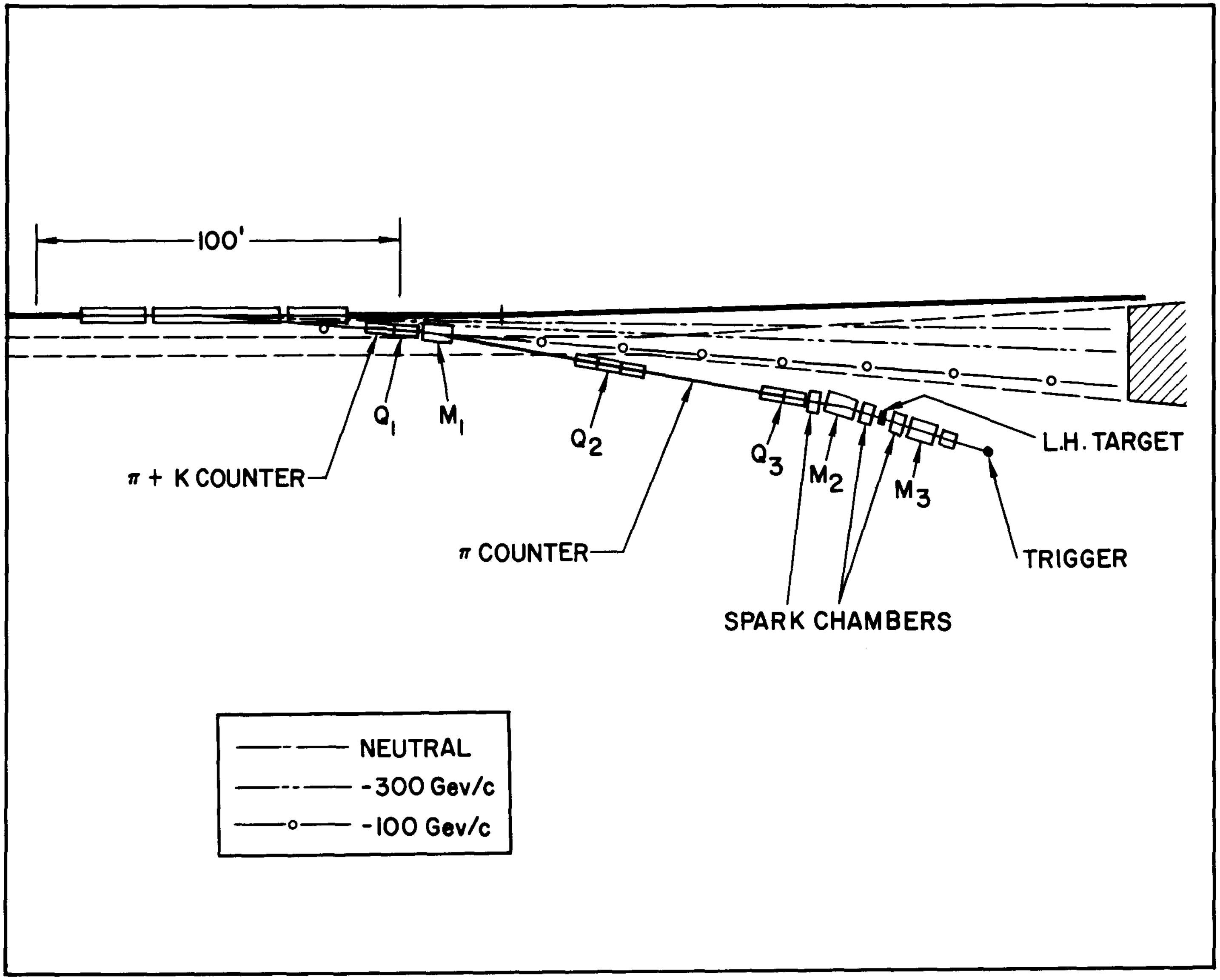
100'
Q_1
M_1
Q_2
Q_3
M_2
M_3
L.H. TARGET
π + K COUNTER
π COUNTER
TRIGGER
SPARK CHAMBERS
NEUTRAL
-300 Gev/c
-100 Gev/c

Fig. S9-2.

Cerenkov counters as much as 100 feet long. In addition, the estimate of fluxes of secondary particles from the target of such a machine leads one to believe that even the secondary beams from such a machine will constitute a rather severe radiation hazard and will probably have to be backstopped in much the same way as the external beams from present machines. Thus, a very large amount of heavy shielding will be used in the experimental areas. The foundation for the experimental area may turn out to be just as difficult a problem as the machine itself! These problems will all be answered with more study.

9. PART II. SEPARATION OF PARTICLE BEAMS AT HIGH ENERGIES.

Denis Keefe

July 7, 1961

Introduction

This report is not intended to be a survey of all possible methods of selecting particles of different masses, but rather a presentation of some relevant numbers, mainly on Cerenkov counters. Some of us have considered a number of specific experiments that will certainly be done with a high-energy accelerator, in order that we may estimate the required dimensions of the beam-transport equipment and particle-detection systems. A typical series of experiments that we considered, on the assumption that mass separation would be available, was

a. total cross sections for $\pi^{\pm}$, $K^{\pm}$, p, and $\bar{p}$,

b. elastic diffraction scattering (up to about 6 mr at 100 Gev),

c. elastic large-angle scattering,

d. inelastic interactions, multiplicities.

Many difficulties present at low energies become less important at high energies, because the interesting region of solid angle in the lab system is strongly forward-peaked. For studying jets, the constant transverse-momentum effect leads to a quite rapid gain in this respect. Thus, the limitations set by small magnet apertures on conventional lower-energy scattering experiments become less severe at high energies.

Table S9-I shows the momenta, γ and $\Delta\beta$, where $\Delta\beta = 1 - \beta$, for π mesons, K mesons, and p (or $\bar{p}$) in the region of projected energies.

Methods of separation hitherto used or examined on paper may be listed as follows.

Table S9-I.

Values of γ and $1-\beta$ for various momenta

Momentum (Gev/c)	π		K		p	
	γ	$\Delta\beta$	γ	$\Delta\beta$	γ	$\Delta\beta$
50	360	38×10^{-7}	101	49×10^{-6}	53	48×10^{-5}
100	720	9.6×10^{-7}	202	12×10^{-6}	106	4.4×10^{-5}
150	1075	4.3×10^{-7}	304	5.5×10^{-6}	160	2.0×10^{-5}
200	1430	2.4×10^{-7}	405	3.0×10^{-6}	213	1.1×10^{-5}
250	1800	1.5×10^{-7}	506	2.0×10^{-6}	266	0.7×10^{-5}

Spatial Separation

Radio-frequency and electrostatic separators

Requirements for precision in the beam optics become increasingly stringent as the energy increases. Separators have not yet been used beyond 2 Gev/c, and many of us feel that a practical limit may be reached at about 10 Gev/c.

Interaction separation

For special beams — e.g., enriched antineutron beams — the Goldhabers and Peters have proposed a scheme of interaction separation (discussed later in this series) which utilizes the forward peaking of inelastic charge exchanges. Clearly, other schemes based on the same principle are possible; e.g., for low fluxes π^+ and p can be separated because they have different total cross sections. Beams of muons and neutrinos are an extreme example of interaction separation.

Degradation separation

The Goldhabers have also studied the possibility of using the mass dependence of dp/dx in a constant-momentum beam to induce a small difference in momentum. This scheme is well known at low momentum where the ionization curve is steep. At high energies the relativistic rise has to be utilized; the main sources of difficulty are the Fermi density effect, the Landau fluctuations, and the rather large mass of degrader. The Goldhabers have shown that enrichment is probably attainable by using cesium at CERN energies, but extension to much higher energies looks doubtful.

Triggered deflection

This scheme (Brody) depends on electronic identification of the particle, whereupon a deflector (O'Neill and Korenman) is triggered to deflect the required particle several milliradians out of the main course of the beam into the chosen detector. The main requirement is a bending magnet to turn the secondary beam back through 180° at the end of a flight path of approximately 200 feet. The long return path is needed to allow time for the ferrite magnet to be pulsed.

All the above methods of separation end up essentially with low flux, approximately 10 to 100 particles per pulse, primarily suited to bubble chambers.

Time Separation

Time of flight

Below 2 Gev/c, time of flight over lengths of 30 or 40 feet is a useful method of enrichment. A glance at Table S9-I shows, however, that even if resolving times were 10 times as short as today's, let us say 0.1 nsec, the flight path needed to separate protons and pions at even 50 Gev/c would be approximately 1000 feet. Thus, time of flight is almost certainly out of the question.

Gas Cerenkov counters

This technique becomes simpler in many respects at higher energies, largely because of the small angles and low pressures involved. This is discussed in detail later.

Relativistic rise

The calculations by Budini and by Sternheimer on differential energy loss show that in the region 10 to 300 Gev/c for a chosen momentum there is a difference of 6 to 7% between protons and K's, and a difference of 9 to 10% between K's and π's in noble gases at about atmospheric pressure. In solids and liquids the density effect limits the highest momentum at which separation is possible, so that gaseous scintillators would probably be needed. The relativistic rise has been observed for grain density in emulsions, bubble density in bubble chambers, and droplet density in cloud chambers, and it is plausible to assume that it is present in scintillation light. However, since any of these ionization parameters samples only certain aspects of the total energy loss, some aspects could be more useful than others. For example, droplet formation in a cloud chamber depends largely on ionization, whereas scintillation in xenon appears to depend largely on atomic excitation. A preliminary measurement by Yuan at Brookhaven has shown that the scintillation light from xenon has a fast component (approx 10^{-8} sec) and that the relativistic rise is observable. The Landau fluctuations again are troublesome in making measurements of ionization to a few per- cent, and it seems likely that several small counters, possibly ten 1-gram NTP counters, could be used with suitable electronic logic to sample the energy loss of a particle and decide on its probable identity. From what follows on Cerenkov counters, it will appear that the most useful feature of gas scintillation counters will be in selecting out π mesons which would otherwise require very long gas Cerenkov counters. In contrast with Cerenkov counters, note that with scintillation counters the difference in effect be- tween π's and K's is greater than that between K's and p's .

Synchrotron radiation

Lawrence Jones has calculated the number of quanta emitted when a secondary beam passes through a reasonably sized magnet. He found the light output too small to be useful, although not more than one order of magnitude away from usefulness.

Gas Cerenkov Counters

Threshold Counters

The half angle Θ of the Cerenkov cone is given by

$$\cos \Theta = \frac{1}{n\beta} ,$$

where n = refractive index of gas. At high ener- gies, where $n \approx 1$, $\beta \approx 1$, and $\cos\Theta \approx 1$, if one writes

$$\cos \Theta = 1 - \Delta C,$$

$$\beta = 1 - \Delta\beta \text{ (as before)},$$

one then has $$n = 1 + \Delta n .$$

Then the Cerenkov relation is $\Delta n = \Delta C + \Delta\beta$,

where $$\Delta\beta = \frac{1}{2\gamma^2} ,$$

and $$\Delta C = 1/2\ \Theta^2 .$$

For a perfect gas Δn is proportional to pressure, i.e., $\Delta n = \eta p$. For p in atmospheres, η for some useful gases is as follows:

	η
hydrogen	1.4×10^{-4}
methane	4.4×10^{-4}
ethylene	7.3×10^{-4}
nitrogen	3.0×10^{-4}

These gases are arranged in descending order of refractivity per g/cm^2 . Thus, for a given refractive index, H_2 requires the introduction of the least number of g/cm^2 into the beam, methane requires twice as many as H_2 , ethylene three times as many, and nitrogen six times as many.

The threshold pressure at which a particle begins to give Cerenkov light is given by

$$\Delta C = 0 , \quad \text{or} \quad p_t = \frac{\Delta\beta}{\eta} = \frac{1}{2\gamma^2\eta} .$$

From this formula emerges one feature of mass separation by use of gas Cerenkov counters which remains the same at all high energies. In a beam of defined momentum $p = m_1\gamma_1 = m_2\gamma_2$, the threshold pressures for two different mass com- ponents are related by

$$\frac{(p_t)_1}{(p_t)_2} = \frac{2\gamma_2^2\eta}{2\gamma_1^2\eta} = \frac{m_2^2\gamma_2^2}{m_1^2\gamma_1^2} \cdot \frac{m_1^2}{m_2^2} = \frac{m_1^2}{m_2^2} ,$$

so that the threshold pressures remain in the ratio of the squares of the masses. Thus, there arise no special problems that require careful pressure control.

Light output

The number of photons emitted per cm into the wavelength interval $\lambda_2 - \lambda_1$ is given by

$$\frac{dN}{d\ell} = 2\pi\alpha\left(\frac{1}{\lambda_2} - \frac{1}{\lambda_1}\right) \sin^2 \Theta .$$

For an S-11 photocathode, we use the values

$$\frac{dN}{d\ell} = 500 \sin^2 \Theta$$

$$= 1000\ \eta p \text{ photons/cm.}$$

These are believed to be pessimistic estimates, and the use of quartz optics everywhere will increase the useful number of photons.

Selection of π Mesons Only

For convenience, consider the gas used to be methane. (To obtain values for the other gases mentioned, one need only scale the pressure in accordance with the figures in the listing of η values above.) The simplest form of threshold detector (Fig. S9-3) is a long cylindrical pipe coated internally with a reflector, with a 45° mirror at the downstream end to deflect the light out through a side lens onto a photomultiplier tube.

The pressure is set just below the threshold for counting K mesons, and Table S9-II summarizes the important relevant numbers. The required number of photons is arbitrarily and conservatively taken to be 50, giving about 10 photelectrons at the photocathode. In practice, it may be better to use more than one mirror and photomultiplier tube and to sum the output signals.

The required pressures are quite small, and using such a counter in the whole beam channel is not too different from using a vacuum pipe or helium bag. Note that to obtain a given light output the required length is roughly proportional to p^2. This is not necessarily as disadvantageous as it may seem, since, for given magnet limitations, the length of a beam channel also will be roughly proportional to p^2.

Selection of π's and K's

If the pressure is set just below the threshold for counting p or $\bar{p}$, the pertinent data are as shown in Table S9-III.

Note that the lengths are much shorter than those in Table S9-II. Note also that, since $\Theta\pi$

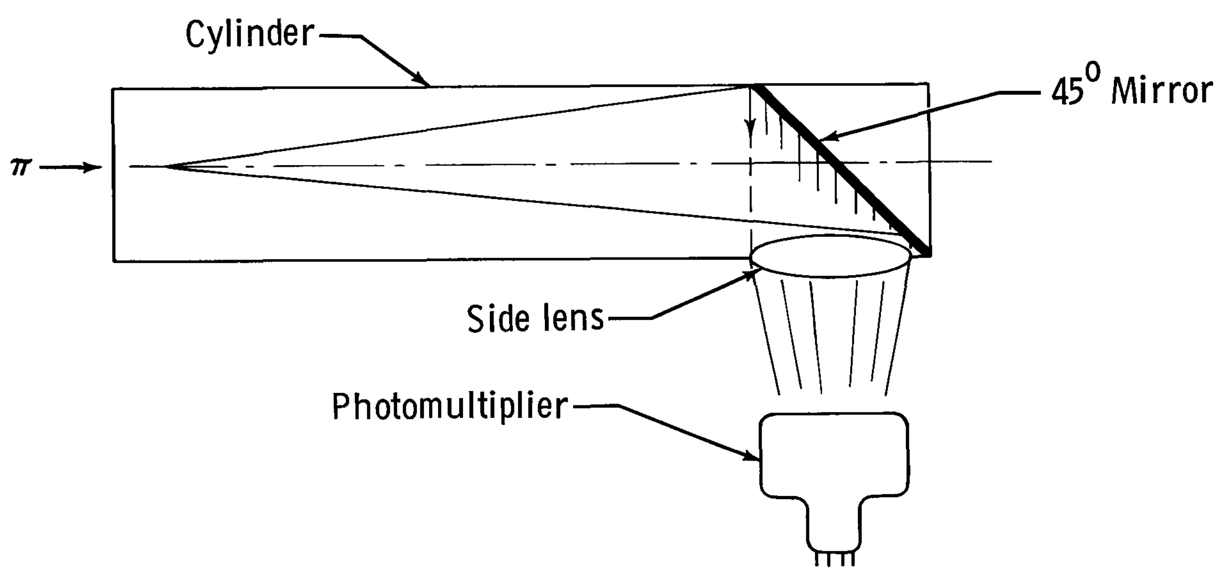

Fig. S9-3. π -meson threshold counter.

Table S9-II.

Parameters for selection of π mesons (counting π's only) in threshold counter; $p = (p_t)_K$.

Momentum (Gev/c)	Θ (mr)	$h\nu/m$	Length for 50 $h\nu$ (ft)	Pressure (cm Hg)
50	9.4	4.40	36	8.4
100	4.5	1.00	160	2.1
150	3.1	0.47	340	1.0
200	2.3	0.26	620	0.5
250	1.9	0.18	900	0.3

and Θ_K are not very different, the pulse heights from both types of particle will be similar.

To select π beams, one π counter should be adequate; to select K beams, two π anti-counters (i. e., pion counters in anticoincidence) and one $\pi + K$ counter would probably be needed; while for $\bar{p}$ beams, two $\pi + K$ anti-counters would suffice. In selecting K^+ mesons in the presence of large numbers of protons, knock-on electrons from protons in the $\pi + K$ counter can be removed with a few sweeping magnets — however, the cross section for production of δ rays above threshold diminishes

Table S9-III.

Parameters for selecting π and K mesons in threshold counter; $p = (p_t)_p$.

Momentum (Gev/c)	Θ_π (mr)	Θ_K (mr)	Length for 50 $h\nu$ from K meson (ft)	Pressure (cm Hg)
50	19.0	16.0	13	31.0
100	9.4	8.0	52	7.5
150	6.3	5.2	120	3.4
200	4.7	4.0	210	1.9
250	3.6	3.1	340	1.2

with increasing energy, and this problem is not likely to be serious at very high energies. The most inconvenient beams, with respect to length, are clearly K beams, which require very long π anticounters. It is hoped that at least one π anticounter might be replaced by gas scintillation counters. One possibility at high energies, which arises partly from the convenient pressure ranges and partly from the small angles involved in many of the interactions, is to place a gas Cerenkov counter downstream from the hydrogen target and detectors so as to complete identification after the particle has interacted. For example, in elastic K-p scattering the diffraction peak should lie within 6 mr at 100 Gev/c, so that one π anticounter about 2 feet in diameter could be placed behind the scattering detector and still have a large enough aperture to record the particles of interest.

Differential Cerenkov Counters

The distinctive feature of this type of counter (Fig. S9-4) is that radiation occurs from more than one mass component and the appropriate cone of light is selected on the basis of its angle. The usual procedure is to pass the Cerenkov light through a spherical lens to produce ring images in the focal plane. The angular radius of the focal ring is the same as the angle of Cerenkov light. An annular slit in the focal plane selects the desired ring. The velocity resolution is usually described by

$$\frac{\delta\beta}{\beta} = \tan\Theta \cdot \delta\Theta ,$$

where $\delta\Theta$ is the minimum angle between cones that can be clearly resolved.

Several gas Cerenkov counters have been made quite successfully with $\delta\beta/\beta \approx 10^{-3}$, and the best hitherto constructed (Kycia and Jenkins) can select K mesons or antiprotons at 20 Gev/c and reject the unwanted particles successfully. In this counter $\Theta = 4.5°$ and $\delta\beta/\beta \approx 2 \times 10^{-4}$. Since $\delta\beta/\beta = \tan\Theta \cdot \delta\Theta \propto \Theta$, the resolution can be improved by using smaller angles (optimum resolution is at $\Theta = 0$, threshold), but at the expense of a much longer device to achieve the same light output. On examining the usual limiting factors — beam divergence, multiple scattering, momentum spread, optical dispersion — it seems feasible to build such a counter, with $\Theta \approx 0.5°$ or 1° and about 30 feet long, to operate up to 50 to 60 Gev. The great advantage to the differential Cerenkov counter is the saving in required length by eliminating a separate threshold counter to reject pions.

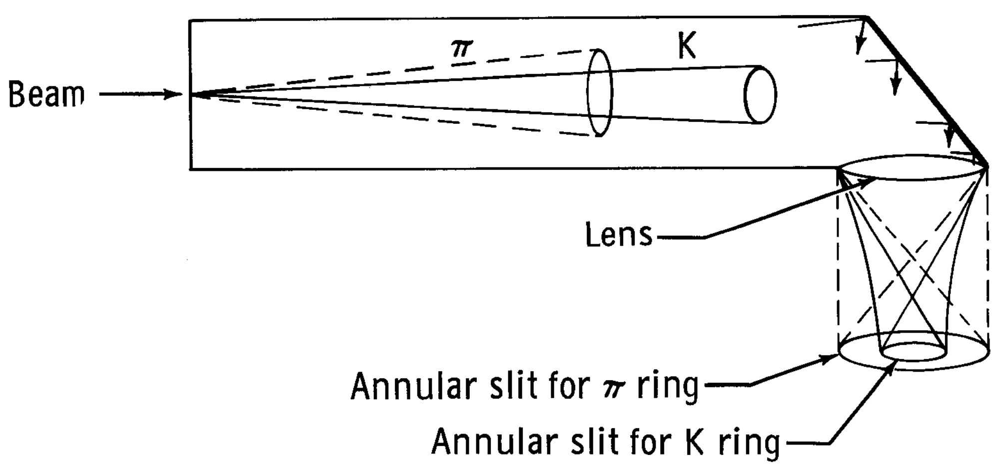

Fig. S9-4. Differential Cerenkov counter.

10 and 11. RESULTS FROM COSMIC-RAY EXPERIMENTS

Donald H. Perkins

July 10 and 11, 1961

Introduction

The integral energy spectrum of primary cosmic-ray nucleons above energies of 1 Gev can be approximated by the power law $N(>E) = k\,E^{-\gamma}$. The index γ is approximately 1.5 for $E < 100$ Gev, and appears to increase slowly at high energies, reaching a value $\gamma \approx 3.0$ at $E = 10^8$ Gev. With E in Gev, and $k \approx 1$, the formula gives the flux of particles per cm^2 per sr per sec. An impression of the low flux at high energies can be gained from the fact that, to obtain 1 μamp of cosmic-ray beam above 1000 Gev, one needs to integrate over the entire surface of the earth (and even then one has a completely unfocused beam with no momentum resolution). One can therefore understand that the character and quality of experiments carried out with cosmic rays on the one hand, and with accelerators on the other, are in no way comparable. In cosmic-ray experiments, one can hope, at best, to measure the major features of the interactions, never the detailed characteristics.

The final results of such a qualitative analysis of the cosmic-ray data are that the parameters measured either remain remarkably constant or vary only slowly and smoothly with variations in energy. So, the cosmic-ray data can be of considerable help in extrapolating secondary-particle spectra, etc., from the 25-Gev region up to 300 or 1000 Gev.

Elastic Cross Sections

Elastic cross sections were not measured in these experiments.

"Total" Inelastic Cross Sections

Reliable cosmic-ray measurements of collision cross sections resulting in appreciable energy loss ($\gtrsim 10\%$) have been made on medium-weight and heavy nuclei only. The results are shown in Fig. S10/11-1. The observed cross section has been expressed in terms of σ_0; the "geometric" cross section has been calculated for an opaque nucleus of radius $1.28\,A^{1/3}$ fermis. This value of σ_0 was chosen to give agreement with low-energy results from accelerators. Non-uniform-density models with partial transparency give values of σ not significantly different from the ones shown.

The cosmic-ray data are from:

a. The rate of penetrating showers observed with counters and absorbers.[1,2] Primaries are nucleons between 20 and 200 Gev.

b. The scanning of jet tracks of secondaries in emulsion stacks to determine the interaction mean free path. The particles are mostly pions; energies range from 50 to 500 Gev.[3]

c. The maximum-likelihood analysis concerning positions of interactions of primary particles (predominantly nucleons) in ionization calorimeters or "sandwich" stacks of heavy elements and emulsions.[4,5]

Conclusions

Over the energy range 5 to 20,000 Gev, σ appears to be constant. The results are consistent with an elementary particle-nucleon cross section which is constant at all energies above 100 Gev and for all strongly interacting particles (π, p, K, etc.).

There appears to be no probability of a decrease in collision cross section at very high energies (10^7 to 10^9 Gev). The interaction length in air of primaries producing large extensive air showers must be less than the rate-attenuation

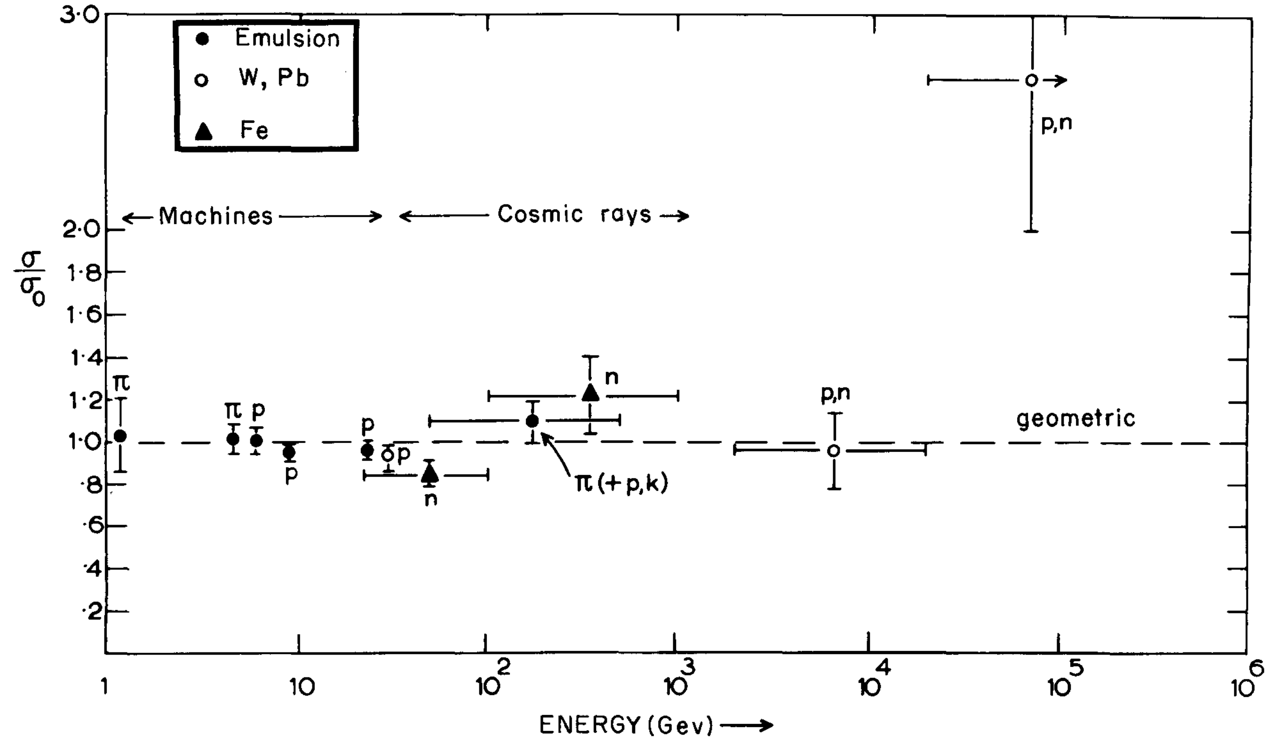

Fig. S10/11-1. Total inelastic cross section in medium and heavy nuclei.

length; this sets a lower limit to σ/σ_0 in nitrogen of 0.8.

Attenuation Length of Shower-Producing Radiation

When, as in cosmic rays, the incident nucleon beam is not monoenergetic, but has the form of a power-law spectrum with nearly constant index, information on the partition of energy in the collisions can be obtained from the attenuation length λ. The term λ is the amount of material, in g/cm^2 (air), required to reduce the number of nuclear-active particles above a given energy by the factor e. Experimentally, the logarithmic derivative with respect to depth, i.e., $(-1/\lambda)$ of the counting rate of secondary showers above a given multiplicity or total energy, is found to be constant where atmospheric depth is sufficient for the radiation being measured to have attained equilibrium with the (nucleon) source.

Determinations of λ (shown in Fig. S10/11-2) have been made by measurement of:

a. Variation with atmospheric depth of the number of local penetrating showers (counters and emulsions, range 10 to 100 Gev);

b. Zenith-angle and altitude variation of the number of "jets" above a given primary energy;[6] or of the number of electron-photon cascades of a given energy produced in local absorbing material[7] (emulsions, primary energy range 10^3 to 10^5 Gev);

c. Altitude and zenith-angle variation, and barometric coefficients of extensive air showers;[8,9] equilibrium conditions with constant λ obtain in the lower third of the atmosphere (counter experiments, energy range 10^4 to 10^8 Gev).

From 10 to 10^6 Gev, λ appears to be remarkably constant, with a mean value of 120 g/cm^2 of air. One can interpret this result as follows: Suppose that, in an interaction, a particular nuclear-active secondary particle j acquires a

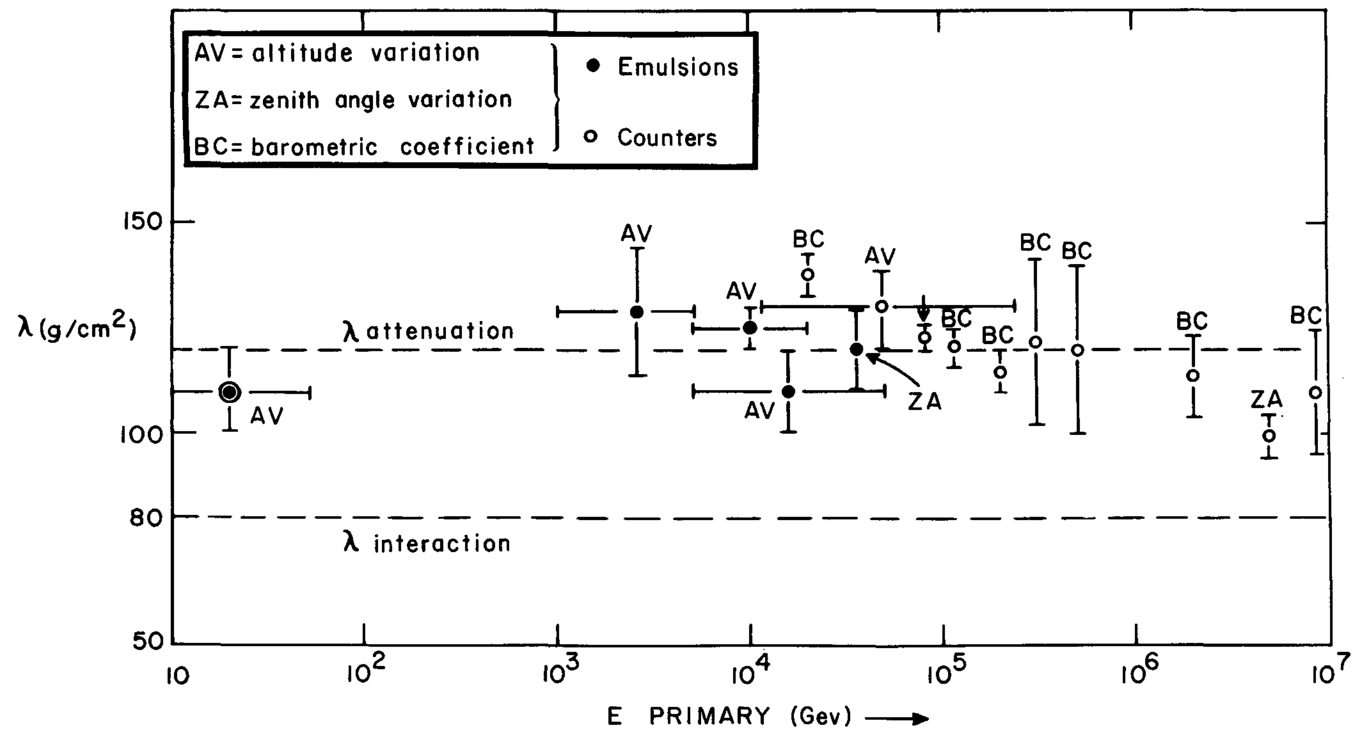

Fig. S10/11-2. Attenuation length in air

fraction f_j of the primary energy. Then if λ_i is the interaction length, and γ is the index of the integral energy spectrum of the nuclear-active component (assumed constant), we have

$$\lambda = \frac{\lambda_i}{1-\sum_j f_j^{\gamma}} .$$

Thus, for $\lambda_i = 80$ g, we have $\Sigma f_j^{\gamma} = 0.33$. The γ is known to vary slowly from 1.5 at low energies (a few Gev) to 1.8 at high energies (10^6 Gev). With $\gamma = 1.8$, the assumption of equipartition of primary energy among n secondaries (all assumed capable of further interaction) would lead to

$$n = 3^{1/\gamma - 1} \approx 4 \text{ to } 5 .$$

Observed multiplicities at high energies (see below) are greater by an order of magnitude and, in any case, equipartition is unlikely. Hence, we must assume that the bulk of the secondary energy is carried off by only one or two particles. If f_0 is the value of f for the most energetic nuclear-active secondary, and $f << 1$ for all other secondaries, one obtains

$$f_0 = 3^{-1/\gamma} \approx 0.5 .$$

This result is usually interpreted as meaning that, on the average, the incident nucleon re-emerges from the collision with about half of its original energy* (i. e., inelasticity $K \approx 0.5$). Nothing is known about the distribution in K, but it seems to be well established that the average value of K is less than unity and is remarkably independent of energy.

At the very highest energies (10^8 Gev), there is some evidence[10, 11] that λ may decrease

* It may, of course, emerge in an "excited" state as a hyperon or other baryon.

to about 100 g/cm^2. This effect may be due to the increase of γ (to 2.0) rather than to a change in elasticity of the collisions. It should be noted that the assumption λ_i = 80 g/cm^2 can well be questioned. The demonstration that the collision cross section is constant and "geometric" in heavy elements does not necessarily imply either a constant or geometric cross section for an air nucleus, and an increase of inelasticity at high energies cannot be ruled out.

Conclusions

The results on the attenuation length are consistent with a mean inelasticity coefficient of 0.5 for all energies from 10^2 to 10^7 Gev. This result is in agreement with the observations on Gev beams from accelerators (Dubna).

Multiplicity

Figure S10/11-3 shows that the multiplicity n_s of the charged secondary relativistic particles depends on energy. Most of the observations were made in emulsions. They have been divided into those of low and high N_h, respectively, where N_h is the number of associated heavily ionized tracks. The former are thought to be rather close approximations of peripheral collisions with a single nucleon of the target.

The fluctuations in multiplicity are very wide; the standard deviation about the mean value of n_s at a particular energy is approximately 0.5 n_s for $N_h \leqslant 3$, and approximately 1.0 n_s for $N_h \approx 4$. For both groups of N_h, there is a steady increase of n_s with primary energy E_p. The results are consistent with the relation $n_s = 1.8\,E_p^{1/4}$ with E_p in Gev for $E_p \leqslant 10^4$ Gev, for "peripheral" collisions in emulsions and collisions in light elements.

Points marked "π" at high energies refer to interactions of secondaries (80% of which are pions) from the "primary jets."

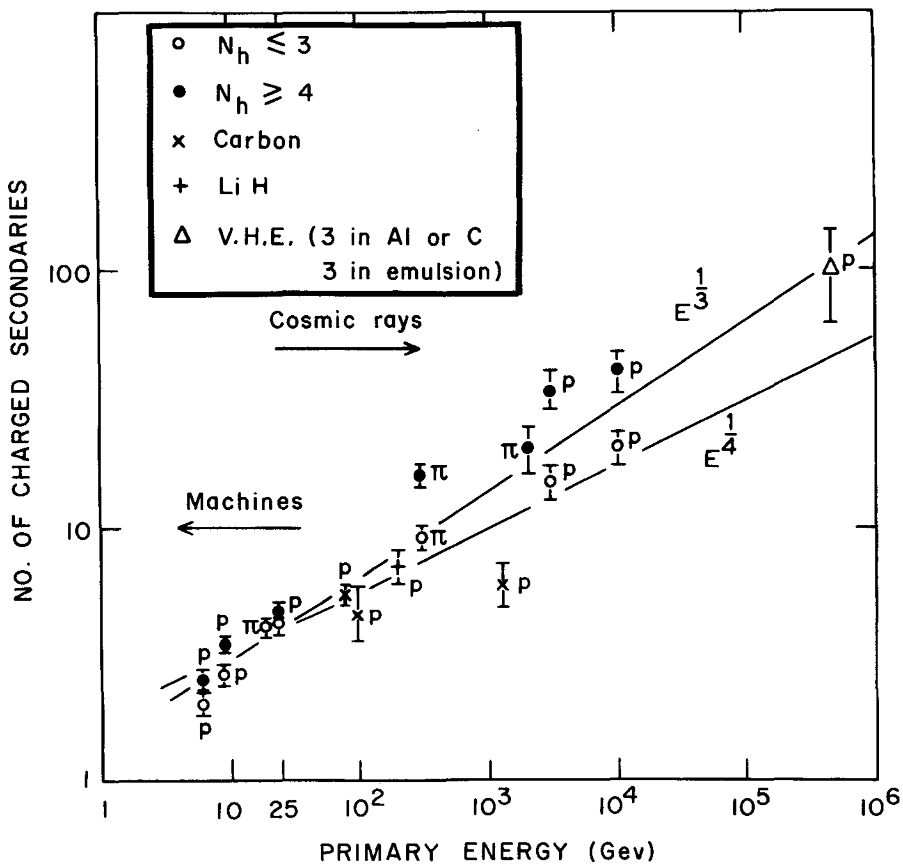

Fig. S10/11-3.

The cosmic-ray events in emulsions were found by detection of the associated soft cascades. The primary energies were estimated either from a kinematical analysis or by multiplying the cascade energy by a suitable factor, such as 10. The average energies plotted are probably correct within a factor of 2.

Differential Cross Sections for Production of Different Particle Types

Relative Numbers Averaged over Secondary Energies and Angles

It is well established that, even at the highest energies attainable in cosmic rays, pions are the most copiously produced particles in nuclear collisions. The important question of the relative numbers of strange particles and baryons, however, has not yet been well resolved.

a. In the emulsion work, one estimate of the proportion of pions has been obtained by measuring the number of γ rays converting into electron pairs in the cores of "jets." Assuming all the γ rays come from π^0 decay, and that $N_{\pi^\pm}$ equals $2N_{\pi^0}$, one finds, from the world survey of emulsion data, [3]

$$\frac{\text{number of charged pions}}{\text{all charged secondaries}} = 0.82 \pm 0.05.$$

In individual cases of higher energy up to 10^6 Gev, the ratio is the same within statistical errors.[12]

In order to find the proportion of pions among the created particles, one must allow for the primary nucleon(s) projected into the forward cone of the jet. If we denote charged and neutral created heavy particles $X^\pm$ and X^0, respectively, we obtain

$$\frac{N_{X^\pm}}{N_{X^\pm} + N_{\pi^\pm}} = 0.14 \pm 0.05 . \qquad (1)$$

A second approach has been to determine the ratio of numbers of secondary interactions produced by neutral and charged secondaries — the former, of course, are due to nonpions. Again, making allowance for primary nucleons, one finds

$$\frac{N_{X^0}}{N_{X^\pm} + N_{\pi^\pm}} = 0.15 \pm 0.05 . \qquad (2)$$

From the ratios (1) and (2) we obtain

$$\frac{\text{created heavy particles}}{\text{all created particles}} = 0.20 \pm 0.05 .$$

These ratios apply to the primary energy range 10^3 to 10^5 Gev.

b. Quite similar observations have been made with multiplate cloud chambers.[13] The primary energies were in the region 10 to 120 Gev. The ratio (1) was 0.20 ± 0.08, and the ratio (2), 0.16 ± 0.06. It is noteworthy that in these experiments about half of the secondary K^0 particles would decay rather than interact, whereas in the emulsion work decay is negligible. The consistency between the ratios in the two methods is some indication that the X particles are not made up exclusively of K mesons, but the errors are too large to give a meaningful baryon/K ratio.

c. Observations made with a magnetic cloud chamber[14] that has targets of light elements placed above the chamber allow identification of secondaries, by measuring momentum and ionization, up to energies of about 20 Gev. The proportion of heavy particles agrees well with that deduced by the previous methods; the primary energy in this case was approximately 300 Gev.

The results of the measurements described above are summarized in Table S10/11-I.

Conclusion

Averaged over all secondary energies in the interactions and over all forward angles in the center-of-mass system, K particles plus baryons constitute approximately 20% of the created particles. Between 20 Gev and 10^6 Gev primary energy, this fraction appears to vary little. Heavy-meson and baryon production never become comparable to pion production, even at the highest energies so far investigated. This is pionization *a fortiori.*

Table S10/11-I.

Relative abundance of heavy created particles

$\frac{\text{Heavy created particles}}{\text{all created particles}}$	Primary energy (Gev)	Method and	reference
0.20 ±0.06	10 - 120	Multiplate chamber (interactions in carbon)	13
0.22 ±0.06	50 - 1000	Magnetic cloud chamber (interactions in carbon)	14
0.20 ±0.05	$10^3 - 10^5$	Emulsions	3
0.18 ±0.07	$10^6 (n_s \approx 400)$	Emulsions (1 event in Al) (see Fig. S10/11-8)	12

The Relative Numbers of K Particles and Pions above a Given Energy

Limits on the K/π ratio have recently been set by comparing the γ-ray flux observed in the atmosphere with the muon flux at sea level.[15] First, by assuming that directly produced pions are the sole source, one can compute the muon flux from the γ flux. The expected and observed fluxes agree within the limits of error (approximately 20%) over the common energy range 250 to 1000 Gev (see Fig. S10/11-4). Above 1000 Gev the muon flux, determined from the range spectrum underground, becomes rather uncertain owing to (a) discrepancies between results of different observers and (b) possible errors in the energy-loss formula and the fluctuations therein.

The magnitude of the effects of (b) is indicated by the horizontal lines attached to the high-energy points. The energy corresponding to the left-hand side of each line has been calculated by using the formula

$$dE/dR = 2.5 + bE \quad \text{in Mev/g/cm}^2 \text{ in rock,}$$

with $b = 0.003$ and E in Gev; for the right-hand side of the horizontal lines, the value taken for b in the second term was 0.006. The first term in the formula corresponds to collision loss; the second, to pair production, nuclear interaction, and bremsstrahlung. Since the radiation length of a muon in rock is $5 \cdot 10^5$ g/cm^2, whereas the range of a muon of 1000 Gev is approximately $2 \cdot 10^5$ g/cm^2, it is clear that fluctuations in bremsstrahlung energy loss are extremely important. At present, fresh experiments on the muon flux at great depths are (or soon will be) in progress, as are also the Monte Carlo calculations on the distribution of energy loss. For the time being, however, no meaningful comparison between photon and muon fluxes above 1000 Gev is possible.

If K mesons rather than π mesons were the main source of μ's and γ's, the observed μ flux would be expected to be higher by a factor of about 10 than that computed above.* This factor stems largely from the fact that $K^{\pm}$ mesons have (roughly) a 7-fold greater decay probability than do $\pi^{\pm}$ mesons, at a given high energy. The conclusion is that the ratio $N_{K^{\pm}}/N_{\pi^{\pm}}$, above a given energy, is < 0.15 over the range 250 to 1000 Gev. This result applies to the primary energy range 1000 to 10,000 Gev.

Conclusion

K mesons are not only much less numerous than pions, but also carry much less total energy (i.e., the "partial inelasticity" K_K is much less than K_π).

* If hyperons, rather than K mesons, were the intermediate particles, the μ/γ ratio would be almost the same as for directly produced pions.

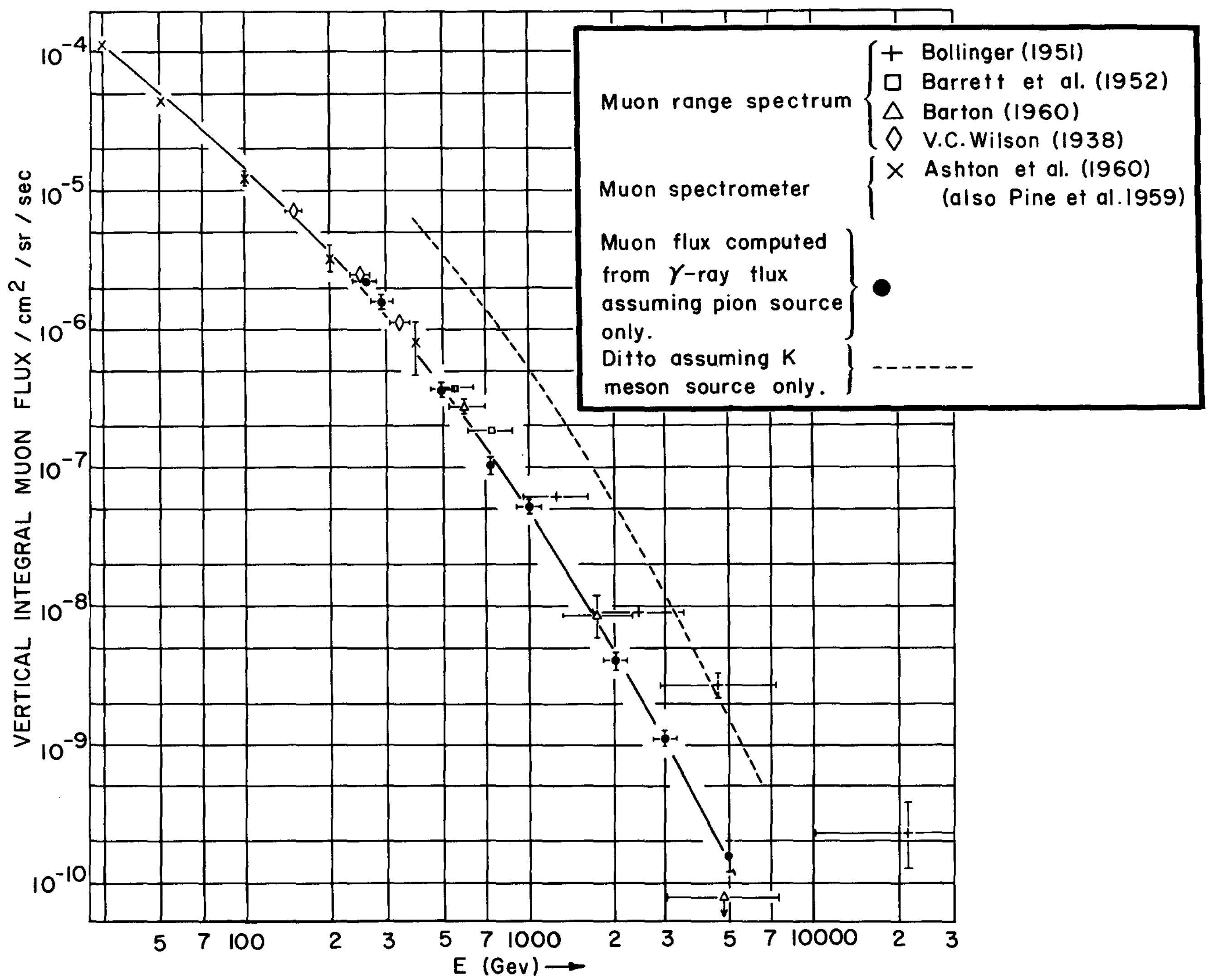

Fig. S10/11-4. Expected and observed muon flux.

The Relative Numbers of Pions and Baryons Above a Given Energy

The small fractional energy transferred to individual pions in high-energy nucleon-nucleus collisions is emphasized by the measurements of the proportion of pions among the nuclear-active particles above a given energy. Cosmic-ray observations have been made concerning:

a. The pion flux computed from the γ-ray flux at high altitudes. It was found, for example, that, at above 500 Gev energy, the production rate of charged and neutral pions, per g of atmosphere at the top, is only 7% of the number of interacting primary nucleons per g of atmosphere above the same energy.

b. The relative numbers of interactions at aircraft and mountain altitudes produced by neutral and charged primaries. When allowance has been made for the residual positive excess in the nucleon component (because the primaries incident at the top of the atmosphere are positively charged), the relative numbers of charged and neutral primaries of showers at great depths will be determined by the ratio of pions (all charged) to nucleons or other heavy particles (equal numbers charged and neutral). For incident particles producing secondary cascades above a given energy, the emulsion experiments indicate that the ratio of pions to nucleons is approximately 20%. Since an incident pion of given energy is likely to transfer more energy to π^0's in a collision than is a nucleon, the ratio of pions to nucleons above a given energy is considerably less than 20%. The primary energies considered here are in the range 2000 to 10,000 Gev. A similar result is obtained from the charged/neutral ratio in the radiation that produces local penetrating showers (primary energy 100 to 1000 Gev).[13]

Energy Distribution of Pions (c.m.s.)

The differential spectrum of total energy of pions in the center-of-momentum system of the collisions (averaged over all angles of emission) shows that, over a wide range of primary energy, the most probable pion energy is 2 to 3 $m_\pi c^2$. Beyond the maximum, the intensity drops off roughly exponentially with energy. Spectra have been obtained from the π^- beams produced by CERN 25-Gev protons on an aluminum target;[16] from cloud-chamber observations in the 200-Gev region with a carbon target;[14] from emulsion results at higher primary energy (obtained from scattering measurements on the particles projected backwards in the c. m. system[17]); from measurements of energies of individual γ rays from π^0 decay; and from observations on "families" of parallel cascades in young air showers intercepted by stacks of "sandwiches" of emulsion and a heavy element.

If we approximate these distributions by exponentials, the effective temperature T (i. e., mean kinetic energy) of the pions increases roughly as $E_p^{1/4}$, from about 0.3 Gev at E_p = 30 Gev to 2 to 3 Gev at $E_p = 3 \times 10^4$ Gev. Apparently, however, this trend does not continue. For laboratory-system photon energies below 2000 Gev, the integral spectrum of individual pions — measured from the γ-ray flux (see Fig. S10/11-5) — is of the form $E^{-2.3}$, as compared with the integral spectrum of the total photon energy liberated in a nuclear collision (Fig. S10/11-6), which has a constant index (-2.0) nearly equal to that of the primary nucleons (corresponding to a nearly constant fraction of the primary energy dissipated into pion secondaries). This difference in slope (0.3) is exactly what would be expected if the effective photon (hence pion) multiplicity were to rise as $E_p^{1/4}$. Above approximately 2000 Gev, there seems to be a definite steepening of the γ-ray spectrum, corresponding to a more rapid rate of increase of multiplicity per collision. For a multiplicity rising as $E_p^{1/2}$, one expects an integral photon spectrum of the form $E^{-3.0}$, rather close to what is observed in the region 3,000 to 10,000 Gev. If the fractional primary energy liberated as pions in a collision is to remain constant, a multiplicity rising as $E_p^{1/2}$ implies a constant c. m. energy for the pions (or photons). Hence, at some critical primary energy, about 30,000 Gev (γ_c = 100 to 150), the c. m. pion temperature, having reached 2 or 3 Gev, ceases to rise further.

The consequence of the magnitudes of the multiplicity and "temperature" of the pions in the c. m. system is that, for primary energies $< 3 \times 10^4$ Gev, the bulk of the total pion energy is carried off by only one or two particles. This finding is confirmed as follows. Electron-photon cascades above a certain energy in emulsion sandwich stacks are due either to (a) single γ rays or electrons or both from interactions in the overlying atmosphere, or to (b) local nuclear interactions in the assembly. For cascade energies below 2000 Gev, the equality in the numbers of the two types indicates that the bulk of the total photon energy in a nuclear collision must be accounted for in terms of a single π^0 meson. The only way around this conclusion would be to postulate that very-high-energy hyperons are an important constituent of the interaction products. These would decay in the atmosphere, liberating γ rays, but would not decay in solid matter.

Angular Distribution in the c. m. System

General Characteristics

Figure S10/11-7 shows some samples of angular distributions (c. m.) in high-energy events. The emulsion data refer to collisions with low N_h, and represent averages over many events.

The degree of anisotropy of the angular distribution increases slowly with primary energy. If the distribution is approximated by the expression $|\cos^n \Theta| \times d\Omega$, then at $E_p \approx 30,000$ Gev,

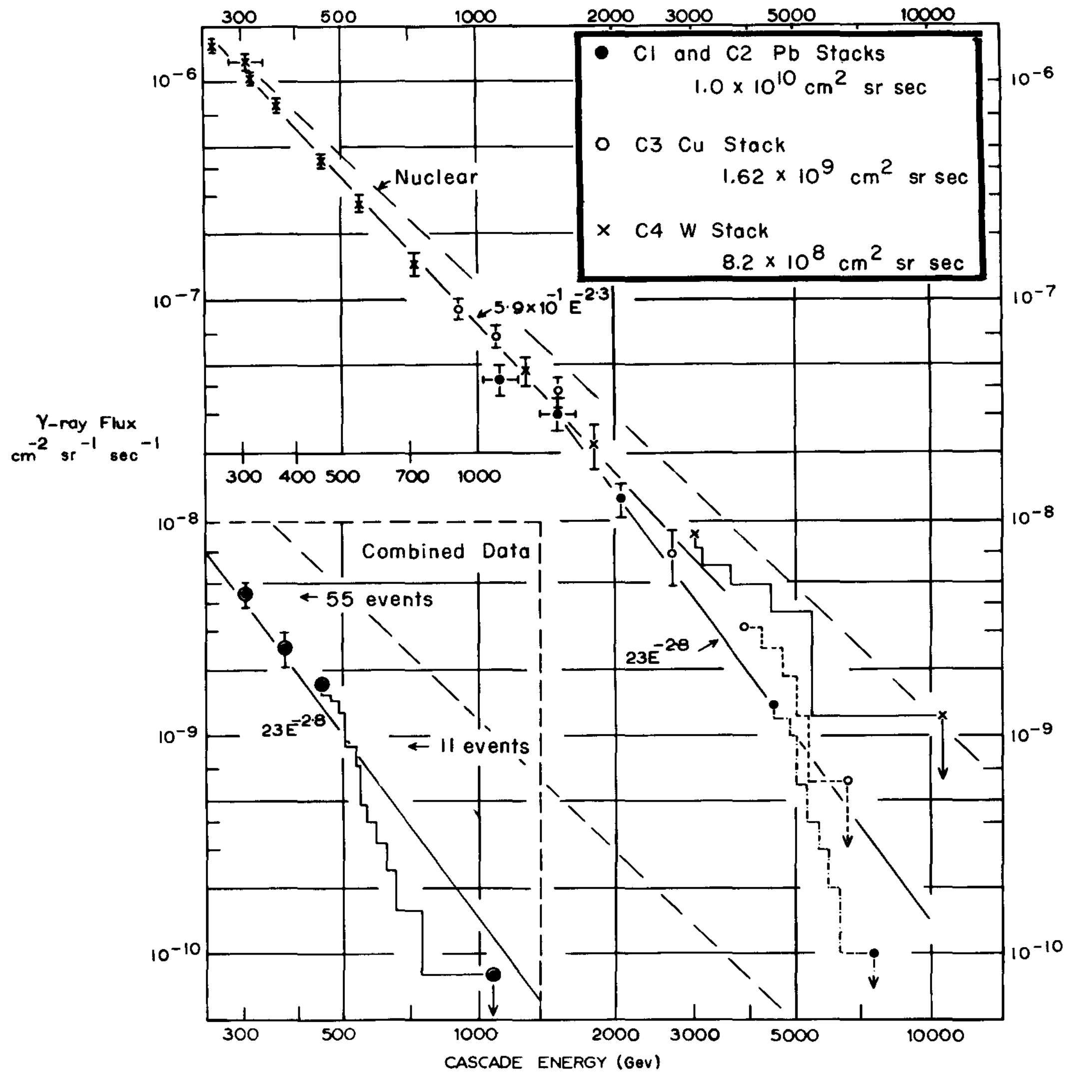

Fig. S10/11-5. Integral energy spectrum of γ rays and (or) electrons in comet stacks (220 g/cm^2).

$n \approx 2$ to 3, in comparison with the value $n = 0$ (isotropy) at accelerator energies ($E_p \leq 25$ Gev). It must be emphasized that the distributions in Fig. S10/11-7 represent averages over many events; the degree of anisotropy in individual cases varies considerably. Very large values of n (up to 2,000) have been observed but appear to be extremely rare. *

The distributions in Fig. S10/11-7 refer to all charged secondaries regardless of type. Direct mass measurements in the cloud-chamber work indicate that the K mesons and baryons

* Apparently the degree of anisotropy in the cloud chamber events is greater than those in emulsions, even though the energies of the latter are greater. The reason may be that, in every event, the original primary particle is likely to re-emerge at a very small forward angle (< 10°). If this event is subtracted, the discrepancy is largely removed. Another possible source of difference may lie in the fact that the angles in the emulsion data are measured relative to the primary direction, whereas those in the cloud chamber data are measured relative to the resultant momentum vector of the charged secondaries.

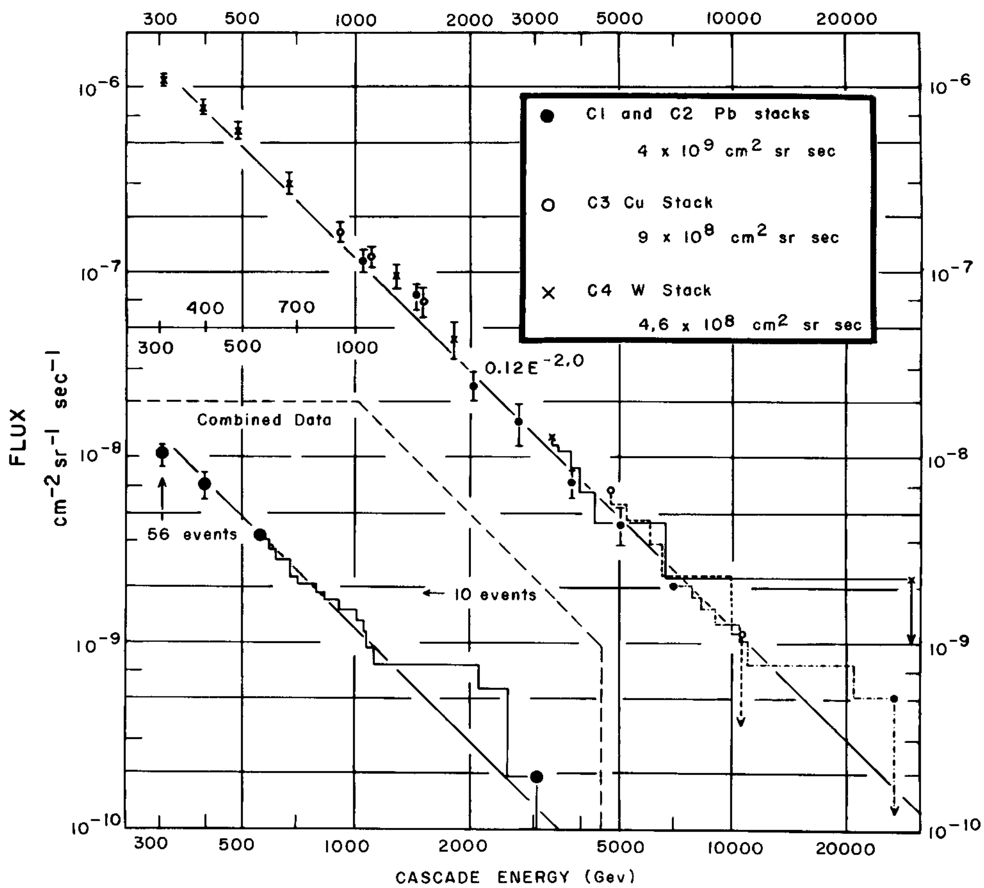

Fig. S10/11-6. Integral energy spectrum of electromagnetic cascades initiated by local nuclear interactions in comet stacks (220 g/cm^2).

have a substantially more anisotropic distribution than do the pions.

Of significance for a colliding-beam experiment is the essential feature emerging from these results; namely, that the proportion of particles emerging at small c. m. angles is quite low. At a mean energy $\overline{E}_p = 30,000$ Gev , 8% of the particles lie in the range $0°$ to $5°$ and $175°$ to $180°$; the corresponding figure for $E_p = 2,000$ Gev is 5%.

Double maxima and asymmetric showers

Within the last few years, there have been two interesting developments arising from the analysis of the angular distribution of the shower particles in high-energy collisions:

The first was the observation that, for primary energies above 1000 Gev, the angular anisotropy in the emulsion events could be interpreted in terms of isotropic emission from two separate centers, moving in opposite directions in the c. m. system.[18, 19, 20] These have been discussed already by Ticho. The second important discovery was the backward-forward asymmetry of the shower particles in the c. m. system in the ionization-calorimeter experiments at primary energies of approximately 100 Gev.[21] Both of these phenomena have been interpreted as the result of the dominance of pion-exchange processes (π-core, π-π, and core-π collisions) in peripheral interactions.[21, 22]

Transverse Momentum

One of the best-known features of high-energy collisions is the apparent constancy, with respect to primary energy or angle of emission, of the transverse component of momentum p_T of the secondaries.[3, 23]

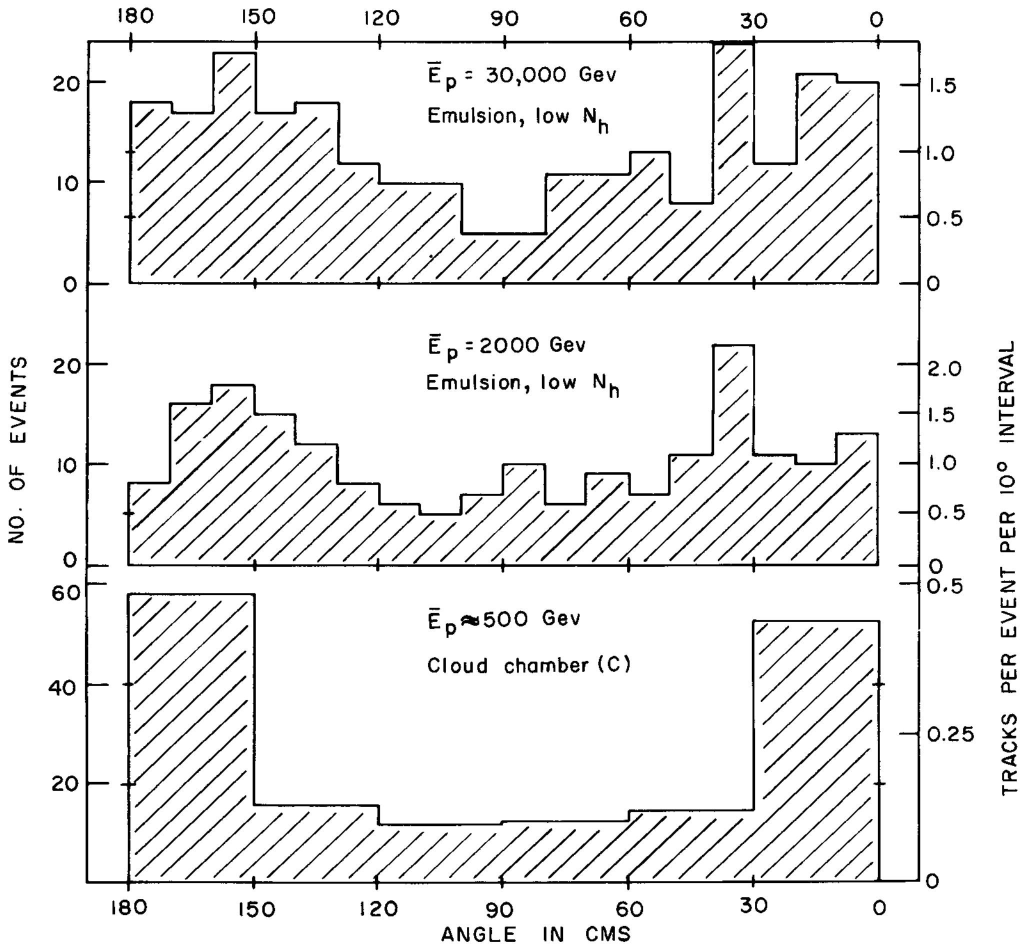

Fig. S10/11-7. Angular distributions (c. m. system) of high-energy events.

In the cosmic-ray experiments, reliable measurements of p_T have been made over a wide primary energy range (100 Gev to 10^6 Gev) for the pions (via the decay $\pi^0 \rightarrow 2\gamma$). In particular, the p_T distribution of photons has been shown to be nearly exponential as in

$$\left[\frac{dN\,(p_T)}{dp_T}\right]_{\gamma's} = \text{const. } \exp(-p_T/0.22),$$

where p_T is given in Gev/c.

This result implies that the distribution for the pions has roughly the form of a Maxwell distribution as in

$$\left[\frac{dN\,(p_T)}{dp_T}\right]_{\pi's} = \text{const. } p_T \exp(-p_T/0.22),$$

where $\langle p_T \rangle_\pi = 0.44$ Gev/c.

Essentially the same distribution (with $\langle p_T \rangle_\pi = 0.4$ Gev/c) has since been observed at CERN (see Cocconi's report) for p-p collisions at 24 Gev. As indicated by this formula, the fraction of pions with $p_T > 1$ Gev/c is very small ($\lesssim 1\%$). At the very highest energies investigated (10^6 Gev), there is tentative evidence for a long "tail" extending to several Gev/c; e. g., in one Bristol event (Fig. S10/11-8) containing more than 200 photons from a collision in aluminum, five energetic photon cascades are observed at wide angles, corresponding to p_T values between 2 and 5 Gev/c.

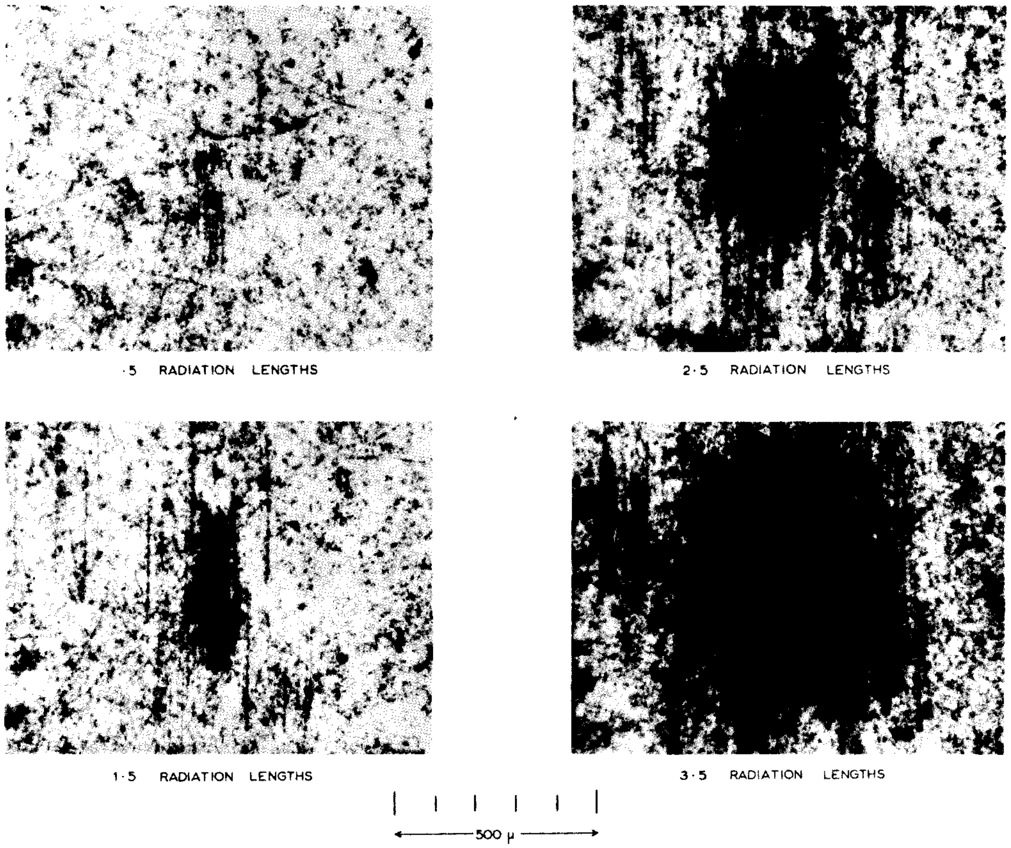

Fig. S10/11-8. Development of photon cascades at various distances from point of origin.

For heavy particles, results on p_T have been conflicting. Emulsion results are meager; they are based on the analysis of interactions of secondary neutral particles of jets, and suggest $p_T \approx 1$ to 2 Gev/c.[3] On the other hand, the Berkeley cloud-chamber measurements on identified K-particle and proton secondaries (of $p < 20$ Gev/c, however) give a mean value of p_T equal within the errors (10%) to that for pions,[14] as do also the CERN results for protons, Σ, etc. (see Cocconi's report, Seminars 3 and 4).

Inelasticity of the Collisions

The evidence from the rate of absorption of high-energy showers in the atmosphere indicates that the overall average energy used up in the creation of new particles in a collision between a nucleon and a light nucleus is of the order of 50% of the primary energy. (Refer to "Attenuation Length of Shower-Producing Radiation," above.)

One of the urgent questions at present concerns the subdivision of the energy radiated among the created particles. Unfortunately, cosmic-ray measurements do not give precise indications.

Fractional Energy Radiated as Pions (K_π)

The energy associated with the γ rays resulting from decay of π° mesons created in a collision can be determined fairly well; most determinations of K_π depend on this.

Emulsion work

In individual events the primary energy has been estimated from angular distributions of shower particles and assumptions of angular symmetry in the c. m. system. Values of K range from 1% to 100% (or more!). It appears that there are large fluctuations in K_π from collision to collision. Biases are introduced, which can give the appearance of a dependence of K_π on primary energy, since a low-energy K_π event would be detectable for high E_p but not for low. Averaged over primary energies from 500 to 50,000 Gev, the value of K_π is 0.25.[3]

Ionization calorimeter (in conjunction with magnetic cloud chamber)

The principle in this type of measurement is to determine the total electron track-length integral (TLI) over the nucleon cascade developing in a deep chamber (iron).[21] When extrapolated to infinite thickness, the TLI multiplied by the critical energy gives the primary energy directly. The interactions occurred in an LiH block between two magnetic cloud chambers, with the calorimeter placed underneath. The primary energy was compared with the photon energy liberated in the first interaction (measured calorimetrically), and also the energy of the charged secondary particles in the cloud chamber. Average values of $K_\pi = 0.30$ are found for $E_p \approx$ 200 Gev. The most probable value of K_π was 0.2, individual values ranging from 0.05 to 1.0. Some of this spread must be due to errors in the estimate of primary energy, which were quoted at 30%.

Intensity of cascades produced by nuclear-active component

In heavy-element-emulsion sandwich stacks we can determine the number N of electron-photon cascades that are above a given energy E_{π^0} and that are associated with local nuclear interactions.[12, 24] From the data on EAS[8, 25] one can compute the primary energy E_p, above which there would be N nucleons interacting in the assembly. If there is a one-to-one correspondence between primary energy and cascade energy, then the ratio $E_{\pi 0}/E_p$ is a measure of K_π. By this method, one obtains values of $K_{\pi 0} = 0.09$ for $E_p = 2{,}000$ Gev, and $K_{\pi 0} = 0.06$ for $E_p = 10^5$ Gev. Since the bulk of the pion energy is believed to be carried by only a few pions at the lower primary energy, fluctuations in the neutral-to-charged ratio are important, with the result $K_\pi \approx 2.2\, K_{\pi 0}$; thus, there is an average value of $K_\pi = 0.2$ for the energy region 5×10^3 to 10^5 Gev. There are probably uncertainties of a factor of 2 or more in the absolute value of K_π because of possible errors in the primary spectrum (converting EAS sizes to primary energy). The important feature, here, is that K_π does not change appreciably over a large interval in primary energy. Note that here the values of K_π refer to collisions in heavy nuclei.

Cloud chambers

Estimates of K_π have been made also for collisions produced in light elements placed above cloud chambers with magnetic fields,[14] and in multiplate chambers.[13] Values of K (an upper limit to K_π) ranging from 0.4 at $E_p = 100$ Gev to 0.1 at $E_p = 1000$ Gev have been reported by the Berkeley group.[14] This rapid fall of K (hence K_π) with energy is not substantiated by the other experiments, or by the evidence from the attenuation length. The Russian cloud chamber results with LiH targets give $K_\pi = 0.3$ (refer to "Ionization Calorimeter ..." above).

Multiplate chamber measurements of K_π [13] depend on estimates of primary energy from the angular distributions, in comparison with the energy liberated in the form of π^0 mesons.

A summary of the observed values of K_π is given in Table S10/11-II.

Conclusion

The mean energy radiated as pions lies between 20% and 30% of the primary energy. Large fluctuations occur in individual events. There is no evidence that K_π changes appreciably with energy, over the range 100 Gev $< E_p < 10^5$ Gev.

Fractional energy radiated as heavy particles

Strange-particle production

As previously discussed (refer to "The Relative Numbers of K Particles and Pions..." above), present evidence suggests that the total energy

Table S10/11-II. Summary of values of K_π observed by various methods.

(K_π) average	Primary energy (Gev)	Method
0.25	5×10^2 to 5×10^4	Emulsions, analysis of individual events.[a] (Ref. 3)
0.30	200	Ionization calorimeter + cloud chambers. (Ref. 21)
0.20	5×10^3	Emulsions, spectrum of energy in soft cascades, compared with primary spectrum. (Refs. 12, 24)
0.20	10^5	
0.40	10^2	Magnetic cloud chamber. (Ref. 14)
0.10	10^3	
0.24	10 to 10^2	Multiplate chamber.[a] (Ref. 13)

[a] Depends on primary-energy estimate from angular distribution of shower particles.

radiated in the form of K mesons, K_k, is considerably less than K_π.

Baryon production

Production of nucleon (and hyperon) pairs is expected, according to the statistical theories, to become increasingly important at very high energies. No direct measurements of $K_{n\bar{n}}$ have been made; if we set $K_{n\bar{n}} = K - K_\pi$, then we obtain $K_{n\bar{n}} \leqslant K_\pi$. Certainly, the energy radiated in the form of baryon pairs does not appear to predominate over that in the pion component.

Summary: Phenomenological Models

Let us now summarize the above results.

First, it seems to be fairly well established that the inelastic cross sections for high-energy collisions in heavy nuclei are close to the values obtained at accelerator energies (i.e., in the region of a few Gev). The multiplicity of the secondary particles increases slowly with energy (roughly as $E^{1/4}$) in the range 10 to 10^4 Gev. At all energies, pions are the most numerous secondaries, accounting for about 80% of the total. The energy division among the secondaries is not uniform. If a single secondary particle – presumably the original primary nucleon – is mainly responsible for the propagation of the nuclear cascade, it acquires on the average about 50% of the original primary energy. In this case, it may not be possible to account for all the energy radiated (50%) in terms of the pion component alone. Indeed, the amounts of energy radiated as pions and heavier particles may be about equal. The majority of these heavy particles must be baryons, for the energy content of the K particles is known to be much smaller than that of the pions. The energy distribution among the pions themselves is also very nonuniform; the bulk of the energy is usually carried by only one or two particles.

In the main, these results are not dramatically different from those observed at lower energies. One important conclusion that emerges from them and to which attention has been repeatedly drawn – particularly by Russian cosmic-ray physicists – is that the Fermi-Landau statistical theory, which completely neglects the structure of the nucleon, is unable to account for the low value of the inelasticity coefficient in the majority of the collisions.

Although the statistical theory may well apply to core-core (N-N) collisions, these are evidently rather rare. Peripheral collisions are much more probable, and it has been proposed that the dominant mechanism, in this case, is virtual-pion exchange between the nucleons.

The double maximum in the angular distributions of the shower particles (in the symmetrical events) has, as mentioned above, been interpreted as isotropic emission from unstable isobars ("fireballs"). In order to account for the low inelasticity, these must be pion isobars, which "trail behind" the nucleons after the collision. It would be interesting, of course, to demonstrate that such isobars are formed as a result of resonances in the π-π system. Unfortunately there seems to be no clear evidence that fireballs of reasonably well-defined masses or energies are formed.

New Processes

In the nuclear interactions at high energies, as we have seen, there is the unexpected result with respect to the change in form of the pion-production spectrum (c. m.) at a primary energy in the region of 10^5 Gev. This change manifests itself as a steepening in the spectrum of individual photons intercepted by emulsion stacks flown at aircraft altitudes. This steepening is also borne out by the experiments of the Japanese emulsion group at mountain altitudes,[26] and, with less certainty, by the muon spectrum at sea level. This result can be interpreted in terms of a limiting value, in the region of 3 Gev, to the mean c. m. energy of individual pions, so that the number of high-energy pions begins to rise quickly (as $E_p^{1/2}$) above a primary energy of 10^5 Gev, maintaining the total energy content of pions produced in a nuclear collision steady at about 20% of the primary energy.

This is not the first time that peculiarities have been observed in phenomena at energies of about 10^5 Gev. Some years ago, experiments by Nikolsky and others[27] indicated a dramatic increase in the number of nuclear-active particles in air showers in the region 10^5 to 10^6 Gev. This result, however, has not been confirmed in other laboratories.

A second class of phenomena, which we observed recently in Bristol, concerns electromagnetic interactions at very high energy (3000 Gev). We observed four cases of anomalous development of electron-photon cascades initiated apparently by γ rays or electrons. In one case, for example, the cascade grows to a maximum at the expected depth, about 7 radiation lengths from the ouside of the stack, and then begins to die out. We then find a second cascade developing exactly along the axis of the first. This second cascade has a profile of exactly the right shape, but with a maximum at 14 or 15 radiation lengths. The energy in each of the two "humps" is about the same (3000 Gev). In another case, no double maximum is observed, but a single rather broad maximum is observed at a position 5 or 6 radiation lengths deeper than expected from cascade theory. We are sure that such anomalous cascades cannot be explained by ordinary cascade fluctuations.

These findings indicate that entirely new phenomena may exist in the very-high-energy region. In cosmic rays, owing to the low fluxes and the difficulties of accurate measurements, we observe strange effects only when they are rather dramatic, that is, when the process in question is well above the energy threshold for its appearance. It is not unreasonable, therefore, to expect that, with more refined measurements, such phenomena could be detected at much lower energies, perhaps in the region of a few hundred Gev.

References

1. A. E. Brenner and R. W. Williams, Phys. Rev. 106, 1020 (1957).

2. G. Bozoki, E. Fenyves, and L. Janossy, Nuclear Phys. 24, 412 (1961).

3. For review up to 1958: D. H. Perkins, in Progress in Cosmic Ray and Elementary Particle Physics, Vol. 5 (North-Holland Publishing Co., Amsterdam, 1960).

4. J. Duthie, Ph. D. thesis, University of Bristol, 1961.

5. C. Babayan, N. Grigorov, M. Dubrovin, L. Mishchenko, V. Murzin, L. Sarycheva, V. Sobiniakov, and I. Rapoport, in Proceedings of the IUPAP Conference in Cosmic Rays, Moscow, 1959.

6. M. Kaplon, J. Klose, and D. Ritson, Phys. Rev. 91, 1573 (1953).

7. J.G. Duthie, C. Fisher, P. Fowler, A. Kaddoura, D. Perkins, and K. Pinkau, Phil. Mag. 6, 89, 113 (1961).

8. For review, see K. Greisen, in Progress in Cosmic Ray Physics, Vol. 3 (North-Holland Publishing Co., Amsterdam, 1956).

9. For review, see T. Cranshaw and W. Galbraith, Phil. Mag. 3, 811 (1958).

10. B. Rossi, in Proceedings of the IUPAP Conference on Cosmic Rays, Moscow, 1959, Vol. 2, p. 18.

11. T. Cranshaw and A. Hillas, in Proceedings of the IUPAP Conference on Cosmic Rays, Moscow, 1959, Vol. 2, p. 210.

12. P. Fowler; in Proceedings of the 1960 Rochester Conference on High-Energy Physics (Interscience Publishers, Inc., New York, 1960), p. 829.

13. S. Lal, Pal Yash, and R. Raghavan; private communication.

14. L. Hansen and W. Fretter, Phys. Rev. 118, 812 (1960).

15. J. Duthie, P. Fowler, A. Kaddoura, D. Perkins, K. Pinkau, and W. Wolter, in press.

16. G. Cocconi, in Proceedings of the 1960 Rochester Conference on High-Energy Physics (Interscience Publishers, Inc., New York, 1960), p. 799.

17. M. Schein, D. Haskin, E. Lohrmann, and M. Teucher, in Proceedings of the IUPAP Conference on Cosmic Rays, Moscow, 1959, Vol. 1, 6.

18. P. Ciok, S. Cogben, J. Gierula, R. Holynsky, A. Jurak, M. Miesowicz, S. Saniewska, and J. Pernegr, Nuovo cimento 10, 741 (1958).

19. G. Cocconi, Phys. Rev. 111, 1699 (1958).

20. K. Niu, Nuovo cimento 10, 994 (1958).

21. N. Grigorov, V. Murzin, and I. Rapoport; Soviet Phys. JETP 7, 348 (1958); N. Grigorov, N. Kondratiev, A. Savelieva, V. Sobinyakov, A. Podgurskaya, and V. Ya. Shestoperov, in Proc. IUPAP Conference on Cosmic Rays, Moscow, 1959; N. A. Dobrotin and S. A. Slavatinsky, in Proceedings of the 1960 Rochester Conference on High-Energy Physics, p. 819.

22. E. Feinberg, Soviet Physics Uspekhi 3, 147 (1960).

23. Cooperative Emulsion Group in Japan: Suppl. Nuovo cimento 8, 761 (1958).

24. J. Duthie, C. Fisher, P. Fowler, A. Kaddoura, D. Perkins, and K. Pinkau, in Proceedings of the IUPAP Conference on Cosmic Rays, Moscow, 1959.

25. G. Clark, J. Earl, W. Kraushear, J. Linsley, B. Rossi, and F. Scherb, Nature 180, 353 (1957).

26. J. Nishimura, in Proceedings of the IUPAP Conference on Cosmic Rays, Moscow, 1959.

27. S. Nikolsky and A. Pomansky, in Proceedings of the IUPAP Conference on Cosmic Rays, Moscow, 1959, Vol. 2, p. 214.

12. COLLIDING-BEAM TECHNIQUES*

Gerald K. O'Neill

July 13, 1961

The Princeton-Stanford Colliding-Beam Experiment

This experiment was designed in 1957-8 and authorized in 1959 for the purpose of observing the elastic scattering of electrons on electrons, at a total energy of 1 Gev (c. m.) so that the behavior of quantum electrodynamics might be explored to distances of approximately 10^{-14} cm or less. The design maximum circulating current is 1 amp which is calculated to give a rate of 3 counts/sec integrated over all counters observing a differential cross section of about 10^{-31} cm^2/sr. Barber, Gittelman, O'Neill, Panofsky, and Richter are the physicists assigned to this experiment.

Status After Approximately Two Years of Construction

Magnets

The magnets are finished, in place, and tested.

Rf system

The rf system is finished, in place, and tested.

Inflectors (dc and pulsed)

The dc pulsed inflectors are finished, in place, and tested.

Counters

The counters are unfinished but well along in construction.

Vacuum system

Assembled and tested in Princeton, five-eighths of the vacuum system reached a pressure of 5×10^{-10} mm after two bakes at 400° C. The entire system reached 5×10^{-9} mm after 1 hour's bake. After testing, the vacuum system was disassembled and shipped to Stanford for reassembly, which should be completed in September. We do not expect to begin storage tests until at least October of this year.

Cost

The entire experiment — including all salaries, a building, design, and construction — will have cost about $1, 000, 000 by the end of this year. The cost is about 15% above initial estimates.

Later plans

It is somewhat premature to look beyond the initial experiment, but it is planned that, if the first is successful, we shall

a. look for pions and muons made directly or indirectly in e-e collisions, and

b. modify the apparatus to store electrons and positrons, so that pure final states of two pions or two muons can be produced. The energy is insufficient for the pair production of heavier particles.

The Frascati Storage Ring

This 250-Mev ring, built and now operating, was designed for the study of electron-positron

* A summary of an informal seminar talk, given in July 1961, at a meeting of the Berkeley Summer Study Group. An attempt has been made to recall some of the more significant questions asked, but no claim to completeness is made. The summary is expanded from notes used in the talk, but is not a verbatim report.

injection, as a first step toward construction of a larger device for electron-positron experiments of the kind discussed under (b) above. A countable number of electrons (about 14) has been stored, with mean lifetimes of 2 to 4 min at pressures of about 0.5×10^{-6} mm. A new device, larger than the Princeton-Stanford rings, would be advantageous for the study of K-meson interactions.

CERN Studies on Colliding Beams

Designs for a 25-Gev ring have been studied in considerable detail by Dr. Schoch's group. A low-energy electron model is being built to test some of the basic accelerator-theory questions involved.

The tentative proposal put forward by Dr. Schoch's group was for a pair of rings with either one or two interaction regions, to be located near the existing proton synchroton (P.S.). The estimated cost is 1 to 1.5 "CERN P.S. Units", and the design is appealing from a practical viewpoint: it could be located at the present site, whereas no larger machine could. The laboratory administration was willing to consider the proposal. However, a number of experimental physicists at CERN — worried lest a large and possibly difficult-to-use new machine with limited application be authorized without adequate scientific justification — formed a study group which met four times for about 2 hours each session to consider the proposal, and concluded that it should be shelved. My own conclusions, based on a detailed account furnished by Dr. G. Cocconi, are:

a. concern because a fairly definite proposal was made at such an early stage, prior to detailed study of the experimental techniques, advantages, and disadvantages associated with colliding-beam experiments;

b. regret that a number of the experimental possibilities suggested to the experimentalists were, in my opinion, of negligible interest and a waste of the very limited time of the committee; and

c. accord with the general feeling that no proposal for a new and untried approach to any problem can succeed unless there is someone available with a genuine personal interest in using the new approach, exploiting its possibilities, and inventing ways around its disadvantages. In the case of the CERN review, for lack of such an advocate, only a very few of all the significant questions involved were even mentioned for discussion. The CERN experimentalists did their review job conscientiously and with all possible fairness, but they had no more than a small portion of the input data normally required as a basis for a decision.

Theoretical Studies at Princeton

During the past three years, J. Woods, P. Herzberg, and F. Gross have studied several problems related to storage-ring design. Developments since the most recent CERN accelerator conference are as follows:

a. F. Gross has developed and tested a 704 computer program which optimizes the design of a storage ring by satisfying several minimization problems at once. It is also useful for conventional synchrotrons in that all form factors, misalignment sensitivities, etc., are approximately identical for concentric storage rings and conventional synchrotrons of the same energy; the varying radii of curvature in a concentric ring add no problems; also, in all of the designs considered, the requirement that all equilibrium orbits be approximately tangent in all six straight sections is simultaneously satisfied.

b. E.J. Woods has developed several programs for studying the effect of the electromagnetic forces of one beam on the other at the interaction points. He found that stability could exist for one beam crossing a fixed current distribution of even several thousand amperes. He is now working on the much more difficult problem of approximating the real case in which both beams are free to move and distort under their mutual interactions. By tracing 50 to 100 clusters of charge in each beam and dealing with currents of several thousand amperes, he infers results applying to the real case within 10^5 to 10^6 crossings of the interaction region. Still in progress, the work is made difficult by the fact that the small number of "particles" used makes possible the introduction of apparent instabilities, which result from the approximations used rather than from the physics involved in the real case.

The Princeton-Pennsylvania Study Group on Colliding Beams

A small group met several times this spring, and will resume in the fall with one or two additional members. So far, the group has consisted of the following members:

M. G. White	H. Primakoff
E. P. Wigner	S. B. Treiman
A. K. Mann	G. K. O'Neill

The group will consider theoretical guesses about the high-energy physics questions which may be of interest ten years from now, and compare corresponding conventional and colliding-beam experiments as to feasibility, experimental convenience, and inherent accuracy. We intend to continue this in a relaxed way, without making any specific proposal for at least several months. Our study will not necessarily result in a proposal for a machine at Princeton; rather than our starting with a piece of hardware and trying to decide whether it is worth building, we would prefer having the physics under consideration force us to some conclusion.

Portions of the following two sections of this report are the result of meetings of the colliding-beam study group, but should not be considered conclusive; as a group, we shall deliberately avoid making definite statements or suggestions for at least several months.

Limitations and Disadvantages of Proton-proton Colliding-Beam Systems

Intensity

As far as is presently known, the most severe upper limit to the circulating beam in a proton storage ring is set by the single-beam longitudinal space-charge instability. At an energy of 25 Gev, with a 2% beam energy spread, this limit is approximately 130 amperes. To fill to this limit from an accelerator with 5×10^{11} protons per pulse, for example, would require 4,000 pulses and a filling time of 6 hours. If, as has been suggested, the source accelerator were raised to 5×10^{13} protons per pulse by construction of a new high-energy injector, the filling time would be reduced to 3 min (40 pulses). Even in this upper-limit situation, the interaction rate in a storage ring would be much lower than in a conventional synchrotron; for example, with 130 amp of circulating current, the total interaction rate would be lower by a factor 15 to 50 than that of a 25-Gev synchrotron with a 1-meter liquid hydrogen target. The rate would therefore be equivalent to that of a conventional machine with 1 to 3×10^{10} protons per pulse. If the conventional machine used for comparison were bombarding a solid target, with multiple traversals, the "equivalent intensity" of the storage ring would be 0.3 to 1×10^{10} protons per pulse. If the storage ring had a-factor-of-10 less current, the equivalent intensity ratio relative to a synchrotron with 5×10^{11} protons per pulse would be 10^{-3} to 10^{-4}.

For a circulating current of 130 amp, the interaction-rate density in a storage ring would be equal to that of a conventional machine of 10^{10} protons per pulse on a liquid hydrogen target.

In the CERN study referred to earlier, the intensity factor quoted is 10^5 to 10^7, based on an assumed circulating current of 0.5 to 5 amp. This is equivalent to assuming no increase of the injecting accelerator current during the next several years beyond that now achieved by the CERN proton synchrotron, and allowing generous safety factors.

Source Size

By use of thin targets and multiple traversals, the source size in conventional machines can be made very small, therefore easy to refocus on a small target or counter. In a storage ring, the source regions would be 1 × 1 × 10 cm, during maximum-intensity operation. This would limit the magnification that could be used in magnetic-lens systems used to form secondary beams from such a source.

The Impossibility of Putting a Detector at the Primary Production Point

In a storage ring, the closest approach one could make to the primary production point would be 1 to 2 cm at 90° (c.m.) or 2 to 4 cm at 30° (c.m.).

Low Intensity and Low Energy of Secondary Beams

The maximum energy for secondary beams would be approximately the energy of the injecting synchrotron. Here it is worth noting that by secondary beams we mean really K's, pions, muons, and neutrinos. The generation of separated beams of unstable hyperons in any machine is almost certainly impractical, because, at the energies at which time dilation makes decay lengths reasonable, the beams are much too stiff for separation.

The Comparative Inconvenience of Applying an Analyzing Magnetic Field to the Active Region

In a conventional synchrotron (at least up to 3 Gev) one can extract the proton beam and let it interact in a bubble chamber located, for example, in a highly inhomogeneous magnetic field of the kind that is easy to make. In a storage ring, however, the analyzing field would have to be designed with great care, and properly shaped so as not to introduce a lens action which would disturb the focusing properties of the ring.

Note that, in any reasonable colliding-beam design, backgrounds due to residual gas would be very small (10^{-2} to 10^{-6} of the colliding-beam interaction rate in the source region), for which reason backgrounds are not listed among the limitations.

Advantages of Doing Experiments by Colliding Beams

This section is frankly partisan, and can be taken as a tract in support of colliding beams. Its purpose is partly to interest other experimentalists in designing colliding-beam experiments, and partly to point out some of the advantages to be gained thereby.

Higher Energies (c.m. system)

It is difficult to see how else the extension of experiments to really high energies will ever be made. Even the most extreme proposals made for "third-generation" synchrotrons (1000 Gev), at a cost of 15 to 30 times that of the CERN synchrotron, will not exceed 40 to 45 Gev in the c.m. system. By contrast, even a "first-generation" storage ring, costing 1 to 2 CERN units, would already give 50 to 60 Gev in the c.m. system. At still higher energies, the contrast increasingly favors colliding beams.

Interaction Rates

Although interaction rates would be considerably lower in a storage ring, they would not be so much lower that important physics is likely to be missed. The CERN group has estimated, quite conservatively, that the minimum detectable cross section for colliding beams (10 interactions per day) would be about 10^{-35} cm^2. If the theoretical limits in current could be approached, this number could be pushed down still further, to 10^{-38} cm^2. From the geometrical proton-proton cross section of 3×10^{-26} cm^2 to the intensity limit of 10^{-35} to 10^{-38} there is a huge range, and, if the area of interesting physics consists of even a very small fraction of the total cross section, the limit on finding this fraction (starting with either conventional or colliding-beam machines) will be set by details of experimental procedures, and by detection techniques which one or the other method makes possible, rather than by available interaction rates.

Production Point

The production point is not nearly as "invisible" as one may think. The area of interesting physics is likely to be found in the high-momentum-transfer events which are characterized by a high degree of multiple pion production ("pionization" in Cocconi's phrase), and, in any 4π photographic detector, these pion tracks will locate the production point to within less than 1 mm.

Secondary Pion Beams

Since it is now clear that the proton is mostly pion cloud, it is unlikely that there will be much difference, either in the physics or the experimental analysis, between high-energy pion-proton and proton-proton collisions. In my opinion, therefore, the lack of intense secondary pion beams is relatively unimportant. On the other hand, at low energies, where our present experience is based, the situation is entirely different.

Source-Particle Annihilation

There is one bit of low-energy experience which is likely to hold true at all energies; namely, it is often convenient to have source particles which can disappear in the reaction, so that the final state is simplified. Examples of studies facilitated by such final states are as follows: the studies of positron annihilation at low energy; more recently, the efforts now being started by two groups to study the π-π interaction by high-energy electron-positron annihilation; also, already partly completed, the studies of the final states resulting from p-$\bar{p}$ annihilation. Since, in any accelerator, only protons and neutrons are available as strongly interacting target particles, the possibility of storing antiprotons in a ring already includes all the advantages that could be found for high-energy strong-interaction disappearing-particle experiments. At low currents, a ring would be an ideal antiproton separator for stationary-target experiments. If the stored currents can be made high enough (for example, by continuous injection of antiprotons to a ring by hyperon decay, which bypasses phase-space limits), colliding beams of protons and antiprotons would be worth considerable effort to achieve. It is true that the p-$\bar{p}$ system is an isobaric mixture, in contrast to p-p, but its zero baryon number more than compensates for this difficulty.

Strange Particles

The only useful strange-particle secondary beams which can be made by any accelerator are, as far as is known, K^+ and K^-. They would be nice to have, but since they carry only strangeness ±1, it is difficult to believe that their absence, in a colliding-beam system able to make cascade pairs with strangeness ±2, would prevent discovery of new high-strangeness particles, if such exist.

The next two points to be listed ("Unity Duty Cycle" and "Simultaneous Mass Analysis") are of critical importance; to emphasize their significance I shall digress on a matter of experimental technique: Within the past year the prospect for experimentation on colliding beams has been changed enormously by a development still so new that most people have not heard of it — namely, the high-resolution momentum-analyzing spark chamber. It is essentially a perfect match to a colliding-beam source. Figure S12-1 shows the present state of the art on this detector. Shown is a spark chamber with 50 gaps, each just 3 mm wide, with a magnetic field of 14 kgauss along the line of sight. We have found that the precision with which individual sparks represent the actual path of the particle increases with decreasing gap spacing; for the chamber shown, the sparks scatter about the particle path with a full width at half-maximum of just 15 to 20 mils. The density and scattering of this chamber are less than those of liquid hydrogen, and, although the chamber is only 30 cm long, it has a maximum detectable momentum of 16 Gev/c. For a larger chamber of the same kind, p_{max} should vary as the length to the 5/2 power, so that, in the 30 × 30 × 60-cm chamber now being built, p_{max} should be about 130 Gev/c. There is no equivalent of the convection currents that limit the accuracy in large bubble chambers. This chamber, of course, has an ultimate time resolution of 1 microsecond or better, and is triggerable. In the experiment in which we plan to use it first, the spark chamber will be integrated into a system of scintillation and Cerenkov counters, which will identify the one in 10^5 of incoming K mesons that produces a particular rare decay mode; we need not take pictures of the unwanted events.

In considering the following two major advantages of colliding beams, one should keep this type of photographic detector in mind.

Unity Duty Cycle

In detecting rare events of the complicated kind expected at high energies, a continuous source would be a great advantage. In many, if not in most, experiments, the increase by a factor of 30 to 100 in the duty cycle of storage rings over that of conventional machines, will be worth as much as (and in many cases more than) an equal amount of added interaction rate. In many experiments now going on at conventional synchrotrons, the limitation on the rate of gathering information is set, not by the total

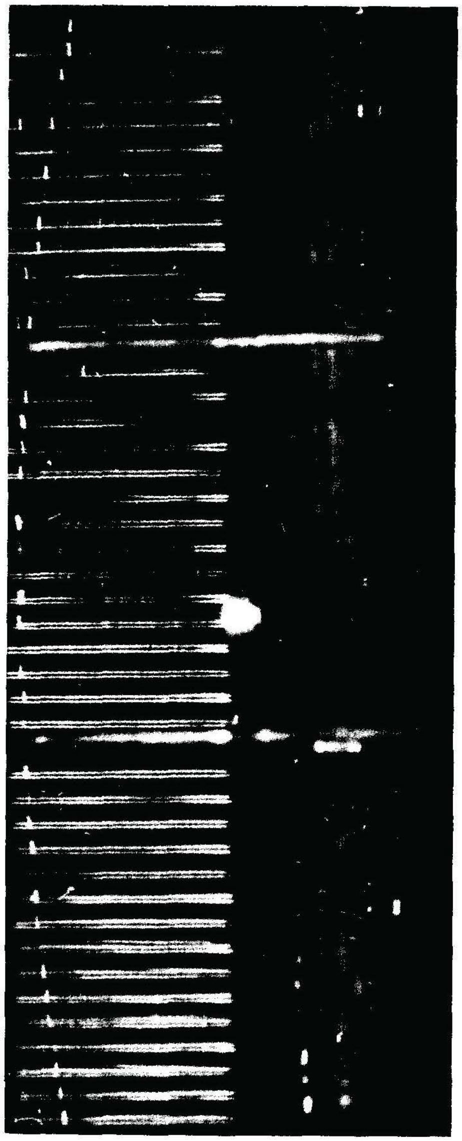

Figure S12-1. Track of a mu meson of approximately 250 Mev/c momentum, in a 50-gap spark chamber. A magnetic field of 14 kgauss existed normal to the view presented. The gaps (0.3 cm) are separated by hollow aluminum frames, 0.3 cm thick, covered on each side by 0.0025-cm aluminum foils. The average density and scattering are less than that of liquid hydrogen. The scatter in the positions of individual sparks is 0.04 cm, so that the maximum detectable momentum in this 30-cm chamber is approximately 16 Gev/c.

interaction rate of the machine, but by the saturation of the analyzing counting system on high instantaneous rates; in a 5-amp storage ring, for example, the interaction rate at each of six points would be 1 per 50 μsec. This is just about optimum for the counting electronics and for spark chambers; an increase in circulating current by a factor of 10 would make the rate 1 per 1/2 μsec, which would be too much for a 4π photographic detector. At 5 amp, however, an event occurring with a total cross section of 10^{-33} cm^2 could be detected and photographed at the rate of several per hour.

Simultaneous Mass Analysis

A very serious limitation of conventional machines in the very-high-energy range is the fact that it is extremely difficult (at present, impossible) to make mass measurements on more than one relativistic secondary from a single interaction. At present, only gas Cerenkov counters of small aperture and very small angular acceptance can measure masses above a momentum of about 1.5 Gev/c (lab). This limitation bites very hard; all strange particles are made in associated production, in which the simultaneous measurement of masses for several particles from a single interaction is essential to learning the full story. If one wishes to study a typical interaction in which two short-lived strange particles are made, each of which decays, giving four detectable charged secondaries, one can (in conventional machines at extreme energy) find out what is going on only in the very small (probably not representative) fraction of cases in which all four subsequent decay products go backward in the center-of-mass system, so that they are at low energy in the laboratory system. The smallness of this fraction can be seen by the observation that for a 1,000-Gev event, the gamma of the center-of-mass system is 22; thus, a particle emerging at low energy in the c.m. system at 90° is thrown forward so that it appears in the lab system with a gamma of 22 or higher. A similar limitation exists for resonant states — none has been seen at the 25-Gev machines, not only because these machines have not been operating long, but because the detection of resonant states involves in an essential way simultaneous mass and momentum measurements on two or more products of a single interaction. By contrast, in a colliding-beam event nearly every secondary comes out in a favorable range for mass analysis.

Specific Recommendations

It is not the purpose of this report to try to show that machines above 25 Gev are not useful; however, I want to urge the designers of such a machine to seriously consider optimizing the design in such a way that the machine will be a good injector for storage rings. This need not be painful. Nearly every change in design that makes a synchrotron better as a ring injector also makes it better as a conventional machine. I also feel that any experimentalist willing to spend time in the design of experiments and new techniques for colliding beams will discover for himself the advantages I have listed above; the exercise is an instructive one for those of us now also designing experiments for the existing machines.

As an example of such a design comparison, I shall cite the following experiment, presently of interest to me. Consider the electronic decay mode of the K^0 meson: $K^0 \to \pi^{\pm} + e^{\mp} + \nu$. This reaction and its charge conjugate can be used in a sensitive test of the $\Delta S/\Delta Q$ rule. We are planning to measure this reaction with the momentum-analyzing spark chamber, coupled with scintillation counters and velocity-selecting and threshold Cerenkovs. In a 1.6-Gev/c positive beam at the Brookhaven AGS, we can approach to within 60 ft of the target. At an assumed intensity of 4×10^{11} per pulse, with a 100-msec beam spill, we can expect to get about 5 counts per hour. If we had an electrostatic separator, the rate (now limited by pion accidentals) could be raised, but by no more than a factor of 30. I have chosen this experiment for comparison because it is about the worst choice for a colliding-beam source that could be made; it uses a secondary K beam, does not require extreme energies, and is extremely wasteful of the incoming beam: the decay mode we are looking for is only one part in 1,500 of the total, and we lose a further factor of 100 in charge exchange. Even in this case, however, the corresponding colliding-beam experiment is suprisingly competitive: if we had a ring set with a 5-amp circulating current, a primary source rate of 2×10^4/sec would exist at each of six points. Based on cross sections measured at only 6 Gev (c.m. system), we should get about 10^3 K^+ per second. About one-third would be in an interesting momentum interval, and about one-third of those would be in a favorable solid angle. The K trigger could be obtained rather more simply than at present, by observing the corresponding hyperon decay. Of the 10^2 K's per second available for charge exchange, about one per second would exchange its charge, and we would end up with about one or two useful events per hour. It is no small advantage that the experiment could be going on in just one straight section, while five other people did simultaneous experiments in other sections. It is also worth noting that, even if a more careful design should show the estimates above to be optimistic by a factor of 10, the available rate still would be several events per day. In this sort of experiment, a reasonable number (50 to 100) of good events is quite enough to clinch the matter.

Questions

Q. (Goldhaber): Why quote a limit of 1.5 Gev/c for bubble chambers? The CERN work mentioned was done with a small chamber, but with larger ones it is possible to go much higher.

A. In momentum measurement, yes; but the point is that measurements of particle mass, essential for identification, cannot be made at much higher momenta because the velocity is then too close to c. (Occasionally, of course, a high-energy δ ray can be used to set a lower limit on the gamma of the incoming particle, but this happens rarely enough not to be reliable and positive for most tracks.)

Q. Even at very high energies, though, the backward cone of particles comes out at low energy in the lab system.

A. Yes, but as indicated by the example quoted, the low-energy "backward cone" comes from far less than half of the solid angle (c.m.), in energetic collisions, so that the probability that all the interesting particles will have simultaneously measurable masses becomes, in a stationary-target experiment, extremely small;

those few events which would be completely measurable would represent a very biased sample.

Q. (Masek): Would the location of the source region in a storage ring be fixed or would it fluctuate?

A. The equations of motion are such that if a large stored current can be built up at all, then the resulting distribution will be very stable indeed.

Q. How can you tell where the target region is?

A. With many thousand high-multiplicity events per second, a few seconds of data taking, by either spark chambers or counters, is enough for an accurate survey of the source region. Also, it turns out that even in ultrahigh vacuum the deexcitation of atoms of the residual gas through which the beam is passing is enough to allow direct photography of the beam with exposure times of a few seconds. This has been checked experimentally by using smaller beams presently available.

Q. (Blewett): What are the relative difficulties of measuring elastic proton-proton scattering by colliding beams and by conventional synchrotrons?

A. It's so easy either way that I have not considered it as a test experiment.

(Q. Made clear that the point of the question was the observation of very-low-probability events with large momentum transfer.)

A. (By Cocconi): That is a clear case in which the colliding-beam experiment would be much easier, because the momentum measurements on both outcoming protons must be made to an error of less than half a pion mass, to assure elasticity.

Q. (Jones): We have noticed that one of the ways to make use of high-field superconductors would be to build a colliding-beam vacuum pipe of material in such a state, so that a strong magnetic field outside could be perfectly shielded from the circulating beams.

A. Good idea. This must, however, be balanced against the desirability of having a magnetic field in the source region to aid in analysis.

Q. (Johnsen): I would like to clear the record in regard to the CERN work on storage rings. So far no actual proposal has been made. Our discussions with experimentalists were very preliminary, and were intended to raise questions and suggest topics for useful study by all concerned. Since there is confusion on that point even in CERN itself, I would like to clear it up.

Also, a technical note of interest: two weeks ago we accelerated the proton beam in the proton synchrotron to 10 Gev, and held it there, quite stable, for 2 minutes. Then we had to stop or our magnet power supply would have overheated.

A. Thank you. I discussed the CERN study in detail mainly because it has been widely represented, during the past few weeks, as formal, exhaustive, and final. It took direct conversation with Dr. Cocconi before I was able to get an accurate story.

Q. I don't yet see the geometry of the experimental areas in a storage ring.

A. The diamond-shaped interaction region, $1 \times 1 \times 10$ cm, would be at the center of a 15- to 30-foot straight section, ended by the ring magnets, which would be about 3×3 feet. The vacuum pipes, crossing at a small angle, would be 2 to 4 cm in diameter, of thin stainless steel.

Q. How close to the forward direction can you get in a colliding-beam experiment?

A. It depends on the reaction. Actually the center of mass is moving slowly (at about 0.10 c) radially out of the vacuum chamber. In the two-center approximation, the source regions would follow the primary protons (but moving slowly) along the thin vacuum pipes. For reactions in which one is interested, particularly in the directions of the primary protons, the cases are:

a. Charged products longer-lived than 1 or 2×10^{-10} sec; they are deflected outward in an analyzing field, or, with no field, the minimum angle for their escape from the vacuum chamber before decay is 5° to 10°.

b. Neutral shorter-lived secondaries: there is no minimum angle there (at least in high-multiplicity events) because the charged tertiaries extrapolate to a point which can be reconstructed.

c. Charged, shorter-lived products: the extrapolation of the charged tertiary makes clear the existence of the short-lived secondary producing it, but the entire kinematics is not seen in one event.

Q. (Kerth): Would the rings have to be shielded?

A. For experimental convenience, it is worth avoiding shielding as far as possible. During the injection period, of course, one could not work close to the rings, even though most of the injection losses would occur in a narrow region. After injection stops, though, it might well be possible to work close to the rings in safety. It depends on the degree to which a magnet or vacuum failure can be made to lead always to controlled beam dumping in a known, locally shielded place. The speed with which vacuum failures can occur in a steel system, or in which magnetic fields can change in solid iron magnets, is inherently much slower than the circulation frequency in the ring. In any case, it would certainly not be necessary to locate massive shielding close to the rings; at most, one might have to provide earth dikes 50 or 100 feet away to stop the direct radiation in the event of an uncontrollable beam dump.

13. ROUND TABLE DISCUSSION OF THEORETICAL INTEREST IN 300-Gev PROTON ACCELERATOR

(Amati, Case, Chew, Dombey, Frautschi, Gasiorowicz, Goebel, Wong)

July 14, 1961

Introduction (Chew)

After 4 weeks of discussion and crude calculations, some fairly definite opinions about the impact on theory of a proton accelerator of approximately 300-Gev lab energy are beginning to emerge. These opinions are certain to change with time, and in at least one important area, as we shall hear, there is still an almost complete absence of concrete reasoning. Nevertheless, it was felt appropriate at this mid-point of the summer study to bring all the participants collectively up to date on the activities of the theoretical members.

The organization of this round-table discussion will be based on the melancholy fact that the energies we are talking about are, almost certainly, not sufficiently high to unify the traditional three-way division of particle physics according to interaction strength. Weak interactions are not expected to become strong, at least until E_{lab} approximates 10^4 Gev (if ever), and electromagnetic interactions, presumably, stay well below the unitarity limit until. log E approximates 137. There is no reason to think, therefore, that the contemplated step-up in energy will be a crucial factor in relating the three types of interaction. In fact, it may be said in general that current theory does not pinpoint any characteristic energy in the region of 10 to 30 Gev, the center-of-mass energies under consideration.

Let us consider, in order, the theory of strong, weak, and electromagnetic interactions as related to a proton accelerator of approximately 300 Gev. Certain experiments, of course, may bear on more than one interaction type.

Strong Interactions (Chew)

One can imagine at least three qualitatively different situations with respect to strong interactions at these energies.

Metastable Strongly Interacting Particles

One possibility is that there exist hitherto undiscovered symmetries and associated conservation laws (like strangeness), broken at most by weak or electromagnetic interactions, that lead to metastable strongly interacting particles (lifetimes $\gtrsim 10^{-20}$ sec) of mass greater than a few Gev. There has been no clear theoretical call for such particles, as there was for pions and antiprotons—but then, of course, no call was made for strange particles either. Without a definite motivation for a particular particle, the experimenter must be prepared to make general fishing expeditions, and theorists will not be of much help in such a situation. Basically, our reason for expecting to find something is historical: in the past, something new has always turned up when the energy was increased by a big factor.

Froissart:

Will it be possible to observe particles with lifetimes less than approximately 10^{-15} sec, if their properties are not predicted in advance?

Chew:

The π^0 (lifetime approximately 10^{-16} sec) was discovered without significant help from theory (even though it had been predicted).

Dombey:

One can always look for "missing mass" peaks in the momentum spectra of known particles.

Unstable Particles of Unpredictable Masses
(Chew)

A second possibility for strong interactions is that there are "hidden" symmetries, broken violently at low energies by the existence of masses and implying only unstable particles of unpredictable masses with lifetimes of approximately 10^{-23} sec which are difficult to distinguish from dynamical resonances. Such symmetries, however, may become apparent at energies and momentum transfers at which masses are unimportant. Many theoretical proposals of this type have been made, but so far no experimental test has been suggested. For example, even if one believes that pions and kaons are equivalent in some fundamental sense, it does not follow that one should expect $\sigma^{tot}_{\pi N}$ to approach σ^{tot}_{KN} at high energies. It may be that a relation such as

$$\left(\frac{d\sigma^{el}_{\pi N}}{d\Omega}\right) \rightarrow \left(\frac{d\sigma^{el}_{KN}}{d\Omega}\right) ,$$

at a finite nonzero angle, is to be expected. Dombey and Gasiorowicz are concentrating on problems of this type—as probably will Gell-Mann and Zachariasen when they arrive.

The Testing of Underlying Symmetries
(Gasiorowicz)

The statement that "in the absence of such-and-such coupling, such-and-such symmetry holds exactly," is often heard, and, in view of the fact that, unfortunately, we cannot "switch off" couplings at will, it is necessary to think about the meaning of such statements. The form of the statement springs from conventional field theory in which the various interactions between particles are introduced additively into a Lagrangian function, which, together with the canonical commutation relations, supposedly defines the problem completely. With such a theory, it is easy to imagine some interactions removed, and calculations performed without them: the effect of introducing an additional interaction, which might mask an underlying symmetry, is calculable, and, in this sense, the statement has a meaning. The practical difficulties in actually carrying out the necessary calculations do not really change the situation: thus, for example, the belief in charge independence is based on the fact that the deviations from this symmetry, such as mass differences, are of such an order of magnitude as to conform with our expectation that they come from the symmetry-violating electromagnetic interaction, and, even though quantitative estimates are unreliable and often wrong, we do not question the principle of charge independence. The practical difficulties of calculating the "symmetry-breaking corrections" begin to be much more important when we do not have even a qualitative idea of how important such corrections should be: in that case, the underlying symmetry is very uncertain. It is easy to give examples:

a. Global symmetry: because the interactions which supposedly break the symmetry are fairly strong, we have no way of estimating their effect, and, therefore, 4 years after the symmetry has been proposed, we still do not know whether it prevails or not.

b. It is generally believed that the weak interactions have a universal V-A structure. It is something of a surprise that the corrections due to the strong interactions are very small—of the order of 25%. On the other hand, the leptonic decays of the strange particles appear to be depressed by a factor of 10; is this a strong-interaction effect, or does this mean that the underlying "universality," when generalized to include the strange particles, already accounts for this factor?

The detection of underlying symmetries thus presents us with a major practical problem, even if the question is well defined, as it is in conventional field theory. If we try to abandon conventional field theory, we run into difficulties in principle: "bare coupling constants" do not exist in an S-matrix theory, and, thus, relations between such quantities (e.g., equality between G_V and G_A) have no meaning. Since the S-matrix theory is supposed to provide a complete description of all phenomena, the absence of a place for "hidden symmetries" in it is disturbing. There are several—unfortunately equivocal—hints to where we should look for the "bare structure":

a. In theories with a cutoff, such as the Chew-Low static-meson theory, the scattering amplitude approaches that calculated by perturbation theory, with bare coupling constants, for energies much in excess of the cutoff energy.

b. In quantum electrodynamics, on the assumption that all renormalization effects are finite and the theory is not too pathological, Källén was able to prove that the form factors approach the unrenormalized perturbation-theory result at high energies. Unfortunately, this result then leads to infinite renormalization constants, so that there is a contradiction somewhere.

c. Many symmetries are destroyed by mass terms only (e.g., chirality) and, in the limit in which these can be neglected (i.e., at high energies, if at all), the symmetries should reappear.

It has been suggested by Gell-Mann and Zachariasen that "hidden symmetries" are to be looked for at high energies. When several variables are involved, such as in scattering, one must go to the high-energy limit in both the energy and the momentum-transfer variable, but in the study of form factors the high-energy limit is well defined, though it is not clear where it is reached. This topic will surely be discussed at later seminars by one or the other of the authors. I shall just "deduce," in order to illustrate the arguments, that the muon and electron form factors should approach one another at high energies.

The form factors are defined by

$$\left\langle p' \left| j_\mu^{(\text{electron})} \right| p \right\rangle = \sqrt{\frac{m^2}{p_0\, p_0'}}\; e\, \bar{U}(p') \left[i\gamma_\mu F_1(q^2) + i\sigma_{\mu\nu} q_\nu F_2(q^2) \right] u(p),$$

where $q = p' - p$,

and perturbation theory suggests that at high energies

$$F_1(q^2) >> F_2(q^2) .$$

Furthermore, at high energies the electric form factor is assumed to approach asymptotically the value Z_2, the electron (or muon) wave-function renormalization constant, as suggested by the form of the interaction $L_{int} = iZ_2 \bar{\psi}\gamma_\mu\psi \cdot eA_\mu$. Thus,

$$\lim_{q^2\to\infty} F_1(q^2/m^2) = \lim_{q^2\to\infty} Z_2(q^2/m^2) = Z_2 ,$$

and

$$\frac{F_1^{\text{elect}}(q^2/m^2)}{F_1^{\text{muon}}(q^2/m^2)} \approx \frac{Z_2^{\text{el}}(q^2/m^2)}{Z_2^{\text{muon}}(q^2/m^2)} \approx \frac{Z_2^{\text{el}}}{Z_2^{\text{muon}}} .$$

On the other hand, as pointed out by Feinberg, the ratio $Z_2^{\text{el}}/Z_2^{\text{muon}}$ must be very close to unity, because only if this is so will the ratio

$$\frac{\Gamma(\pi \to e + \nu)}{\Gamma(\pi \to \mu + \nu)} = \frac{Z_2^{\text{el}}}{Z_2^{\text{muon}}} \quad (1.3 \times 10^{-4})$$

agree with experiment. Hence,

$$\frac{F_1^{\text{elect}}(q^2/m^2)}{F_1^{\text{muon}}(q^2/m^2)} \approx 1 ,$$

even though each probably approaches zero.

S-Matrix Theory (Chew)

A third possibility, and presumably the least exciting from the point of view of a new accelerator, is that no further symmetries (conservation laws) exist, hidden or manifest, and that S-matrix theory will explain everything to be observed in the strong-interaction domain. As was clear from my seminar three weeks ago, I am personally betting on this eventuality, and commitment to such a point of view unquestionably damages one's objectivity with respect to the accelerator. In my opinion, there will certainly be many interesting experimental strong-interaction questions to be answered by an additional factor of 10 in lab energy, even if the S matrix is the whole story; but ten years from now I would expect the completeness or lack of completeness of S-matrix theory to have been established to most people's satisfaction. At present, progress in this area is very rapid, and no really basic stumbling blocks are apparent. Ten years is a long time.

Regardless of one's point of view, it may be worthwhile here to go into some details about the kind of strong-interaction experiments that should be interesting, even if no new particles or symmetries are discovered. Amati, Frautschi, Goebel, and I have considered a few of the possible implications of the peripheral approach to S-matrix theory, and have distributed among you a summary of our discussion. A related question concerns the possible quantum numbers of systems of large numbers of particles. Ken Case is making himself an expert on this subject.

Classification of general n-particle states (Case)

While it is a little premature, since I have no definite results to present, I can make a few remarks on what I have been thinking about. The program in mind is rather pedestrian but also somewhat ambitious; namely, to classify general n-particle states. The applications would be:

a. To obtain possible selection rules. While there are undoubtedly some of these, it is doubtful whether these are as definite as for Z-particle systems.

b. To find possible correlations.

c. To develop a language for the states typically arising in high-energy processes.

Mathematically, the problem is not quite so difficult as it might appear. The main problem is to reduce direct products of representations of the inhomogeneous Lorentz group. Fortunately, most of the results can be obtained by considering the three-dimensional Euclidean group. This, in turn, is rather simple, since

a. this group is a limit of the four-dimensional rotation group,

b. the four-dimensional rotation group is homomorphic to the direct product of two two-dimensional unimodular unitary groups—about which we know all.

As a result of these "accidents" it is expected that a rather complete classification of n-particle states should be simple to obtain.

Oppenheimer's View of the Strong-Interaction Picture (Chew)

So as not to leave the strong-interaction picture on a low note, let me quote from a resumé by Oppenheimer of a discussion held last fall at Rochester on exactly the same subject as our summer study.

"The clearest reason for a super-high-energy machine is the same reason that motivated the present generation of accelerators, from the Gev electron synchrotrons, the electron linac, and the Cosmotron to the 30-Gev A.G. synchrotrons in Brookhaven and Geneva: we do not know what we shall find, what finer structure of matter, what new heavier ingredients. There are some new points.

"(1) In the past, cosmic rays were enough to reveal, but not fully to describe, new particles and new processes. This is not happening today, and one can hardly be confident that it will, for new particles will probably be too short-lived and new processes too rare.

"(2) Our description of nuclear and subnuclear physics is incomplete, full of arbitrary and ununderstood numbers and parameters, and wide open; there appear to be essential clues that are missing, buried in high-energy phenomena. Such are the nucleon 'core,' the masses of the 'elementary particles,' the interaction constants themselves.

"(3) Highly unstable heavy particles will probably be found. Stable, or relatively stable, new particles, with new quantum numbers, may be analogous for the baryon-meson system to the μ meson in relation to the electron.

"(4) Today, we do not in any real sense understand the nuclear and subnuclear world. We think it likely that essential novelty will appear at the 'super-high energies' that will promote this understanding. We are confident that a knowledge of what does in fact occur in this domain will take us a long way toward this understanding."

Oppenheimer, at least, does not share my feelings about the S matrix.

Smith:

Would you care to comment on the statement by Van Hove that he would rather see a very-high-intensity machine constructed, even if it had no higher energy than about 50 Gev?

Chew:

From what I have heard of the estimated intensity of the proposed 300-Gev machine, it seems more than adequate.

Goldhaber:

Experiments as yet unknown to us may require higher intensity.

Amati:

I understood Dr. Kerth to say that the proposed 300-Gev machine would have a very high intensity when operated at about 50 Gev.

Johnsen:

The increase in intensity to be realized as the energy is dropped is not simply inversely proportional to the energy. It depends on the injector, which would have to run at the higher repetition rate without the corresponding drop in energy.

Blewett:

When the energy, and therefore the circumference, is increased by a factor of 10, you may have 10 times as many particles per pulse at the full energy, if the injector can provide them. Thus, one may have 10^{13} particles per pulse at 300 Gev.

Cocconi:

In addition to this, the intensity of the secondary beams is increased by a factor of 10 in going from 30 to 300 Gev because of the flux concentration in the forward direction.

Weak Interactions (Chew)

We have heard a survey by Dombey of various neutrino beam experiments. The impression I got was that all but the qualitative measurements are out of reach with techniques presently available or on the horizon. What are the qualitative questions so far recognized?

1. Does the increase ($\propto E_{lab}$) with energy of weak-interaction cross sections—predicted by the Fermi theory—actually occur? Even if this question is partially answered by the 30-Gev accelerators, it seems likely that another factor of 10 in energy will be of interest.

Dombey:

It is not obvious that an increase of 10 in lab energy will help matters considerably. In neutrino-lepton collisions, and with the lowest-possible-mass intermediate boson, a neutrino lab energy of 250 Gev is necessary to determine the deviations from the four-point interaction. In neutrino-nucleon interactions structure effects, which cut down the spectacular increase in cross section with energy, are present anyway. However, it is possible that, with storage rings, nucleon-nucleon interactions of approximately 100 Gev (c.m.) may show weak effects. For example, parity-violating effects may well be much more important at these energies.

Bludman:

At 600 Gev in the center-of-mass system, the weak interactions may be strong.

Greenberg:

Have storage rings been considered?

Smith:

Not very seriously. Since each ring has a 5-mile circumference, the specifications for the construction site become more severe, and the technical problems formidable.

Chew:

2. Are there two kinds of neutrinos? This question probably will be settled by the 30-Gev machines.

3. Is there an intermediate vector boson (W particle) and, if so, what is its mass? Should the mass turn out to be several Gev, it would be missed at CERN and Brookhaven but might be found with the accelerator we are discussing. In this connection, it may turn out that the photon beam is a more effective source of W particles than the neutrino beam. This possibility will be discussed next week by Bludman and Wong.

Blewett:

Will it be possible to search for Dirac monopoles?

Bradner:

We still have no idea of the mass, but the currents mentioned for the proposed 300-Gev machine are ample to set a new lower limit on the mass.

Electromagnetic Interactions (Chew)

Since time has run out, we shall defer this topic until the seminar by Frautschi and Masek next week on muon experiments.

14. INTERACTION OF 11.3-Gev PIONS WITH PROTONS

William B. Fretter

July 17, 1961

Introduction

The work described here is still in progress and the present report should be understood as an indication of what might be done rather than a report on definitive results. My collaborator in this work is Peter Hoang.

The idea of the experiment was to use the fact that π^0 mesons could often be observed coming from nuclear interactions as a useful additional tool in the analysis of the multiple-production process. As the experiment developed, we have attempted to interpret the results in terms of the one-pion exchange model (OPE model), pushing this model to the very limit of its applicability.

Apparatus

The detector was the propane-freon chamber of the École Polytechnique, built by a group under the direction of A. Lagarrigue. The chamber has the approximate inside dimensions of 1 meter × 50 cm × 50 cm, and is rectangular in shape. During November 1960, the chamber was exposed to pion beams at CERN, Geneva, having energies of 6, 11.3, and 17.8 Gev. Approximately 30,000 photographs were taken at 6 Gev, 30,000 at 17.8 Gev, and 11,000 at 11.3 Gev. We chose to study the 11.3-Gev photographs because of the relatively easy measurements possible. Other groups in Paris, Geneva, Turin, Milan, and Padua are also working with the photographs, at the various energies, studying the production of pions and strange particles.

The chamber contained a mixture of propane (86%) and freon (14%), giving a density of 0.55 and a radiation length of about 70 cm. It was in a magnetic field of 17.1 kilogauss.

Measurement Procedure

Nuclear interaction events were selected for measurement which fulfilled the following criteria:

1. Events occurring in a limited region near the entrance aperture to the chamber were measured. This selection made possible simple optical corrections, and gave a long path for materialization of γ rays produced in the decay of π^0 mesons.

2. Events satisfying the usual criteria for interactions of negative pions with protons were measured. These included balance of charge, lack of evaporation prongs in the event, and certain dynamic criteria.

It was important, however, not to confuse the struck proton in a peripheral collision, which often imparts little momentum to the proton, with evaporation prongs from an excited nucleus.

If more than one such positive heavy particle was present, the event was rejected. Thus, there is a background among the events measured which consists of interactions on protons on the periphery of a nucleus. These are complicated by the Fermi motion of the proton in the nucleus. However, we believe that the main features of these high-energy interactions are not seriously affected by this, and the advantage of seeing the π^0 γ rays with good probability outweigh at this stage the uncertainties due to the bound protons.

The measurements were made by hand on the scanning table, and track reconstructions and Lorentz transformations were done graphically, wherever possible. Calculations have been repeated by use of a simple IBM program.

Experimental Results

We measured systematically 110 events which satisfied our criteria. The average multiplicity of charged particles in these events was 4.0 ±0.2 (in agreement with results in the 30-cm hydrogen chamber at CERN) with pions of 16 Gev. Among these 110 events were 27 in which we were able to identify the proton, either by its stopping in the chamber or by its ionization, which is adequate for identifying protons up to about 1.3 Gev/c momentum.

Measurements were also made on 18 additional events in which the proton was identified.

The distribution of momentum of the identified protons is, within statistical accuracy, consistent with the momentum distribution obtained by the British group at CERN by analyzing the interactions of 16-Gev negative pions in the 30-cm hydrogen bubble chamber, except at low momenta where the range of the proton is less than 3 mm in our chamber.

The conventional display of results in such an experiment as this would involve giving angular and energy distributions of the events in the laboratory and c.m. systems, and attempting to interpret these distributions in terms of a theoretical model. Rather than do this, we first categorize the various events in terms of the OPE model, and then give results in each category, looking for regularities in the distributions.

The assignment to categories is never certain, owing to the lack of certainty in detection of π^0 mesons. In each case, we have assigned the event to the most reasonable category. The events in which the proton was identified have been much easier to categorize than the others, and the present paper deals only with those.

The basis for assignment to categories is the angular distribution of particles in the c.m. system. Consider, for example, the process of Fig. S14-1.

If the negative pion emitted from the proton vertex has relatively low energy—i.e., the nucleon excitation energy is not too high—this pion goes backward in the c.m. system whereas

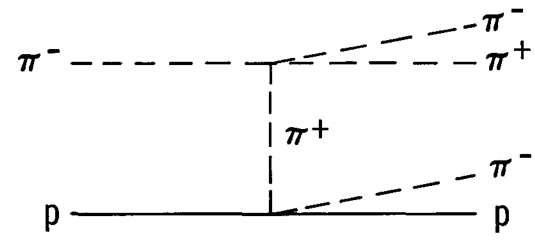

Fig. S14-1

the other two pions go forward in the c.m. system. Thus, we take particles going forward in the c.m. system as coming from the pion vertex, and those going backward in the c.m. system as coming from the proton vertex. No subtleties such as multiple centers of production along the virtual pion line are considered here.

Using this simple procedure, we have divided the events with the identified proton according to the number of negative particles observed, and then according to the OPE model which seems the most reasonable. The categories are indicated and labeled in Figs. S14-2, -3, and -4, and the data given in Table S14-I.

Discussion

It is obvious that each category contains an insufficient number of events for us to draw quantitative conclusions. There are, however, certain qualitative and semiquantitative comments to be made.

Proton Momenta

Since these events are selected according to the fact that the proton was identified, and therefore had low momentum, it is a biased selection. However, the proton momentum—or the value of Δ^2, the four-momentum transfer to the proton—seems not to depend much on the category. The predominance of low momentum transfers is shown, however, by the following argument. In the unbiased sample of 110 events, 27 involved stopped or identified protons, hence low momentum. Most such cases involve exchange of a π^0 meson. The probability of a proton's emitting a virtual π^+ meson is twice as large as the probability of its emitting a π^0

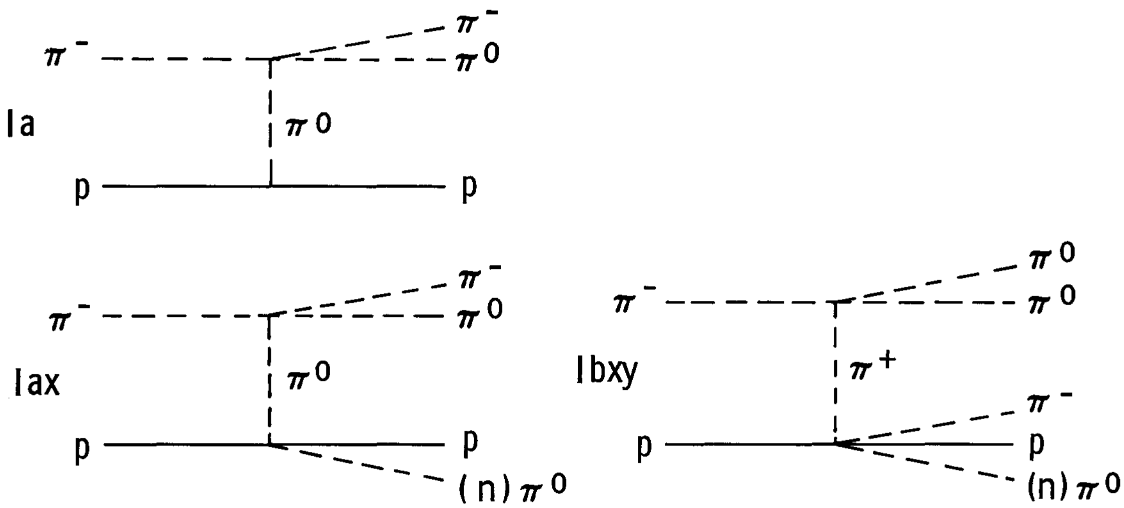

Fig. S14-2. Categories of one-negative events observed (9 events).

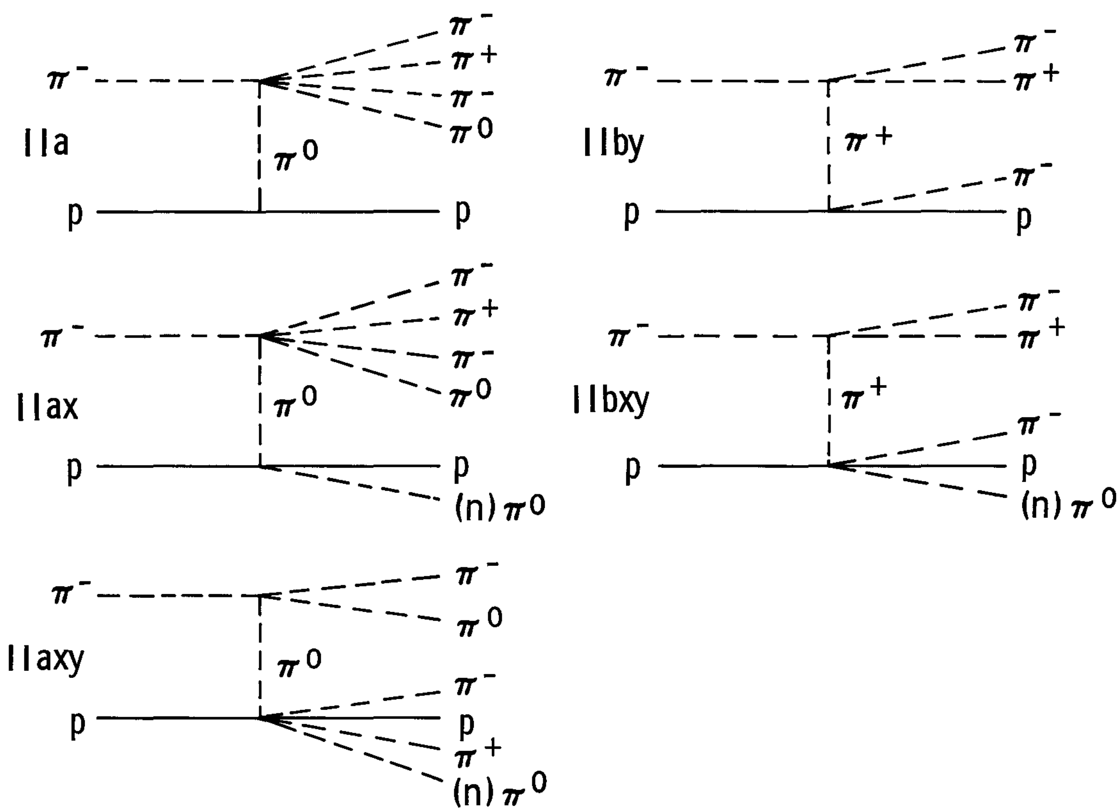

Fig. S14-3. Categories of two-negative events observed (26 events).

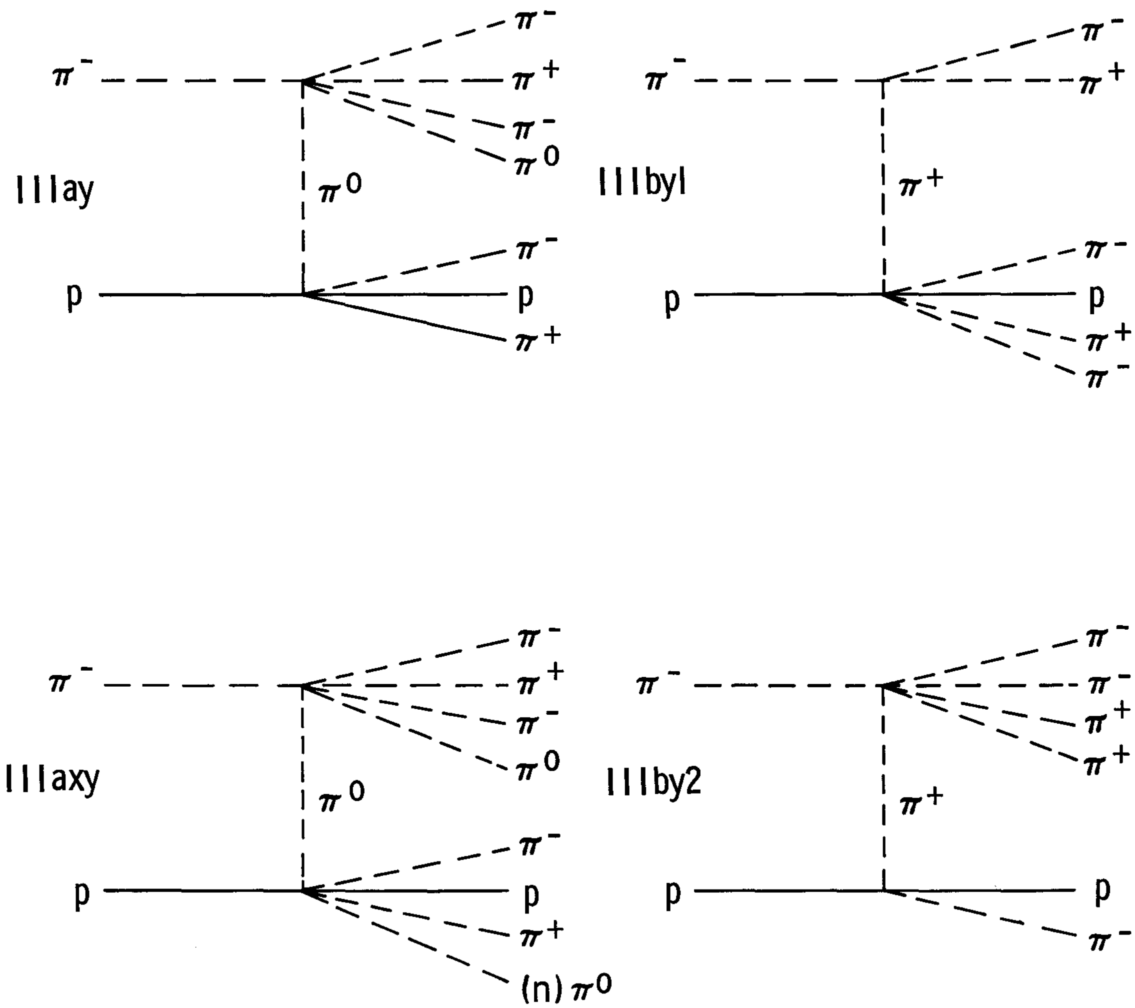

Fig. S14-4. Categories of three-negative events observed. Three additional events were observed which could not be classified in the OPE model. Two four-negative events were observed; neither could be classified reasonably.

Table S14-I

Momenta in Gev/c (lab)

Category	Picture No.	No. of γ's	Σp_ℓ	p_{prot}	p_{π^-}		K_p	K_{π^-}	Δ^2_p
Ia	306610	2	10.9	0.44	6.7		0.09	0.41	0.184
	306774	1	12.8	0.44	12.3		0.01	-0.10	0.184
	306794(b)	1	9.9	0.19	9.5		0.20	0.13	0.035
	307735	1	10.2	0.36	9.5		0.09	0.14	0.125
	307871	1	10.2	0.78	7.4		0.56	0.36	0.529

Table S14-I (cont'd.)

Category	Picture No.	No. of γ's	Σp_{ℓ}	p_{prot}	$p_{\pi-}$			K_p	$K_{\pi-}$	$\Delta^2 p$
Mean values				0.44	9.1			0.19	0.19	0.211
Iax	306373	4	9.8	0.43	4.6			0.31	0.61	0.172
	307712	4	8.7	0.16	5.5			0.19	0.53	0.025
	310052	4	4.2	0.36	1.8			0.42	0.87	0.125
Mean values				0.31	4.0			0.31	0.67	0.107
Ibxy	307008a	6	10.9	0.21	0.54			0.27	0.97	0.044
						$p_{\pi+}$	$p_{\pi-}$			
IIa	305958	2	10.4	0.41	5.6	1.2	2.2	0.28	0.51	0.159
	306255	2	11.8	0.37	5.1	3.9	0.55	0.36	0.33	0.129
	306660	2	11.7	0.15	3.5	5.9	1.0	0.12	0.72	0.023
	306860	0	11.1	0.36	5.1	1.6	3.4	0.05	0.57	0.122
	307120	0	7.9	0.87	3.1	1.4	2.8	0.46	0.74	0.645
	307645	1	10.8	0.54	5.0	1.5	2.2	0.05	0.57	0.266
	307767	0	11.4	0.13	4.3	3.9	3.3	0.08	0.66	0.016
	307847	0	12.2	1.26	6.7	0.62	4.3	0.09	0.38	1.190
	310615	2	10.1	1.42	3.9	2.2	2.2	0.16	0.69	1.430
Mean values				0.61	4.7	2.5	2.4	0.18	0.57	0.440
IIax	306863	2(+)	9.3	0.48	6.2	0.96	1.1	0.40	0.43	0.217
	307095	3	5.2	0.45	1.3	0.66	1.3	0.00	0.93	0.433
	307252	5	12.0	0.74	5.0	1.3	2.7	0.74	0.53	0.482
	310127	4	11.6	0.30	3.0	2.2	1.6	0.11	0.76	0.088
	310192	3	11.2	0.14	4.1	2.2	3.3	0.04	0.62	0.019
Mean values				0.40	3.9	1.5	2.0	0.26	0.65	0.248

Table S14-I (cont'd.)

Category	Picture No.	No. of γ's	Σp_{ℓ}	p_{prot}	$p_{\pi -}$	$p_{\pi +}$	$p_{\pi -}$	K_p	$K_{\pi -}$	$\Delta^2 p$
IIaxy	305832	2	7.8	0.48	3.5	1.79	0.22	0.13	0.72	0.210
	306335	0	10.9	0.52	9.5	1.12	0.34	0.44	0.16	0.251
	306869	0	4.3	1.03	2.5	0.70	0.09	0.83	0.81	0.852
	307117	4	7.7	0.41	1.6	0.85	0.32	0.25	0.84	0.161
	310044	2?	9.8	0.36	8.7	1.39	0.08	0.00	0.24	0.125
	305364	0	9.1	0.56	8.6	0.12	0.10	0.59	0.25	0.290
Mean values				0.56	5.7	1.0	0.19	0.37	0.50	0.314
IIby	306163	0	12.2	1.30	9.4	1.11	1.05	0.91	0.17	1.240
	307008b	0	10.1	0.13	8.4	1.51	0.41	0.05	0.22	0.016
	307799	0	11.1	0.38	9.5	1.09	0.51	0.00	0.16	0.139
	310239	0	10.1	0.82	6.3	3.36	0.82	0.65	0.40	0.574
Mean values				0.66	8.4	1.77	0.70	0.40	0.24	0.492
IIbxy	306291	2	8.8	0.60	6.4	1.40	0.41	0.65	0.45	0.326
	307017	1	8.3	0.44	1.3	6.2	0.19	0.30	0.93	0.180

Category	Picture No.	No. of γ's	Σp_{ℓ}	p_{prot}	$p_{\pi -}$	$p_{\pi +}$	$p_{\pi -}$	$p_{\pi +}$	$p_{\pi -}$	K_p	$K_{\pi -}$	$\Delta^2 p$
IIIay	306983	0	10.3	0.30	1.16	7.3	1.12	0.24	0.60	0.08	0.93	0.087
IIIby1	306351	0	10.8	0.43	6.7	3.3	0.52	0.21	0.45	0.22	0.37	0.176
IIIby2	306644	0	11.2	0.51	7.0	0.96	2.08	0.78	0.31	0.34	0.40	0.244

meson. Hence, there were roughly 2 × 27 = 54 cases in which a low-momentum neutron emerged, leaving 110- (54 + 27) = 29 cases in which the nucleon had momentum above 1.3 Gev/c. Thus, roughly three-fourths of the pion-proton events at 11 Gev are peripheral, involving a small momentum transfer to the nucleon.

Proton Inelasticity

A related quantity is the proton inelasticity K_p. This is defined as $K_p = (T_a - T_{c.m.})/T_a$, where T_a is the kinetic energy of the proton in the c.m. system before the collision, and $T_{c.m.}$ is the kinetic energy of the proton in the c.m.

system after the collision. The average value of K in the various categories ranges from 0.19 to 0.40 and the overall average is 0.28.

π^- Inelasticity

A similar quantity was calculated for the highest-energy π^- in the laboratory system. The average value of this quantity is 0.50 for all events listed. Variations between categories are noticeable, however. When only two particles are produced at the pion vertex, the negative pion is usually the more energetic particle in the laboratory system; it appears to retain its identity just as the baryon does. Occasionally, events are observed in which the struck virtual pion gains high energy, either as a positive or as a neutral pion; this seems to be the exception, however. (Category IIby shows this clearly.) Even in the two-negative events, category IIa, note that the second π^- has the same average energy as the π^+ produced forward, suggesting retention of the negative charge on the incident negative pion.

Mean Values

Mean values in certain categories may be misleading. For example, category IIaxy seems to contain two subcategories, with either quite high or quite low energies for the first (highest-energy) negative pion.

Primary Momentum

Although there are only a few events with three or four negative particles, it seems clear from those observed that 11 Gev/c is too low a primary momentum to separate clearly the two vertices in these events. Three-negative events may be separable in the 18-Gev events, but it is clear that considerably higher-energy pions will be required to investigate higher-multiplicity events by this method. Even at 11 Gev and with two-negative events, some mistakes in classification are possible.

Conclusion

The method outlined shows promise of clarifying the process of multiple production of pions. It makes possible the separation of the $\pi - \pi$ interaction from the process in which the nucleon becomes excited by emitting or absorbing a virtual pion. It depends, to a large extent but not entirely, upon the ability to detect the γ rays that are produced from π^0-meson decay, and upon the fact that an even number of pions must be emitted from a pion-pion vertex. Because this rule does not hold at the proton vertex, and because the chamber is less efficient in the detection of γ rays emitted at large angles, the method is not quantitative with regard to the proton vertex.

15. PART I. MUON BEAMS FROM A 300-Gev ACCELERATOR AND THEIR APPLICATION TO MUON-PROTON SCATTERING AND THE PROCESS $\mu + p \to \nu + N$.

George F. Masek

July 18, 1961

Introduction

It is the purpose of this report to estimate the magnitude and quality of muon beams that might be expected from the proposed 300-Gev accelerator, and to apply these beams to several experiments that might be of interest. In particular, we look at the yields from elastic muon-proton scattering and also those from the weak interaction process $\mu + p \to \nu + N$. Detailed analysis of experimental arrangements is not attempted; rather, counting rates are estimated and possible experimental difficulties are outlined.

The principal conclusions of this report are:

a. Muon beams of relatively high intensity (10^5 to 10^9 muons per Gev per 10^{12} protons over an area of about 300 cm^2) and high energy (20 to 50 Gev) are available;

b. these beams will allow investigation of momentum transfers in μ-p elastic collisions to about 13 Gev/c (about three times that available to the proposed Stanford 15-Gev electron accelerator), and will allow rather accurate comparison experiments between e-p and μ-p elastic scattering; and

c. if the proton current can be increased to 10^{13} protons per pulse, the yields for experiments that investigate the weak-interaction process $\mu + p \to N + \nu$ seem reasonable.

Muon Beams

Pion decays in flight are the source for the muon beams, and a sketch of a "one-quadrupole" beam is shown in Fig. S15-1. Kaons, because their mean life is about half that of pions, might seem a better choice. However, the number of kaons in high-energy collisions is about 15% of the pions. Further, the decay cone is much larger for the same energy, and hence the focusing problems become more severe. To estimate the pion fluxes that might be available from a 300-Gev accelerator, we have used the relation (Report 6 in the APG Reports)

$$\frac{d N_\pi}{d\Omega\, d E_\pi} = \frac{n}{2\pi\, p_0^2\, T} E_\pi^2\, e^{-E_\pi (1/T + \Theta/p_0)} ,$$

where $n = 1.28\, E_p^{1/4}$, $T = 0.293\, E_p^{3/4}$, $p_0 = 0.18$, and E_p is the primary proton energy. This has been derived by fitting the yields from the Brookhaven AGS and assuming that n and T scale as above. The relation gives rather good agreement when tried with AGS angles other than the one chosen for evaluating the constants. It should be noted that the 0° agreement with the CERN data[1] is very poor, and, similarly, the 0° Ticho results[2] do not agree. In Fig. S15-2 are shown the results of integrating this expression, from 0° out to an angle Θ, for $E_p = 300$ Gev. The most striking feature is that almost all the beam, even at quite low energies (approximately 50 Gev), is contained within a very small angle (approximately 8×10^{-3} radian). Accordingly, we have designed the muon beam in the following way. We select a muon-beam size determined by the decay angle—which also permits a reasonable experimental setup. This is chosen to be 20 cm. We choose the quadrupole aperture a to be of this diameter also. The quadrupole will focus a momentum spread in such a way that the highest momentum focuses at infinity, and the lowest, at one-half the distance from the quadrupole to the scattering region. The distance ℓ between the machine target and the quadrupole is chosen so that 80% of the beam

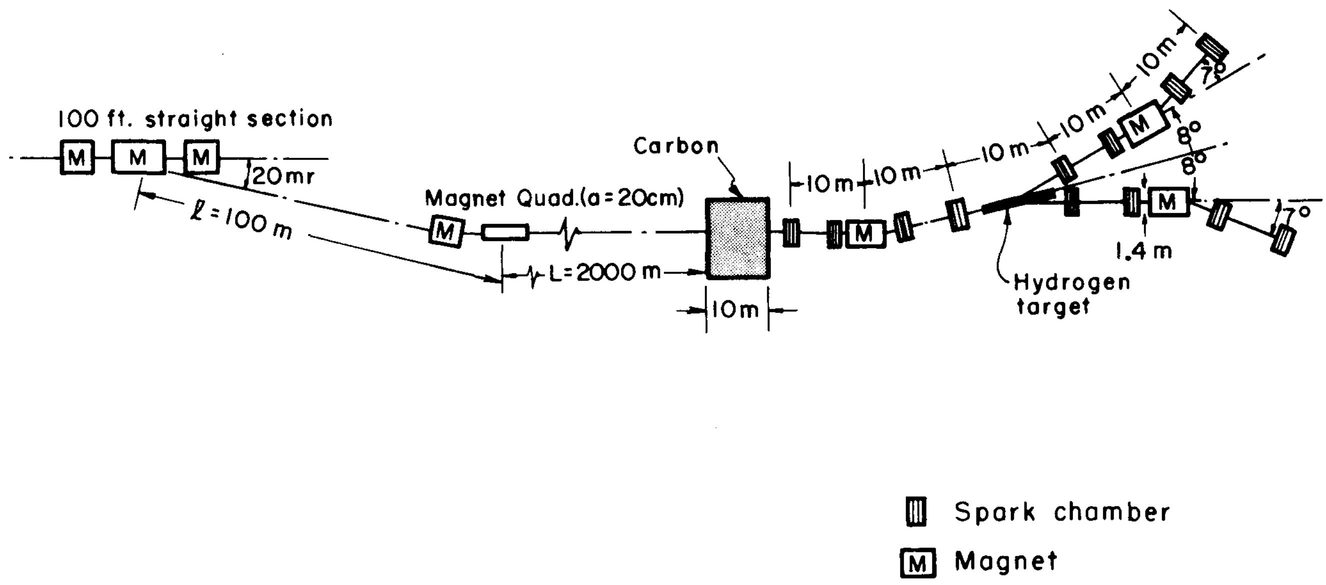

Fig. S15-1. Setup for a "one-quadrupole" beam.

(at a pion energy E_π) is contained by the 20-cm quadrupole aperture, i.e., $\ell = a/2\Delta\Theta_{80\%}$. A magnet is placed between the target and the quadrupole to remove the dispersion introduced by the machine. Given ℓ and the requirement on the momentum focusing, the distance L is determined from the relation $L = 2(\ell/f)$, where f is the momentum fraction $\Delta p/p$ accepted. One further condition must be imposed: the fraction of pions, F, that will decay in the length L is $F = L/\ell_\pi$, where ℓ_π is the mean decay length for the pions. Although the product Ff is independent of L, an acceptance of large momentum results in additional loss, since the pion yield falls off rapidly with energy (i.e., $e^{-E_\pi/T}$). Conversely, a large L is expensive in real estate. We have chosen $\Delta p/p$ to be 0.20 for $E_\pi = 200$ Gev, and 0.10 for the lower energies. These quantities, together with the other parameters discussed above, are summarized in Table S15-I. Also in Table S15-I are given the corresponding pion yields (using the results of Fig. S15-2), muon yields per Gev, and, finally, the maximum muon-decay angle.

The beam outlined here is the simplest design. Improvements could be made by using one of the multiple-quadrupole systems that have been discussed (e.g., Citron[3]). One might expect to contain the beam for longer distances—but this probably would be useful only at the lower energies, since the lengths at higher energies are already prohibitive. Also, one might be able to contain a slightly larger momentum spread and confine it to smaller apertures—but, again, these would not be a great improvement. Actually, the beam spread may be desirable; since the number of particles passing into the experimental region will be of the order of 10^8 to 10^{10} per pulse, this will be extremely difficult to resolve with single counters, and a spread-out array may be needed.

In summary, the main points concerning the muon beam are:

a. one needs large distance to allow for the decays (approximately 2000 m for the higher energies).

b. once one has accepted the large distances (and a vacuum system to go with it—e.g., the multiple scattering at atmospheric pressure would diverge the beam to about 10 m diameter

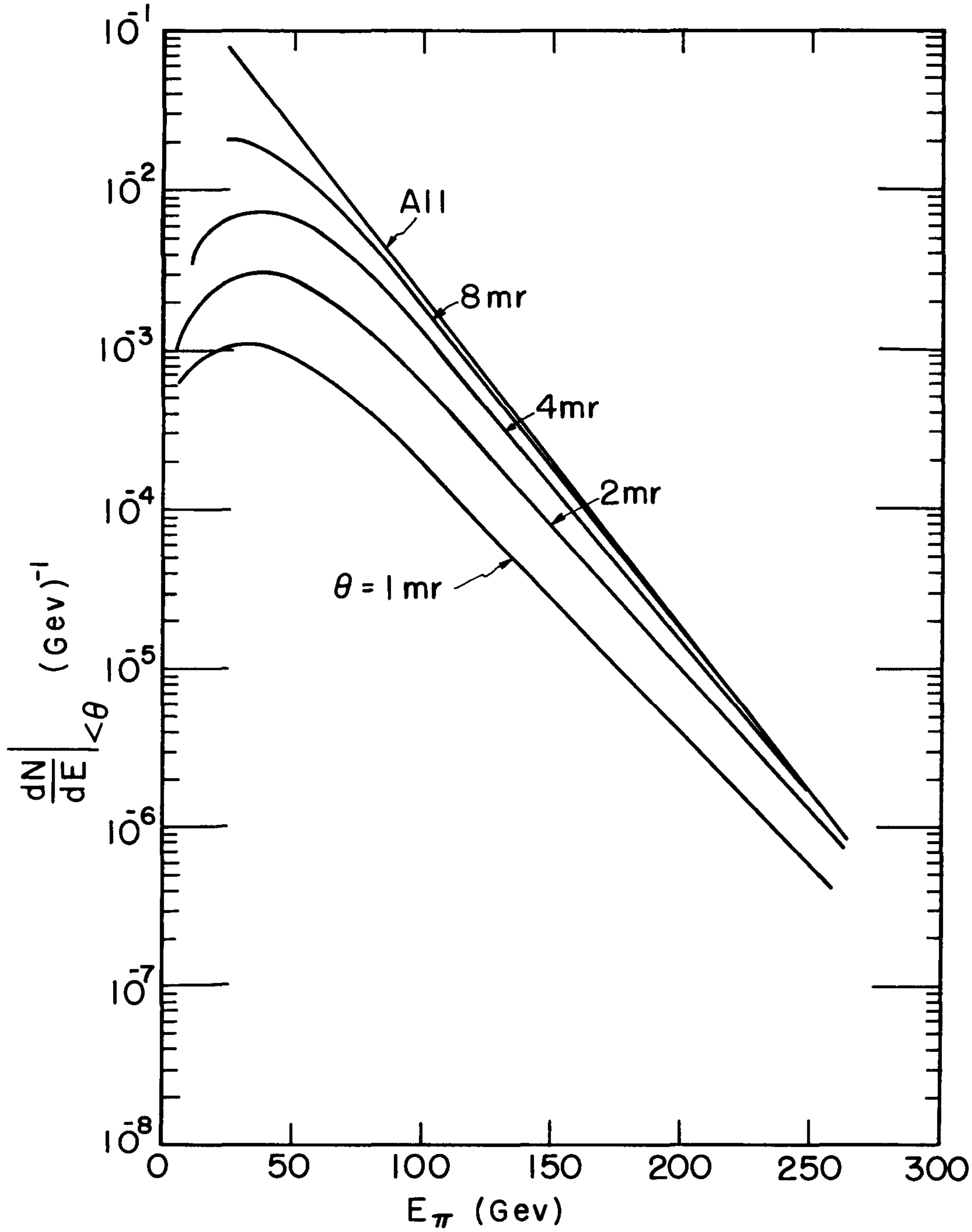

Fig. S15-2. $\left.\frac{dN}{dE}\right|_{<\Theta}$, yield of all π^+, π^-, π^0 pions for angles from $0°$ to Θ vs E_π per incident proton of 300 Gev.

Table S15-I.

E_π (Gev)	$\theta_{80\%}$ (mrad)	ℓ (m)	Bend angle, θ (mrad)	Effective $\Delta p/p$ accepted	L (m)	ℓ_π (m)
220	2	200	10	0.20	2000	13200
105	4	100	20	0.10	2000	6600
53	8	50	40	0.10	1000	3300
26	16	25	80	0.10	500	1600
13	32	13	160	0.10	250	800

E_π (Gev)	Resolution factor	(a) $\frac{dN}{dE_\pi}$ per Gev	(a) N_π	E_μ (Gev)	(a) $\frac{dN_\mu}{dE_\mu}$ per Gev	$\frac{1}{2}\theta$ (mrad)
220	0.37	1.8×10^6	3.8×10^7	200	3.2×10^5	0.2
105	0.46	2.6×10^8	1.4×10^9	100	2.5×10^7	0.4
53	0.49	4.0×10^9	1.1×10^{10}	50	4.0×10^8	0.8
26	0.50	1.3×10^{10}	1.8×10^{10}	25	1.3×10^9	1.6
13	0.50	2.0×10^{10}	1.3×10^{10}	13	1.8×10^9	3.2

(a) Assumes 10^{12} protons per pulse.

for the 50-Gev beam), the muon fluxes are quite large.

c. the beam diameter is due primarily to the large-momentum band pass in the pion beam (approximately 20 cm for the beams outlined here).

To see how large these fluxes are, we may compare them to the electron beams obtainable from the proposed Stanford 15-Gev electron accelerator. At about 10 Gev, the above numbers show that we may expect 0.6×10^9 muons per second into a 10% momentum spread. For Stanford's machine, the electron current is expected to be approximately 6×10^{13} into a 0.5% spread. However, one should compare not just the particle fluxes but also the product of the flux times the "usable proton targets." If one uses a 1-g/cm^2 hydrogen target (Cassel's report on e-p scattering[4]) with electrons, they will be spread 2% in momentum owing to radiation. The limitation on hydrogen targets for the muon beams is one of practical lengths which can be used in experiments; for the μ - p scattering outlined in Section 2, a target of 70 g/cm^2 has been assumed. Thus, the ratio

$$\frac{N_\mu\ (\Delta p/p = .02) \times \text{Number of target protons available to muon experiment}}{N_e\ (\Delta p/p = .02) \times \text{Number of target protons available to electron experiment}} \approx 10^{-4},$$

which clearly shows that muons cannot compete with electrons when counting rates are the dominant factor.

Muon-Proton Elastic Scattering

We now look at the elastic scattering of muons on protons with these beams. Of primary interest is the question: How high a momentum transfer can be investigated with reasonable counting rates?

The kinematics for the process are shown in Fig. S15-3. One sees that both the recoil angle and the scattering angle are peaked strongly forward for practically all regions of interest. The implication is that angular determinations, in themselves, are not good criteria for elastic scatterings. But, because the particles are peaked forward, one may expect to make momentum analyses on both particles with a reasonable solid-angle acceptance at the spectrometer. For example, if a pion is created in the scattering process and it remains at rest in the c.m. system, the following table gives the change in angle expected for the muon and proton with respect to elastic scattering; also shown is the change in their outgoing energies E':

Particle	q	E	Θ	$d\Theta/\Theta$	$\frac{dE'}{E'}$
recoil proton	7	50	10°	2.5×10^{-4}	0.0135
scattered muon	7	50	12°	5.0×10^{-6}	0.0135

The case of the pion at rest in the lab system leads to a dE'/E' of approximately 0.005, and even smaller for the higher energies. Thus, the changes in angles are much too small to be detected, while the changes in momenta offer a reasonable chance of detection. Even the detection of coplanarity is difficult, e.g., if the pion has transverse momenta of the order of $m_\pi c$, the muon will be noncoplanar by $\approx \frac{m_\pi c}{p'_\mu} \approx 5 \times 10^{-3}$ rad.

To examine this problem in greater detail, one must look at the actual cross sections for electromagnetic pion production and thereby ascertain to what extent truly elastic scattering can be measured.

The cross section for the elastic scattering at small angles can be written in the form

$$\frac{d\sigma}{dq} = 8\pi\, r_0^2 \frac{m_e^2}{q^3} (1 - x)\, F_1^2 \left(1 + 1/2\, \frac{x^2}{1 - x}\right),$$

where r_0 is the classical electron radius, q is the four-momentum transfer, m_e is electron mass, $x = \frac{q^2}{2EM}$, M is the proton mass, and E is the incident muon energy (c = 1). Also F_2 has been set equal to zero, and in the evaluations that follow, F_1^2 has been set equal to a constant value of 0.17. If one wishes to use other form factors, it is a simple matter to scale the final numbers by an appropriate factor.

The cross sections shown in Fig. S15-4 and the muon beams given in Table S15-I have been used to compute the yields for elastic scattering, as shown in Fig. S15-5. It is assumed that the target consists of 70 g/cm^2 of hydrogen, and that no factors have been included for spectrometer efficiency, i.e., that these are the total yields into dq = 1 Gev from a beam width ΔE_μ = 1 Gev (these intervals represent the order of magnitude of the parameters dq and ΔE_μ that can be measured simultaneously in a single experimental setup).

The yield that might be expected in an actual experimental arrangement has been estimated for the setup shown in Fig. S15-1, with E_μ = 100 Gev. Here, we also show a 10-meter carbon absorber which reduces the pions to one part in 10^8 of the muons and which allows these cross sections to be measured with negligible pion interference. Three analyzing magnets (one for the incident muons, one for the scattered muons, and one for the recoil protons) are shown together with their associated spark chambers which, in principle, would allow momentum determinations of the order of 0.3%. Assuming 10-cm gaps for downstream magnets, and the geometrical arrangement shown in Fig. S15-1, the solid-angle acceptance is about 10^{-3} sr.

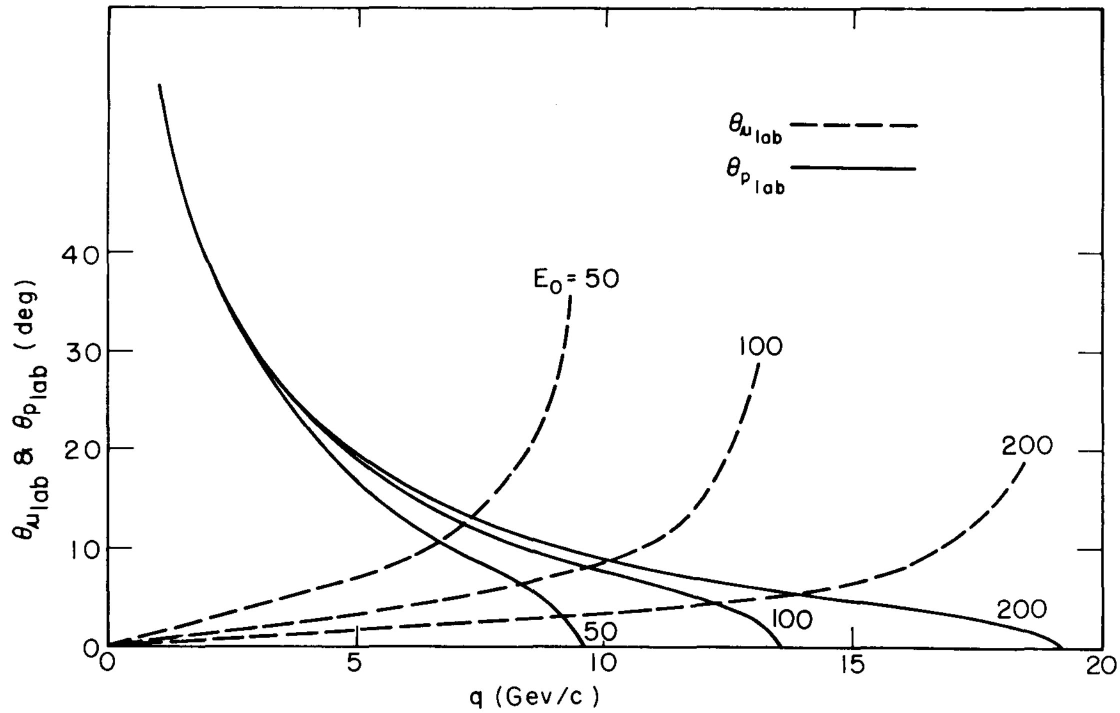

Fig. S15-3. Muon-proton scattering kinematics (elastic): $\Theta_{\mu\ \mathrm{lab}}$ and $\Theta_{\mathrm{p\,lab}}$ vs q .

These magnets will accept a dq $\approx$ 1 Gev/c, giving a yield of about one count per hour for q's between 9.5 and 10.5 Gev/c. Thus, measurements of q's up to 10 Gev, and probably up to 13 Gev/c, can be made with 5% to 10% statistical accuracy, and with momentum determinations sufficient to distinguish elastic scattering. Further, Fig. S15-5 shows that, in general, to measure a particular q, it is best to use the lowest-energy muons which still give reasonable forward angles for this q. Figure S15-5 probably overemphasizes the difference in yields for different E's and the same q, since $d\sigma/dq$ is shown instead of $d\sigma/d\Omega$. Using $d\sigma/d\Omega$ would introduce an E^2 into the numerator of the cross section expression and, hence, help the higher energies. However, this solid-angle factor for higher energies may be reduced somewhat, if we assume that, to get the necessary momentum accuracy, we must push the analyzing magnets to their limits—in which case, for example, to get the same momentum accuracy, we would have to reduce the magnet gaps for the higher energies.

In summary, we list the main features of the μ -p elastic scattering:

a. Cross sections with momentum transfers of the order of 13 Gev/c can be measured with 5 to 10% statistical accuracy and with sufficient momentum accuracy to define elastic scattering, assuming $F_1^2 = 0.17$ and $F_2 = 0$. These momentum transfers are about three times those obtainable with Stanford's proposed 15-Gev machine.

b. Muon experiments to compare muons and electrons at q's of approximately 5 Gev/c are quite easy from the standpoint of counting rate.

c. Muon experiments to explore the proton form factor in the region of q $\approx$ 5 Gev/c cannot compete with similar electron experiments.

d. For a given q which is available with a number of different $E\mu$'s, it is best, from the standpoint of counting rate and probably the ease of the experiment, to use the lowest possible $E\mu$.

Yield for the Process $\mu + p \rightarrow \nu + N$

The weak-interaction process $\mu + p \rightarrow \nu + N$ has been suggested as another method for investigating the weak interactions at high energies.

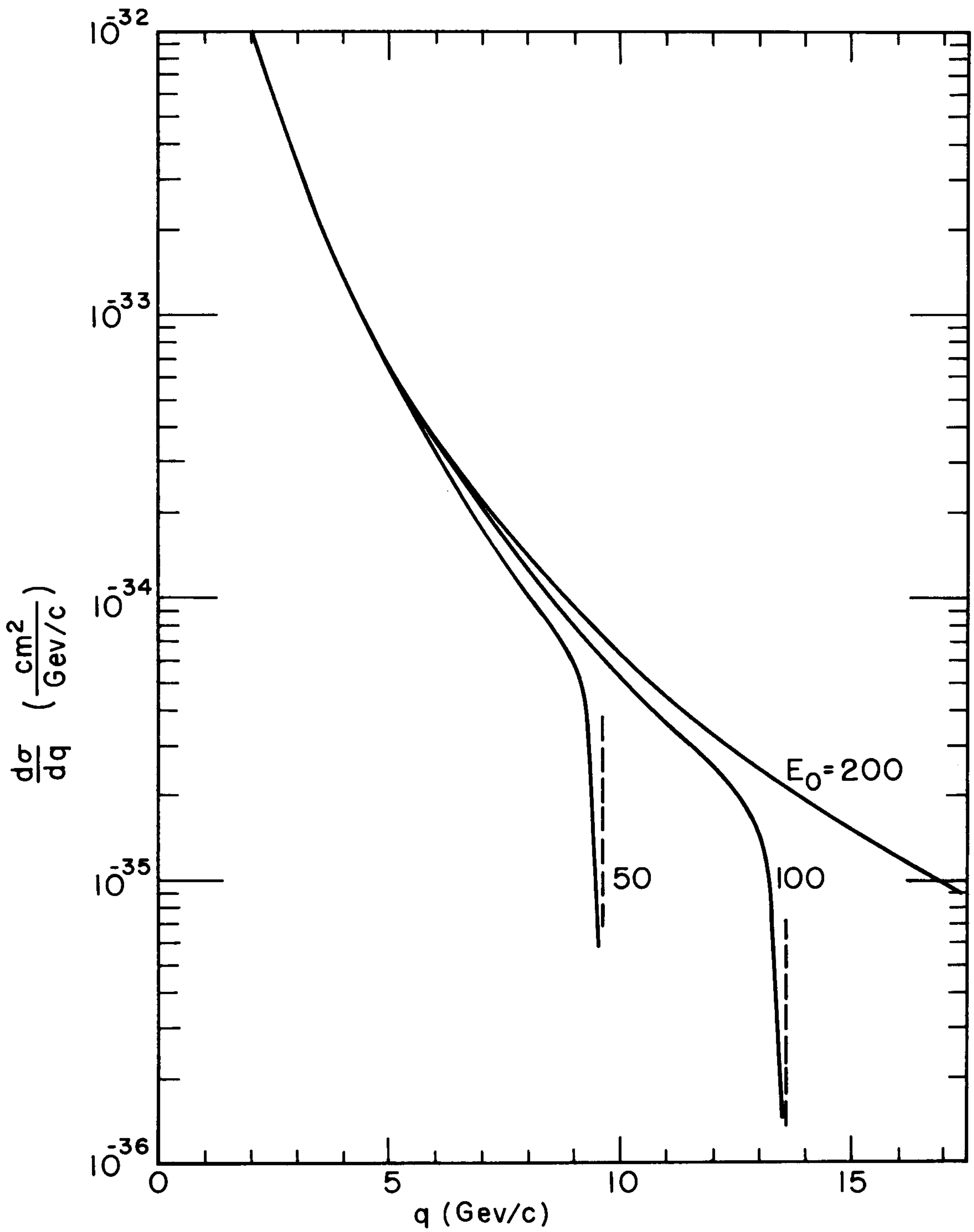

Fig. S15-4. Muon-proton elastic scattering; $\frac{d\sigma}{dq}$ vs q; assumes F_1^2 = constant = 0.17, $F_2^2 = 0$.

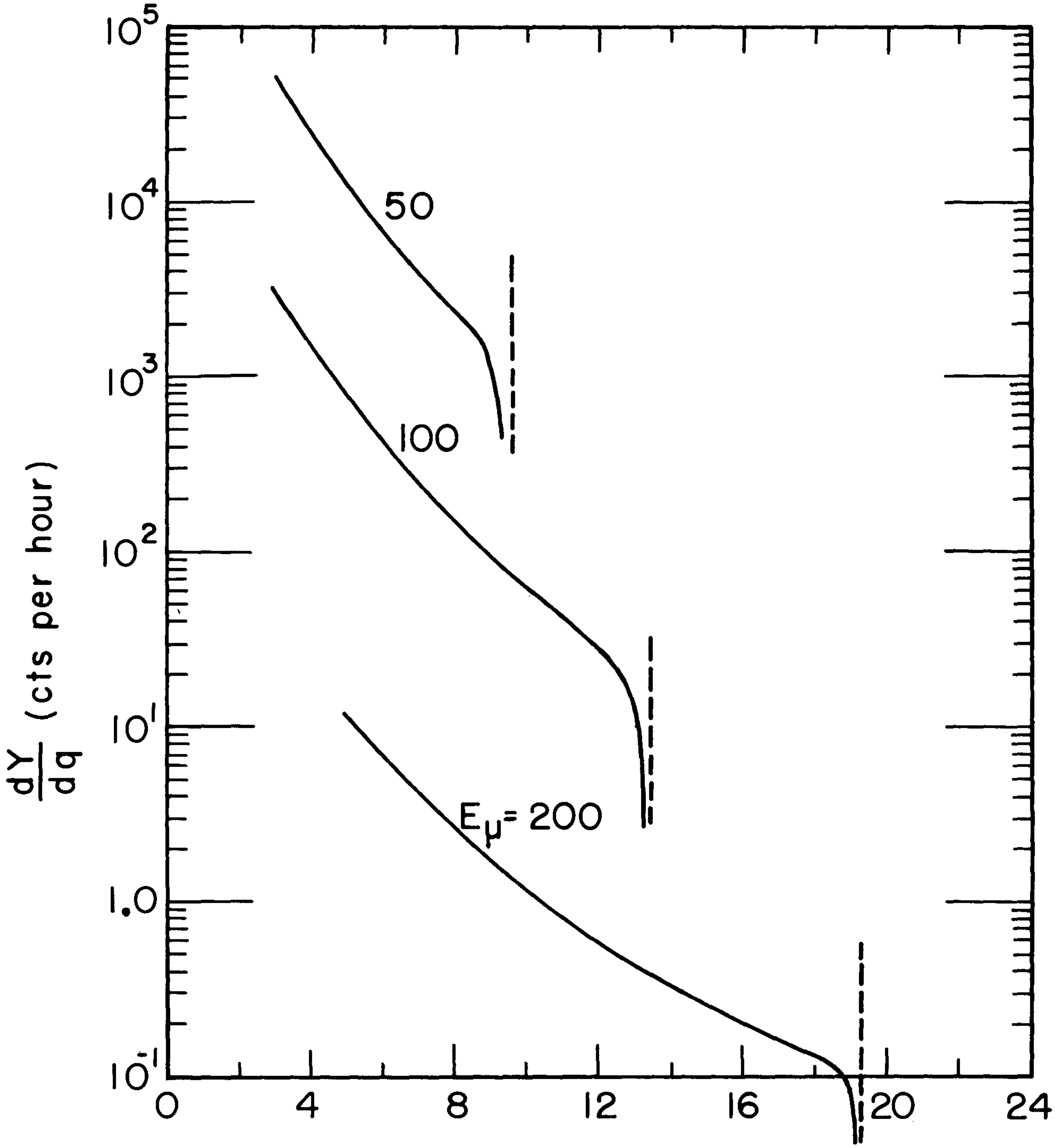

Fig. S15-5. Elastic μ - p scattering yields;
$\frac{dY}{dq}$ vs q for 10^{12} protons per pulse;
ΔE_μ is 1 Gev, and the target is 70 g/cm^2 of hydrogen.

Conceptually, it has many of the same requirements as μ-p elastic scattering (large muon fluxes and good pion rejection) and has the distinctive experimental feature that the muon disappears. The yield is estimated for 50-Gev muons on 140 g/cm^2 of hydrogen (the target could, of course, be any nucleus and probably would be the plates of a spark chamber). Assuming a cross section of approximately 10^{-38} cm^2, we get

Yield per hour per 10^{12} protons per pulse ≈ 3.

There have been several estimates which place the beam intensities at 10^{13}, in which case, the above becomes an attractive possibility.

References

1. G. Cocconi, in Proceedings of the 1960 Rochester Conference on High-Energy Physics (Interscience Publishers, Inc., New York, 1960), p. 799.

2. H. Ticho, Flux Estimates for a 300-Gev Proton Accelerator, UCLA Technical Report No. 1, June 1961.

3. A. Citron, A High-Intensity μ-Meson Beam from the 600-Mev CERN Synchrocyclotron, in Proceedings of an International Conference on Instrumentation for High-Energy Physics, 1960 (Interscience Publishers, New York, 1961) p. 286-288.

4. J. M. Cassels, Electron-Proton Scattering in the Gev Range, W. W. Hansen Laboratories of Physics, Stanford University, July 13, 1960 (unpublished).

15. PART II. MUON BEAMS.

Steven C. Frautschi

July 18, 1961

A 300-Gev accelerator would produce beams of highly energetic pions. These pions would decay chiefly in the modes

$$\pi^{\pm} \rightarrow \mu^{\pm} + \nu \tag{1}$$

and

$$\pi^{0} \rightarrow 2\gamma\ , \tag{2}$$

the decay products also being energetic and concentrated in a small forward cone. I shall indicate how energetic muons and photons produced in this way, and used in concert with the well-established theory of quantum electrodynamics, would allow us to study some questions of fundamental interest. These remarks are intended to complement the companion work by George Masek, who has estimated the muon intensity as a function of energy and the counting rates for muon reactions in hydrogen.

Let us consider energetic muons or photons incident upon a hydrogen target: Low-momentum-transfer events in reactions such as

$$\mu + p \rightarrow \mu + p \tag{3}$$

and

$$\gamma + p \rightarrow e^{+} + e^{-} + p \tag{4}$$

are strongly peaked in a narrow forward cone. These are "peripheral collisions" par excellence, involving the exchange of one photon, and can be predicted with considerable reliability by standard quantum electrodynamics. Bludman, Koester, and Wong have described how one might use the pair-production reaction $\gamma + p \rightarrow W^{+} + W^{-} + p$ as a tool in looking for charged vector bosons.

At larger momentum transfers, one-photon-exchange calculations remain valid, thanks to the smallness of the electric charge. Thus, in electrodynamics, peripheral collisions find quantitative application over a much wider range of momentum transfer than in strong interactions. The most straightforward application for our purposes is to describe $\mu + p \rightarrow \mu + p$ by one-photon exchange (Fig. S15-6). Since fundamental information is most directly obtainable from the elastic reaction, it is desirable to use hydrogen targets, for which the energy resolution need be good enough only to exclude pion production, rather than complex nuclei, in spite of the higher counting rates obtainable from the latter. The unavoidable inelasticity due to photon emission can be corrected for reliably by use of standard quantum electrodynamics.

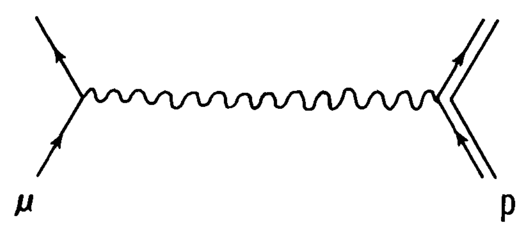

Fig. S15-6. One-photon-exchange diagram for $\mu + p \rightarrow \mu + p$.

If in Fig. S15-6 we associate form factors $F_\mu(\Delta^2)$ and $F_p(\Delta^2)$ with the muon and proton vertices, respectively (neglecting the proton anomalous moment for simplicity), the cross section $\sigma(\mu + p \rightarrow \mu + p)$ for momentum transfer Δ is proportional to $F_\mu^2(\Delta^2)\ F_p^2(\Delta^2)$. In similar fashion, we have

$$\sigma(e + p \rightarrow e + p) \propto F_e^2\ (\Delta^2)\ F_p^2\ (\Delta^2)\ . \tag{5}$$

In the accompanying paper, Masek finds that the counting rate for $\mu + p \rightarrow \mu + p$ would allow experimentation up to about Δ = 10 Gev. At the proposed Stanford 15-Gev electron accelerator, the maximum momentum transfer kinematically obtainable in $e + p \to e + p$ is $\Delta \approx 5$ Gev. Thus, muon scattering could test $F_\mu F_p$ up to about 10 Gev; when combined with electron-scattering results from Stanford, it could test F_μ / F_e up to about 5 Gev. Of course, the latter ratio is unity if both muon and electron behave according to pure quantum electrodynamics, as indicated by all previous experiments at lower Δ.

The proton form factor at large Δ gives a measure of the proton charge and magnetic-moment distribution at small distances; if the proton has a "core" we may expect $F_p^2 \neq 0$, but if the charge and moment are smoothly spread out, it is likely that $F_p^2 \to 0$ as Δ increases. The estimate of F_p^2 strongly affects the cross section, counting rate, and even the interpretation of $\sigma(\mu + p \to \mu + p)$. Masek has extrapolated the values which F_{1p} ("charge form factor") and F_{2p} ("anomalous moment form factor") presently exhibit at $\Delta \approx 1$ Gev as $F_{1p}^2 = 0.17$ and $F_{2p}^2 \approx 0$ at $\Delta > 1$ Gev. In view of the assumption that F_{1p}^2 remains constant, his cross section should probably be considered as an upper bound. If F_{1p}^2 and F_{2p}^2 become very small at large Δ, the two-photon exchange (Fig. S15-7), which is not limited by F_{1p} and F_{2p}, might conceivably become a competitive process and seriously complicate the interpretation of the experiment.

Can the information provided by $\mu + p \to \mu + p$ at $\Delta = 10$ Gev with considerable experimental errors be obtained from lower-energy higher-precision studies? In terms of the minimum distance studied, we find

muon g - 2 (in 1961):

$$10^{-14}\,\text{cm} \;; \tag{6}$$

$e + e \to e + e$ (O'Neill, 1962?):

$$3 \times 10^{-15}\,\text{cm} \;; \tag{7}$$

$\mu + p \to \mu + p$ (in 1970?):

$$2 \times 10^{-15}\,\text{cm} \;. \tag{8}$$

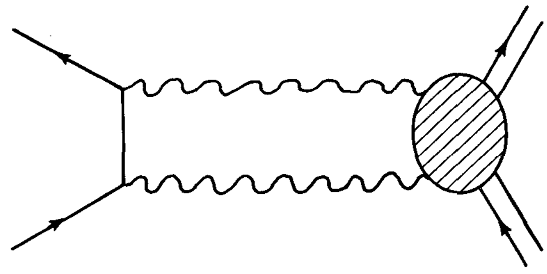

Fig. S15-7. Two-photon-exchange diagram for $\mu + p \to \mu + p$.

Of course, these experiments involve different combinations of muon vertices, electron vertices, muon propagators, etc. But it should further be emphasized that the colliding electron beams [reaction (7)] involve about 1 Gev maximum momentum transfer (2×10^{-14} cm), and cannot tell us anything about larger momentum transfers without some assumption that a possible breakdown of electrodynamics at $\Delta > 1$ Gev would occur in a smooth manner, leading to deviations detectable by high-precision measurement at $\Delta \approx 1$ Gev. In the case of muon g-2, the theory involves an integration over large momentum transfers, weighted so that the effect of a breakdown at $\Delta = \Lambda$ on g-2 would vary as Λ^{-2}. The accuracy of g-2 experiments must be improved by a factor of 25 in order to extend the distance studied from 10^{-14} cm to 2×10^{-15} cm. Thus, it appears that $\mu + p \to \mu + p$ at $\Delta = 10$ Gev might provide a useful and independent piece of information.

Wide-angle pair production of electrons ($\gamma + p \to e^+ + e^- + p$), or other charged pairs, could also be used to study electrodynamics at small distances, but we find it less immediately appealing than $\mu + p \to \mu + p$ for several reasons: experimentally, the energy of the incoming photon is harder to determine; three final-state particles are perhaps harder to study than two; and we have the cross section $\sigma(\gamma + p \to e^+ + e^- + p) \approx \alpha^3$ (see Fig. S15-8), whereas $\sigma(\mu + p \to \mu + p) \approx \alpha^2$. Also, the theoretical interpretation is clouded by the presence, in lowest order, of diagrams such as Fig. S15-8 (b), where the nucleon currents enter twice and are not readily calculable. The relative importance of such undesirable diagrams could be reduced by minimizing the momentum transfer to the proton. But then, the electron propagator in Fig. S15-8 (a) could be pushed far off the mass shell, where small distances come in, only by using the high-energy tail of the photon spectrum, where intensity is very low.

Finally, we remark that a polarized muon beam can be obtained from pion decay, but we have been unable to find any good use for it.

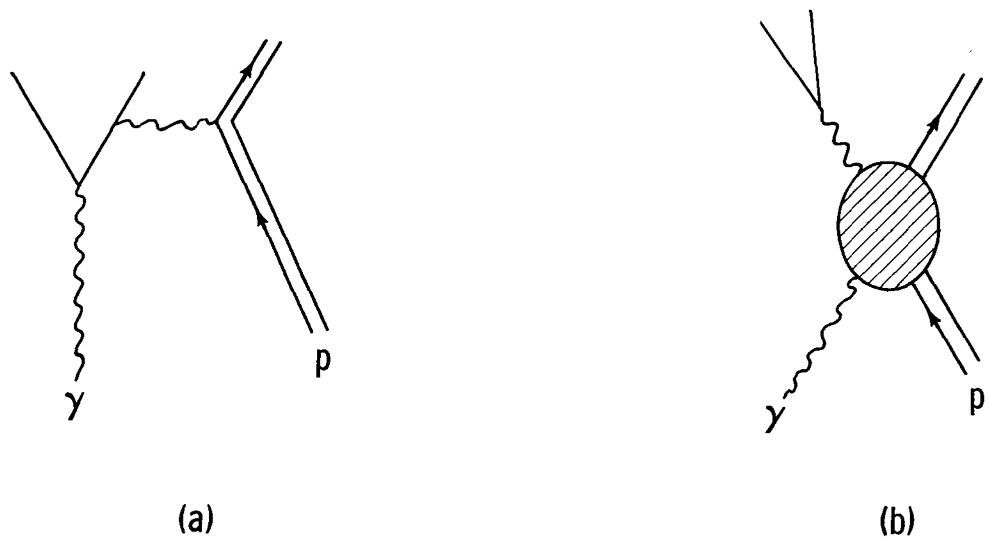

Fig. S15-8. Some representative lowest-order diagrams for $\gamma + p \to e^+ + e^- + p$.

16. PARTICLE SEPARATION AT HIGH ENERGIES

Sulamith Goldhaber

July 20, 1961

The technical difficulty of identifying particles of different masses increases almost exponentially as the difference in their respective velocity decreases. For momenta of 15 Gev and above, these difficulties become prohibitive for detectors that require not just tagging of particles of different masses, but also their spatial separation. For bubble chambers, a preselected enriched beam of particles whose interactions one wishes to study is a prerequisite. Velocity selection, such as crossed electric and magnetic fields, has been used to obtain spatial separation and can give satisfactory results up to a momentum of 6 Gev/c and probably even up to 10 Gev/c. Beyond that limit it seems hopeless to use electromagnetic separation by presently known techniques. If bubble chambers are to have an important place in future high-energy particle research, a number of problems must be solved. I shall divide these problems into two major classes:

a. Enrichment of primary particle beams and identification of the primary particle.

b. Analysis and identification of the secondary particles in the bubble chamber itself.

The latter problem becomes more acute at high energies when multiple particle production with many neutral particles sets in. Kinematical fittings can no longer be utilized under such conditions.

Today, I shall deal mainly with the first part of the first problem; namely, the enrichment of the primary particle beam whose interaction with matter one wishes to study. A discussion of bubble chamber analysis problems will be covered under a separate section by Dr. George Trilling and Dr. Gerald R. Lynch.

Before starting my discussion of a sophisticated separation scheme by which one may obtain enriched particle beams, I think it appropriate to mention one important experiment that can be done well in the hydrogen bubble chamber with a scattered proton beam; namely, the investigation of high-energy proton-proton collisions. Dr. Perkins has given us an extensive summary of the results on high-energy collisions in cosmic-ray research. The difficulties and uncertainties in explaining some of the phenomena were tied to the uncertainty of the mass of the primary particle and the identity of the target nucleus. The understanding of the fireball model, which is tied to questions such as inelasticity of the collision and accurate momenta spectra of secondaries, might be achieved by studying high-energy p-p collisions in a hydrogen bubble chamber. In particular, notice that, owing to the complete symmetry of the proton-proton system, the backward hemisphere in the center-of-mass system tells us the entire story of the collision. This, of course, has the signal advantage that in the laboratory system the particles will be slow, so that the identification will not be a major problem.

If, however, one wants to tackle problems of antibaryon and strange-particle research, enriched beams become a must.

While at CERN, Gerson and I investigated two separation schemes.

The first is based on the utilization of the relativistic rise in the energy loss of charged particles. I will not discuss this part in detail but will merely state that we expect this method, with suitable absorbers, to give useful spatial separation up to 10 Gev/c. A detailed description of this work is included in the report that begins on page 194.

The second scheme was the brainchild of Gerson, Bernard Peters, and myself. This work has been published.[1] Discussing the difficulties one encounters in sorting particles with conventional techniques, we started looking for some characteristic type of interaction of the particle we wanted to sort. We soon found that proper utilization of characteristic differential cross sections can give us the desired result.

Let me now briefly describe the method that we worked out in some detail for enriching an antineutron beam of 8 Gev/c, and show you that the method can be extended to higher energies.

The principle is simple: Imagine a negative momentum-selected beam consisting of pions, K^- mesons, and antiprotons striking a hydrogen target. What are the dominant types of interactions one would observe?

$$\bar{p} + p \rightarrow \bar{N} + N + X\pi \ , \qquad (1a)$$

$$\bar{p} + p \rightarrow X\pi \ \text{(annihilation)} \ ; \qquad (1b)$$

$$K^- + p \rightarrow \bar{K}^0 + N + X\pi \ ; \qquad (2)$$

$$\pi^- + p \rightarrow N + X\pi \ , \qquad (3a)$$

$$\pi^- + p \rightarrow K + Y + X\pi \ . \qquad (3b)$$

Out of the products of these reactions, we can preferentially select the antineutrons produced, if we remember three important experimental facts:

a. The $\bar{p}$ charge-exchange cross section remains up to 3 Gev/c about 10% of the total interaction cross section (Fig. S16-1).

b. The differential charge-exchange cross section is strongly forward peaked, indicating small momentum transfer (Fig. S16-2).

c. In the pion-nucleon collision, the baryon is emitted backward in the center-of-mass system (Fig. S16-3).

1. Nuclear Physics 25, 502 (1961)

References to these experiments are given in our published work.[1]

The kind of arrangement we visualized, keeping these three facts in mind, for obtaining the separation is shown in Fig. S16-4.

A momentum-selected negative beam passes through an absorber A in which it interacts to produce charged and neutral particles, as indicated in reactions (1), (2), and (3). The charged secondaries are swept out of the beam by magnet H_1. The neutral beam, consisting of antineutrons, neutrons, K_2^0, and γ rays from π^0 decays, is now passed through a lead converter followed by a second sweeping magnet H_2. The remaining beam consists now of antineutrons, K_2^0, and some neutrons.

Our calculations show that, for a beam of 10^6 negative particles with a momentum of 8 Gev/c, solid angle of 10^{-4} steradian, and a $\bar{p}/\pi$ ratio of 1% at production, one expects yields given in Table S16-I, Column 2.

Table S16-I

Particle	Estimated yield per 10^6 pions	Observed preliminary yield per 10^6 pions
$\bar{n}$	1 - 8	approx 1
K_2^0	2 - 5	Not measured
n	1 - 2	approx 2

A preliminary test of these ideas, carried out in CERN,[2] proved most encouraging. The preliminary results, which were obtained without optimizing the system, showed a yield within the estimated limits. Figure S16-5 shows a schematic drawing of the actual setup. A momentum-selected beam focused onto detector L was passed through a LiH absorber, followed by sweeping magnet F . The γ rays are

2. Work done jointly with Gerson Goldhaber, G. von Dardell, B. Hyams, Y. Goldschmidt-Clermont, L. Montanet, and R. Mc Leod.

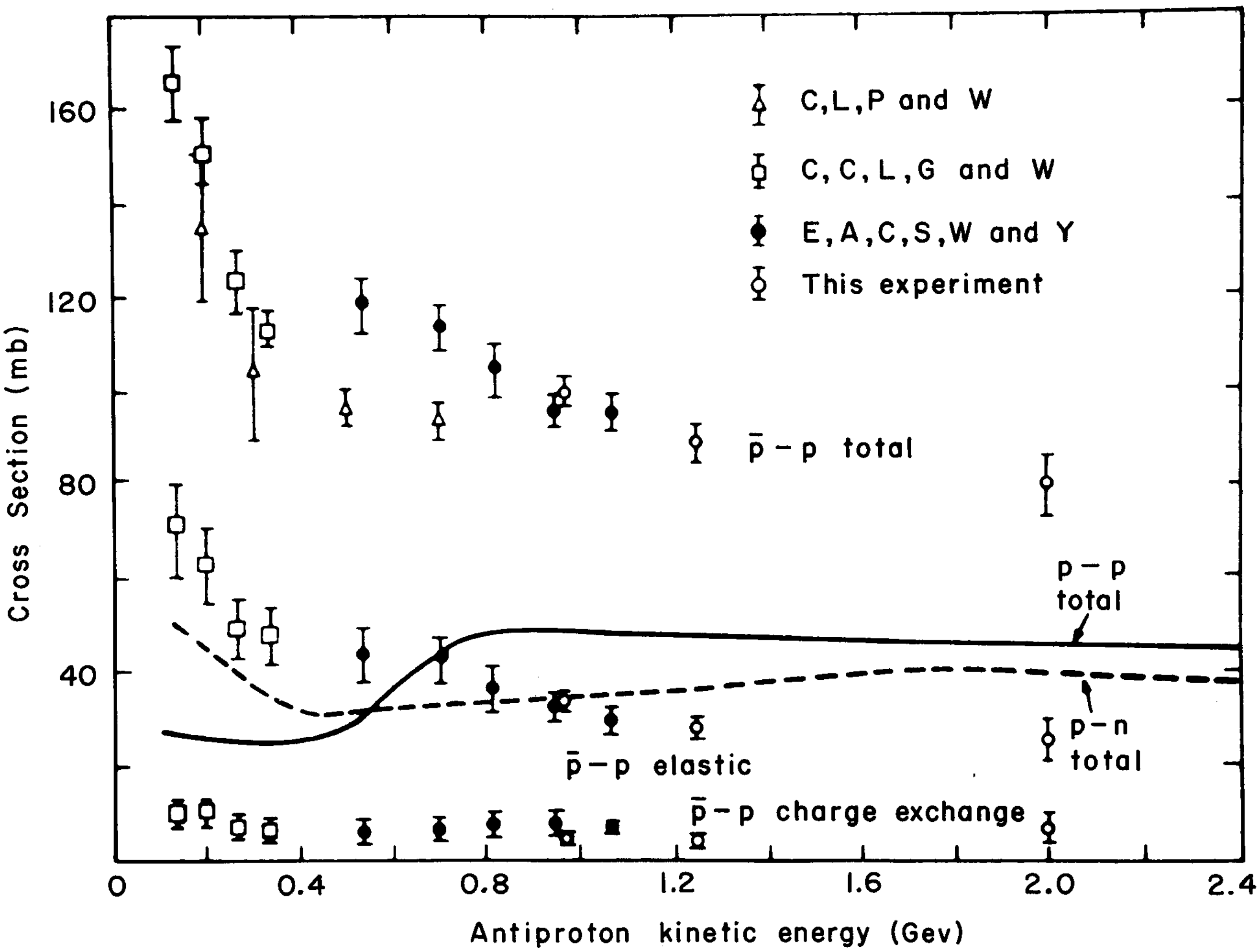

Fig. S16-1. Measured $\bar{p}$-p cross sections.

converted in absorber G , and the resulting electron pairs removed by sweeping magnet H . The final detector was a total-energy-loss counter, designed by Hyams, and consisted of 40 scintillation counters sandwiched between forty 1-cm iron plates. The output was put through a pulse-height analyzer. Further tests are now in progress. A higher flux of the initial negative beam seems definitely in the realm of possibility. It should also be possible to compress such a system and increase the solid angle without increasing the background appreciably. In particular, high-field magnets would be a great asset to schemes of this sort. There are a number of possible extensions to such a scheme; for example:

a. a double charge-exchange scheme to yield a purified $\bar{p}$ beam; and

b. double charge exchange yielding pure K^+ and K^- beams, starting initially with particles of the opposite charge.

Now I shall present some of the arguments that lead us to believe that separation by strong interaction should be applicable at ultrahigh energy and may therefore find prominent application with machines of 100 to 1000 Gev.

Again, the principle that collisions with small momentum transfer dominate the inelastic charge exchange at small angles is important. In other

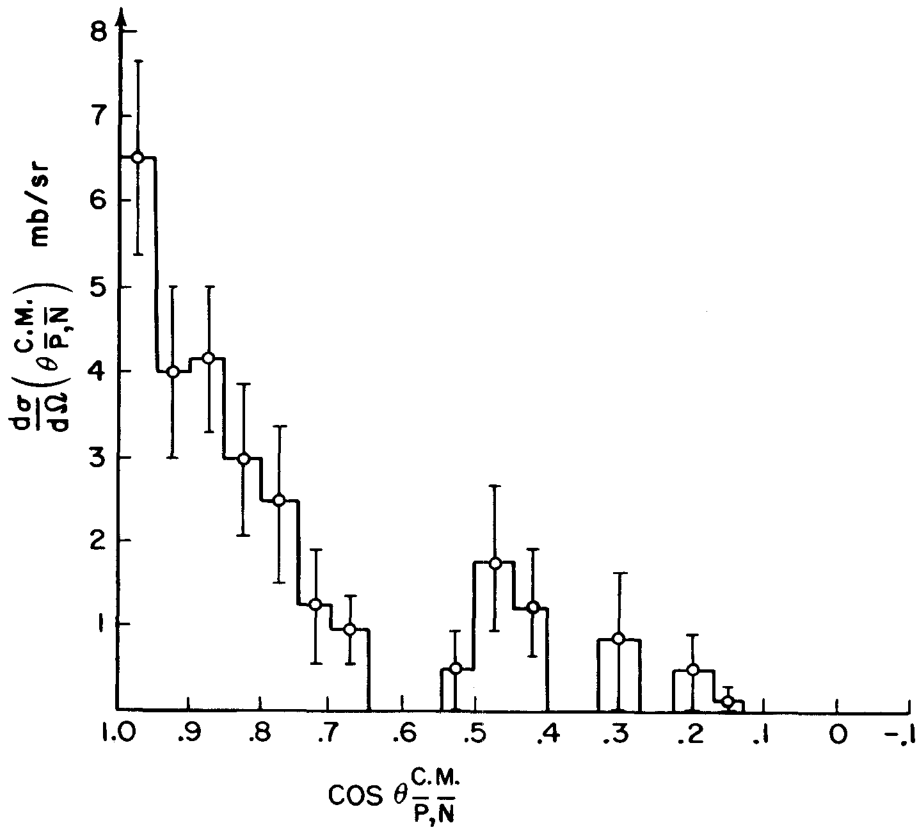

Fig. S16-2. Angular distribution of $\bar{p} + p \rightarrow \bar{n} + n$ events.

words, the interaction occurs via large impact parameters, and the particles continue in the same direction they had prior to the collision. We also know, from results obtained with cosmic rays, that the average transverse momentum of particles emitted in high-energy collisions is of the order of 2 pion masses. Combining these two pieces of information, one deduces that in a $\bar{p}$-p charge-exchange reaction half the antineutrons would be contained in an angle

$$\Theta(\bar{n}) \approx \frac{2m_\pi}{P_0}, \tag{4}$$

where P_0 is the incident momentum. If we assumed an inelasticity K in the interaction, this angle would be modified to

$$\Theta(\bar{n}) \approx \frac{2m_\pi}{(1 - K)\, P_0}; \tag{5}$$

for $K = 0.25$ and $P_0 = 100$ Gev/c, $\Theta \approx 0.25$ deg. The angle Θ thus varies inversely as the incident momentum.

The neutrons, on the other hand, will be emitted backward in the c.m. system [see reaction (2)]. To evaluate the laboratory-system angle of neutron emission as a function of energy, let us consider the most unfavorable case for our separation scheme, namely, emission at 90°. This means that we give the neutrons only transverse momentum.

Let us define the angle into which half the neutrons are emitted as

$$\Theta(n) = \frac{\langle P_\perp \rangle}{P_{\parallel}^{lab}}, \tag{6}$$

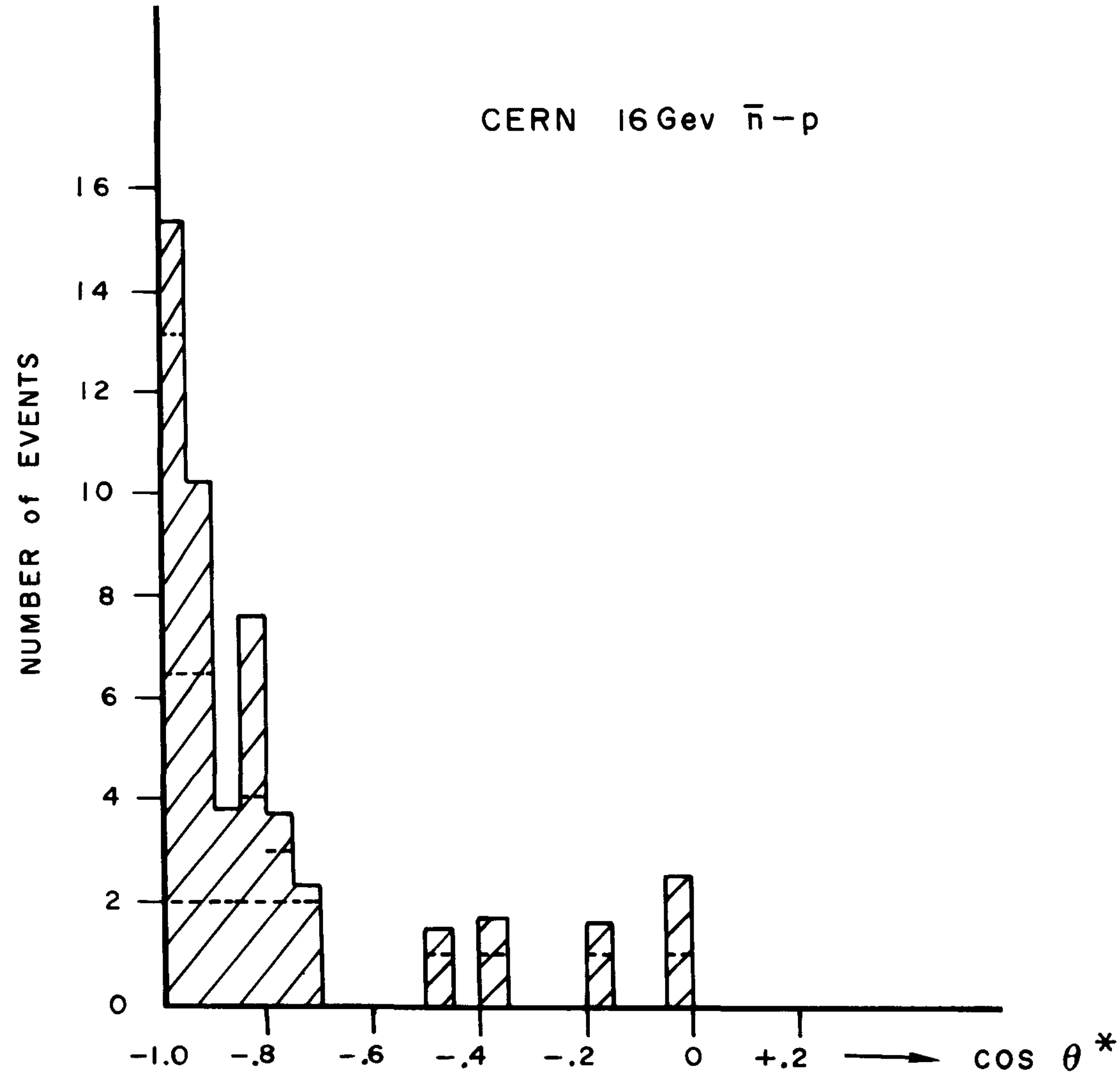

Fig. S16-3. The angular distribution (c.m.) for the Λ^0.

where $\langle P_\perp \rangle$ is the average transverse momentum, and $P_{\parallel}$ is the longitudinal momentum; then,

$$P_{\parallel}^{lab} = \bar{\gamma}\,(P^{c.m.} \cos \Theta^{c.m.} + \bar{\beta}\, E^{c.m.})$$

$$= \bar{\gamma}\, P^{c.m.} \left(\cos \Theta^{c.m.} + \bar{\beta}/\beta^{c.m.}\right) , \tag{7}$$

where $\bar{\beta}$ and $\bar{\gamma}$ correspond to the velocity of the center of mass, and $\beta^{c.m.}$ the velocity in the center-of-mass system. Since we chose the condition of emission at 90°, we have $\cos \Theta^{c.m.} = 0$, so that

$$P_{\parallel}^{lab} = \bar{\gamma}\, P^{c.m.}\, \bar{\beta}/\beta^{c.m.} \text{ , where } \bar{\beta} \approx 1 ; \tag{8}$$

$$P^{c.m.} = P_\perp \text{ , for our case ;} \tag{9}$$

$$P_{\parallel}^{lab} = \bar{\gamma}\, P_\perp\, 1/\beta^{c.m.} ; \tag{10}$$

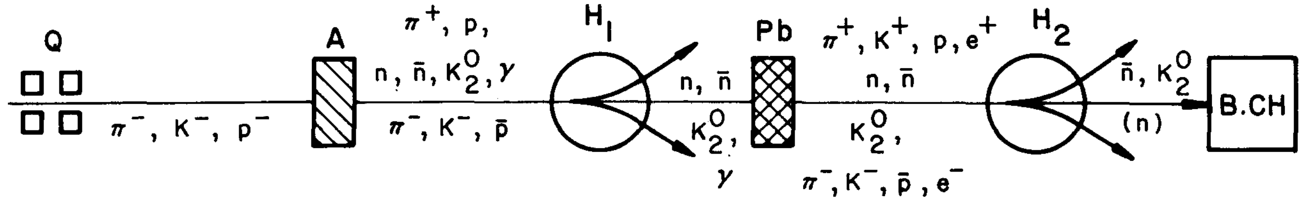

Fig. S16-4.

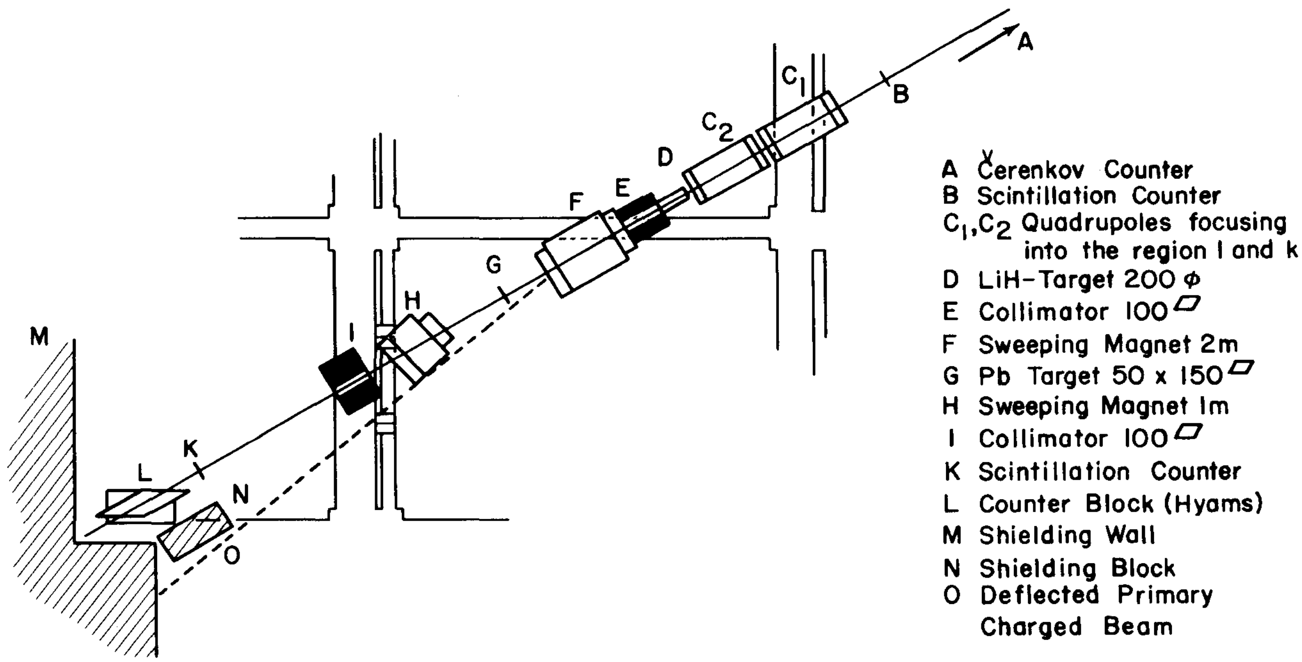

Fig. S16-5.

$$\Theta(n) = \frac{P_\perp}{P_{||}} = \frac{P_\perp}{\bar{\gamma} P_\perp} \cdot \beta^{c.m.} = \frac{1}{\bar{\gamma}} \cdot \beta^{c.m.} ; \tag{11}$$

but

$$\bar{\gamma} \approx \sqrt{\frac{P_0}{2M_p}} ,$$

so that

$$\Theta(n) \propto 1/\sqrt{P_0} \tag{12}$$

In the above derivation, we have shown that the neutron-emission angle varies inversely as the square root of the incident momentum, and will thus decrease more slowly as a function of energy than the antineutron angle. We expect therefore that separation by strong interaction, once shown to work at lower energies (8 Gev/c), should work as well, if not better, at higher energies (100 Gev and above).

Before concluding, I shall mention the possible application of the relativistic rise in the energy loss to identifying particles of different masses, rather than to obtaining spatial separation between them. The idea is to pass a momentum-selected beam of particles through a scintillator and identify the masses by the difference in their pulse heights. Pions will have the larger energy losses and, therefore, larger pulse heights than protons of the same momentum. The limiting factor is the Fermi density effect, which counteracts the relativistic rise in the energy loss. One gram of xenon gas at 1 atmosphere may be a good scintillator, since density effects in this medium are still small up to momenta of 100 Gev/c.

Figure S16-6 gives an example of particle separation at 100 Gev for 1 gram of Xe at 1 atm pressure (approximately 2 meters long). By judicious utilization of the information from several such counters in series, it should be possible to separate antiprotons from K mesons and pions.

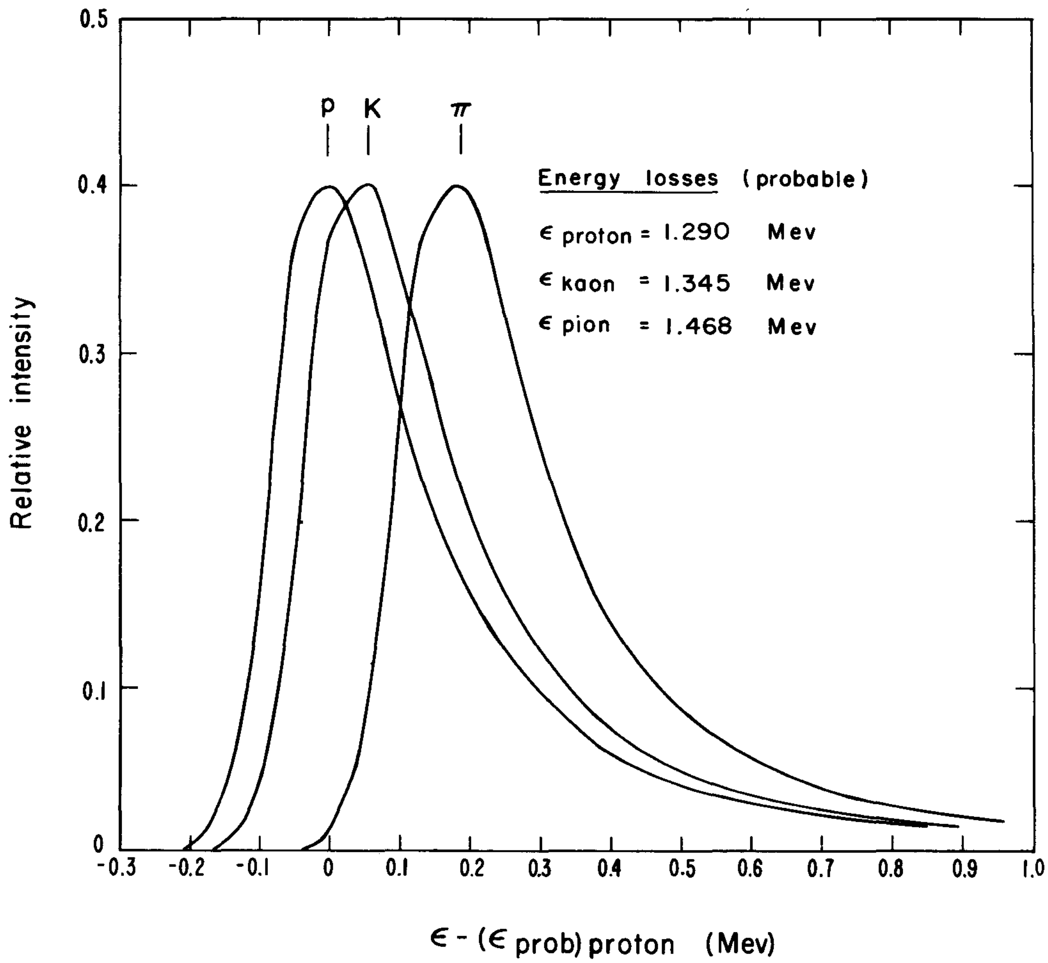

Fig. S16-6. Landau distributions of energy loss for 100-Gev particles in 1 g xenon at 1 atm. Density effects are taken into account.

17. ELECTROMAGNETIC PRODUCTION OF CHARGED VECTOR MESONS*

Sidney A. Bludman† and James A. Young‡

July 21, 1961

I. Introduction

Charged vector mesons have recently been hypothesized as possible intermediary quanta in the weak and strong interactions. In this paper, we wish to consider the standard electromagnetic processes—Coulomb scattering, Compton scattering, bremsstrahlung, and pair production—as applied to mesons of spin 1. We are specifically interested in the possibility of photoproduction of $B^{\pm}$ pairs in the Coulomb field of some nucleus of charge eZ. The cross section σ_P for this second-order electromagnetic process is of order $\alpha Z^2(e^2/M_Bc^2)^2$, or about a thousand times the cross section $\sigma_\nu \propto \alpha^2 Z^2 G$ for the semiweak process in which weakly coupled vector mesons are supposed to be produced by high-energy neutrinos in the nuclear Coulomb field eZ.

The most interesting feature of this cross section, σ_P, is that for the production of high-energy vector mesons, when the momentum transfer to the Coulomb field is small, σ_P is (in the Born approximation) expected to increase linearly with photon energy. This increase of the cross section with energy is well known for the bremsstrahlung by charged S = 1 mesons, and is the basis of Christy and Kusaka's conclusion from the size of cosmic-ray bursts that the spin of cosmic-ray mesons had to be less than 1.[1] Nevertheless, this increase in cross section at high energies does not obtain for particles with S = 0, 1/2 and cannot be expected to continue indefinitely with increasing energy. Therefore, we compare the Coulomb and Compton scattering of S = 1 particles with that of S = 0, 1/2 particles. We find that the increasing cross section is associated with the longitudinal polarization state, which does not exist for S = 0, 1/2. Application of the unitarity limit to the Compton cross section will enable us to obtain a theoretical limit for the applicability of our formulae.

We then use the Compton cross sections obtained in order to calculate, by the Weizsäcker-Williams method,[2] the cross sections for bremsstrahlung and pair production in the low-momentum-transfer limit, and finally discuss qualitatively some of the experimental difficulties associated with electromagnetic—as compared with neutrino—production of B mesons.

II. Coulomb Scattering

The cross sections for vector-meson processes turn out to have a much stronger energy dependence than those for S = 0, 1/2 particles and, in the Born approximation, increase indefinitely with energy. When we investigate the Coulomb scattering of vector mesons we can show that this singular behavior is associated with the extra longitudinal-spin degree of freedom that S = 1 particles possess.

We begin with the plane-wave expansion of the free vector-meson field,

$$U_\mu(x) = (2\pi)^{-3/2} \sum_{r=1}^{3} \int \frac{d^3p}{\sqrt{2E}} \left[\epsilon_\mu^r a^r e^{-ip\cdot x} + \epsilon_\mu^{r+} b^{r+} e^{ip\cdot x}\right], \quad (2.1)$$

where E is the meson energy, and a^r and b^r are, respectively, destruction and creation operators for particles and antiparticles of spin polarization ϵ_μ^r (r = 1, 2, 3). Because of the subsidiary condition, $\partial_\mu U_\mu = 0$, we have

$$p \cdot \epsilon^r = \underset{\sim}{p} \cdot \underset{\sim}{\epsilon}^r - E\epsilon_0^r = 0.$$

If we choose the z axis in the direction of propagation, so that

$$\underset{\sim}{p} = (0,\ 0,\ p),$$

then, in the two transverse polarization states ($r = 1, 2$), we have $\epsilon_3^r = \epsilon_0^r = 0$, and ϵ^1 and ϵ^2 are unit vectors in the xy plane. For the longitudinal polarization state, we can write

$$\underset{\sim}{\epsilon}^3 = (0,\ 0,\ E/M), \quad \epsilon_0^3 = p/M. \qquad (2.2)$$

In the plane-wave expansion (2.1), the amplitude of the longitudinally polarized state therefore exceeds that of the transverse polarized states by the factor E/M, which can be large for a fast-moving vector meson. In the rest frame there is, of course, no distinction among the three possible polarization states.

Because $\underset{\sim}{\epsilon}^1$, $\underset{\sim}{\epsilon}^2$, and $\underset{\sim}{p}/|p|$ are orthogonal unit vectors, we have

$$\sum_{r=1}^{2} \epsilon_i^r \epsilon_j^r = \delta_{ij} - p_i p_j/p^2, \qquad (2.3)$$

for $i, j = 1, 2, 3$. The covariant polarization sum is given by

$$\sum_{r=1}^{3} \epsilon_\mu^r\, \epsilon_\nu^r = \delta_{\mu\nu} + p_\mu p_\nu/M^2, \qquad (2.4)$$

for $\mu, \nu = 1, 2, 3, 4$.

For the interaction Lagrangian we have

$$\begin{aligned}\mathcal{L} = {} & (1/2) U_{\mu\nu}^+ (\pi_\mu U_\nu - \pi_\nu U_\mu) \\ & + (1/2)(\pi_\mu U_\nu^+ - \pi_\nu U_\mu^+) U_{\mu\nu} - 1/2\, U_{\mu\nu}^+ U_{\mu\nu} \\ & + M^2 U_\mu^+ U_\mu + (ie\,\gamma/2)(U_\mu^+ U_\nu - U_\nu^+ U_\mu) F_{\mu\nu} \\ & + (ie\, q/4M^2) \left[U_{\mu\nu}^+ U_\lambda - U_\lambda^+ U_{\mu\nu} \right] \partial_\lambda F_{\mu\nu}\,, \end{aligned} \qquad (2.5)$$

where $\pi_\mu = \partial_\mu - ie A_\mu$, and γ and q are specific magnetic-moment and electric-quadrupole moment factors respectively. In this paper, we assume $q = 0$ and consider only $\gamma = 0$, i.e. vector mesons of unit magnetic moment $\frac{e\hbar}{2Mc}$ (or, in Sections III and IV, $\gamma = -1$, and zero magnetic moment). The matrix element of the vector-meson current operator between free-particle states of momentum p and p' is then

$$\begin{aligned}\left\langle p' \middle| J_\mu \middle| p \right\rangle = {} & -\frac{e}{2}(2\pi)^{-3} (EE')^{-1/2} \\ & \Big[(p_\mu + p'_\mu)\, \epsilon \cdot \epsilon' \\ & + (1+\gamma)(p_\nu - p'_\nu)(\epsilon'_\mu \epsilon_\nu \\ & - \epsilon'_\nu \epsilon_\mu) \Big]\ . \end{aligned} \qquad (2.6)$$

For the differential cross section for Coulomb scattering, we find (for $\gamma = 0$)

$$\begin{aligned} d\sigma_{Coul}/d\Omega = {} & \sigma_R \frac{1}{4E^2} \Big[4(p\cdot n)^2 (\epsilon\cdot\epsilon')^2 \\ & + (p\cdot\epsilon')^2 (n\cdot\epsilon)^2 + (p'\cdot\epsilon)^2 (n\cdot\epsilon')^2 \\ & + 2(p\cdot\epsilon')(p'\cdot\epsilon)(n\cdot\epsilon)(n\cdot\epsilon') \\ & - 4(p\cdot n)(p\cdot\epsilon')(n\cdot\epsilon)(\epsilon\cdot\epsilon') \\ & - 4(p'\cdot\epsilon)(\epsilon'\cdot n)(p\cdot n)(\epsilon\cdot\epsilon') \Big]\,, \end{aligned} \qquad (2.7)$$

where n_μ is the polarization of the virtual photon and

$$\sigma_R = \left(\frac{\alpha Z}{2pv} \Big/ \sin^2 \Theta/2 \right)^2 = \frac{1}{4} Z^2 r_0^2 \left(\frac{1}{\beta^2 \gamma} \right)^2 \times \frac{1}{\sin^4 \Theta/2} \qquad (2.8)$$

is the relativistic Rutherford cross section for scattering through the angle Θ, and

$$\gamma = E/Mc^2,\ \beta = p/E,\ r_0 = e^2/Mc^2 \quad .$$

Consider three types of spin transitions:

a. Transverse-Transverse Spin Transitions. When both the initial and final mesons are transverse polarized, Eq. (2.7) gives

$$d\sigma/d\Omega = \sigma_R\ (\underset{\sim}{\epsilon} \cdot \underset{\sim}{\epsilon}')^2 \ ,$$

or, if Eq. (2.3) is used to sum over the transverse polarizations,

$$d\sigma/d\Omega = \sigma_R\ (1 + \cos^2\Theta). \text{ (trans. -trans.)} \qquad (2.9)$$

b. Longitudinal-Longitudinal Spin Transitions. When both the initial and final mesons are longitudinally polarized, Eqs. (2.2) and (2.7) give

$$d\sigma/d\Omega = \sigma_R \cos^2\Theta. \text{ (long. -long.)} \qquad (2.10)$$

c. Transverse-Longitudinal Spin Transitions. Finally, when the initial meson is transversely polarized and the longitudinal meson longitudinally polarized (or vice versa), we have

$$d\sigma/d\Omega = \sigma_R \left(\frac{E^2 + M^2}{2ME}\right)^2 \left(\frac{\underset{\sim}{p}' \cdot \underset{\sim}{\epsilon}}{|\underset{\sim}{p}|}\right)^2 .$$

By summing over the transverse polarizations, we obtain

$$d\sigma_{Coul}/d\Omega = \sigma_R \left[(1+\gamma^2)/2\gamma\right]^2 . \text{ (trans. -long.)} \qquad (2.11)$$

We sum over final polarizations and average over initial polarizations by adding Eqs. (2.9), (2.10), and twice Eq. (2.11) (to account for both transverse-longitudinal and longitudinal-transverse transitions) and then dividing the statistical weight of the initial state by 3. We then obtain,[3] for $S = 1$,

$$d\sigma_{Coul}/d\Omega = \sigma_R\ (1 + \tfrac{1}{6}\beta^4\gamma^2 \sin^2\Theta)\ . \qquad (2.12)$$

For comparison, the cross sections for the Coulomb scattering of particles with $S = 0$ and 1/2 are, respectively,

$$d\sigma_{Coul}/d\Omega = \sigma_R \qquad (2.13)$$

and

$$d\sigma_{Coul}/d\Omega = \sigma_R\ (1 - \beta^2 \sin^2\Theta/2)\ . \qquad (2.14)$$

Of course, in the nonrelativistic limit ($\beta \to 0$), the Coulomb cross section is given in all cases by the classical Rutherford formula. The cross section (2.12) increases with increasing energy $\gamma\, Mc^2$ of the vector meson. By reference to Eq. (2.11), we see that this increase of the cross section with increasing energy is due to the increase with energy of the matrix element for spin-flip transitions. In the next section, we shall see that transitions involving longitudinal vector mesons also lead to Compton, bremsstrahlung, and pair-production cross sections that (in the Born approximation) increase with energy.

The Born-approximation cross section for Coulomb scattering is exact.[4] Since Eq. (2.11) or (2.12) would become infinite in the limit $M \to 0\ (\gamma \to \infty)$, this suggests that massless vector mesons cannot be coupled to the electromagnetic field.[5] This is owing to the singular role the longitudinal degree of freedom would play, and obtains even when, as in this example, the electromagnetic field is unquantized. Since the electrodynamics of vector mesons is not renormalizable for nonzero mass,[6] this result shows there is no renormalizable vector-meson electrodynamics. Since zero-mass charged vector mesons together with the electromagnetic field would constitute a Yang-Mills triplet, the implication is that a symmetric Yang-Mills field can exist only if its mass is nonvanishing.

III. Compton Effect

The scattering of photons off vector mesons of unit magnetic moment has been calculated by

Booth and Wilson,[7] who obtain, in the rest frame of the initial meson,

$$d\sigma_{\mathrm{Com}}/d\Omega = \sigma_C \left[1 + \cos^2\Theta + \frac{kk'}{12M^2} (7 - 16\cos\Theta + 3\cos^2\Theta) + \frac{k^2 + k'^2}{48M^2} (29 - 16\cos\Theta + \cos^2\Theta) \right] \quad (g = 1), \tag{3.1}$$

where

$$\sigma_C = \frac{1}{2} r_0^2 \left(\frac{k'}{k}\right)^2 . \tag{3.2}$$

Here k and k' are the momenta of the incident and scattered photon, respectively, and Θ is the scattering angle, so that

$$\frac{k'}{k} = \frac{M}{M + k(1 - \cos\Theta)} = \frac{M - k'(1 - \cos\Theta)}{M} . \tag{3.3}$$

This cross section also increases for increasing k^2.

We have recalculated the Compton cross section for vector mesons of zero magnetic moment (gyromagnetic ratio $g = 0$, or $\gamma = -1$) and obtain

$$d\sigma_{\mathrm{Com}}/d\Omega = \sigma_C \left[1 + \cos^2\Theta - \frac{4}{3}\frac{kk'}{M^2}\cos\Theta (1 - \cos\Theta) + \frac{k^2 + k'^2}{3M^2} (5 + \cos^2\Theta) \right] \quad (g = 0) . \tag{3.4}$$

That Eq. (3.4) shows the same increase with energy as Eq. (3.1) suggests that this effect is not associated with the precise value of the magnetic moment but is again associated with the third kinematic degree of freedom.

For comparison, the Compton cross sections for particles with $S = 0$, $1/2$ are

$$d\sigma_{\mathrm{Com}}/d\Omega = \sigma_C \left(1 + \cos^2\Theta\right) \quad (\text{for } S = 0) \tag{3.5}$$

and

$$d\sigma_{\mathrm{Com}}/d\Omega = \sigma_C \left(1 + \cos^2\Theta + \frac{k'}{k} + \frac{k}{k'} - 2\right) \quad (\text{for } S = 1/2) . \tag{3.6}$$

In the long-wave-length limit ($k \to 0$), these cross sections all reduce, of course, to the Thomson cross section (3.5). In the forward direction ($k' = k$), the Klein-Nishina formula (3.6) agrees with the Thomson formula (3.5), but $S = 1$ cross sections [Eqs. (3.1) and (3.4)] do not. This difference between the $S = 1$ forward scattering and the classical result is again due to longitudinal-transverse vector-meson ($\Delta M = 1$) transitions at the absorption and emission of the electromagnetic quantum. This overall $\Delta M = 2$ transition leads to forward scattering of the photon with spin flip ($\Delta m = 2$); in the scattering of $S = 1/2$ particles, on the other hand, $\Delta m = 2$ is impossible.

The Compton cross sections (3.1) and (3.4) cannot increase indefinitely with energy. It is interesting to impose unitarity as a limit on the validity of these formulae. For this purpose, one must express the Compton cross section in the photon-particle center-of-mass (c.m.) system (designated with subscript c).[8] Now $d\sigma$ is invariant. Introducing the invariants

$$\bar{s} = (p + k)^2 - M^2 = 2p_c (E_c + p_c) ,$$

$$\bar{t} = (p - p')^2 = -2p_c^2 (1 - \cos\Theta_c) ,$$

$$\bar{u} = (p - k')^2 - M^2 = -2p_c (E_c + p_c \cos\Theta_c) , \tag{3.7}$$

so that

$$\bar{s} + \bar{t} + \bar{u} = 0 ,$$

we obtain

$$\sigma_C \, d\Omega_{lab} = \frac{1}{2} r_0^2 \, \frac{M^2}{\bar{s} + M^2} \, d\Omega_c , \qquad (3.8)$$

and

$$1 - \cos\Theta = (1 - \cos\Theta_c) \, \frac{1 - \beta}{1 + \beta \cos\Theta_c} , (3.9)$$

where $\beta = (p/E)_c$ is the velocity of the center of mass relative to the meson rest frame. Equation (3.9) is the relativistic angular-aberration formula. The right-hand side of Eq. (3.8) contains no dependence on the c.m. scattering angle Θ_c. The angular dependence of $(d\sigma/d\Omega)_c$ is therefore contained in the square brackets of Eqs. (3.1), (3.4), (3.5), and (3.6). In terms of the invariants (3.7), we have

$$\cos\Theta = 1 - 2M^2\bar{t}/\bar{s}(\bar{s} + \bar{t}) , \qquad (3.10)$$

$$\frac{k}{k'} + \frac{k'}{k} - 2 = \frac{\bar{t}^2}{\bar{s}(\bar{s} + \bar{t})} ,$$

$$kk'/M^2 = \bar{s}(\bar{s} + \bar{t})/\left(2M^2\right)^2 ,$$

$$(k^2 + k'^2)/M^2 = \left[\bar{s}^2 + (\bar{s} + \bar{t})^2\right]/\left(2M^2\right)^2 ,$$

so that—particularly when $\bar{s}$ (the energy available in the center of mass) is large—none of the square-bracketed terms is very sensitive to $\bar{t}$, which contains the dependence on Θ_c. The angular distribution $(d\sigma_{Com}/d\Omega)_c$ is therefore relatively flat, which suggests that, in the c.m. system, only a few partial waves contribute to the Compton scattering. These cross sections are therefore limited by unitarity to some few multiples of π/p^2, or

$$\text{unitarity limit} \approx N/\bar{s} , \quad N \approx 10. \qquad (3.11)$$

Referring to Eqs. (3.1) and (3.4), we have, for the Compton scattering by vector mesons,

$$d\sigma_{Com}/d\Omega_c \lesssim r_0^2 \bar{s}/8M^2 . \qquad (3.12)$$

The requirement that Eq. (3.12) not exceed (3.11) unitarity limit restricts the validity of Eqs. (3.1) and (3.4) to

$$\bar{s}/M^2 \leqslant (8N)^{1/2} (137). \qquad (3.13)$$

Since, in the laboratory frame, we have $\bar{s}/M^2 = 2k/M$, the vector-meson Compton-scattering formulae (3.1) and (3.4) will not violate unitarity for photon energies

$$k < 500 \text{ M}. \qquad (3.14)$$

This result allows us to confidently apply these Compton-scattering formula to the calculation of pair production.[9]

IV. Bremsstrahlung and Pair Production

Coherent and Incoherent Pair Production

Our principal purpose is to arrive at a cross section for the electromagnetic production of vector-meson pairs in the Coulomb field of a nucleus of charge eZ and radius d. We define d as the radius of the equivalent uniform charge distribution so that for heavy nuclei[10] we have

$$d = (1.2) \, A^{1/3} \text{ fermi}, \qquad (4.1)$$

and

$$q_{max} = \hbar/d \qquad (4.2)$$

is the maximum momentum value occurring in the analysis of the nuclear momentum distribution. Thus $\hbar/Mcd \approx (m_\pi/M) A^{-1/3}$. For an individual nucleon, we have[10]

$$d = 1.4 \text{ fermi} \qquad (4.3)$$

and

$$q_{max} = 500 \text{ Mev/c}. \qquad (4.4)$$

In the production of charged particles of mass M by photons of momentum k ,

$$q_{min} = M^2/2k \tag{4.5}$$

is the minimum possible momentum transfer to the nucleus. For

$$k < M^2/2q_{max} , \tag{4.6}$$

the pair production will be off individual nucleons rather than the nucleus as a whole. The cross section for the pair production coherently off the nucleus as a whole is proportional to $Z^2 F^2(q)$, where $F(q)$ is the nuclear form factor. In the high-momentum-transfer limit, this factor is replaced by $ZF_0^2(q)$, where $F_0(q)$ is the nucleon form factor. According to Eq. (4.6), for B mesons with the mass of the K meson produced off lead, coherent production is to be expected for photon energies $k > 16$ Gev. It thus appears that for existing or presently envisaged electron synchrotrons or linear accelerators, any B mesons produced will be produced incoherently off individual nucleons, and that, for B mesons produced in really high-energy accelerators, the coherent production off heavy nuclei will be more important.

For low photon energies (high momentum transfer), the meson-spin degrees of freedom cannot be excited, and the cross section for the production of pairs of $S = 1$ mesons will be similar to that of $S = 0$, 1/2 particles. (This is clear for bremsstrahlung, where a threshold theorem applies; pair production and bremsstrahlung are, of course, related by the substitution rule.) We therefore devote ourselves to the calculation of vector-meson pair production in the opposite limit of high energies or low momentum transfer. In this limit, features specifically characteristic of vector mesons do appear. The most interesting of these features is that the cross section (4.38) or (4.39) is expected to increase with increasing photon energy. This means that the coherent pair production by photons of energy k is ultimately expected to exceed the incoherent production by the factor

$$Z^2 \frac{k}{M} \frac{\hbar}{Mcd} / Z F^2(q) \approx Z^{2/3} \frac{k}{M} \cdot \frac{1}{F^2(q)} \left(\frac{M_\pi}{M} \right) . \tag{4.7}$$

Weizsäcker-Williams Approximation

In the low-momentum-transfer limit we can calculate pair production from the Compton cross-section formulae in Sec. III by using the method of Weizsäcker and Williams.[2] We first calculate bremsstrahlung in the low-momentum-transfer limit and obtain the pair-production formulae by the usual substitution rule. The bremsstrahlung from vector mesons of unit magnetic moment was calculated by Christy and Kusaka in this way.[1]

In the Weizsäcker-Williams method, the bremsstrahlung from a meson moving rapidly past a nucleus at rest is calculated by going to the opposite Lorentz frame in which the meson is at rest and the heavy nucleus is passing by rapidly. In this frame, the bremsstrahlung of photons off the meson is viewed as the Compton scattering of virtual photons of initial energy k^* (from the electromagnetic field of the fast moving nucleus) to give (real) photons of energy k'^*. (Unstarred and starred quantities are, respectively, in the laboratory frame, where the nucleus is at rest, and in the meson rest frame. We recall that the Compton cross sections (3.1), (3.4), (3.5) and (3.6),

$$d\sigma_{Com} = d\Omega^* \sigma_C \left[\quad \right] \tag{4.8}$$

were all calculated in the particle rest frame. Therefore the Ω, Θ, k, and k' appearing in these formulae will, in this section, all carry stars.)

If, by using Eq. (3.3), we express the angle of scattering in terms of the scattered quantum energy k'^*, then Eq. (4.8) becomes

$$d\sigma_{Com} = \pi r_0^2 \frac{M}{k^{*2}} dk'^{*} \left[\quad \right] \tag{4.9}$$

For a fast-moving meson, the Lorentz transformation from the nuclear rest frame to the meson rest frame gives

$$k^{*} = (2E/M)\, k \tag{4.10}$$

$$k'^{*} = (2E'/M)\, k \tag{4.11}$$

where $E' \equiv E - k'$, and we have assumed $E >> k$. From Eqs. (4.10) and (4.11), we have

$$dk'^{*}/k^{*2} = dk'/Ek^{*} , \tag{4.12}$$

so that in terms of the bremsstrahlung quantum energy k' in the laboratory frame, we can write

$$d\sigma_{Com} = \pi r_0^2 \frac{M dk'}{E k^{*}} \left[\quad \right] \equiv \Phi (k', k^{*})\, dk' . \tag{4.12.1}$$

In the brackets, $\cos \Theta^{*}$ is also to be expressed in terms of k^{*} and k'; we have

$$\frac{1}{2} (1 - \cos \Theta^{*}) = k^{*}_{min}/k^{*} , \tag{4.13}$$

where

$$k^{*}_{min} = \frac{M}{2} \cdot \frac{k'}{E'}$$

is, by Eqs. (3.3) and (4.11), the minimum momentum transfer permitted by the kinematics.

It is useful to define

$$y \equiv k^{*}_{min}/k^{*} = \frac{1}{2} (1 - \cos \Theta^{*}) , \tag{4.14}$$

which runs between the limits

$$B \lesssim y \lesssim 1,$$

where

$$B = k^{*}_{min}/k^{*}_{max} = (k'/2E') \left(\frac{Mcd}{\hbar} \right) << 1 .$$

Then, in the four cases considered we have

$$\left[(S = 0)\right] = 2 - 4y + 4y^2 , \tag{4.15}$$

$$\left[(S = 1/2)\right] = E/E' + E'/E - 4y + 4y^2 , \tag{4.16}$$

$$\begin{aligned} \left[(S = 1),\ (g = 1)\right] = {} & 1 + (1 - 2y)^2 + y^{-2}(k'^2/48\, EE') \\ & \left[7 - 16(1 - 2y) + 3(1 - 2y)^2 \right] \\ & + y^{-2} (k'^2/192)(1/E'^2 + 1/E^2) \\ & \left[29 - 16(1 - 2y) + (1 - 2y)^2 \right], \end{aligned} \tag{4.17}$$

$$\begin{aligned} \left[(S = 1),\ (g = 0)\right] = {} & 1 + (1 - 2y)^2 - y^{-2}(k'^2/3\, EE') \\ & (1 - 2y)\, 2y + y^{-2}(k'^2/12) \\ & (1/E'^2 + 1/E^2) \left[5 + (1 - 2y)^2 \right] . \end{aligned} \tag{4.18}$$

The cross section for the bremsstrahlung of a photon of energy k is thus given by

$$d\sigma_B = \int_{k^{*}_{min}}^{k^{*}_{max}} q(k^{*})\, dk^{*}\ \Phi\, (k', k^{*})\, dk' . \tag{4.19}$$

Here $q(k^{*})\, dk^{*}$ is the equivalent number of virtual quanta with energies between k^{*} and $k^{*} + dk^{*}$ that is contained in the Coulomb field of the nucleus. The integration over virtual quantum energies in Eq. (4.19) extends from a k^{*}_{min} determined by the kinematics to a k^{*}_{max} determined by the spatial extension of the nucleus.

The number of equivalent quanta of momentum k^* is determined by integrating over impact parameters the quantity $p(\nu)\,d\nu$, which is the number of equivalent photons of frequency $\nu^* = k^*/\hbar$ appearing at impact parameter b in the electromagnetic field of the fast moving nucleus. Thus we have

$$q(k^*)\,dk^* = \int_{b_{min}}^{b_{max}} p(\nu)\,d\nu\, 2\pi\, b\,db \ . \quad (4.20)$$

By the condition that

$$\int_0^\infty p(\nu^*)\, h\nu^*\, d\nu^*$$

gives the Poynting flux at distance b, one obtains

$$p(\nu) \approx \frac{\alpha Z^2}{\pi^2} \cdot \frac{1}{\nu^*} \cdot \frac{1}{b^2} \ . \qquad (4.21)$$

Equation (4.21) is restricted, by an approximation involved in estimating the Poynting flux, to values

$$b < b_{max} = \frac{E}{k^*} \cdot \frac{\hbar}{Mc}, \qquad (4.22)$$

where E is the meson energy in the nuclear rest frame. (We are neglecting screening, i.e., assuming $b_{max} < 137\,(\hbar/Mc)\,Z^{-1/3}$, the atomic radius on the Thomas-Fermi model.)

The lower limit in the integral (4.20) is determined by the nuclear size,

$$b_{min} = d. \qquad (4.23)$$

(For a point nucleus, b_{min} is determined by the requirement that the impact parameter be considerably larger than the wave-packet size in order for the Weizsäcker-Williams classical picture to apply; then we have

$$b_{min} = \hbar/Mc.)$$

Thus we can write

$$q(k^*)\,dk^* = \frac{2\,\alpha Z^2}{\pi} \cdot \frac{dk^*}{k^*} \ln \frac{b_{max}}{b_{min}}, \quad (4.24)$$

where $b_{max}/b_{min} = (E/k^*)\,(\hbar/Mcd)$ for an extended nucleus, and $b_{max}/b_{min} = E/k^*$ for a point nucleus.

From Eqs. (4.19) and (4.12), we have

$$d\sigma_B = 2\bar{\Phi}dk' \left[\int_{k^*_{min}}^{k^*_{max}} \frac{dk^*}{k^{*2}} \left[\quad \right] \frac{M}{E} \ln\left(\frac{E}{k^*} \cdot \frac{\hbar}{Mcd}\right) \right] \qquad (4.25)$$

where

$$\bar{\Phi} = \alpha Z^2 r_0^2 \approx Z^2\,(6 \times 10^{-34}\,\text{cm}^2)\,(M_K/M_B)^2 \ .$$

For a point nucleus the logarithm should be replaced by $\ln E/k^*$. Finally, we have

$$d\sigma_B = 4\bar{\Phi} \cdot \frac{dk'}{k'} \cdot \frac{E'}{E} \left[\int_B^1 dx \left[\quad \right] \ln Ax \right], \qquad (4.26)$$

where $A = (2\,EE'/Mk')\,(\hbar/Mcd)$ for an extended nucleus, and $A = 2\,EE'/Mk$ for a point nucleus, and the expression in the brackets is given by Eqs. (4.15) through (4.18) for the four cases being considered.

<u>Bremsstrahlung Cross Sections</u>

Carrying out the integration (4.26), we obtain, in the no-screening relativistic limit (E, $E' >> M$),

$$d\sigma_B = 4\bar{\Phi}\ \ell n\, A\ \frac{4E'}{3E} \cdot \frac{dk'}{k'} \qquad (\text{for } S = 0)\ , \qquad (4.27)$$

$$d\sigma_B = 4\bar{\Phi}\ \ell n\, A\ \frac{E^2 - \frac{2}{3}EE' + E'^2}{E^2} \cdot \frac{dk'}{k'}$$

$$(\text{for } S = 1/2)\ , \qquad (4.28)$$

$$d\sigma_B = 4\bar{\Phi}\left[\frac{7E^2 - 12EE' + 7E'^2}{48\,EM^2 d} + \frac{7E^2 + 20EE' + 7E'^2}{96\,E^2} \cdot \frac{E - E'}{E'}\ \ln A + \left(\frac{4}{3} \cdot \frac{E'}{E - E'} - \frac{E - E'}{E'} \cdot \frac{5E^2 - 36EE' + 5E'^2}{96E^2}\right) \ln A - \frac{13}{3} \cdot \frac{E'}{E - E'} - \frac{E^2 + 12EE' + E'^2}{48E^2} \cdot \frac{E - E'}{E'}\right] \frac{dk'}{E} \qquad (\text{for } S = 1,\ g = 1)\ , \qquad (4.29)$$

$$d\sigma_B = 4\bar{\Phi}\ \frac{E^2 + E'^2}{2E^2}\left(\frac{\hbar}{Mcd}\right)\frac{dk'}{Mc^2}$$

$$(S = 1;\ g = 0)\ . \qquad (4.30)$$

In obtaining Eqs. (4.28) and (4.30) we have retained only the leading terms in k^* or y^{-1}. The remarkable difference between the two $S = 1$ cases and the $S = 0$, $1/2$ cases is due to the singular energy dependence of the vector-meson electrodynamics expressed in the energy-increasing Compton cross sections (4.1) and (4.4).

Cross sections (4.27) through (4.29) are the same as those quoted by Pauli (for an extended nucleus),[11] together with original references. Cross section (4.29) is qualitatively no different from that of (4.28), obtained by Christy and Kusaka[1] with the same method. Our result merely serves to suggest that energy-increasing cross sections obtained in vector-meson electrodynamics are not peculiar to any particular value of magnetic moment.

<u>Pair Production</u>

To go from bremsstrahlung to pair production, we merely change k' to k, change the sign of E relative to E' (except in the logarithm), and change the phase-space factors

$$\frac{p'}{p} \cdot \frac{dk'}{k'} \rightarrow (2S + 1)\,\frac{1}{2} \cdot \frac{pp'\,dE}{k^3}\ . \qquad (4.31)$$

On the right side, p and p' refer to the momenta of the two charged particles produced, and $k = E + E'$. The spin phase-space factors ($2S + 1$) and $1/2$ are present because, whereas in bremsstrahlung we average over spins of the incident particle and sum over the two photon polarization states, in pair production we sum over spins of the emergent antiparticle and average over the photon polarization states.

The cross sections for the production of charged particles of energy E and $E' = k - E$ that are obtained in this way are

$$d\sigma_P = \bar{\Phi} \cdot \ \ln B \cdot \frac{8\,EE'}{3\,k^3}\ dE \quad (\text{for } S = 0)\ , \qquad (4.32)$$

$$d\sigma_P = \bar{\Phi} \cdot \ \ln B \cdot \frac{4(E^2 + E'^2 + \frac{2}{3}EE')}{k^3}\ dE$$

$$(\text{for } S = 1/2)\ . \qquad (4.33)$$

$$d\sigma_P = \bar{\Phi}\left[\frac{7E^2 + 12EE' + 7E'^2}{8M^2 dk} - \frac{7k^2 - 34EE'}{16EE'}\right.$$

$$\times \ln^2 B$$

$$+ \left(\frac{26EE' + 5k^2}{16EE'} - \frac{8EE'}{k^2}\right)\ln B$$

$$\left. + \frac{26}{3}\frac{EE'}{k^2} + \frac{k^2 - 14EE'}{8EE'}\right]\frac{dE}{k}$$

$$(\text{for } S = 1,\ g = 1) \qquad (4.34)$$

$$d\sigma_P = \bar{\Phi}\left(\frac{\hbar}{Mcd}\right)\cdot\frac{3(E^2 + E'^2)}{Mc^2 k^2}\, dE$$

$$(\text{for } S = 1,\ g = 0)\ , \qquad (4.35)$$

where $B = (2\,EE'/Mk)\,(\hbar/Mcd)$ for an extended nucleus, and $B = 2\,EE'/kM$ for a point nucleus. In these formulae we have taken $E,\ E' >> Mc^2$ but screening has been neglected, i.e., $2\,E'/Mk << 137\,Z^{-1/3}$. Equation (4.33) is a standard result.[12] Equation (4.32) differs, as Drell has already noted,[13] by a factor of two from the result quoted by Pauli for $S = 0$.[11]

Integrating Eqs. (4.32) through (4.35) from $E = M$ to $k - M$, we obtain the total cross sections for the production of pairs by quanta of energy k (assumed to be large compared with M):

$$\sigma_T = \bar{\Phi}\ \ln\xi\ \cdot\frac{4}{9} \qquad (\text{for } S = 0)\ , \qquad (4.36)$$

$$\sigma_T = \bar{\Phi}\ \ln\xi\ \cdot\frac{28}{9} \qquad (\text{for } S = 1/2)\ , \qquad (4.37)$$

$$\sigma_T = \bar{\Phi}\left[\frac{5}{12}\xi + \frac{5}{12}\ln^3\xi + \frac{39}{16}\ln^2\xi + \frac{13}{24}\ln\xi\right]$$

$$(\text{for } S = 1,\ g = 1)\ , \qquad (4.38)$$

$$\sigma_T = \bar{\Phi}\xi \qquad (\text{for } S = 1,\ g = 0)\ , \qquad (4.39)$$

where $\xi = (2k/M)\,(\hbar/Mcd)$ for an extended nucleus and $\xi = 2k/M$ for a point nucleus. Dividing Eqs. (4.32) through (4.35) by the corresponding quantities σ_T in Eqs. (4.36) through (4.39), we obtain the normalized probabilities of producing a pair with energies E and E'. In units of the photon energy $[E \equiv kx,\ E' \equiv k(1 - x)]$, this distribution is given by

$$d\sigma_B/\sigma_T = 6x(1 - x)\,dx \qquad (\text{for } S = 0)\ , \qquad (4.40)$$

$$= \frac{3}{7}(4x^2 - 4x + 3)\,dx \qquad (\text{for } S = 1/2)\ , \qquad (4.41)$$

$$= \frac{3}{20}(2x^2 - 2x + 7)\,dx$$

$$(\text{for } S = 1,\ g = 1)\ , \qquad (4.42)$$

$$= \frac{3}{2}(2x^2 - 2x + 1)\,dx$$

$$(\text{for } S = 1,\ g = 0)\ . \qquad (4.43)$$

The probability of producing a pair of spinless mesons is thus a maximum for $E = E' = k/2$ and falls to zero for E or $E' = 0$. On the other hand, for a Dirac particle and for the two vector-meson cases considered, the probability that one member of the pair will take all of the photon energy is respectively 3/2, 21/20, and 2 times the probability that the photon energy will be divided equally. The energy distribution of vector mesons produced is thus rather flatter or steeper than the energy distribution for relativistic spin one-half particles, according to whether the meson magnetic moment is zero or one-meson magneton.

V. Conclusions

The total cross section for the production of single B mesons in the Coulomb field of a nucleus by neutrinos of momentum k is[14]

$$\sigma_\nu = \alpha Z^2\left(G/6\pi\sqrt{2}\right)\left\{(g - 2)(\ln\xi)^3 - \left[\frac{7}{2}(g - 2)^2 + 24(g - 1)\right](\ln\xi)^2 + \cdots\right\}, \qquad (5.1)$$

in the same low-momentum-transfer approximation as was used to calculate Eqs. (4.38) and (4.39). This cross section increases only logarithmically with k, because the greatest contribution to the neutrino production is at relatively large impact parameters in the Coulomb field. The ratio of Eq. (4.38) or (4.39) to (5.1) is about

$$\alpha\,(\hbar/Mcd)\,(k/Mc^2)\,6\pi\,\sqrt{2}\,/\,GM^2 \approx$$

$$2000\,(m_\pi/M)A^{-1/3}\,(k/Mc^2)\,. \qquad (5.2)$$

The cross section for the electromagnetic production of vector mesons is thus large compared with that for the neutrino production. The probability of competing electromagnetic processes is also extremely large. This "background" will consist principally of photoproduced pions which decay into muons and electrons, and of pairs of electrons and of muons (for which $\overline{\Phi}$ is at least 10^6 or 25 times as large, respectively, as for B mesons).

The B meson is to be distinguished from this large background by its large mass and prompt decay. On both these accounts, the B-meson decay products will tend to appear at relatively large angles compared with directly produced particles. Two interesting B-meson signatures would seem to be wide-angle $\mu^+\mu^-$ or $\mu^\pm e^\mp$ coincidences. Each of these leptons will, typically, have one-quarter the original photon energy, while with directly produced pairs each of the particles obtains on the average one-half the photon energy. The lepton products of the semiweak B-meson decay will also be partially polarized.

It would seem that the neutrino and electromagnetic production of B mesons may constitute parts of two different programs: one a study of weak neutrino interactions, the other a study of the electromagnetic creation of new charged particles.

References

* A preliminary version of this paper appeared in Proceedings of the 1960 International Conference on High Energy Physics at Rochester (Interscience Publishers, Inc. New York, 1960), p. 564. It is based in part on a thesis submitted by J. A. Young in partial fulfillment of the requirements for the doctoral degree at the University of California (Lawrence Radiation Laboratory Report UCRL-9563, Feb. 8, 1961).

† Now at the University of Pennsylvania, Philadelphia, Pennsylvania.

‡ Now at General Electric Company, Vallecitos Atomic Laboratory, Pleasanton, California.

1. R. F. Christy and S. Kusaka, Phys. Rev. 59, 414 (1941).

2. C. F. v. Weizsäcker, Z. Physik 88, 612 (1934); E. J. Williams. Phys. Rev. 45, 729 (1934); W. Heitler, The Quantum Theory of Radiation, Third Edition (Oxford University Press, New York, 1954), Appendix.

3. H. S. W. Massey and H. C. Corben, Proc. Cambridge Phil. Soc. 35, 463 (1939).

4. R. H. Dalitz, Proc. Roy. Soc. (London) A206, 509 (1951).

5. We are indebted to Professor Stephen Gasiorowicz (University of Minnesota) for a stimulating discussion of this question.

6. H. Umezawa and S. Kamefuchi, Nuclear Phys. 23, 399 (1960).

7. F. Booth and A. H. Wilson, Proc. Roy. Soc. (London) 175, 483 (1940).

8. We are indebted to Dr. S. Frautschi for helpful discussions of this point.

9. The same limit to the Born approximation has been derived by J. R. Oppenheimer, Phys. Rev. 59, 462 (1941) and by L. Landau, J. Phys. U.S.S.R. 2, 483 (1940). Oppenheimer requires that the interaction energy in the center of mass be small compared with the total energy. Landau requires that the cross section for all competing processes be small compared with the cross section in question.

10. R. Hofstadter, Ann. Rev. Nuclear Sci. 7, 231, (1957).

11. W. Pauli, Revs. Modern Phys. 13, 203 (1941).

12. W. Heitler, The Quantum Theory of Radiation, Third Edition (Oxford University Press, New York, 1954).

13. S. D. Drell, Phys. Rev. Letters 5, 278 (1960).

14. T. D. Lee, in Proceedings of the 1960 Annual International Conference on High Energy Physics at Rochester (Interscience Publishers, Inc., New York, 1961), p. 567.

20. OUTLINE OF AGS EXPERIMENTS AND 1000-Gev ACCELERATOR STUDIES

PART I. EXPERIMENTS AT THE BROOKHAVEN AGS

PART II. STUDIES FOR 1000-Gev ACCELERATOR

Luke Yuan

July 27, 1961

I. AGS Experiments

Beam Surveys

The first major experiment on the AGS was an investigation of the composition of beams coming from an internal target, and measurements of the distribution of the various particles in energy and angle. This work had two objectives:

a. To provide the necessary information concerning particle intensities required for the detailed planning of most future experiments.

b. To provide a detailed enough study of the particle-production characteristics to allow both phenomenological and other theoretical analyses of the basic high-energy particle-production mechanism.

Intensities were measured with a momentum-analyzed beam, using a scintillation counter telescope and a differential gas Cerenkov counter to identify the individual particles. It was possible to distinguish among K's, π's, and p's up to 20 Gev/c. At this time, the average primary beam intensity was 4×10^{10} protons per pulse, and the targets used, 37 g/cm^2 of Al and 21 g/cm^2 of Be, were about 50% efficient. Measurements were made at target angles of 4.75°, 9°, 13°, and 20°, and also at 30° and 90°. The analyzed beams had a momentum spread of ±2% and a solid angle of 2×10^{-7} sr.

Figure S20-1 shows the experimental area, Fig. S20-2 one of the gas Cerenkov counters. Diagrams of the optical arrangement are shown in Figs. S20-3 and -4, and a typical curve of counting rate versus pressure for a negative beam is shown in Fig. S20-5.

Secondary fluxes of pions and protons for a beam energy of 30 Gev are given in Fig. S20-6 at various angles, for both Be and Al targets. The ratio of fluxes from Be and Al targets ranges from 1.1 to 1.4. Figure S20-7 gives the fluxes of pions for proton beam energies of 10, 20, and 30 Gev.

Figures S20-8 and S20-9 show the variation of the ratio of K^+/π^+, K^-/π^-, and $\bar{p}/\pi^-$ as a function of secondary momentum, for different values of the circulating proton beam energy, and at 4.75° and 9° to the target.

From these data, we can conclude that the ratio K^+/π^+ is not sensitive to incident energy, and tends to increase toward higher K^+ momenta; and that the ratio K^-/π^- falls rapidly with decreasing incident proton energy and also falls rapidly with increasing K^- momentum. At low momenta these two ratios tend to approach equality. These results may imply that the production of K's of low momenta occurs predominantly through K-pair production, whereas for large p_{K+} associated production predominates.

Fitch's group has made observations on particle fluxes at 90° to the circulating beam, using time-of-flight methods for identification. The momentum spectra of pions, protons, deuterons, and tritons are given in Fig. S20-10.

AGS Research in Progress

At present, the primary beam intensity is 3×10^{11} protons per pulse at 33 Gev/c. The following is a list of current experiments.

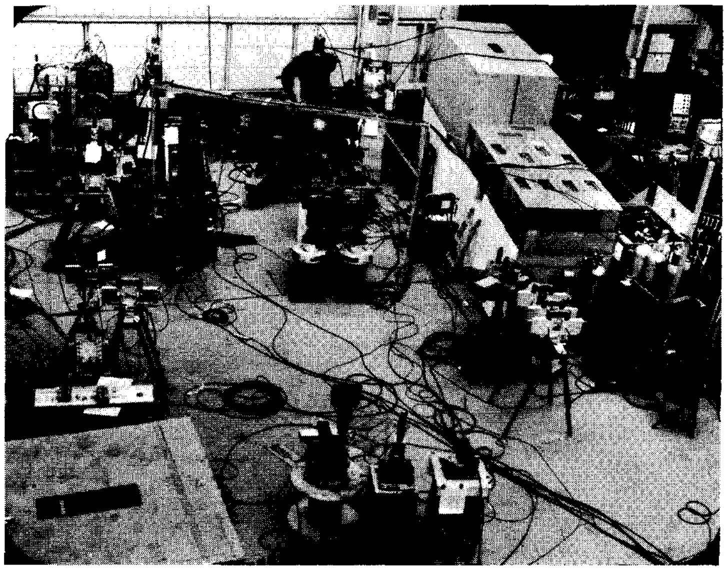

Fig. S20-1. General view of experimental area.

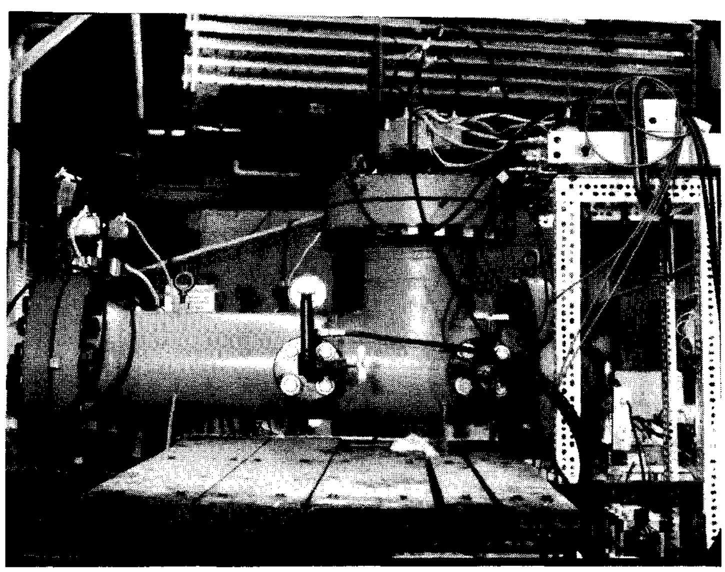

Fig. S20-2. Gas Cerenkov counter.

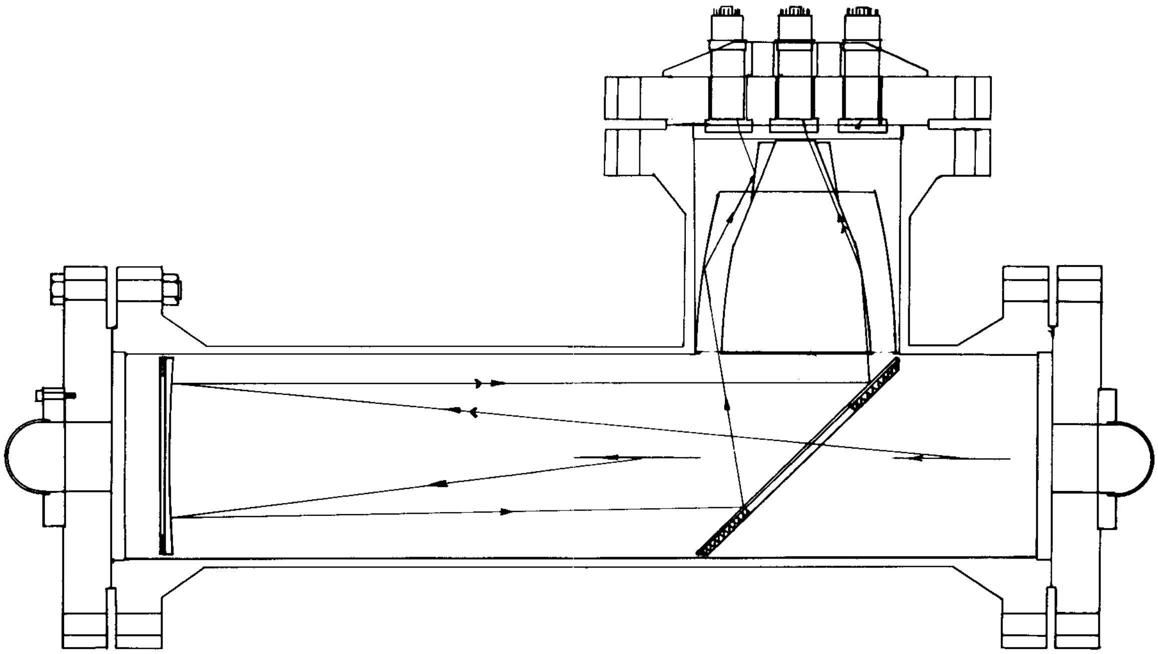

Fig. S20-3. Diagram of optical arrangement.

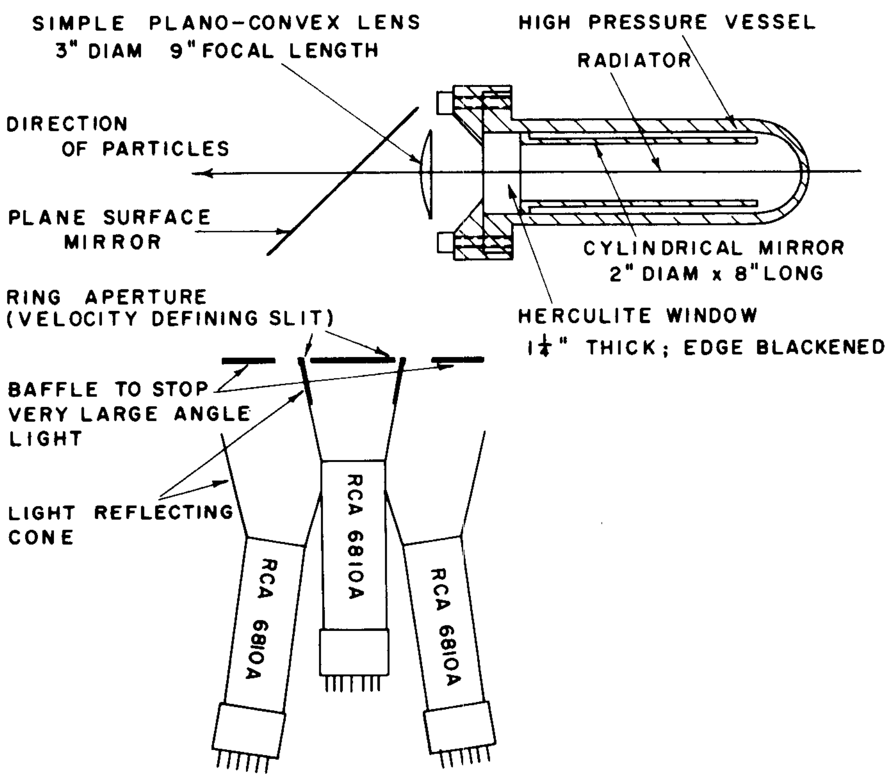

Fig. S20-4. Further details of optical arrangements.

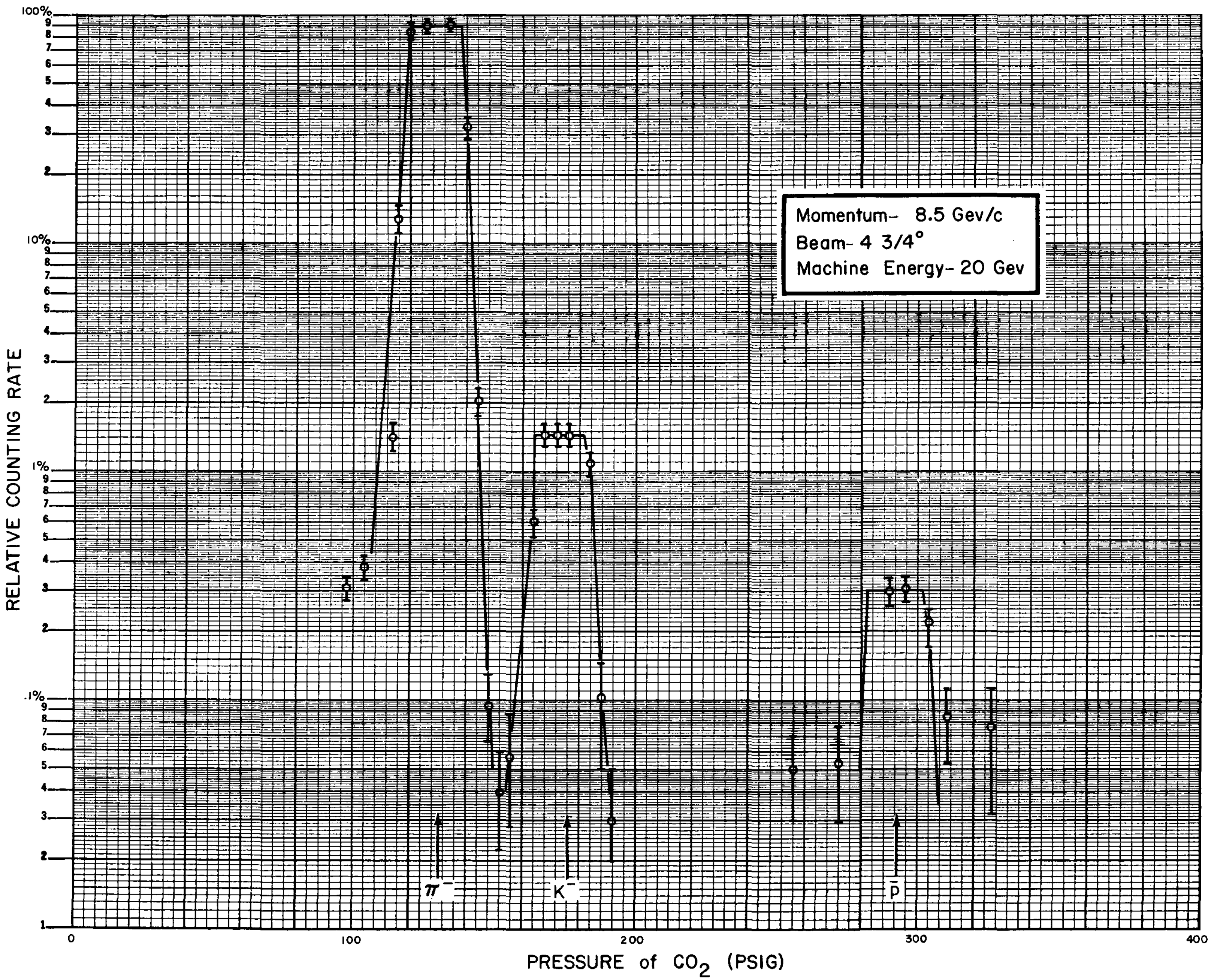

Fig. S20-5. Relative counting rate vs CO_2 pressure in Cerenkov counter.

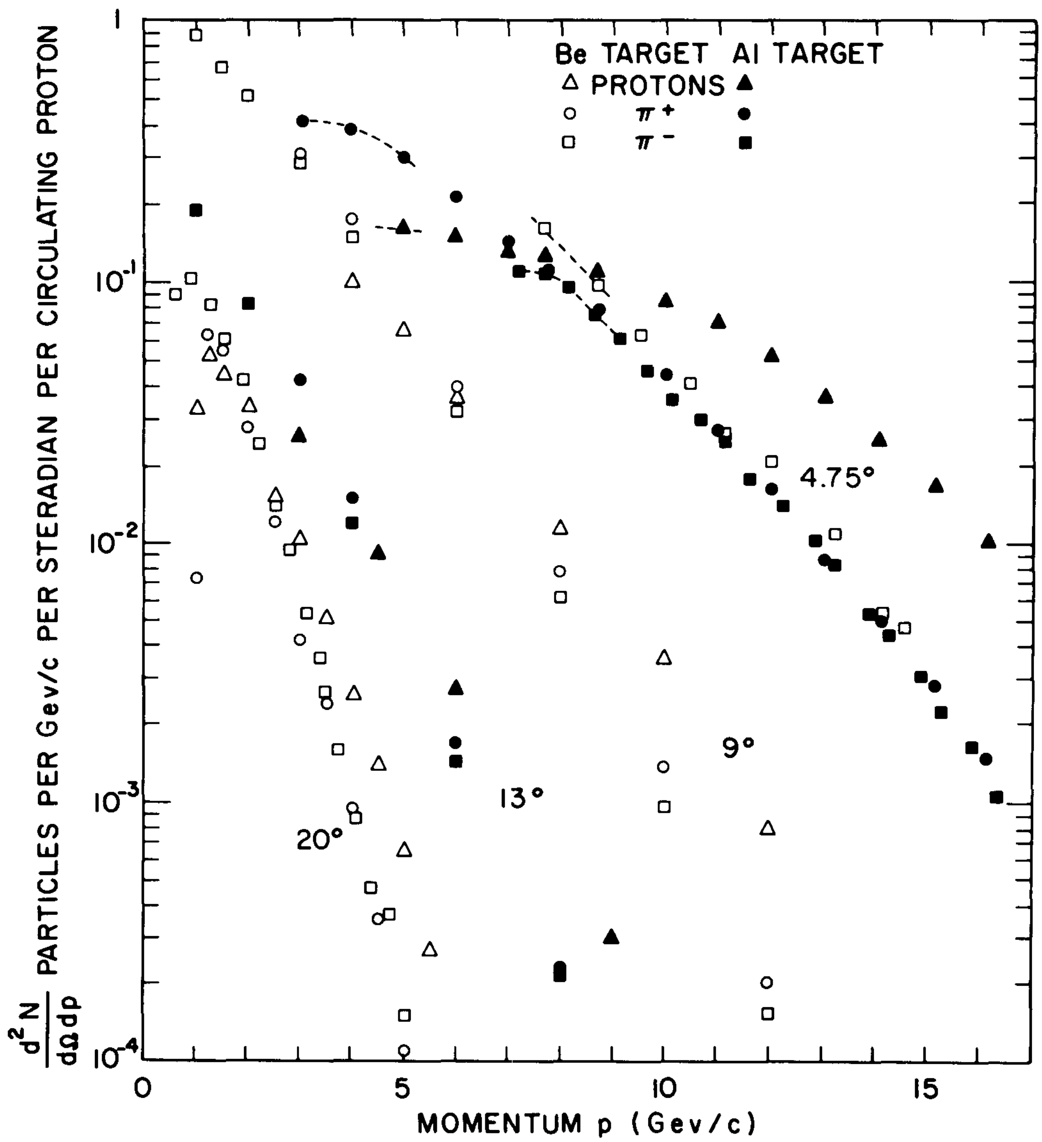

Fig. S20-6. Secondary fluxes for proton beam energy of 30 Gev.

a. $\bar{p}$-p total cross section, C counter telescope.

b. $K^{\pm}$-p experiment; Cool et al.

c. parasitic experiments.

(1) γ rays at 30° to the beam; Al Wattenberg et al. 30-Gev p on carbon

(2) monopole; Purcell et al.

(3) 30° D production in Al about twice that in Be; p production in Al slightly higher

(4) p-p production (C, CH_2) of d, p, K, etc., in the low-momenta region.

Future Experiments

Two major facilities are being set up for the immediate future. These are a separated beam channel to be used by Shutt's group and for a study of ($\bar{p}$, p) interaction by the Yale group, and the large installation for neutrino experiments.

II. Studies for 1000-Gev Accelerator

In connection with the preliminary study being made at Brookhaven on the feasibility of a 1000-

Gev accelerator facility, many people are devoting some time to a study of the utilization of such a machine. The following is a list of topics with the names of the persons responsible for each:

A. Some theoretical considerations on the desirability of a 300- to 1000-Gev accelerator - T. D. Lee, R. Serber, G. C. Wick, C. N. Yang (G. Chew, M. Gell-Mann also for short-period consultation).

B. Review of very-high-energy phenomena in cosmic rays - M. Koshiba.

C. Proposed studies on the experimental feasibilities for a 300- to 1000-Gev accelerator.

1. Beam kinematics, secondary beams expected for both proton and electron primaries
    - a. Intensity and angular characteristics from kinematics and other theoretical considerations; b. Decay beams μ and ν, etc. — S. J. Lindenbaum, R. M. Sternheimer
    - c. Experimental area design — J. P. Blewett, S. J. Lindenbaum
2. Beam separation
    - a. Present available methods; b. Possible new techniques — J. Sandweiss, M. Webster
    - c. Targeting and extraction of secondary beams; d. External beams — B. Culwick, J. Sandweiss
    - e. High-field magnets — J. Jensen, A. Prodell
3. Shielding
    - a. 1000-Gev proton beam at 10^{13} ptcles/pulse; b. 100-Gev electrons at 10^{13} ptcles/pulse — S. J. Lindenbaum
    - c. Target shielding to eliminate μ's — N. Samios
4. Particle detection and identification
    - a. Current available techniques
        - (1) Cloud and bubble chambers — R. Rau, R. Shutt
        - (2) Time-of-flight and chronotron techniques — L. C. L. Yuan
        - (3) Spark chambers — D. Meyer, G. Zorn

4. Particle detection and identification (Continued)	
(4) Scintillation chambers	G. Reynolds
(5) Cerenkov counters and Cerenkov chambers	L. C. L. Yuan
(6) Emulsions	E. Salant
(7) Solid-state detectors	L. Miller L. C. L. Yuan
b. Possible new techniques	
(1) Relativistic rise	E. Purcell L. C. L. Yuan
(2) Electromagnetic interaction	L. C. L. Yuan
(3) Synchrotron radiation, etc.	E. Purcell
D. Considerations in some specific experiments	L. Lederman W. Walker

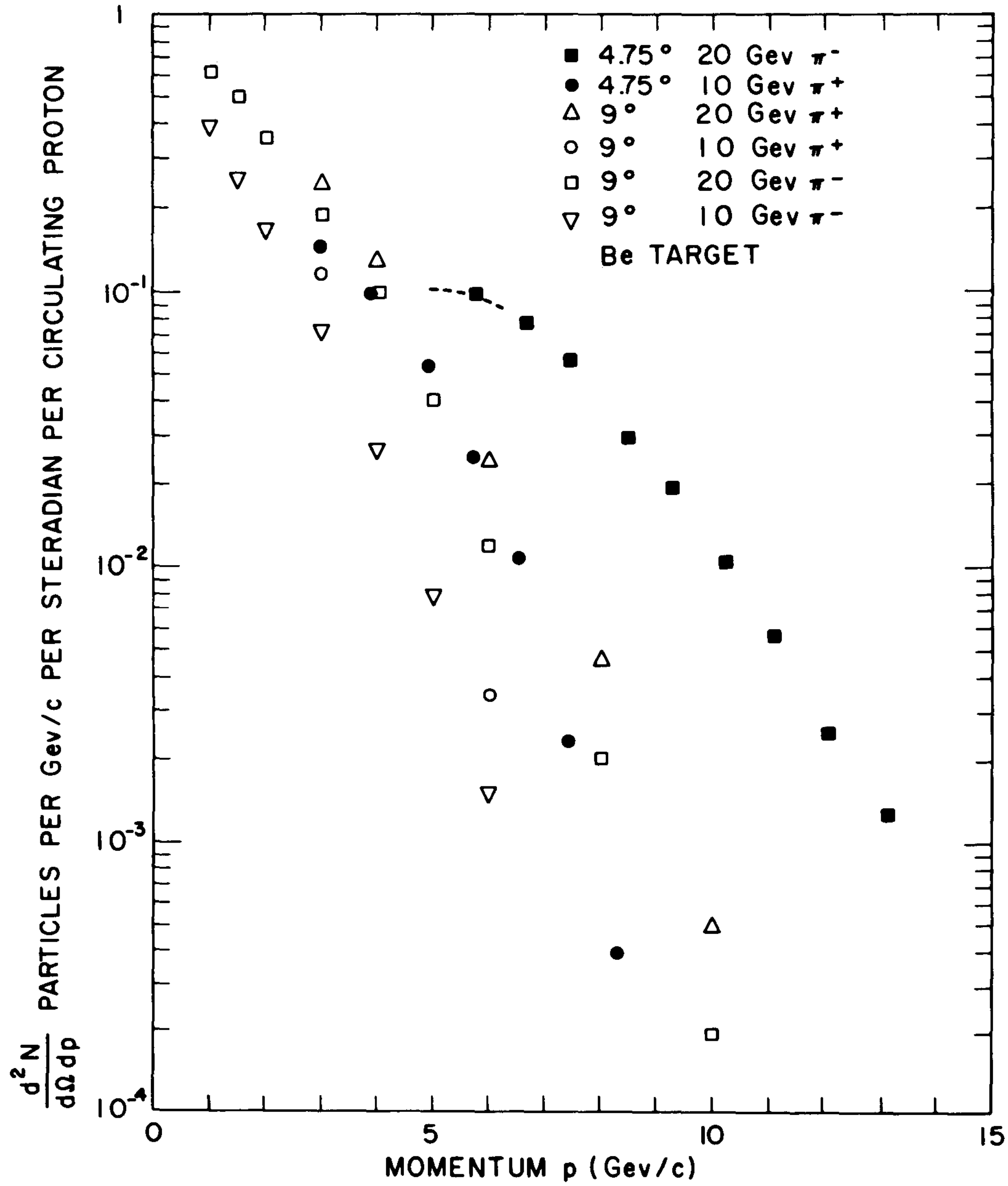

Fig. S20-7. Pion flux for various proton beam energies.

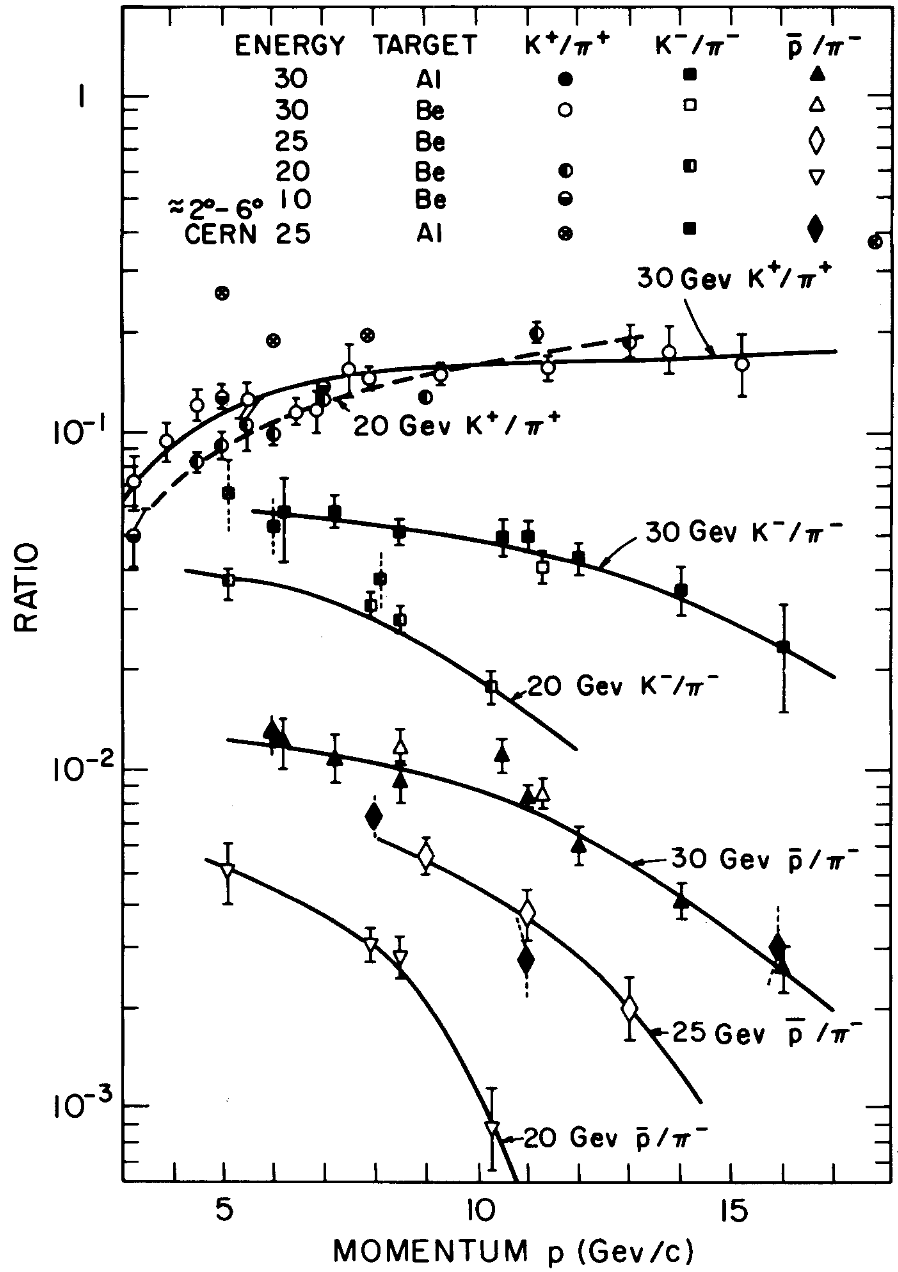

Fig. S20-8. Particle ratios at the target, lab production angle 4.75°.

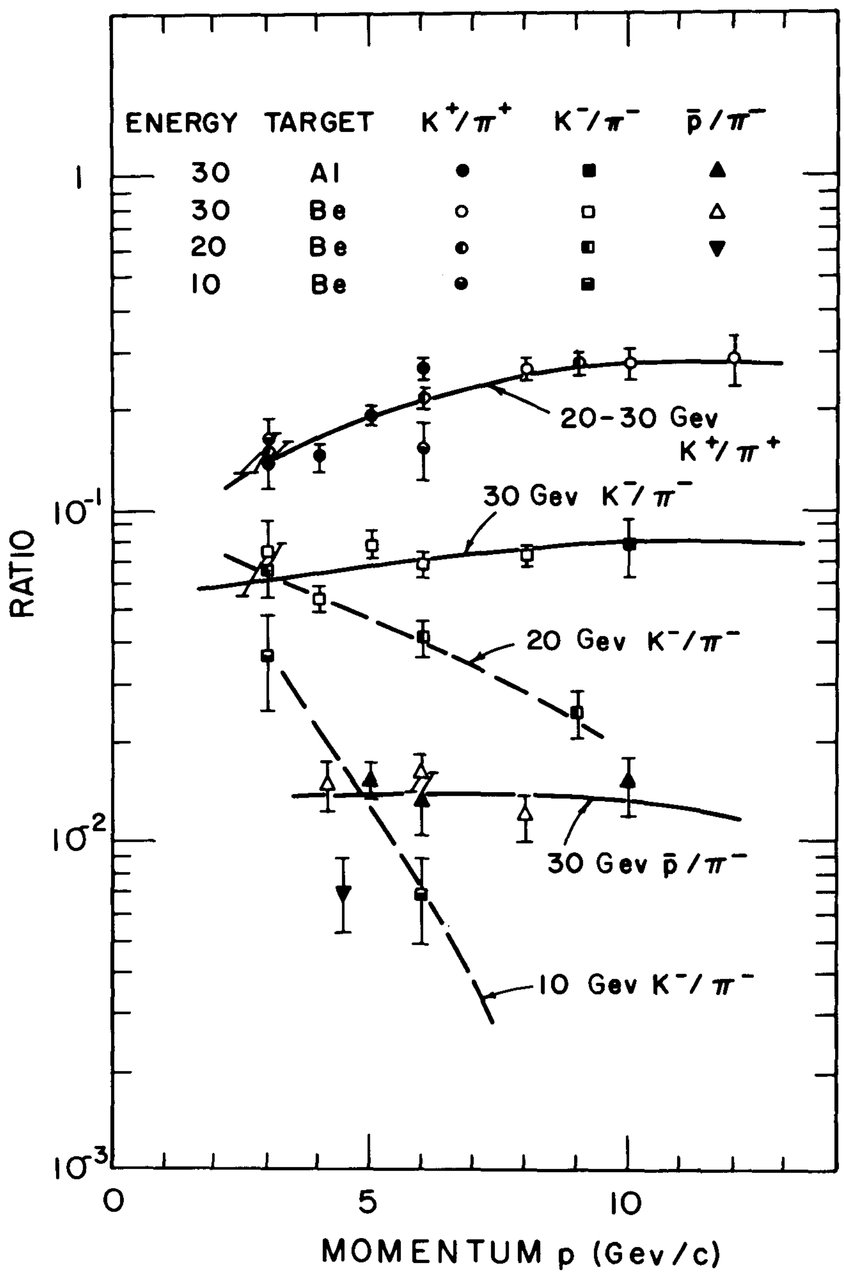

Fig. S20-9. Particle ratios at the target, lab production angle 9°.

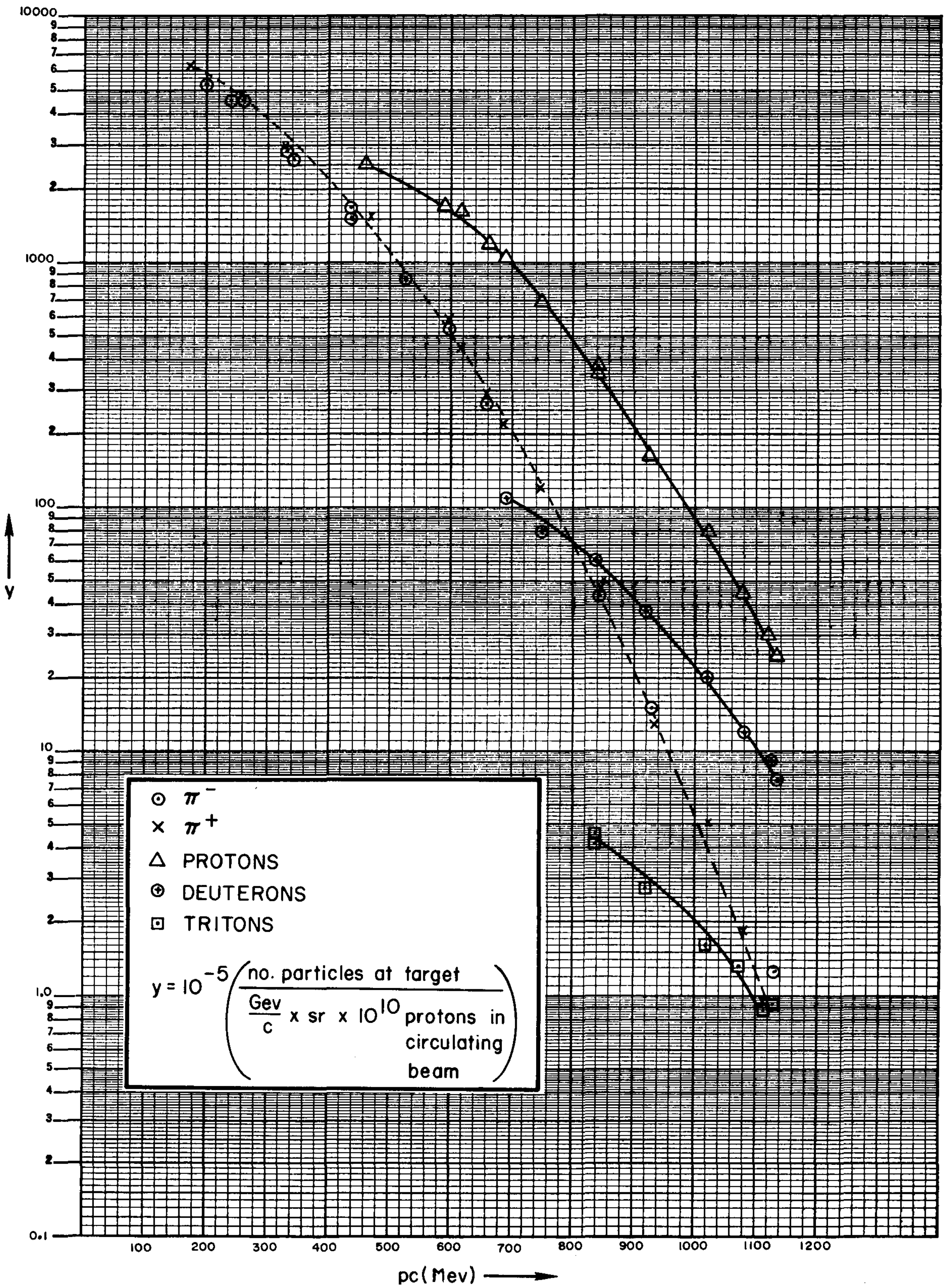

Fig. S20-10. Secondary fluxes at 90° lab. angle.

23. PART I. ON THE DETECTION OF INTERMEDIATE BOSON PAIR PRODUCTION

L. J. Koester, Jr.

August 1, 1961

Bludman (see Seminar 17) has discussed the electrodynamic properties of intermediate bosons $B^{\pm}$, which supposedly are coupled to the weak lepton current. He has pointed out that the cross section for electromagnetic pair production of these charged bosons should be large compared with neutrino cross sections. Rather severe difficulties arise, however, in considering how to identify the pair-production events. First, the mass is unknown. It is supposedly greater than the K-meson mass (500 Mev); otherwise it would be observed in K decays. Presumably, the pair-production cross section decreases as the inverse square of this mass, which may well be greater than the nucleon mass. Second, the mean life is not more than about 10^{-17} sec, so that the $B^{\pm}$ decays at the point where it was created. Third, although the decay is a two-particle decay,

$$B^{\pm} \rightarrow \mu^{\pm} + \nu \text{ or}$$

$$B^{\pm} \rightarrow e^{\pm} + \nu ,$$

the occurrence of an unknown mass in the pair production by a photon of unknown energy, together with two invisible particles in the final system, makes the kinematics almost impossible to unravel. Finally, the large mass of the $B^{\pm}$ requires, on the average, large momentum transfers through the Coulomb field to the nucleus in the pair production. The cross section decreases with increasing momentum transfer, even for a point charge, and more so when a form factor is involved.

In spite of these difficulties, it is tantalizing to consider some features of the kinematics that might make an experiment possible.

Kinematics of Pair Production

Let K = momentum and energy of the incident photon,
M = mass of the recoil nucleus,
$\mathfrak{m}$ = mass of the boson.

The momentum, k, of the recoiling nucleus satisfies the relation, in nonrelativistic approximation for the recoiling nucleus,

$$k = \frac{K}{1 + \frac{K}{M}} \left[\cos\Theta \pm \sqrt{\cos^2\Theta - \frac{w^2}{K^2}\left(1 + \frac{K}{M}\right)} \right] , \qquad (1)$$

where Θ is the lab-system angle of recoil with respect to the direction of the incoming photon and w is the total energy of the pair in its own rest frame.

A number of quantities can be obtained from Eq. (1). Threshold photon energy is obtained by setting the square root equal to zero for $\Theta = 0$ and $w = 2\mathfrak{m}$. This gives

$$K_{threshold} = 2\mathfrak{m}\left(\frac{\mathfrak{m}}{M} + \sqrt{1 + \frac{\mathfrak{m}^2}{M^2}}\right) . \qquad (2)$$

For $K > K_{threshold}$, the minimum momentum transfer is given by Eq. (1), with $\Theta = 0$ and $w = 2\mathfrak{m}$:

$$k_{min} = \frac{K}{1 + \frac{K}{M}} \left[1 - \sqrt{1 - \frac{4\mathfrak{m}^2}{K^2}\left(1 + \frac{K}{M}\right)} \right] \qquad (3)$$

$$\approx \frac{2\mathfrak{m}^2}{K} . \qquad (4)$$

The approximate expression is the familiar result for $M >> K$ and $K >> m$.

The maximum recoil angle is obtained by setting the quantity under the square root sign equal to zero:

$$\cos^2 \Theta_{max} = \frac{w^2}{K^2}\left(1 + \frac{K}{M}\right), \tag{5}$$

from which follows $\Theta_{max} \approx 90°$ for $M >> K >> m$.

Since momentum transfers are crucial in the intensity considerations to follow, a few examples should be noted from Eq. (4). For a lead target and assuming $m = 1$ Gev, k_{min} is 30 Mev/c for $K = 60$ Gev and k_{min} is 200 Mev/c for $K = 10$ Gev. Using the exact expression [Eq. (3)] for a hydrogen target, one has $k_{min} = 250$ Mev/c for $K = 10$ Gev.

The cross section for pair production should be, approximately,

$$\sigma = \frac{\pi}{12}\frac{e^2}{\hbar c}\left(\frac{Ze^2}{mc^2}\right)^2\left(\frac{K}{mc^2} - 2\right)^3$$

$$\approx 1.5 \times 10^{-28} Z^2\left(\frac{m_e}{m}\right)^2\left(\frac{K}{mc^2} - 2\right)^3 ,$$

where m_e is the rest mass of the electron.

This is where the momentum-transfer consideration becomes important. The Z^2 factor for lead would increase the cross section 6400 times, but only if the momentum transfer is small. To estimate the value of momentum transfer beyond which the form factor decreases rapidly, take the nuclear radius to be $10^{-13} A^{1/3}$ cm, which for Pb is 6×10^{-13} cm. The corresponding momentum transfer is about 30 Mev/c.

For momentum transfers much larger than this, the Z^2 factor cannot be realized. For a given pair particle mass m, Eq. (4) gives the minimum useful photon energy K which will fulfill this condition. For example, if lead is the target, and $m = 1$ Gev, then

$$K_{min} \approx \frac{2(\text{Gev})^2}{30 \text{ Mev}} \approx 60 \text{ Gev}.$$

If $m = 500$ Mev, K_{min} drops to 15 Gev.

It is important to keep in mind the ways in which the mass m influences the method of detection.

If larger momentum transfers are desirable, hydrogen should be considered as an alternative. Hofstadter[1] and Wilson[2] have found that the form factor $F_1 = 0.4$ at $q \approx 1$ Gev/c, which means that momentum transfers of this order in hydrogen are only suppressed by a factor $F_1^2 = 0.16$.

If the momentum transfer will be so high that the Pb cross section will only be proportional to Z, 60 cm of liquid hydrogen contains as many protons as does 1 cm of Pb and, important for background considerations, no neutrons. Three types of observation may be considered: pair production in Pb by high-energy photons with small momentum transfer, pair production by photons in hydrogen with large momentum transfer, and pair production by electrons in hydrogen. Of these, only the first is discussed here.

Pair Production in Pb by High-Energy Photons

Since only low momentum transfers are involved, the intermediate boson mass m is the most important unknown and determines the minimum photon energy K through Eq. (4). The pair system has practically all of the energy K and moves directly forward in the laboratory. The pair members B^+ and B^- spread over a cone of half angle m/K, and about 10% of them have energies within 10% of K/2 . The decay particles may appear at larger angles in the laboratory because they are much lighter than m.

For a boson with total energy K/2, its rest system is moving with respect to the lab system according to

$$\gamma = \frac{1}{\sqrt{1-\beta^2}} = \frac{K}{2m}. \tag{6}$$

The lab angle, Θ_μ, of emission of the decay particle with respect to the boson direction is given by

$$\tan \Theta_\mu = \frac{\sin \bar{\Theta}_\mu}{\gamma \left[\cos \bar{\Theta}_\mu + \beta \dfrac{1 + \left(\frac{\mu}{\mathfrak{m}}\right)^2}{1 - \left(\frac{\mu}{\mathfrak{m}}\right)^2} \right]} , \qquad (7)$$

where $\bar{\Theta}_\mu$ is the angle of emission in the boson rest system and μ is the mass of the decay particle (muon or electron). Thus Θ_μ can exceed 90° if the denominator of Eq. (7) can reach zero; that is, for

$$K < \mathfrak{m}^2/\mu . \qquad (8)$$

For $\mathfrak{m} = 1$ Gev and 10 Gev < K < 100 Gev, this can occur for electron decay but not for μ decay.

For most angles, $\bar{\Theta}_\mu$, (7) is, approximately,

$$\tan \Theta_\mu = \frac{1}{\gamma} \tan \frac{\bar{\Theta}_\mu}{2} , \qquad (9)$$

so that values of a few degrees might be expected for the angles of the decay products with respect to the boson direction and with respect to the original photon direction.

The solid-angle transformation is given by

$$\frac{d\bar{\Omega}}{d\Omega} \approx \gamma^2 \left[1 + \beta \frac{1 + \left(\frac{\mu}{\mathfrak{m}}\right)^2}{1 - \left(\frac{\mu}{\mathfrak{m}}\right)^2} \cos \bar{\Theta}_\mu \right]^2 . \qquad (10)$$

The γ^2 factor makes this large for most angles. For example, for $\gamma = 30$ and $\mu/\mathfrak{m} = 0.1$, the ratio is unity for $\bar{\Theta}_\mu \approx 160°$, corresponding to 12° (lab). The energy transformation is more critical, however. Since the energy of the decay particles in the lab system is

$$E_\mu = \frac{\gamma \mathfrak{m}}{2} \left\{ 1 + \left(\frac{\mu}{\mathfrak{m}}\right)^2 + \beta \left[1 - \left(\frac{\mu}{\mathfrak{m}}\right)^2 \right] \cos \bar{\Theta}_\mu \right\}$$
$$\approx \frac{\gamma \mathfrak{m}}{2} \left(1 + \cos \bar{\Theta}_\mu \right) , \qquad (11)$$

the second term can wipe out the first. For $\bar{\Theta}_\mu = 90°$

$$E_\mu \approx \frac{\gamma \mathfrak{m}}{2} = \frac{K}{4} \approx 15 \text{ Gev.}$$

Losing energy at the rate of 2 Mev/ g/cm^2 , such muons may traverse 7500 g/cm^2 in coming to rest. A shield of 4000 g/cm^2 will allow them to pass, but will constitute an order of magnitude of 100 interaction lengths for strongly interacting particles. Thus, the pions will be attenuated by a factor of order e^{-100}. Very few of these pions will decay to muons before they interact.

Assuming a countable γ-ray beam of order 10^7 photons/second and a 1-cm-thick Pb target, the yield of $B^\pm$ pairs in a 10% energy interval would be

$$Y = 10^7 \times 10^{-30} \text{cm}^2 \times 10^{-1} \times \frac{6 \times 10^{23}}{208}$$
$$\times 11 \text{g/cm}^2 = 0.32 \times 10^{-1} \text{ sec}^{-1}$$

which is of the order of 1 per minute.

The choice of cases in which one of the pair members decays into a μ and the other into an electron is in some ways more characteristic. Ordinary pair production of 15-Gev muons is expected to send most μ pairs into a cone of 1/3 degree half angle, but large-angle pairs have to be evaluated. For the $\mu^\pm$, $e^\pm$ case, one cannot pass the electron through a filter without making some showers. Then one must worry about π^0 Dalitz pairs. The idea of "destructive testing" must be kept in mind, however. After the vector momentum of a particle has been measured, it can pass into a lead-plate spark chamber, in which an electron makes showers, a π or nucleon interacts, but a μ just grinds to a halt.

Acknowledgement

I wish to thank Dr. David Wong for many valuable discussions.

References

1. R. Hofstadter, C. de Vries, and R. Herman, Phys. Rev. Letters 6, 290 (1961)

2. D. N. Olson, H. F. Schopper, and R. R. Wilson, Phys. Rev. Letters 6, 286 (1961)

23. PART II. DIFFRACTION SCATTERING OF π^+ MESONS, K^+ MESONS, PROTONS, AND ANTIPROTONS

Leroy T. Kerth

August 1, 1961

Several other papers in this series have dealt with the diffraction scattering of particles at very high energies from a theoretical aspect. The purpose of this paper is to propose an experiment for measuring this diffraction scattering. Before one can measure the scattering of a particle, one must first produce a beam at known momentum and select in this beam the particles of a particular mass.

First we describe the beam and selection system. The magnet arrangement is shown in Figure S9-2 of Seminar 9, Part I. When the achromatic set in the straight section described therein is used, the 100-Gev/c particles of either sign are focused by Q_1 at the field lens Q_2. M_1 provides further momentum analysis than was achieved by the achromatic set in the straight section. Q_3 produces a second image at the point called trigger. Bending magnets M_2 and M_3 serve to recombine momenta at the trigger. M_2 and M_3 are also used in analyzing the scattering. The magnets M_1, M_2, and M_3 are all superconducting, operating at 100,000 gauss. If they are 3.3 meters long, then 100-Gev/c particles are deflected 0.1 radian in each magnet. In the quadrupoles Q_1 and Q_2 are two threshold Cerenkov counters of the type described by Keefe (Seminar 9, Part II). The first is a 13-ft-long counter operating with methane at a pressure of 7.5 cm Hg. This counter will count both π mesons and K mesons in the beam but will not count protons. The counter inserted through Q_2 and extending from M_1 to Q_3 is a 160-ft-long counter operating at a pressure of 2.1 cm of Hg. This counter does not count K mesons and protons, but does count π mesons. By using various coincidence and anticoincidence combinations of C_1 and C_2, one can select any one of the three particles — π mesons, K mesons, or protons — that might be in the beam.

One expects an average momentum transfer in the scattering of approximately 250 Mev/c. This implies a scattering angle of approximately 1 mr. Thus the angular resolution required in the experiment is approximately 0.1 mr. In addition, to assure elasticity in the scattering, the momentum of the ingoing and outgoing particles must be measured accurately. Since the least inelastic interaction that can occur is to produce one π meson in the scattering, one must measure the momentum transfer to an accuracy of less than 140 Mev/c. This implies a momentum resolution for the incident and scattered particles of about 0.1%. The scattering apparatus should consist of two spectrometers, one measuring the momenta of the particles going into the hydrogen target, the other measuring the direction and momentum of the particles emerging from the hydrogen target. By using a ten-gap spark chamber it is possible to locate the horizontal position of a track to about 0.1 mm. Thus, two such chambers placed 1 m apart measure the direction of the particle to an error of about 0.1 mr. Our spectrometers, then, consist of a magnet which, if it is superconducting, will be 3.3 m long (if conventional, five times that long); with four chambers, two are placed on each end. Each spark chamber would have ten gaps and the two at each end would be placed 1 m apart. This system would allow one to measure the direction of a particle going in and out of the magnet to within 0.1 mr. With a 3.3-m magnetic field of 100,000 gauss, the angular deflection is 0.1 radian; thus the momentum is measured to approximately 0.1%. The experiment then consists of using M_2 and M_3 as the spectrometers on each side of the liquid hydrogen target. The four spark chambers coupled with M_2 measure the momentum and the direction of the particle going into the liquid hydrogen target. The four spark chambers and M_3 measure the momentum and direction of the particles emerging from the liquid hydrogen target (LH_2). The chambers would be triggered by a counter placed at the point called trigger. Q_3 can produce a very small image of the target in the machine at the trigger counter. It is possible to arrange the optics of the beam in such a way that a scattering of 0.1 mr would shift the particle outside the trigger counter.

It would seem that the flux needed for this experiment is quite low. On the basis of reasonable guesses at the total cross section for the elastic scattering, a secondary beam of 10^6 particles per pulse — which seems quite reasonable on the basis of the flux estimate made so far — should permit one to obtain 100 scatterings per machine pulse. Thus considerably greater sophistication than has been discussed here would be possible in the experiment without sacrifice of data. It would seem that it is quite feasible to consider carrying out, 10 years from now, an experiment to measure very accurately the diffraction scattering of $\pi^{\pm}$ mesons, $K^{\pm}$ mesons, protons, and antiprotons at 100 Gev/c.

26. THE WEAK INTERACTION AT HIGH ENERGY: PROGRESS OF THE NEUTRINO EXPERIMENTS OF CERN AND POSSIBLE ADVANTAGES OF A 300-GEV MACHINE

Jack Steinberger

August 8, 1961

Questions about the weak interaction that might be answered are:

a. Are there two kinds of neutrinos? The high-energy neutrino fluxes are composed almost entirely of "μ-type" neutrinos, ν_μ. If these are different from "e-type" neutrinos, the reaction $\bar{\nu}_\mu + p \rightarrow e^+ + n$. otherwise allowed, will be forbidden.

b. Is the weak interaction carried by bosons of intermediate mass? Experimentally, all that is known about these particles is that, if they exist, their mass must be greater than the K mass. In high-energy neutrino experiments one looks for the reaction

$$\bar{\nu}_\mu + p \rightarrow B_\mu^- + \mu^+ + p$$
$$\hookrightarrow \mu^- + \bar{\nu}_\mu \quad .$$

The rates for these processes have recently been calculated for complex atoms by Lee and Yang. The momentum exchange with the nucleon is mediated by the electromagnetic field, and the coherence properties (Z or Z^2) are not easily obtained. The resulting cross sections are steeply rising functions of the energy, depending critically on the B mass. Three such curves from Lee and Yang are reproduced in Fig. S26-1.

c. What is the form factor for the weak interaction, and what is the form at higher momentum transfers? Substantial insight would be gained by a detailed study of the processes

$$\bar{\nu} + p \rightarrow \mu^+ + n \quad \text{and}$$

$$\nu + n \rightarrow \mu^- + p \quad .$$

The calculations presented in Fig. S26-2 (Lee and Yang, Yamaguchi) are the predictions according to a model using the Hofstadter electromagnetic form factors, and special assumptions about the form of the Fermi coupling (conserved vector currents). The leveling off at high energy is due to the form factors; the large differences between the two curves are a consequence of the assumed form of the interaction.

The Experimental Problem

The basic experimental problem is due to the smallness of the cross sections at presently available energies. The expected cross sections are of the order of 10^{-38} cm^2, only 10^{-10} to 10^{-12} those for strong or electromagnetic cross sections. It is a special property of the neutrinos that they can be purified from strongly interacting particles without loss of energy and little loss of intensity; this is why, at present, only neutrino reactions are in preparation. The basic plan, then, is as in Fig. S26-3. There is a high-energy pion source, a decay path, a shield, and a detector.

CERN Experiment

The CERN experiment is carried out by a collaboration of three groups under the coordination of Bernardini. These groups support the three detectors: The École Polytechnique Bubble Chamber (1/2 ton of Freon; Lagarrigue), the CERN Bubble Chamber (3/4 ton of Freon; Ramm) and the CERN electronic detector (not yet fully developed; Faissner).

Layout

The pion beam is brought out from an internal target in the proton synchrotron through a 1.5-m

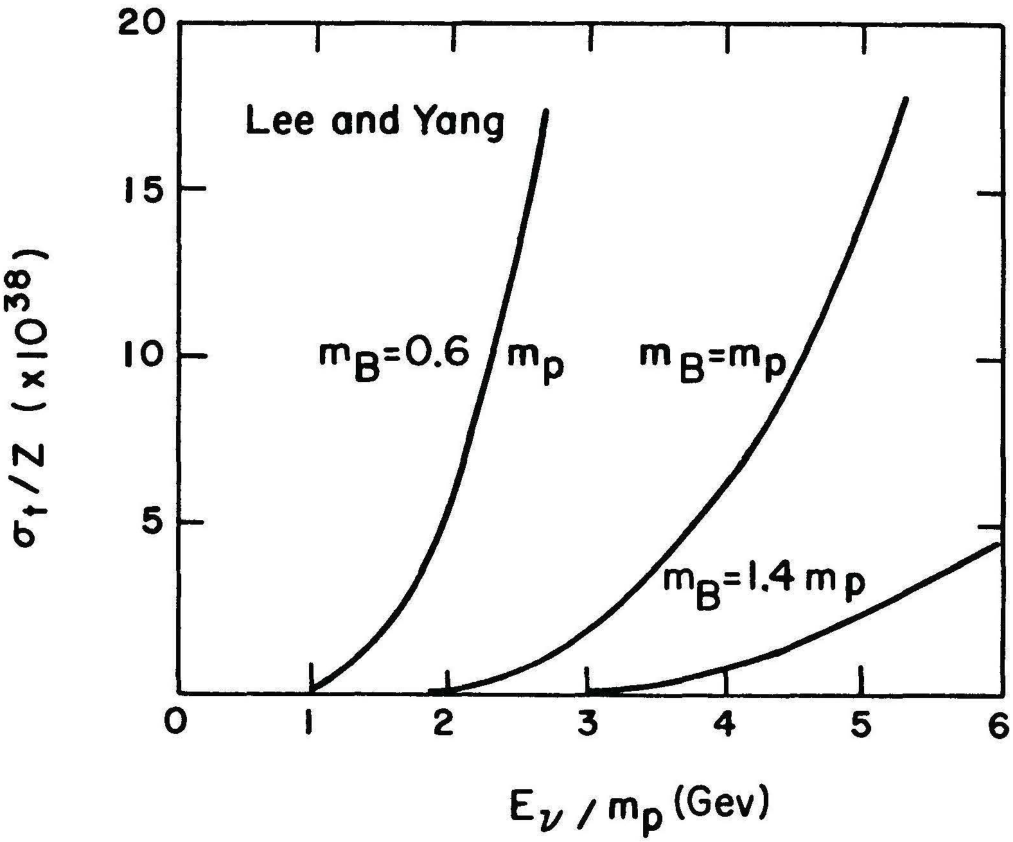

Fig. S26-1. Neutrino-proton cross sections for three values of intermediate boson mass.

straight section at about 7°. The fringing field of the following magnet is such that negative pions are rejected while positive pions are somewhat focused. The pion beam is limited vertically by the copper windings of these magnets, and this obstruction reduces the expected neutrino flux by a substantial factor, perhaps about 3. The decay path of the pions is about 22 m before they strike the shield consisting of 4 m of iron followed by 20 m of heavy concrete. The thickness of the shield in the beam direction is determined chiefly by the need to reduce the high-energy muon flux to a tolerable level (approximately 1/2 μ per pulse).

The Lagarrigue chamber is installed just behind the shield wall, 55 m from the target. The Ramm chamber is at a distance of about 70 m. The electronic detector, which is being redesigned, is between.

Expected Rates and Present Status

Pion flux

This has recently been measured systematically at Brookhaven. At the emission angle of the CERN experiment, the pion flux (pions per Gev per sr per proton circulating in the machine) is as shown in Fig. S26-4.

Neutrino flux

The neutrinos are emitted in a small cone of half angle about $0.1/E_\pi$ (Gev) and with a uniform spectrum between zero and $0.43\ E_\pi$. The expected flux is shown in Fig. S26-5. The curve is shown in the same scale as Fig. S26-4 to emphasize the fact that although the accelerator energy is 25 Gev, the neutrino flux is mainly below 1 Gev.

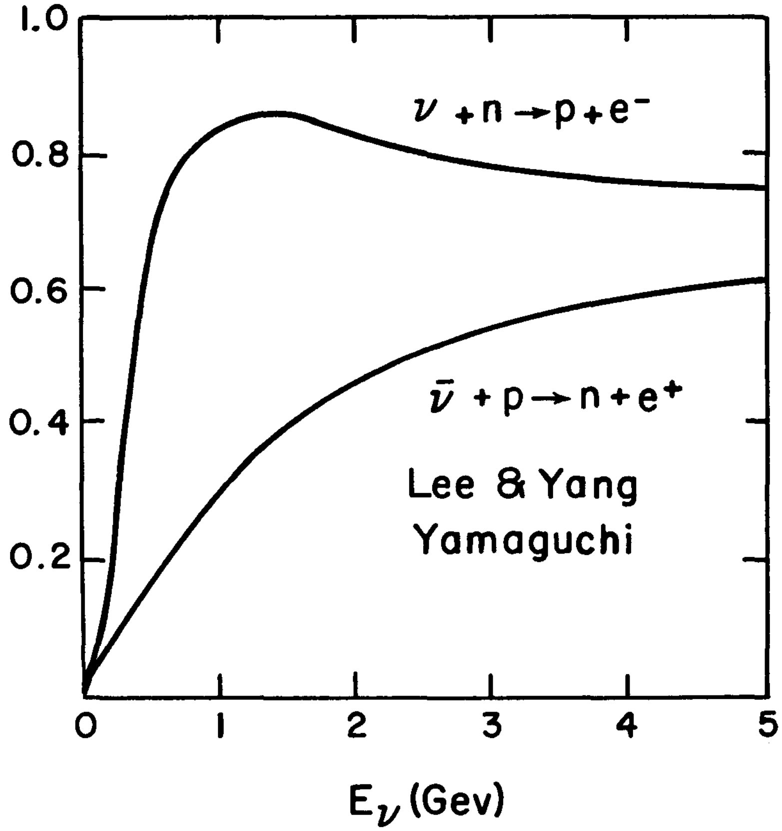

Fig. S26-2. Neutrino-proton cross sections with form factors included.

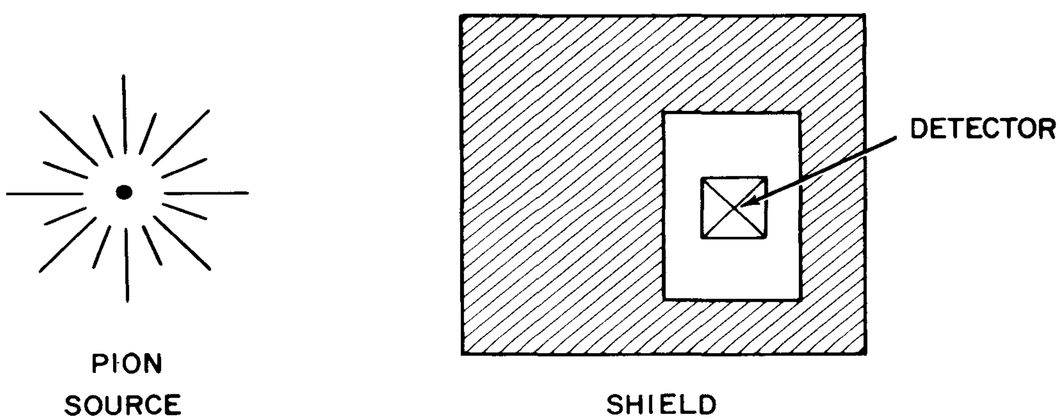

Fig. S26-3. Schematic layout of neutrino experiments.

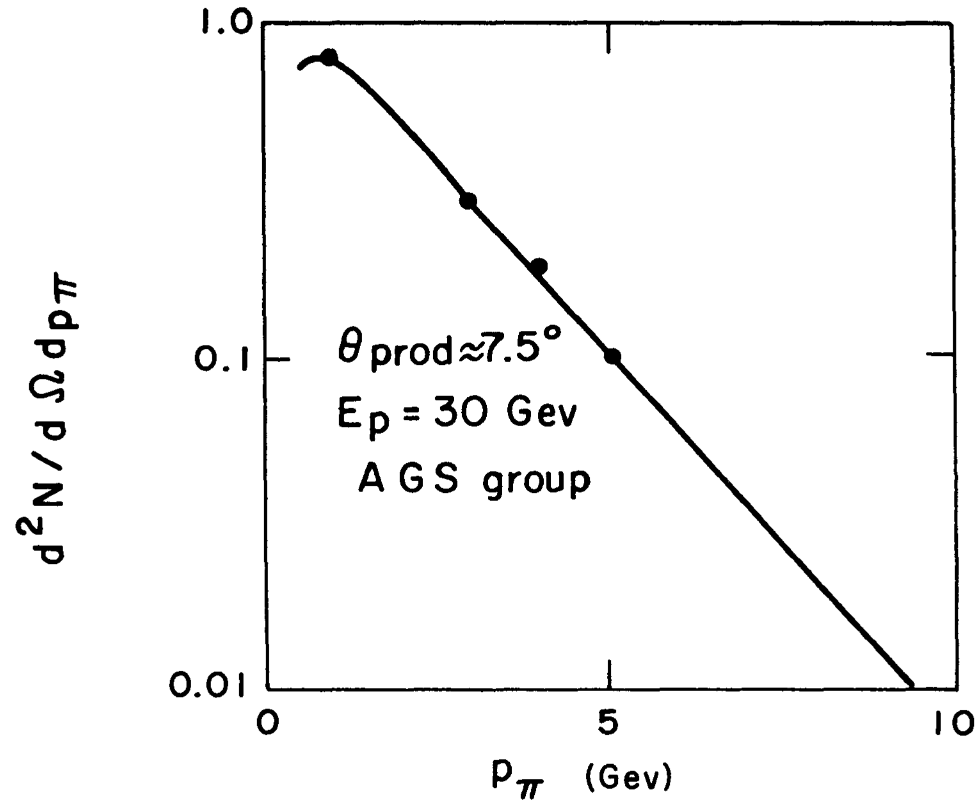

Fig. S26-4. Pion flux as measured at Brookhaven.

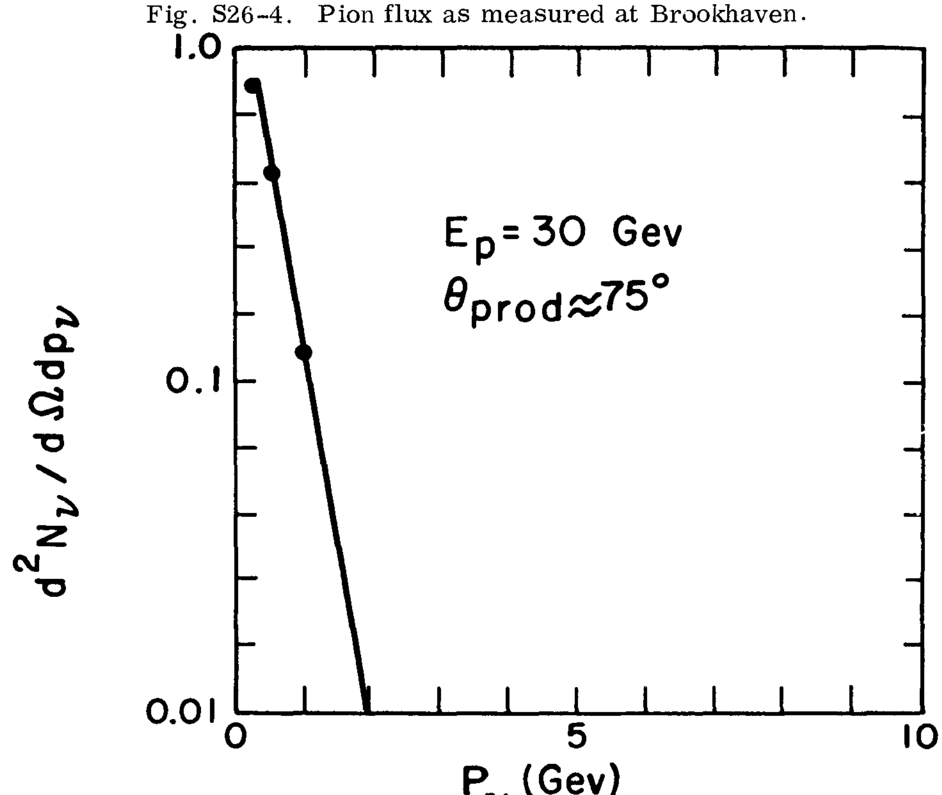

Fig. S26-5. Expected neutrino flux.

Expected number of events for a particular reaction

This is $I_0 \times$ number of pulses per day $\times$ detector efficiency $\times$ $(10^6 \times 6 \times 10^{23} \times \frac{1}{2}) \frac{1}{L^2}$ $\times \int dp_\pi K_\pi$ per day per ton of detector, where

$$K_\pi = \frac{d^2 N_\pi}{d\Omega\, dp_\pi}\left(e^{-m_\pi \ell / p_\pi \tau}\right) \int_0^{0.43 p_\pi} \sigma_\nu (p_\nu)\, dp_\nu ,$$

and

I_0 = number of circulating protons/pulse ,

$\frac{d^2 N_\pi}{d\Omega dp_\pi}$ = number of pions of given charge per Gev per steradian per circulating proton,

L = distance from target to detector,

ℓ = distance from target to shield,

τ = pion mean life,

σ_ν = neutrino cross section for reaction in question.

The function $K_\pi (p_\pi)$ illustrates the contribution of different parts of the pion spectrum to the expected rate (Fig. S26-6). From this, the expected rate of the reaction $\nu + n \rightarrow \mu^- + p$ is 1 in 25 days for the two reactions combined, at present beam intensities ($I_0 = 2 \times 10^{11}$). In addition, the intermediate boson is expected to contribute about 1 event in 75 days, if it has the lowest possible mass, less if the mass is greater, nothing if it doesn't exist. The contribution of events of the type $\nu + n \rightarrow \mu^- + p + \pi^\circ$ is expected to be no more than a small fraction of the elastic events (Berman, Dombey).

The expected rate is therefore dismally low, and some efforts are in progress to improve the neutrino flux. Very little improvement is likely before the external beam is extracted next year.

Background

In three days of actual running during June, at least two events were found in the Ramm chamber that fitted the criteria for neutrino-induced reactions. It was not clear at the time I left (only a few days after they were found) whether these events are likely to be background or not. The background could be of cosmic-ray origin or machine origin. Extrapolating the frequency of low-energy neutron stars found in the chamber to the higher energies characteristic of neutrino events, it did not seem reasonable to attribute these events to background, but nothing could be demonstrated. There was a long sensitive time (approximately 20 msec)and almost no shielding roof. Each picture contained on the average 1 or 2 cosmic-ray μ mesons. The cosmic-ray neutron flux was not known. I am not acquainted with whatever work may be in progress now to investigate the background, but this is clearly vital to the experiment.

AGS Experiment

Layout

The beam is brought out at 8° through a 3-m straight section. It clears the windings and fringing field of the following magnet section, so that both polarities are obtained without attenuation. The internal beam has slightly higher energy (30 Gev as compared with 25) and slightly higher repetition rate (2.5 vs 3 sec) than the CERN P.S. There is a free-flight path of 20 m, and a neutron shield of 22 feet of iron with an additional 14-ft μ stopper. The various factors are all substantially better than at CERN, so that the neutrino flux should be higher by a factor of about 4 for neutrinos, in addition to yielding antineutrinos.

Neutrino Detector

There are 10 (possibly 12) spark chambers, each composed of nine 1-in.aluminum plates 4 × 4 ft, with 3/8-in.gaps (Fig. S26-7). The useful weight of each chamber is 0.9 ton. The chambers are stacked two high and five deep.

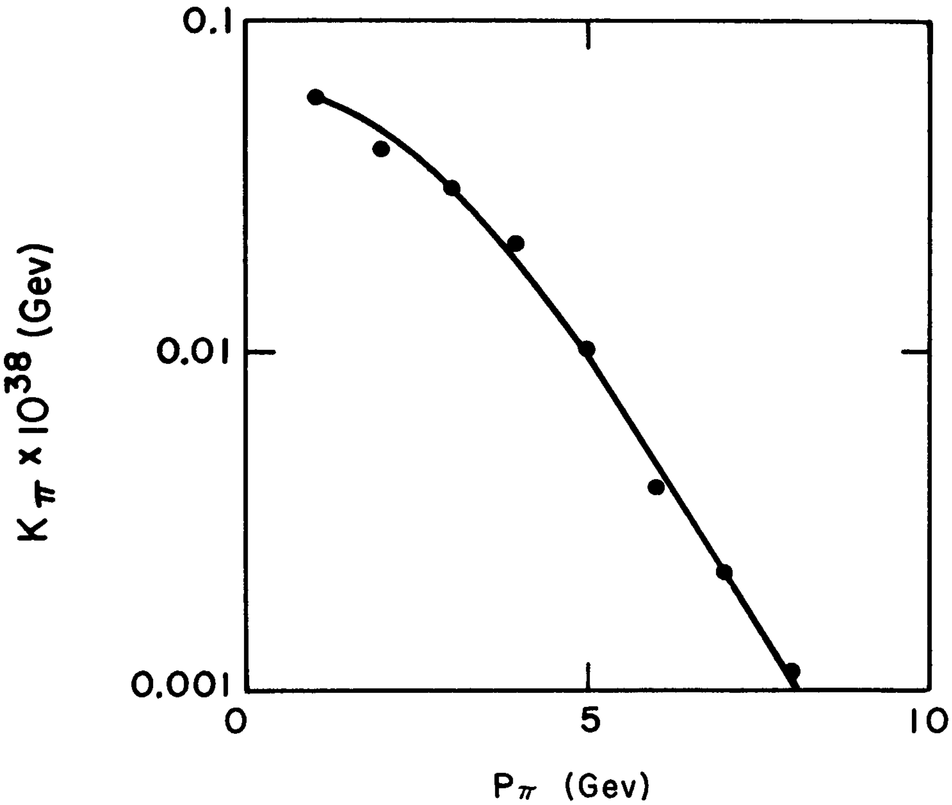

Fig. S26-6. Relative contribution to neutrino reactions from pions of various energies.

Between adjacent counters, there is a double layer of counters separated by 3/4-in. aluminum. A coincidence in any of these sandwiches triggers all chambers, provided it is not vetoed by two 8 × 8-ft anticoincidence layers, one on top, one in front. All counters are plastic scintillators 1 × 4 ft × 1/2 in; there are 112 altogether.

The chambers, counters, and circuits are now almost completed. The neutrino shield will go up in September and the first runs are scheduled for October.

The expected counting rates are 2 counts per day for the "elastic" reactions and less than 1 count per day (depending on its mass) for the production of intermediate bosons, assuming again 2×10^{11} protons circulating. We feel quite confident, on the basis of the CERN results, that the background can be kept low compared with this rate. On the other hand, it is not clear, yet, how much we will learn from each event. The material in the chamber and the thickness have been chosen so that, on the one hand, there should be a good efficiency for triggering on electrons of several hundred Mev, and, on the other hand, there is the hope that the electron showers will be recognizable as such in the chambers. It is therefore likely that at least the question of the existence of two kinds of neutrinos can be settled.

Higher-Energy Experiments

Intermediate Bosons

The production rates at AGS are expected to be very low, even if the mass is the lowest permissible mass. If it is two or three times as high, it is very unlikely that one will succeed in finding the particle with present machines. The cross sections (Fig. S26-1) are very steep functions of energy, and the advantage of a higher-energy machine is clear.

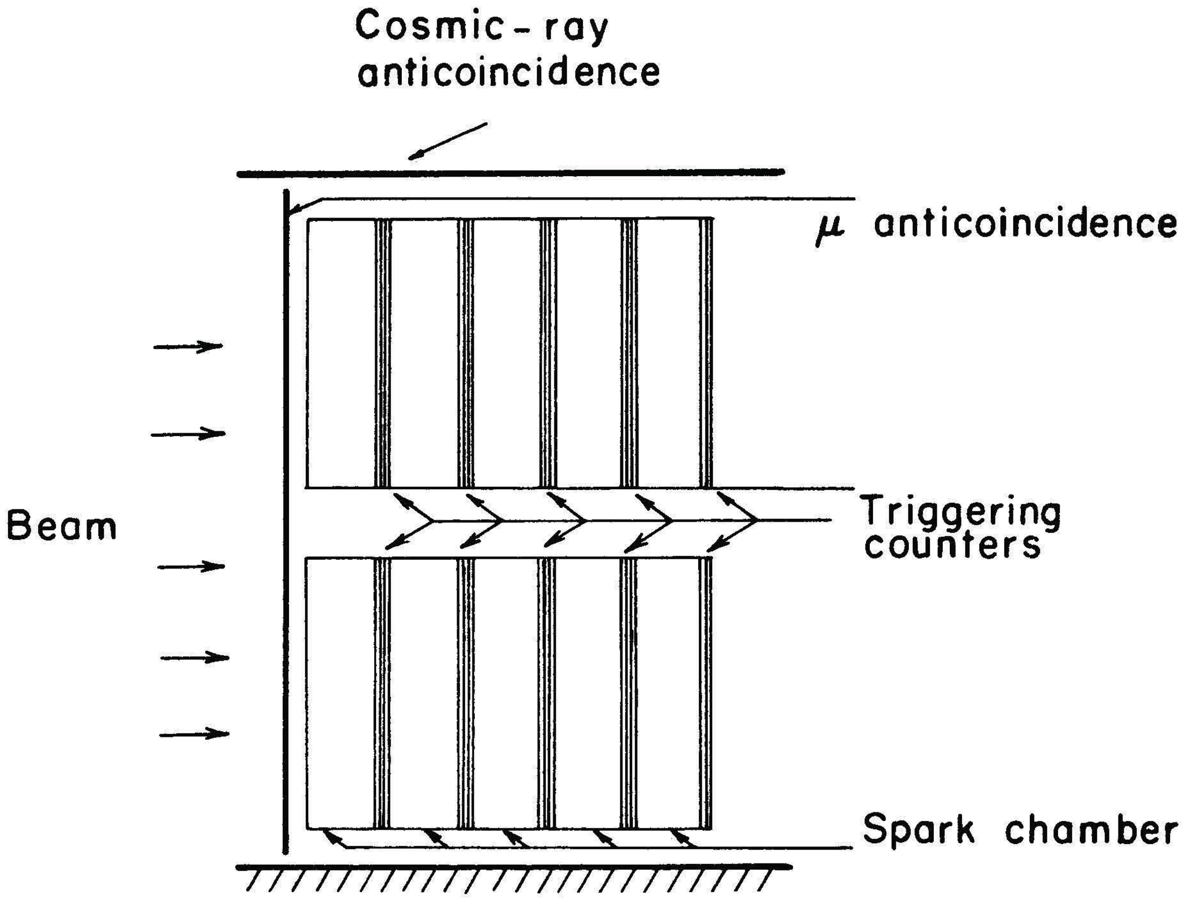

Fig. S26-7. Arrangement of spark chambers at Brookhaven.

Neutrino Intensity for an Experiment of the Type Discussed Here

Given that the average transverse momentum of the pions produced by high-energy protons is independent of proton energy, it is easy to see that the neutrino flux is proportional to the proton energy independent of multiplicity, so that the number of neutrinos goes linearly with machine energy. In addition, the average neutrino energy will also be higher, perhaps in proportion to the square root of the machine energy, and the total neutrino cross section is expected to rise with neutrino energy. On the other hand, the shielding problem against high-energy muons will be more severe.

μ-Induced Reactions

At presently available machines, it is difficult to produce high-energy muon beams that are both intense and adequately free of strongly interacting contaminants. This is so because the easiest purification method is to pass the beam through about 3000 g/cm^2 of absorber; this leaves only the muons of initially high energy, which are few in number, with energy reduced by about 4.5 Gev. If, however, the muons are produced with energies of the order of 10 Gev, instead of 3 to 4 Gev, this method of producing pure muon beams becomes feasible. The problem remains of distinguishing μ-induced weak interactions from their electromagnetic interaction, but there seems at least a reasonable possibility that this may be accomplished.

27. CLASSIFICATION OF MANY-PARTICLE STATES

Kenneth M. Case

August 10, 1961

Introduction

I would like to give a complete classification scheme for n-particle states. Unfortunately I cannot. For various reasons, my own investigations in this direction are still quite incomplete. Instead of describing these, I shall present a case for the detailed use of group theoretical methods in attacking these problems.

We shall proceed as follows.

First, we treat a simple example. No group theory is needed for this and therefore in a certain sense the example is poor. However, it does show the amount of information we must put in, and also indicates why we want a certain type of machinery — and what this should be.

We then state the classification problem in group theoretical terms. This shows us what quantities must be determined and in what order.

Next, we summarize the more important relevant results obtained to date. I might say that the published work furthest along in this direction is that of Jacob and Wick, "General Theory of Collisions," in the Annals of Physics.

Lastly, in response to request, I make a few remarks on Pais's scheme for classifying states involving many π mesons.

Let me emphasize that there is very little that is new in what I have to say today.

The Landau-Yang Theorems

As an elementary introduction, I shall review some of the theorems (Landau and Yang) that relate to particle decays into two photons.

The strongest result is the selection rule that states: A spin-1 particle cannot decay into two photons. A simple proof may be constructed in the following manner. Imagine our vector particle to be at rest. How can we describe the final state? (We work in momentum space.) This state must be constructed from:

(1) The two momentum vectors $\vec{k}_1$ and $\vec{k}_2$, and the two polarization vectors $\vec{e}_1$ and $\vec{e}_2$ of our photons. For simplicity, we take the polarization vectors to be unit vectors in the direction of the respective electric fields. From electrodynamics we have

$$\vec{e}_1 \cdot \vec{k}_1 = \vec{e}_2 \cdot \vec{k}_2 = 0 .$$

Further, since we are talking about a two-particle state, the state function must be bilinear in $\vec{e}_1$ and $\vec{e}_2$.

(2) From momentum conservation we have

$$\vec{k}_1 = -\vec{k}_2 ,$$

so that we have only the single momentum vector

$$\vec{k} = \vec{k}_1$$

to work with.

(3) From angular momentum conservation, we must form a vector from $\vec{e}_i$, $\vec{k}_i$ $(i = 1, 2)$. Clearly, this state can only be of the form

$$\vec{e}_1 \times \vec{e}_2 \, F(k^2).$$

(4) Bose statistics for the photons required the state vector to be symmetric under the interchange e_1 , $k_1 \longleftrightarrow e_2$, k_2 . However, the unique

state we have just constructed is antisymmetric. Hence, the decay cannot occur.

Before analyzing the information put into the above proof, we consider the further statements that can be made about two-photon decays of scalar or pseudoscalar particles.

a. Scalar Decays. Clearly, we can proceed as above. A unique state subject to all our requirements is

$$\vec{e}_1 \cdot \vec{e}_2 F(k^2) .$$

We note that the decay is not forbidden, but the polarization vectors are correlated. (Indeed, we see that the electric vectors must be parallel.)

b. Pseudoscalar Decays. Here our unique state is

$$\vec{e}_1 \times \vec{e}_2 \cdot \vec{k} G(k^2) .$$

Again, we note that the decay is not forbidden, but that there are predicted correlations ($\vec{e}_1 \perp \vec{e}_2$).

The above discussion is an example of how we use group theory without the machinery or language.

Let us now translate the properties (1) through (4) into the appropriate language.

(1) $\vec{e}_i \cdot \vec{k}_i = 0$ is a statement about the massless unitary irreducible representations of the inhomogeneous Lorentz group.

(2) and (3) constitute the statement that the decay processes are invariant under the Euclidean group E_3 (the group of three-dimensional rotations and translations).

The statement that our state vector must be bilinear in $\vec{e}_1$ and $\vec{e}_2$ means that we are to take the direct product of the representations of E_3 with basis vectors as the photon states.

(4) "Bose statistics" requires that we take the symmetrical direct product.

Finally, in considering the scalar and pseudoscalar decays, we have also assumed (implicitly) parity conservation (i.e., the group E_3 has been augmented by the space-reflection operation).

It is clear that the "elementary" derivation has actually incorporated a huge amount of information. Since we could do this so simply, one might ask why we should introduce the machinery of group theory. The reason becomes clear when we modify our original question slightly. For example:

a. What are the selection rules and correlations for decays into two massless particles of spin $\neq 1$?

b. What are the rules for decays into two massive particles?

c. What about three-photon decays?

Classification Schemes - Philosophy

We find (from experiment) or postulate (for later verification) that the equations describing a certain aspect of physics are invariant under a certain group of transformations. Until today, we have found no contradiction with assuming invariance under the proper inhomogeneous Lorentz group.

A fundamental fact of quantum mechanics is that the state vectors form a basis for a unitary representation of the symmetry group.

(Note: Elementary particles are probably best described as entities whose state vectors form the basis of an irreducible representation of the appropriate group.)

The classification of many-particle states then proceeds as follows: We have our invariance group. Each of the particles then has state vectors which are basis vectors of certain unitary representations of the group. The many-particle states then form, in general, the basis of a reducible direct-product representation of our group. We can classify the possible states by decomposing the representation into reducible ones. The states are then labeled by

a. the irreducible representations to which they belong, and

b. the rows of the representation to which they correspond.

We remark that the larger the invariance group the more "quantum numbers" there are at our disposal. Therefore we should use the largest group possible. For example, in strong-interaction physics we would use at least the group obtained as a product of these six groups:

- The proper inhomogeneous Lorentz group
- The group of space and time reflections
- The isotopic spin group
- The charge-conjugation group
- The baryon conservation group
- The strangeness group

(Actually, since the time reflection is represented by an antiunitary operation, it has rather different consequences from all the others and is perhaps better left out of consideration here. For example, the time reflection combined with any of the gauge groups—charge, baryon, or strangeness—implies the charge-conjugation group).

Now, unfortunately, our group may not (and indeed in general will not) be large enough. Thus, no matter how large the group, we find that, for sufficiently large numbers of particles, there are several occurrences of the same irreducible representation in the direct product and therefore several states with the same labels. How are we to proceed then? We invent a new group which is large enough to uniquely characterize all states in the direct product!

A typical example occurs in the case of atomic structure. Here, the representations of the invariance group R_3 (the three-dimensional rotation group) are inadequate to describe the states of a given configuration. We invent the larger group corresponding to separate rotations in position and spin space and use representations of the group to label states (L-S coupling).

This example also serves to show the weaknesses of the invention process. While we may thus uniquely characterize states (and thus solve the counting problem for statistical models), the new group may not be even an approximate symmetry group. Then we obtain almost no predictions as to selection rules and correlations.

A possible example of this is Wigner's Supermultiplet characterization of nuclear states which, unfortunately, turns out not to be as useful as one would like.

Further, even if our "invented" group is at least approximately a symmetry group, it still may not ~~be~~ large enough. Thus, even when Russell-Saunders coupling applies, states may not be uniquely characterized by Configuration + L + S + J + M. Then, as in the case of complex spectra, we need to invent even larger groups.

Program

The general approach to classifying many-particle states is perhaps clear. We proceed as follows.

- Decide on appropriate symmetry groups.
- Classify their unitary, irreducible representations.
- Reduce the direct product of two of these representations.
- In particular, find the decomposition of symmetric and antisymmetric nth-order direct products. (This will yield selection rules.)
- Ideally, we will then construct the basis vectors of the reduced representations in terms of the products of single-particle state vectors. This will then yield predictions as to correlations.

I have been primarily concerned with the proper inhomogeneous Lorentz group (supplemented by the space-reflection operation) and the subgroup of this E_3 .

A Mathematical Complication

The groups of primary interest, here, are technically noncompact. Roughly, this means that the parameters vary over an infinite domain. This is unfortunate, because continuous groups that are compact—like the rotation group R_3—share many of the properties of finite groups. In particular:

a. All representations decompose into irreducible ones.

b. All irreducible representations are equivalent to unitary representations.

c. The coefficients of the irreducible representations form a complete set of functions in group space. These extremely useful properties are not necessarily true for noncompact groups. For example, consider the one-dimensional translation group

$$T(a) : x \to x' = x + a.$$

A representation is

$$T(a) \to \begin{pmatrix} 1 & a \\ 0 & 1 \end{pmatrix}.$$

This representation is

- Reducible, but not completely so.
- Not equivalent to a unitary representation.

However, suppose we restrict ourselves to unitary representations of this group. We note two mathematical facts:

- All reducible unitary representations are completely reducible.
- All irreducible representations of an Abelian (i.e., commutative) group are one-dimensional.

Hence, we see that the unitary irreducible representations of our translation group are of the form

$$T(a) \to e^{ipa} \quad \text{with } p \text{ real.}$$

We note that these representation coefficients are indeed complete—precisely in the sense of the Fourier integral theorem. This result is quite general for the so-called locally compact groups. Fortunately, this is a property common to most of the groups of interest here.

This result is quite analogous to the transition from finite to infinite dimensional vector spaces. Pathologies can occur. However, the restriction to a Hilbert space lets us carry over almost all the conventional properties. The physical requirement of unitary representations does precisely this for our groups of interest.

Boxes

Even if we accept the theorem alluded to about locally compact groups, we still have some technical difficulties. These are similar to the normalization problems common to quantum mechanics and field theory. The easy solution there is to put the system in a "box." Can we do something analogous? That is, can we put our noncompact groups in boxes?

The answer is yes, for the groups we are considering. Explicitly, we mean by this that our noncompact groups (and their unitary irreducible representations) can be obtained by a limiting process applied to compact groups.

This can be shown by an example due to Wigner. We show how to obtain the two-dimensional Euclidean group E_2 (that is, the group of translations in a plane plus rotations about a perpendicular axis) from the group R_3. Intuitively, the process is fairly obvious. R_3 consists of rotations around the 1, 2, 3 axes. Clearly, if we restrict ourselves to infinitesimal rotations around the 1 and 2 axes, we get a set of transformations that are at least like the rotations around the 3 axis plus translations in the directions 1 and 2—i.e., E_2.

Formally, the limit can be obtained as follows:

The group E_2 is the set of transformations of the form

$$x \to x',$$

where

$$x_1' = x_1 \cos \Theta + x_2 \sin \Theta + a_1 ,$$

and

$$x_2' = -x_1 \sin \Theta + x_2 \cos \Theta + a_2 .$$

A simple description, then, is the group of matrices of generic type

$$E(\Theta, a) = \begin{pmatrix} \cos \Theta & \sin \Theta & a_1 \\ -\sin \Theta & \cos \Theta & a_2 \\ 0 & 0 & 1 \end{pmatrix} .$$

Then, writing

$$\begin{pmatrix} x_1' \\ x_2' \\ 1 \end{pmatrix} = E(\Theta, a) \begin{pmatrix} x_1 \\ x_2 \\ 1 \end{pmatrix} ,$$

we see that the transformations of E_2 are reproduced.

The rotation group R_3 is generated by the three independent rotations

$$R^{(1)}(\Theta_1) = \begin{pmatrix} 1 & 0 & 0 \\ 0 & \cos \Theta_1 & \sin \Theta_1 \\ 0 & -\sin \Theta_1 & \cos \Theta_1 \end{pmatrix} ,$$

$$R^{(2)}(\Theta_2) = \begin{pmatrix} \cos \Theta_2 & 0 & -\sin \Theta_2 \\ 0 & 1 & 0 \\ \sin \Theta_2 & 0 & \cos \Theta_2 \end{pmatrix} ,$$

$$R^{(3)}(\Theta) = \begin{pmatrix} \cos \Theta & \sin \Theta & 0 \\ -\sin \Theta & \cos \Theta & 0 \\ 0 & 0 & 1 \end{pmatrix} .$$

In this form, it is rather hard to pass to the desired limit. Suppose, however, that we first transform the rotation matrices with the matrix

$$C = \begin{pmatrix} 1/\xi & 0 & 0 \\ 0 & 1/\xi & 0 \\ 0 & 0 & 1 \end{pmatrix} .$$

(For finite ξ the resulting matrix group is of course isomorphic to the original group of matrices.) We obtain

$$CR^{(3)}(\Theta)\, C^{-1} = R^{(3)}(\Theta) ,$$

$$CR^{(1)}(\Theta_1)C^{-1} = \begin{pmatrix} 1 & 0 & 0 \\ 0 & \cos \Theta_1 & 1/\xi \sin \Theta_1 \\ 0 & -\xi \sin \Theta_1 & \cos \Theta_1 \end{pmatrix} ,$$

$$CR^{(2)}(\Theta_2)C^{-1} = \begin{pmatrix} \cos \Theta_2 & 0 & -1/\xi \sin \Theta_2 \\ 0 & 1 & 0 \\ \xi \sin \Theta & 0 & \cos \Theta_2 \end{pmatrix} .$$

Now we put $\Theta_1 = \xi a_2$, $\Theta_2 = -\xi a_1$, and pass to the limit $\xi \to 0$. We readily find that the general element is just that of E_2.

<u>Representations</u>

Consider the infinitesimal elements of the groups: For the rotation group we have the three elements

$$I_1^{(r)} = \frac{\delta}{\delta \Theta_1} R^{(1)}(\Theta_1) \Big|_{\Theta_1 = 0} ,$$

$$I_2^{(r)} = \frac{\delta}{\delta \Theta_2} R^{(2)}(\Theta_2) \Big|_{\Theta_2 = 0} ,$$

$$I_3^{(r)} = \frac{\delta}{\delta \Theta} R^{(3)}(\Theta) \Big|_{\Theta = 0} ,$$

while for E_2 the elements are

$$I_1^{(E)} = \frac{\delta}{\delta a_1} T(a_1) \Big|_{a_1 = 0} ,$$

$$I_2^{(E)} = \frac{\delta}{\delta a_2} T(a_2) \Big|_{a_2 = 0} ,$$

$$I_3^{(E)} = \frac{\delta}{\delta \Theta} R(\Theta) \Big|_{\Theta = 0} .$$

Since $\Theta_1 = \mathcal{E} a_2$ and $\Theta_2 = -\mathcal{E} a_1$, we see that these infinitesimal elements are related by

$$I_1^{(E)} = \mathcal{E} I_1^{(r)} ,$$

$$I_2^{(E)} = -\mathcal{E} I_2^{(r)} ,$$

$$I_3^{(E)} = I_3^{(r)} .$$

Consider the representation of weight j of R_3 [i.e., the representation in which the square of the angular momentum is $j(j+1)$] : The matrix elements of the infinitesimal operators are well known to be

$$\left\langle m \left| I_3^{(r)} \right| m' \right\rangle = i m \,\delta(m, m'),$$

$$\left\langle m \left| I_1^{(r)} \right| m' \right\rangle =$$

$$\frac{i}{2} \left\{ \sqrt{(j+m)(j-m+1)}\; \delta(m', m-1) + \sqrt{(j-m)(j+m+1)}\; \delta(m', m+1) \right\} ,$$

$$\left\langle m \left| I_2^{(r)} \right| m' \right\rangle =$$

$$\frac{1}{2} \left\{ \sqrt{(j+m)(j-m+1)}\; \delta(m', m-1) - \sqrt{(j-m)(j+m+1)}\; \delta(m', m+1) \right\} .$$

The matrix elements of $I_i^{(E)}$ (for $i = 1, 2, 3$) are obtained by multiplication of $I_1^{(r)}$ with $\mathcal{E}$, $I_2^{(r)}$ with $-\mathcal{E}$, and passage to the limit $\mathcal{E} \to 0$. Two possibilities occur.

a. j finite

Here $\left\langle m \left| I_3^{(E)} \right| m' \right\rangle = i m \,\delta(m', m)$,

$$\left\langle m \left| I_{1,2}^{(E)} \right| m' \right\rangle = 0 .$$

It is seen that we thus obtain one-dimensional representations with the translations represented by the identity.

b. $\mathcal{E} j$ = finite = p . [Notice that m must be kept finite for $I_3^{(E)}$ to be meaningful.] We have

$$I_3^{(E)} = i m \,\delta(m, m'),$$

$$I_1^{(E)} = \frac{i}{2} p \left\{ \delta(m', m-1) + \delta(m', m+1) \right\} ,$$

$$I_2^{(E)} = -\frac{p}{2} \left\{ \delta(m', m-1) - \delta(m', m+1) \right\} .$$

Since

$$\left[I_1^{(r)} \right]^2 + \left[I_2^{(r)} \right]^2 + \left[I_3^{(r)} \right]^2 = -j(j+1) ,$$

we see (on multiplying by $\mathcal{E}$) that these representations of E_2 are characterized by

$$\left[I_1^{(E)} \right]^2 + \left[I_2^{(E)} \right]^2 = -p^2$$

Two remarks are in order here:

- By this process, we have obtained all the unitary irreducible representations of E_2 .

- The limiting process, plus the full knowledge of the Clebsch-Gordan coefficients which has been obtained over the years, enables us to treat the reduction of direct products in complete detail.

The Group E_3

This group of three-dimensional rotations and translations is, of course, of considerably greater physical interest than the group E_2 of our previous example. However, it is still simple to "put it in a box." Thus, we can consider E_3 as a limiting case of the four-dimensional rotation group (R_4) obtained by restricting ourselves to infinitesimal rotations in the 14, 24, and 34 planes. The main point here is that, essentially, R_4 is a direct product of two three-dimensional rotation groups. Hence, again, the knowledge of the Clebsch-Gordan coefficients permits a complete treatment of the reduction of direct products.

An enumeration of the unitary irreducible representations of the group is easily obtained.

The general group element is of the form

$$T(\vec{a})\,\mathcal{R}(R) \ ,$$

where $T(\vec{a})$ describes a translation of distance $\vec{a}$ and $\mathcal{R}$ is an arbitrary rotation around the origin.

Consider the Abelian invariant subgroup of translations $T(\vec{a})$. This has only one-dimensional irreducible unitary representations,

$$T(\vec{a}) \to e^{i(\vec{p}\cdot\vec{a})}, \text{ with } \vec{p} \text{ real.}$$

Suppose now that, in an irreducible unitary representation of E_3 , a representation $\vec{p}_0$ of the translation subgroup occurs. That is, we have a state vector $\left|\vec{p}_0\right\rangle$, such that

$$T(\vec{a})\left|\vec{p}_0\right\rangle = e^{i(\vec{p}_0\cdot\vec{a})}\left|\vec{p}_0\right\rangle$$

The multiplication law

$$R\,T(a)\,R^{-1} = T(Ra)$$

shows that

$$T(a)\,\mathcal{R}(R)\left|\vec{p}_0\right\rangle = e^{i(R\vec{p}_0\,,\,\vec{a})}\,R\left|\vec{p}_0\right\rangle \ ;$$

that is,

$$\mathcal{R}(R)\left|\vec{p}_0\right. = \left|R\vec{p}_0\right\rangle \ .$$

In words, this says that, with $\left|\vec{p}_0\right\rangle$, all states $\left|\vec{p}\right\rangle$, where $\vec{p}$ is obtained from $\vec{p}_0$ by some rotation, occur.

There are two possibilities:

a. $\vec{p}_0^{\,2} = 0$. All translations are represented by the identity. We have here a representation which is an irreducible unitary representation of R_3—i.e., a representation of weight j .

b. $\vec{p}_0^{\,2} \neq 0$. These are infinite dimensional representations. We consider them in further detail:

Let $\Gamma(\vec{p})$ be a continuous subgroup of rotations such that $\Gamma(\vec{p})\,\vec{p}_0 = \vec{p}$.

[Note: If, for example, $\vec{p}_0$ is in the Z direction we can take the set Γ to be the rotations of Euler angles $(\alpha, \beta, 0)$.]

We define a standard set of states $\left|\vec{p}\right\rangle$ by $\left|\vec{p}\right\rangle = \mathcal{R}\left[\Gamma(p)\right]\left|\vec{p}_0\right\rangle$. For further characterization, we consider the different states with the same $\vec{p}_0$; i.e., states $\left|\vec{p}_0, i\right\rangle$.

These clearly form a basis for an irreducible representation of the "little group"—i.e., the rotations that leave $\vec{p}_0$ invariant. This group is obviously the two-dimensional rotation group. Its irreducible unitary representations are, as is well known, characterized by any half-integer ν . Thus, the infinite dimensional (faithful) representations of E_3 can be denoted by $D^{(p,\nu)}$, where $\vec{p}_0^{\,2} = p^2$.

Some remarks may be helpful here:

- The irreducible unitary representations of E_3 are therefore $D^{(p,\nu)}$ and $D^{(j)}$.

- Any rotation can be written in the form

$$R = \Gamma(p)\left\{\Gamma^{-1}(p)\,R\,\Gamma\left(R^{-1}p\right)\right\}\Gamma^{-1}\left(R^{-1}p\right).$$

  Here the factor in braces is an element of the little group.

- The basis vectors $\left|\vec{p},\nu\right\rangle$ are merely helicity states.

Reduction of Direct Products

Three classes of products occur, depending on the finite or infinite dimensional character of the individual factors. The simplest is

(1) $$D^{(j_1)} \times D^{(j_2)} .$$

This is merely the direct product of two representations of R_3. Hence, we just have the Clebsch-Gordan series

$$D^{(j_1)} \times D^{(j_2)} = \sum_{j=|j_1-j_2|}^{j_1+j_2} D^{(j)} .$$

(2) Similarly, we find

$$D^{(p,\nu_1)} \times D^{(j)} = \sum_{\nu=\nu_1-j}^{\nu_1+j} D^{(p,\nu)} .$$

For $\nu_1 = 0$, this is equivalent to constructing the spherical harmonics with spin.

(3) The most important products are of the form

$$D^{(p_1,\nu_1)} \times D^{(p_2,\nu_2)} .$$

The reduction gives all (p,ν) where $|p_1 - p_2| \leqslant p \leqslant p_1 + p_2$ and ν runs (separately) over all integers (or half an odd integer) depending on whether $\nu_1 + \nu_2$ is an integer or half an odd integer.

The special case $p_1 = p_2 = \bar{p}$ is particularly important. Reduction gives all representations p, with $0 \leqslant p \leqslant 2\bar{p}$. These representations are then all irreducible, except the mathematically unimportant case $p = 0$.

Physically, this case is extremely important. It describes the center-of-mass states of two particles and decomposes into irreducible representation D^J, where $J \geqslant \big|\,|\nu_1| - |\nu_2|\,\big|$. Explicitly, using angular momentum instead of momentum states, we have

$$\left|J\,M\,\nu_1\,\nu_2\right\rangle = \sum_{\substack{j_1 \geqslant |\nu_1| \\ j_2 \geqslant |\nu_2|}} \sqrt{\frac{(2j_1+1)(2j_2+1)(2J+1)}{4\pi}}$$

$$(-1)^{j_2+\nu_2}\left|j_1\,\nu_1' \,;\, j_2\,\nu_2'\right\rangle$$

$$\times(-1)^{M-(\nu_1-\nu_2)}\begin{pmatrix} \nu_1' & \nu_2' & -M \\ j_1 & j_2 & J \end{pmatrix}$$

$$\begin{pmatrix} j_1 & j_2 & J \\ \nu_1 & -\nu_2 & -(\nu_1-\nu_2) \end{pmatrix} .$$

(Here the elements in parentheses are Wigner's 3-j symbols — i.e., Clebsch-Gordan coefficients up to sign and normalization.)

From the formula the Landau-Yang theorems follow trivially. Further, they are readily extended. For example, consider a particle of spin S, mass zero: The polarization can be $\pm S$. The states $J = 1, 3, 5, \cdots 2S$ of two such particles are ruled out by the appropriate statistics. Thus, a particle of odd spin less than 2S cannot decay into two particles of spin S (and mass zero).

Further, for allowed states the spins are correlated in a fashion which is easily read off. (Additional information can be obtained if we also consider the space reflection transformation.)

The Inhomogeneous Lorentz Group

This can be treated similarly to the group E_3. We merely quote a few results.

Unitary Irreducible Representations

Those of apparent importance in physics are of two classes.

Representations of finite mass m

These have basis vectors which are eigenstates of the translation operators with four-momentum for which $(p, p) = m^2$ — Lorentz metric. There are representations of this type with arbitrary spin S. (This can perhaps be seen easily by repeating the argument given above for E_3. The "little group" is obtained by considering homogeneous Lorentz transformations which leave a fixed vector p_0 with $(p_0, p_0) = m^2$ unchanged. For example, take $p_0 = (m, 0, 0, 0)$. Clearly the "little group" is R_3 and its irreducible representations are just D^S.)

On considering the subgroup E_3, these representations split into the representations $D^{(p, \nu)}$, where $0 \leqslant p < \infty$ and $\nu = -S, -S+1, \cdots S$.

Representations of mass zero

That is, $(p, p) = 0$ and $p^{(0)} > 0$ (or $p^{(0)} < 0$). These representations are characterized by a further "spin index" S. Restricting ourselves to E_3 gives all representations $D^{(p, s)}$ with $0 \leqslant p < \infty$.

It may be noted that we get two helicity states (as for the photon) only when we consider space reflections. This situation is quite different from massive representations. There the $2s + 1$ helicity states occur even without considering reflections. This is readily understood as being due to the existence of a rest system. Thus, taking a state of given helicity and then successively performing

a. a Lorentz transformation to rest,

b. a spatial rotation of 180°, and

c. a Lorentz transformation back to the original momentum gives a state of opposite helicity.

In group theoretical language, the reason for the occurrence of the single helicity S in a given massless irreducible representation is that the "little group" here is isomorphic to the group E_2, which we considered earlier.

Reduction of Direct Products

Very little work seems to have been done in this direction. Some formulae have been obtained which tell into what irreducible representations some of the possible direct products decompose. I have not seen any work giving the analog of the Clebsch-Gordan coefficients.

Pais' Classification of $n\pi$ States

This work falls into the class of our "pure inventions." It is analogous, perhaps, to the treatment of atomic structure.

Consider a "configuration" of $n\pi$ mesons; i.e., the set of states of n such particles with fixed momenta $\vec{p}_1 \cdots \vec{p}_n$: Clearly, there are many such states—obtained by assigning various values to the three-component of the isotopic spin of the various π's.

The permutation group is of fundamental importance here; but we must take care not to be confused. Of course, the π's are taken to satisfy Bose statistics. However, there are still many possible states for a given configuration. We can perhaps visualize these states by considering Bose creation operators applied to a vacuum state. The states of a "configuration" are then of the form

$$\overset{*}{A}_{\vec{p}_1 m_1} \overset{*}{A}_{\vec{p}_2 m_2} \cdots \overset{*}{A}_{\vec{p}_n m_n} \Big| 0 \Big\rangle .$$

These are obviously symmetric. However, giving various values to the m's — i.e.,

$$m_1 = \pm 1,\ 0,$$

$$m_2 = \pm 1,\ 0,$$

$$\vdots$$

$$m_n = \pm 1,\ 0,$$

gives many states — 3^n , to be exact.

To classify these states, we could begin by combining them to get states of fixed I and I_3. Obviously, there are many such states. A further labeling is needed.

Pais' Invention

Let me talk in terms of Hamiltonians. Suppose H were not only charge-independent but did not even depend on the isotopic spin operators. Then we would have invariance, not only under isotopic spin rotations but also under all three-dimensional unitary transformations in isotopic spin space.

The larger group we are talking about is then the three-dimensional unitary group U_3 (i.e., the group of all 3×3 unitary matrices) rather than its subgroup R_3. This is clearly satisfactory for describing free particles. Hence, states of free particles can be labeled in terms of irreducible representations of U_3. Whether or not this is a really useful description depends on how good an approximate symmetry we have inferred.

Mathematics

Let us restrict the discussion to free-particle states. The states of a configuration form the basis of a representation of U_3 which is just the nth Kronecker product. These representations can be reduced by known mathematical techniques.

First, let us consider an example: Take $n = 2$. There are nine states in a configuration

$$A^*_{p_1 m_1} A^*_{p_2 m_2} \Big| 0 \Big\rangle \quad \text{for } m_1,\ m_2 = \pm 1,\ 0 .$$

We can take the symmetrical and antisymmetrical combinations

$$(\alpha) \quad \left\{ A^*_{p_1 m_1} A^*_{p_2 m_2} + A^*_{p_1 m_2} A^*_{p_2 m_1} \right\} \Big| 0 \Big\rangle,$$

and

$$(\beta) \quad \left\{ A^*_{p_1 m_1} A^*_{p_2 m_2} - A^*_{p_1 m_2} A^*_{p_2 m_1} \right\} \Big| 0 \Big\rangle.$$

We note that there are six symmetrical states (α) and three antisymmetrical states (β). Now, under the transformations induced by elements of U_3, the six states α transform among themselves, as do the three states β. It is a fact that the representations of U_3 under which the two sets transform are irreducible. This is not true for the subgroup R_3. Indeed, as a representation of R_3, the representation α splits into $I = 2$ and $I = 0$, while the representation β is irreducible and is $I = 1$. Here, we see that the irreducible representations of U_3 are uniquely characterized by the symmetry. This generalizes!

Consider the states of a configuration of n π mesons. We can write these states as

$$T_{m_1 \cdots m_n} ,$$

to indicate that they transform as a tensor under the group U_3. Next, decompose this tensor into tensors with various symmetries. This is done as follows:

Define the effect of the permutation

$$P = \begin{pmatrix} 1 & 2 & \cdots & n \\ \downarrow & \downarrow & & \downarrow \\ 1' & 2' & \cdots & n' \end{pmatrix}$$

on a tensor by

$$(PT)_{m_1 \cdots m_n} = T_{m_1' \cdots m_n'} .$$

Consider a partition of n into integers

$$n = n_1 + n_2 + \cdots ,$$

where $$n_1 \geqslant n_2 \geqslant n_3 \cdots .$$

Corresponding to this partition we construct a Young tableau

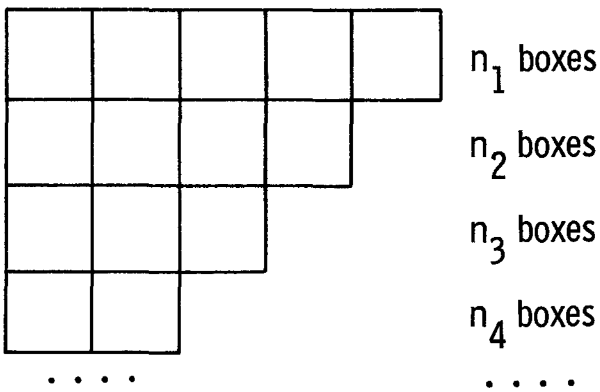

Further, with each tableau we can associate several labeled tableaux. These are obtained by filling the boxes with the numbers 1, 2, ... n , subject to the restrictions that reading from left to right and top to bottom we always have increasing sequences. For example, with the tableau

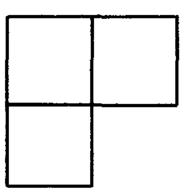

we have the two labeled tableaux

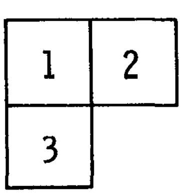

AND

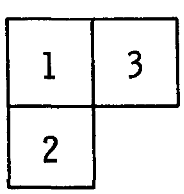

Let P_1 , P_2 ... be all the permutations on N-symbols which carry the elements of a given labeled tableau only into the same row as they were originally. Similarly let Q_1, Q_2 ... be those permutations which keep elements in their original columns. Then, with each labeled tableau { } we can associate the permutation operator

$$Y_{\{\ \}} = \sum_{PQ} (-1)^Q \, QP ,$$

where $(-1)^Q = \pm 1$, depending on whether the permutation Q is even or odd. With these operators, we construct tensors with symmetry by

$$T^{\{\ \}}_{m_1 \ldots m_n} = \left(Y_{\{\ \}} T\right)_{m_1 \ldots m_n} .$$

We note

- Since each m_i can take only three values, we cannot antisymmetrize in more than three indices. Hence, partitions into more than three parts are irrelevant.

- Each labeled tableau symmetrized tensor has, in general, several independent components.

- Since symmetrization and the transformations of the unitary group commute, these independent components transform among themselves under the transformations induced by U_3.

The main mathematical theorem here is that the representations of U_3 so obtained are irreducible. Since permutations and U_3 operations commute, the representations of U_3 corresponding to the same partition are equivalent. Thus, with any partition of $n = n_1 + n_2 + n_3$, we can write the wave functions as a rectangular array

$$\begin{array}{cccc} \psi_a^{\{1\}} & \psi_a^{\{2\}} & \cdots & \psi_a^{\{x\}} \\ \vdots & \vdots & & \vdots \\ \psi_y^{\{1\}} & \psi_y^{\{2\}} & & \psi_y^{\{x\}} \end{array} ,$$

where $\{i\}$ denotes the various labeled tableaux. Under permutations, the columns go into each other. Under the transformations of U_3, the rows go into each other.

We see that we have a complete labeling — essentially by partitions. Under the transformations of the subgroup R_3 of U_3 a given column yields a reducible representation. However, Pais proves that states $I = 0$ or $I = 1$ occur only once and not together. He calls these "cloud states." Then, for cloud states, the partition uniquely characterizes the isotopic spin I of a state.

Many theorems can be developed. The main points, though, seem to be:

- The scheme enables us to count states.
- This may or may not be useful depending on whether it is at least an approximate dynamical symmetry.

28. PART I. SYMMETRIES AT HIGH ENERGIES

Frederick Zachariasen

August 11, 1961

Before I begin, I want to make it very clear that almost nothing that I have to say has been proved in a satisfactory way. The arguments are all based on (a) conventional renormalizable field theories, which are in disrepute, at least around here, and (b) the behavior of the perturbation-series solutions of such theories, which do not necessarily have very much to do with the actual solutions. We hope to be able to obtain reasonable proofs later. At the moment, the hope is merely that the field theory and the perturbation series can be used as a guide to high energies, as it has sometimes been used successfully for other things in the past.

Up to now, the way we express the existence of some kind of broken symmetry is by saying that, if you turn off the symmetry-breaking interactions, the symmetry exists; that is, if you don't include the renormalization effects produced by the symmetry-violating interactions, then various masses, coupling constants, etc., are related. For example, charge independence says $m_p = m_n$ or $m_{\pi^+} = m_{\pi^0}$; yet, actually, these equalities are not true, because electromagnetism breaks the charge-independence symmetry. What we really have to say is $m_p^0 = m_n^0$, where the superscript zero means that we're talking about "bare" or "unrenormalized" masses, without the renormalizations produced by electromagnetism. Here, of course, the difficulty isn't very serious in practice, because the electromagnetic coupling is weak, so that the symmetry is only slightly violated and remains essentially visible. We'd be in the soup, however, if there were, as many people suggest, an underlying symmetry of the strongly interacting particles—e.g., global symmetry—which is broken by an interaction so strong that the symmetry is totally obscured.

What we need, therefore, is some way to experimentally observe bare masses and coupling constants, so that we can see directly if there is any relation between these quantities for different particles.

I'll present an example of how we might be able to do this. I'll arbitrarily base my discussion on pions and nucleons, and try to indicate how we might be able to measure the bare pion-nucleon coupling constant. The argument presupposes that π's and nucleons are elementary particles; if they are not, the conclusions may be very different. However, I use π and N only to illustrate the idea anyway, and if some other particles are really fundamental, the arguments could presumably be transferred to them. What the analogous statements are for nonelementary particles—if, indeed, there are any statements at all—is still unclear.

In the usual renormalizable field theory, one states

$$g_0 = g Z_1 Z_2^{-1} Z_3^{-1/2} ,$$

where g_0 is the bare, g the physical, coupling constant and the Z's are a group of renormalization constants. If one computes the Z's in perturbation theory, they diverge, and one must put in a cutoff Λ to make them finite. Thus, the Z's are functions of Λ and g as in

$$Z = Z(\Lambda^2, g) .$$

Then, in the same way, we get

$$g_0 = g_0(\Lambda^2, g) .$$

As $\Lambda^2 \to \infty$, the Z's, etc., may or may not be infinite. All we know for sure is that each term in an expansion of Z in powers of g^2 diverges as $\Lambda^2 \to \infty$.

Within the usual renormalizable field theory, one can show that the renormalized propagator for a pion, $\Delta_{F1}(s)$, where s = (pion momentum)^2, can be written in the form

$$\Delta_{F1}(s) = \frac{1}{s - \mu^2} + \frac{1}{\pi}\int \frac{\sigma(s')}{s' - s}\, ds' ,$$

where μ^2 is the physical mass, and $\sigma(s')$ is finite and expressed in terms of physical quantities only.

It is possible also to show that, as s gets large,

$$\Delta_{F1}(s) \to \frac{1}{s} Z_3^{-1}(-s, g) ;$$

that is, $Z_3(-s, g)$ is the same function of $-s$ as $Z_3(\Lambda^2, g)$ is of Λ^2. This can be shown, basically, by the fact that each term in the perturbation expansion of $s\Delta_{F1}(s)$ equals the corresponding term of $Z_3(\Lambda^2, g)$ with Λ^2 replaced by $-s$.

In the same way, one can show that the vertex functions approach $Z_1(-s, g)$, where s is the momentum transfer at the vertex. For example, if $F_1^V(s)$ is the charge isovector form factor for a nucleon, then

$$\frac{F_1^V(s)}{F_1^V(0)} \to Z_1(-s, g)$$

where Z_1 is the vertex renormalization of the photon-nucleon vertex. Since the electromagnetic current is conserved, Ward's identity holds, and we have $Z_1(\Lambda^2, g) = Z_2(\Lambda^2, g)$, where Z_2 is the nucleon wave function renormalization (as Z_3 is for mesons). Thus,

$$\frac{F_1^V(s)}{F_1^V(0)} \to Z_2(-s, g) .$$

In the same way, since the isoscalar electromagnetic current is likewise conserved,

$$\frac{F_1^S(s)}{F_1^S(0)} \to Z_2(-s, g) ,$$

where F_1^S is the isoscalar electromagnetic form factor. For the axial weak vertex, for example, we have

$$\frac{F_A(s)}{F_A(0)} \to Z_1(-s).$$

Now, we know experimentally,

$$1.25 = Z_2(\Lambda^2)/Z_1(\Lambda^2);$$

so we find

$$\frac{F_A(s)}{F_A(0)} \to \frac{Z_2(-s, g)}{1.25} ;$$

and so on. This says that all form factors involving the nucleon approach the same function asymptotically, whether they are vertices for conserved currents or not (except for a trivial constant factor like 1.25).

This is all very well, but it isn't enough to let us get g_0, because we still need the Z_1 for the strong vertex. So next, let us look at scattering.

π-N scattering is described by two invariant amplitudes, usually called A and B. As B has an extra power of energy multiplying it, one might guess that B wins at high energies; so we shall forget A. This is supported by perturbation theory, but, certainly, there is no compelling reason for believing it. Whether or not A drops out is something that can be checked by experiment, since, if only B survives, there is helicity conservation in π-N scattering at high energies.

Now the Mandelstam representation for B looks like

$$B(s,t) = \frac{g^2}{s - M^2} + \frac{g^2}{u - M^2} + \frac{1}{\pi}\int \frac{b_1(s')}{s' - s}\,ds'$$

$$+ \frac{1}{\pi}\int \frac{b_2(u')}{u' - u}\,du' + \frac{1}{\pi^2}\iint \frac{B_{13}(s't')}{(s' - s)(t' - t)}\,ds'dt'$$

$$+ \text{ terms in } tu,\ us\ .$$

In addition, there may be Regge terms, such as

$$\beta\,(s)\,\frac{P_{\alpha(s)}\left(1 + t/2q_s^2\right)}{\sin\pi\,\alpha(s)}.$$

Since it is not yet clearly understood just how these come in, or how many there are, we shall forget them and use the old-fashioned Mandelstam representation, as written.

The indications from perturbation theory are that there are no subtractions, so we shall assume this. The pole terms are represented by the diagrams in Fig. S28-1(a) and (b).

(a)

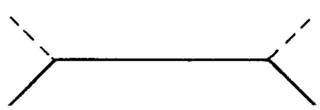

and

(b)

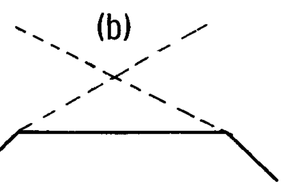

Fig. S28-1.

The single integrals are (Fig. S28-2), e.g.,

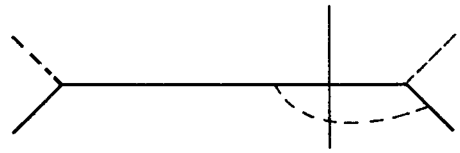

Fig. S28-2.

or (Fig. S28-3)

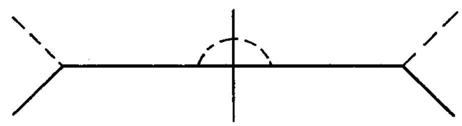

Fig. S28-3.

when sliced as shown. The double integrals include diagrams like (Fig. S28-4)

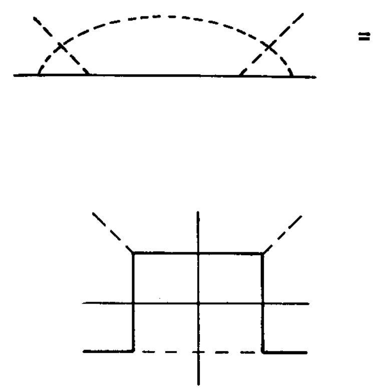

Fig. S28-4.

which can be cut two ways.

If the nucleon is not fundamental, but is a bound state of $N + \pi$, or $K + \Lambda$, then it is probable that the single integrals should not be there, and that there should be a Regge term instead. We shall assume for now that the nucleon is fundamental. Then the single integral and pole in the s channel is the sum of all Feynman graphs such as in (Fig. S28-5)

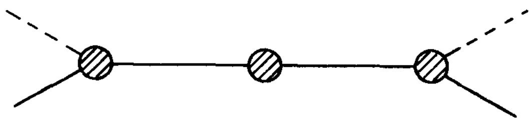

Fig. S28-5.

so that the pole plus single integral is, in the very old-fashioned language, just

$$g^2 \Gamma(s) S_{F1}(s) \Gamma(s) \ .$$

As $s \to \infty$, this approaches

$$g^2 Z_1^2(-s) Z_2^{-1}(-s)/s = g_0^2(-s) Z_2(-s) Z_3(-s)/s \ .$$

Similarly, the crossed pole and single integral approaches

$$g_0^2(-u) Z_2(-u) Z_3(-u)/u$$

as $u \to \infty$.

Thus, we should succeed if we could isolate, let us say, the crossed single integral and examine it for large u.

Now, for $s \to \infty$, an integral of the type

$$\int \frac{f(s')}{s' - s} ds' \to 0.$$

Hence, if we let s, $-t \to \infty$, all the Mandelstam representation for B is eliminated—except what we want. Then, if we let $-u$ be large, we get the limit

$$B \to g_0^2(-u) Z_2(-u) Z_3(-u)/u \ .$$

Having got Z_2 and Z_3 from form-factor experiments, e.g., from $e^+ + e^- \to \pi^+ + \pi^-$, and $e^+ + e^- \to N + \overline{N}$, we now have $g_0(-u)$.

In a bit more detail, the limit we want is this:

a. Fix u at some large (negative) value. Let s, and hence $-t$ (since $s + t + u = 2M^2 + 2\mu^2 \approx 0$), $\to \infty$. Thus, $s >> u$.

b. Do the same for several values of u. This will plot $g_0^2(-u) Z_2(-u) Z_3(-u)/u$ as a function of u.

Since $u = -s/2\,(1 + x)$, where $x = \cos\Theta$, we want to take the limit as $s \to \infty$, and $x = -1-2u/s$, for a fixed value of $-u >> M^2$. This means that we're interested in very backward directions at high energies, but not precisely 180°.

We have no idea when the asymptotic region is reached—i.e., how big we must make u, and how big s. Since as $s \to \infty$, B should become a function of u only, we can say that s is big enough when the result becomes independent of s. We hope that $-u >> M^2$ means $-u = (3 \text{ or } 4 \text{ Gev})^2$ is enough; if the errors are like M^2/u, then this gives only a 10% error.

Also, we don't know how $g_0^2(-u) Z_2(-u) Z_3(-u)$ behaves as $-u$ becomes large; probably it approaches zero—but, since we don't know how fast, we don't know how much cross section there will be left to look at in this limit.

It is also worth observing that, if the guess is correct that there exist single integrals only for fundamental particles, then this limiting procedure provides an experimental test for the fundamentalness of a particle. If no single integral shows up in the limit, it would imply that the particle associated with that single integral is not fundamental.

Finally, as to bare masses, we have nothing much to say yet; only that, if by accident bare masses happen to be finite, they could be observed as a zero in the appropriate scattering amplitude. For example, if m_0 is the bare mass of the nucleon, then the π-N scattering amplitude in the $P_{1/2}$, $T = 1/2$ state has a zero at m_0, provided that the nucleon is an elementary particle.

28. PART II. CALCULATION OF PARTICLE FLUXES FROM PROTON SYNCHROTRONS OF ENERGY 10 TO 1000 Gev

Giuseppe Cocconi, Louis J. Koester, Donald H. Perkins

August 11, 1961

Introduction

Studies with cosmic rays (Seminars 10 and 11) and accelerators (Seminars 3 and 20; also, W. F. Baker et al., Phys. Rev. Letters 7, 101 (1961)) have established the following general characteristics of the secondaries from high-energy interactions of protons with light nuclei:

a. A pion energy spectrum (in the lab system) with a roughly exponential tail, at least up to $E \approx 2/3\, E_0$, where E_0 = proton energy, for $E_0 >$ 20 Gev.

b. A transverse momentum distribution for pions following approximately the Boltzmann law,

$$g(p_\perp)\, dp_\perp = \frac{p_\perp}{p_0^2} \exp\left(\frac{-p_\perp}{p_0}\right) dp_\perp .$$

At E_0 = 25 Gev (CERN), $(p_\perp)_{av} = 2p_0 = 0.36$ Gev/c. Cosmic-ray results give $(p_\perp)_{av} \approx 0.4$ to 0.45 Gev/c, for 10^5 Gev $> E_0 >$ 100 Gev. For $E_0 \gtrsim$ 25 Gev, it can be regarded as established that $p_\perp$ for pions is independent of E_0 and Θ, the angle of emission. For low values of E_0 (let us say 6 Gev) it is known that $p_\perp$ is not independent of Θ; also, just from conservation of energy, the overall $p_\perp$ distribution will be restricted to lower values.

c. The pion multiplicity, n_π, (including π^0, π^+, and π^-) increases slowly with E_0. Data are consistent with a power-law relation

$$n_\pi = aE_0^{1/4} \text{ (with } a = 2.7\text{)}.$$

d. The total energy content of the pions is a fairly constant fraction K_π of the proton energy, and is given by the rough limits $K_\pi \approx 0.3$ to 0.5, for 10^5 Gev $> E_0 >$ 25 Gev.

e. For $E_0 >$ 25 Gev, the ratio of K mesons to pions seems to level off at about 10%. This ratio also appears sensibly independent of the secondary energy E. The $p_\perp$ distribution for K mesons is about the same as that for pions. Thus, rough values of K-meson flux can be obtained by scaling down the pion fluxes by a factor of about 10.

f. In the c. m. system, the proton energy spectrum is peaked towards high values (in contrast with the pion spectrum, peaked towards low values). The CERN results on two-prong inelastic events in a hydrogen chamber indicate a proton momentum spectrum peaked in the vicinity of the maximum possible momentum, and dropping off exponentially as the momentum decreases (Seminar 3). Cosmic-ray results in light elements (with no selection of number of secondary prongs) suggest a (reversed) Boltzmann-like momentum spectrum, with a peak in the region of 0.8 of the maximum possible momentum. The mean energy carried off by the protons is in the region of half the initial energy (K = 0.5) over a very wide range of E_0. Again, the $p_\perp$ distribution of the protons seems to be rather similar to that for the pions.

None of the models of meson production so far proposed (statistical model, fireball model, one-pion-exchange model, etc.) seems able to account for the above features. We have therefore made calculations of particle fluxes simply according to a set of empirical rules suggested by the data.

Two separate approaches have been made in the calculations:

a. The first method was to guess at a pion (or proton) energy spectrum in the laboratory system. Combining this with the transverse momentum distribution, we can obtain an expression for the pion flux in analytical form.

b. The second method was to assume for the pions an exponential longitudinal momentum distribution in the c. m. system. Combination of this distribution with that of $p_\perp$ yields the c. m. momentum distribution, and thus, by a Lorentz transformation, the lab momentum spectrum. The calculation was done numerically, by use of an IBM 709. Proton fluxes were computed in similar fashion.

Analytical Method

The joint probability of obtaining a pion with lab energy E and transverse moment $p_\perp$ has been taken as

$$P\left(E,\ p_\perp\right) = f(E)\ g\left(p_\perp\right). \tag{1}$$

The probability can be expressed as a product in this way, provided $p_\perp$ and E are independent. Clearly, this can be true only for $E >> p_\perp c$, i. e., provided $E > 1$ Gev. Using a Boltzmann distribution for $p_\perp$, and trying a fit with $f(E)$ as a simple exponential, we obtain

$$P\left(E,\ p_\perp\right) dE\,dp_\perp = \frac{1}{p_0^2 T}\ e^{-E/T}\ p_\perp$$

$$\times e^{-p_\perp/p_0}\ dp_\perp\ dE\left(E < E_0\right)$$

$$\text{for } 1 \text{ Gev} < E < E_0,$$

where T is the mean pion energy, for a spectrum extending to $E = \infty$. Since $T << E_0$ (where E_0 = proton energy), the pion energy averaged over the spectrum extending from $E = 0$ to $E = E_0$ is very nearly T. Since $n_\pi T = K_\pi E_0$, and $n_\pi \propto E_0^{1/4}$, it follows that $T \propto E_0^{3/4}$.

Since we have taken $E,\ pc >> p_\perp c$, it follows that the angle of emission Θ is given by

$$\Theta \approx \sin\Theta = \frac{p_\perp}{p}\ ;\quad pc \approx E\ ;\quad p_\perp \approx \frac{E\Theta}{c}\ .$$

Substituting, we obtain for the flux

$$\frac{d^2 N_\pi (E, \Theta)}{dE\,d\Omega} = \frac{n_\pi\ E^2}{2\pi p_0^2 c^2 T}\ e^{-E\left(\frac{1}{T} + \frac{\Theta}{p_0 c}\right)}, \tag{2}$$

where n_π is the effective pion multiplicity. This will be in the region of half the true multiplicity, since only the forward cone of pions (c. m.) can contribute to the high-energy tail (lab). Equation (2) can also be written as

$$\frac{d^2 N_\pi (E, \Theta)}{dE\,d\Omega} = \frac{n_\pi\ T}{2\pi p_0^2 c^2} \left(\frac{E}{T}\right) \cdot e^{-(E/T)\left(1 + \frac{\Theta T}{p_0 c}\right)}$$

$$= \left(n_\pi\ T\right)\phi\left(\frac{E}{T},\ \Theta T\right). \tag{3}$$

Equation (3) suggests a very simple scaling procedure for obtaining fluxes at one value of E_0 (let us say 300 Gev) from those observed at another (let us say 30 Gev). For a given value of E/T, i. e., of $E/E_0^{3/4}$, and ΘT, i. e., $\Theta E_0^{3/4}$, the flux is proportional to $n_\pi T$, i. e., E_0. This procedure does not depend on the explicit forms of f and g. It assumes only that $g(p_\perp)$ is independent of E_0, and that the function $f(E) = f(E/E_{av})$; i. e., always has the same shape.

Equation (2) contains two parameters, n_π and T. As mentioned before, the effective value of n_π is $\approx \frac{a}{2} E_0^{1/4} \approx 1.3\ E_0^{1/4}$. At 30 Gev, this gives $n_\pi = 3.0$. However, n_π can be regarded as a variable parameter to get the best fit with experiment. Figure S28-6 shows the Brookhaven π^+ and π^- spectra from targets of aluminum and beryllium bombarded with 29.5-Gev protons. (Seminar 20; also W.F. Baker et al., Phys. Rev. Letters 7, 101 (1961).) With $p_0 = 0.18$ Gev/c, a fit was made to the flux values at 4.75°, the best result being obtained for $T = 3.75$ Gev, $n_\pi = 1.2\ \times$ targeting factor. Taking the Brookhaven targeting factor

$K_\pi E_0$ is total energy content of pions (postulate d above)

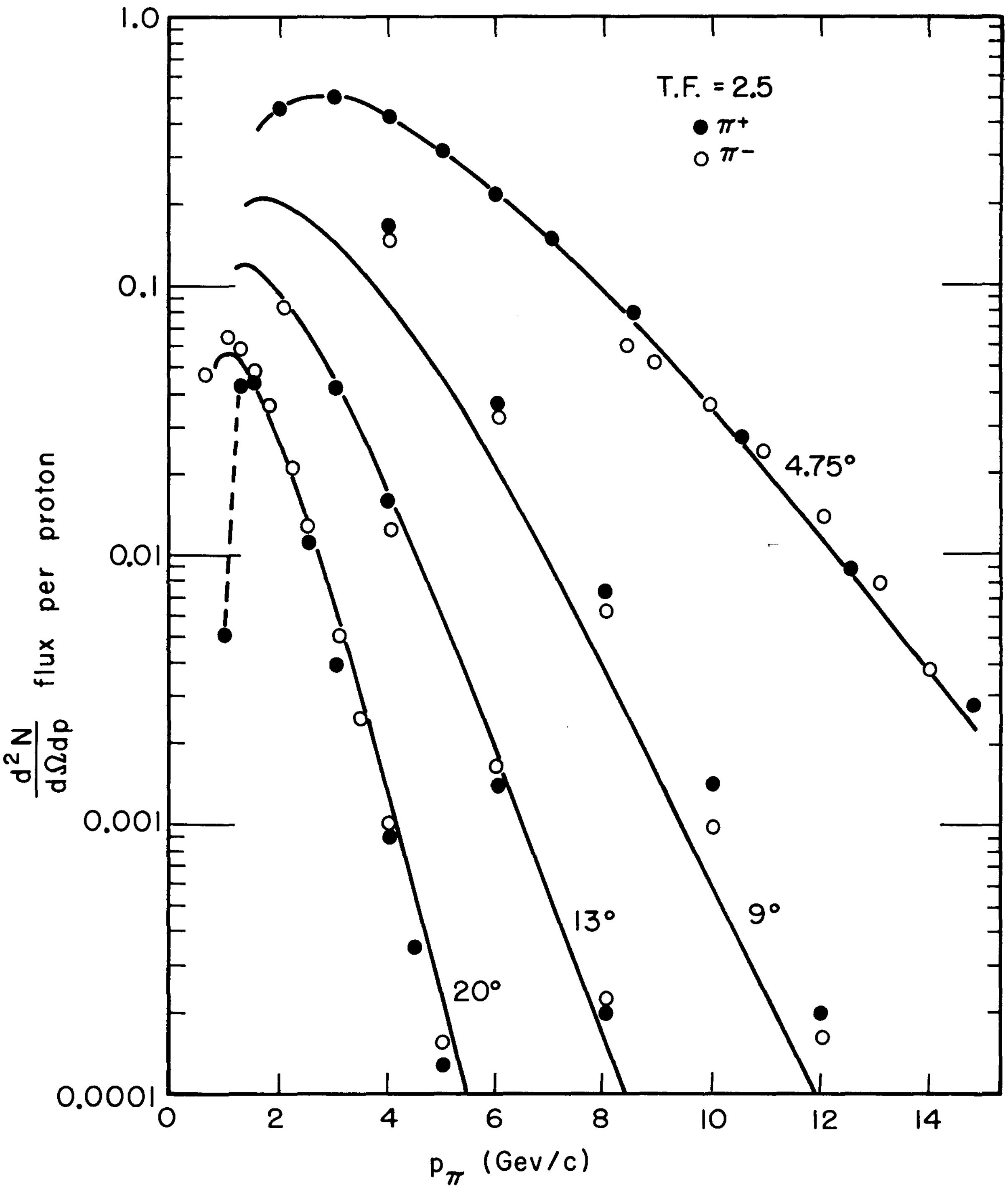

Fig. S28-6. Brookhaven π^+ and π^- spectra from targets of Al and Be bombarded with 29.5-Gev protons. Curves: $n_\pi = 1.2 \times$ T.F. ≈ 3.0

$K_\pi = 0.38$

T = 3.75 Gev; $p_0 = 0.18$ Gev/c.

T.F. ≡ Targeting Factor = (Target efficiency)$^{-1}$

as 2.5 (i.e., 40% target efficiency) yields $n_\pi = 3.0$, in agreement with the previous value. The corresponding value of $K_\pi = \frac{n_\pi T}{E_0} = 0.38$. This value of K_π applies to the high-energy pion secondaries. Those projected backwards in the c.m. system will account for very little lab energy, however, so that the true energy content of the pions is unlikely to exceed $0.45\ E_0$. This figure for the inelasticity is eminently reasonable.

Figure S28-6 also shows the fluxes calculated and observed at 9°, 13°, and 20° to the proton beam. There is a factor-of-2 discrepancy between calculated and experimental fluxes at 9°, but otherwise the agreement is quite good. This agreement confirms that the form taken for the $p_\perp$ distribution is substantially correct, and bears out the value of p_0 obtained from independent direct measurements at CERN. (A 10% change in p_0, for example, would make a factor-of-3 change in the flux at 20° at 5 Gev.) The general agreement between shape of the curves and data also suggests that the choice of an exponential for $f(E)$ is a fairly good one. No simple analytical expression seems likely to give a better fit. Again, it must be emphasized that the curves will underestimate the flux at very low energies ($\lesssim 1$ Gev).

The crucial test of Formula (2) and the relations $n_\pi \propto E_0^{1/4}$, $T \propto E_0^{3/4}$ would be, of course, a comparison with experiments over as wide a range of E_0 as possible. Unfortunately, the range over which this comparison can be made is very limited. Figures S28-7 and 28-8 show this comparison with the Brookhaven results for $E_0 = 20$ Gev and $E_0 = 10$ Gev. The disagreement at 10 Gev most likely results from the fact that, at low proton energies, $p_\perp$ is not independent of Θ, and the angular distributions (c.m.) are indeed nearly isotropic. Evidently, also, the formula does not hold for $E > 2/3\ E_0$. These shortcomings are expected to be less important for large values of E_0, so that we have some confidence that extrapolation upwards to very high energies will be fairly reliable.

From Eq. (2) we can derive the photon flux from the decay $\pi^0 \rightarrow 2\gamma$, under the simplifying assumption that the divergence of the γ rays can be neglected (i.e., setting $m_\pi c << 2p_0$); then

$$\frac{d^2N_\gamma(E,\Theta)}{dE\,d\Omega} = \frac{n_\pi\left[1+E\left(\frac{1}{T}+\frac{\Theta}{p_0c}\right)\right]}{3\pi p_0^2 c^2 T\left(\frac{1}{T}+\frac{\Theta}{p_0c}\right)^2}\, e^{-E\left(\frac{1}{T}+\frac{\Theta}{p_0c}\right)} . \tag{4}$$

Figure S28-9 indicates fair agreement between the fluxes predicted by Eq. (4) and those observed in CERN (Giacomelli et al.). As expected, the neglect of the γ divergence leads to a slight overestimate of flux at small angles. This graph again shows how the formula underestimates fluxes below 1 or 2 Gev secondary energy.

Finally, Figs. S28-10 and S28-11 show the pion beam intensities expected from a 300-Gev proton accelerator, according to the above formulae. Figure S28-10 gives the flux in particles per sr per Gev per interacting proton, at various angles up to 20 mr. The numbers of particles inside different angles are given in Fig. S28-11. The outstanding feature of these distributions is the strong collimation of the beams; for example, more than half the pions of energy $\gtrsim 80$ Gev are confined within a cone of semi-angle 4 mr (0.25°). For comparison, the fluxes from a 1000-Gev synchrotron are given in Fig. S28-12.

Proton Fluxes

It was mentioned in the introduction that direct observations on secondary protons from collisions of 25-Gev protons in a hydrogen bubble chamber at CERN showed that the momentum spectrum was peaked towards high values of momentum, and a similar result has been inferred from the distribution in the inelasticity parameter in cosmic-ray events. Secondary proton fluxes from aluminum and beryllium targets bombarded with 30-Gev protons have been measured at Brookhaven. These measurements extend only up to a momentum of 16 Gev/c, and down to an angle of 4.75°. If Eq. (1) can be applied to the protons, the energy spectrum (lab) can be found from the relation

$$f(E) = \frac{dN_p}{dE} = \frac{d^2N_p}{dE\,d\Omega}\ \frac{2\pi p_0^2 c^2}{E^2} \exp\left(E\Theta/p_0c\right).$$

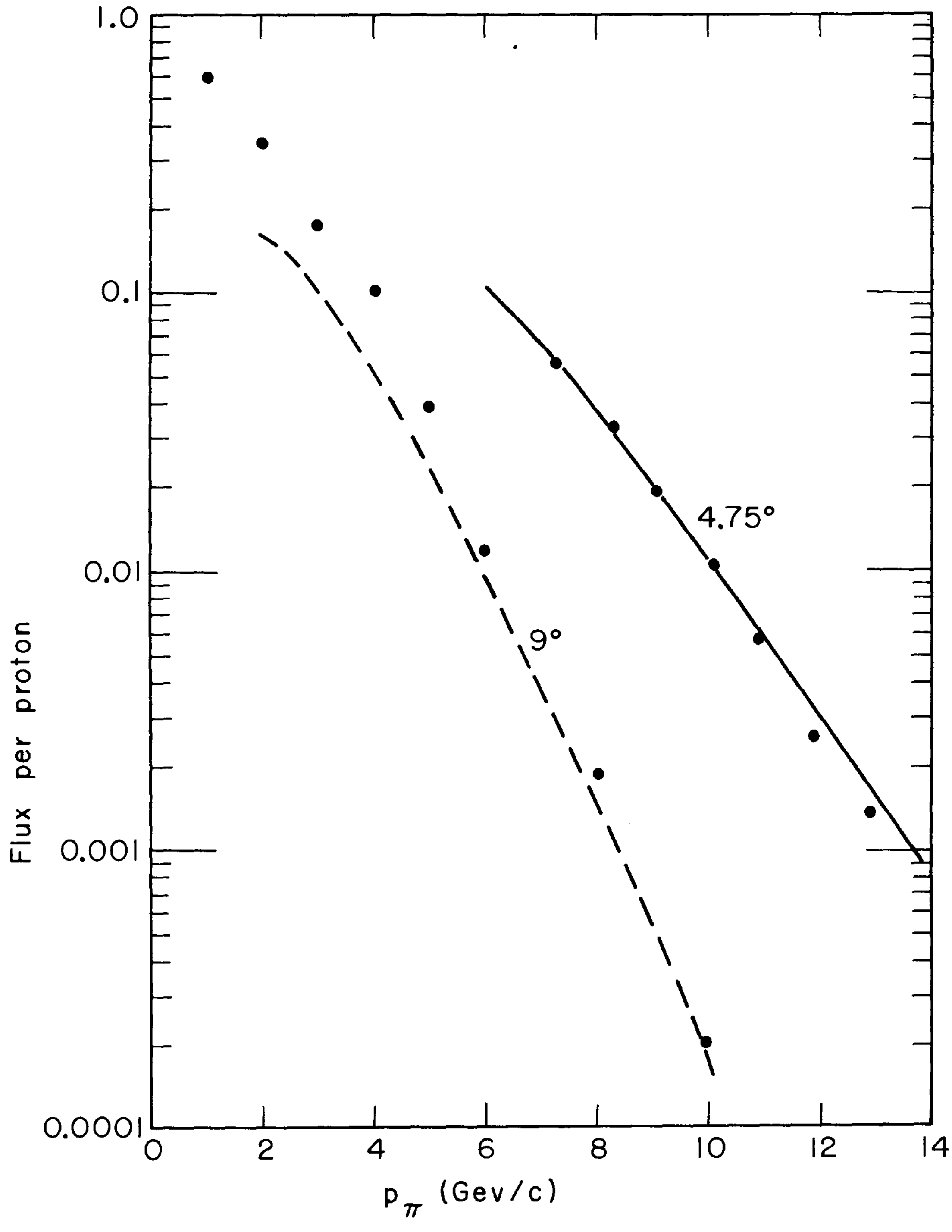

Fig. S28-7. Brookhaven data for 20-Gev protons on Be with T. F. = 2.5 .

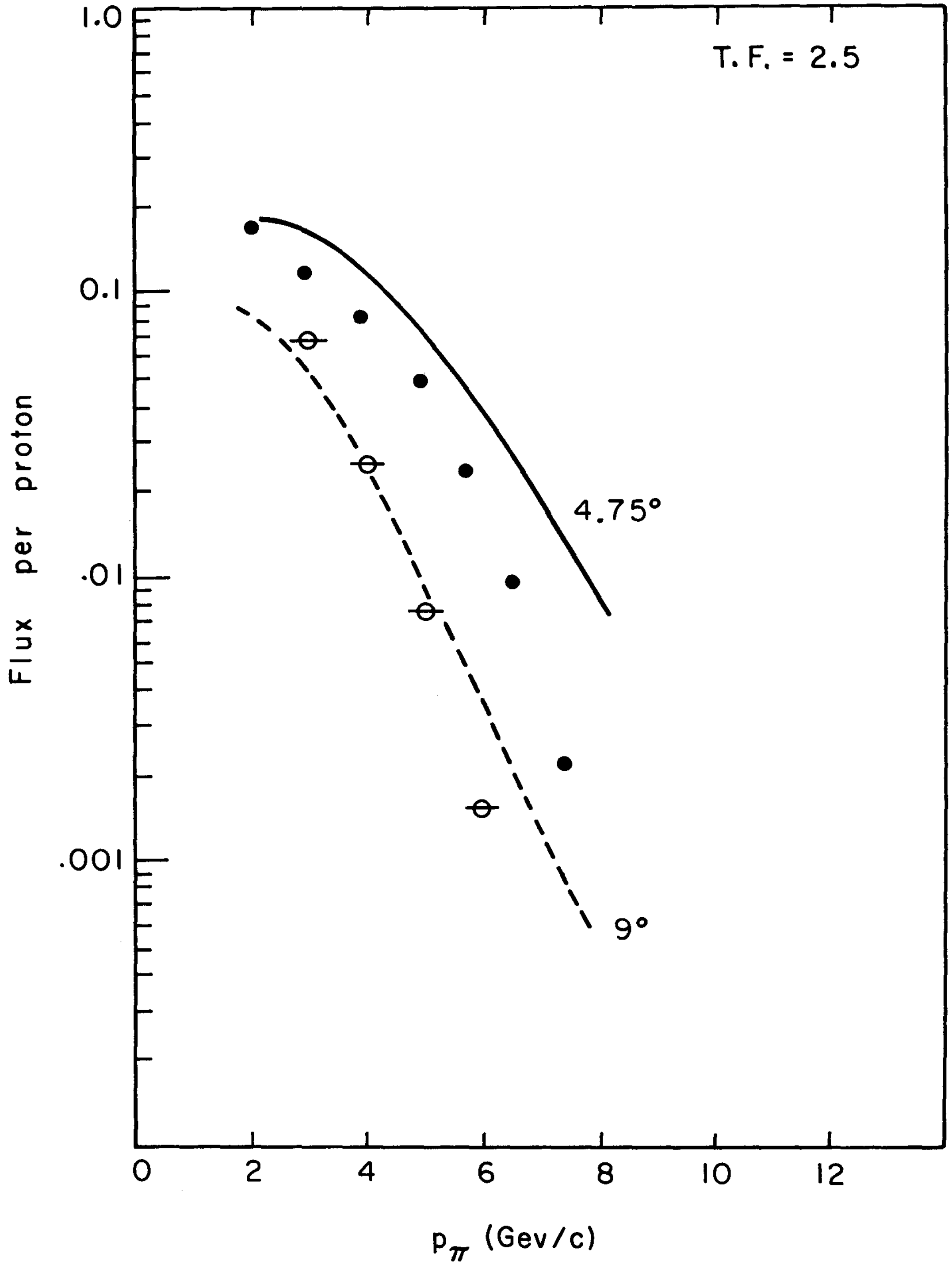

Fig. S28-8. Brookhaven data for 10-Gev protons on Be with T. F. = 2.5 .

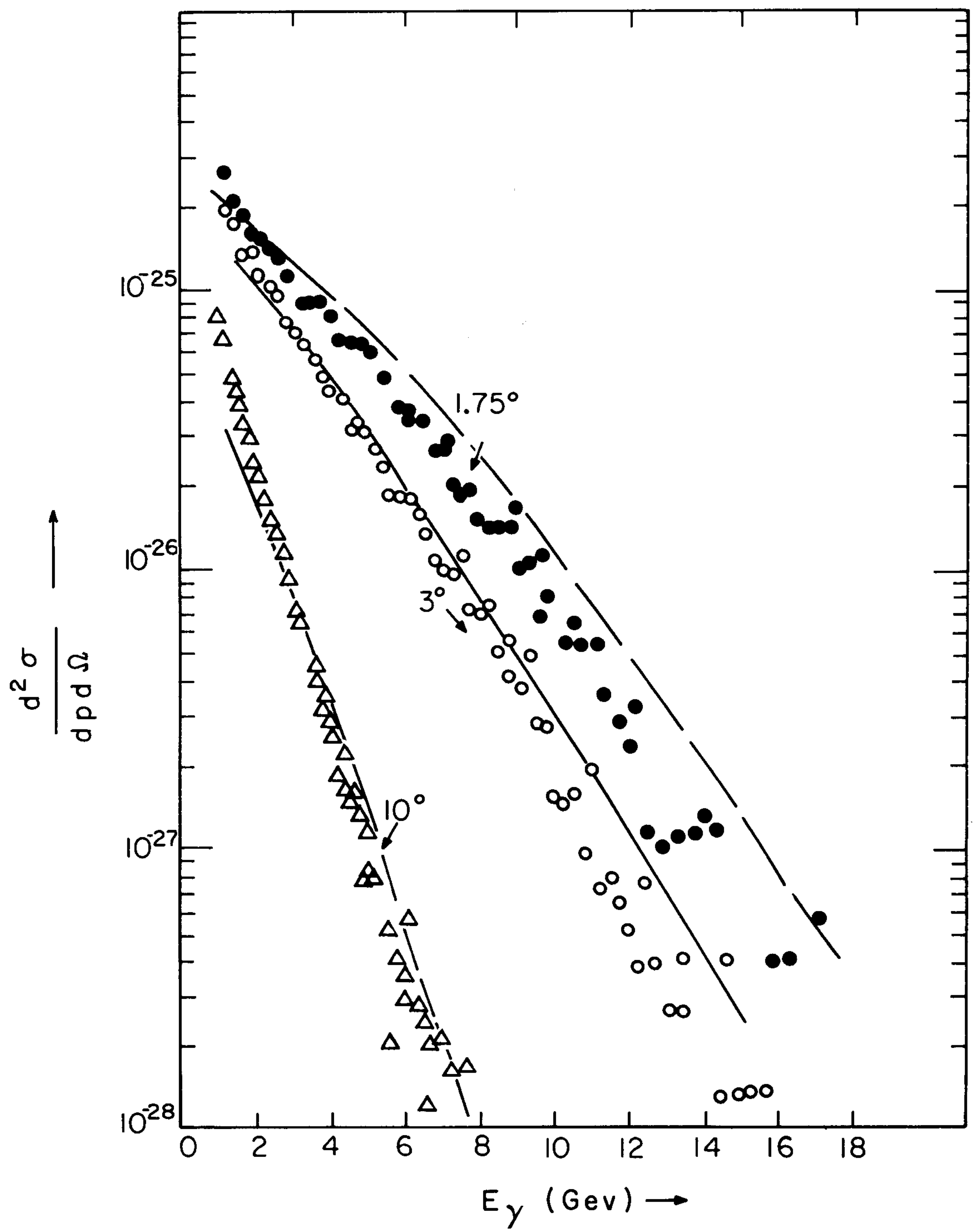

Fig. S28-9. CERN data on γ spectra, p-p at 23 Gev.

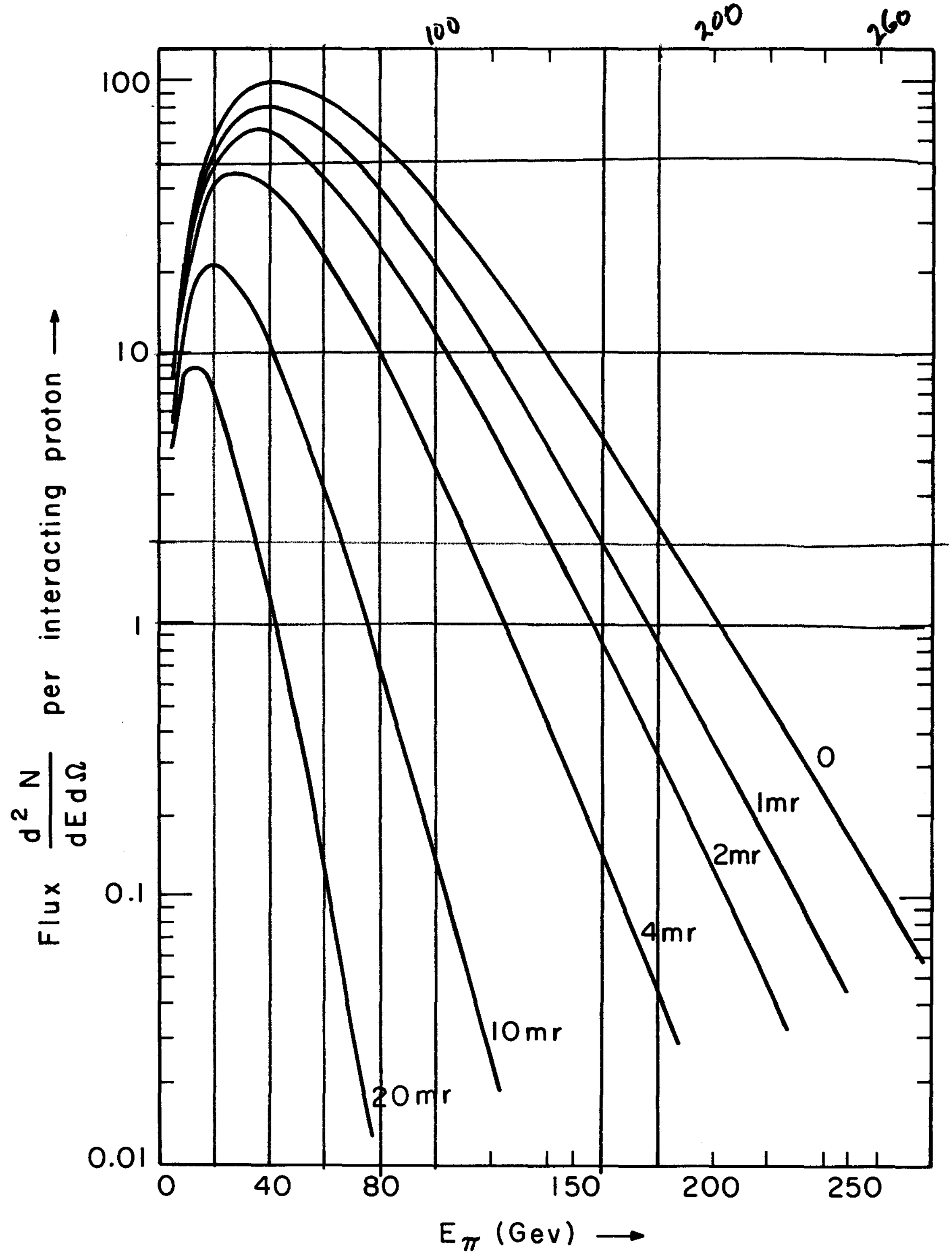

Fig. S28-10. Flux of pions (one sign) from 300-Gev proton beam, at various angles.

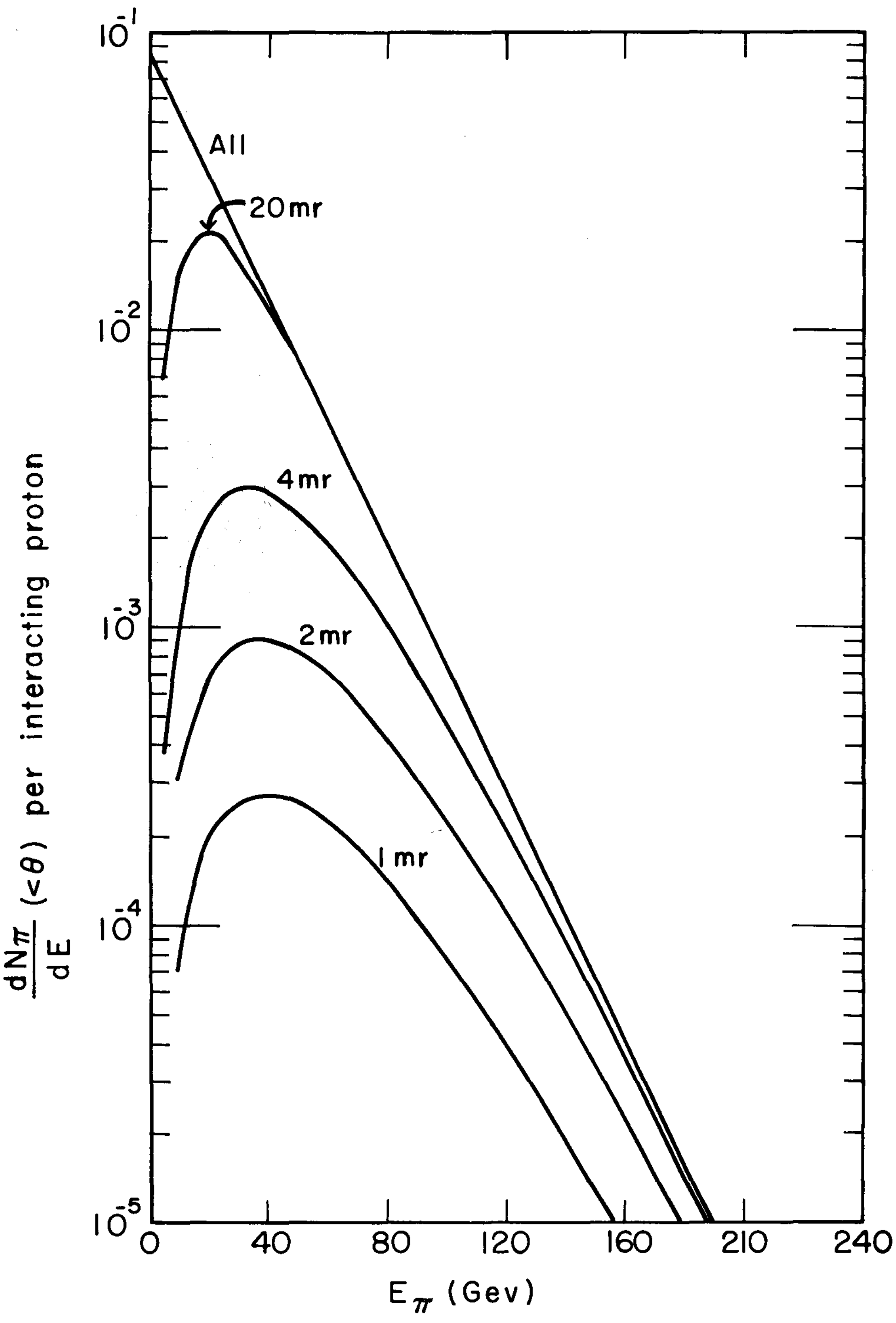

Fig. S28-11. Differential energy spectrum of pions (of one sign) inside angle Θ, produced by 300-Gev protons.

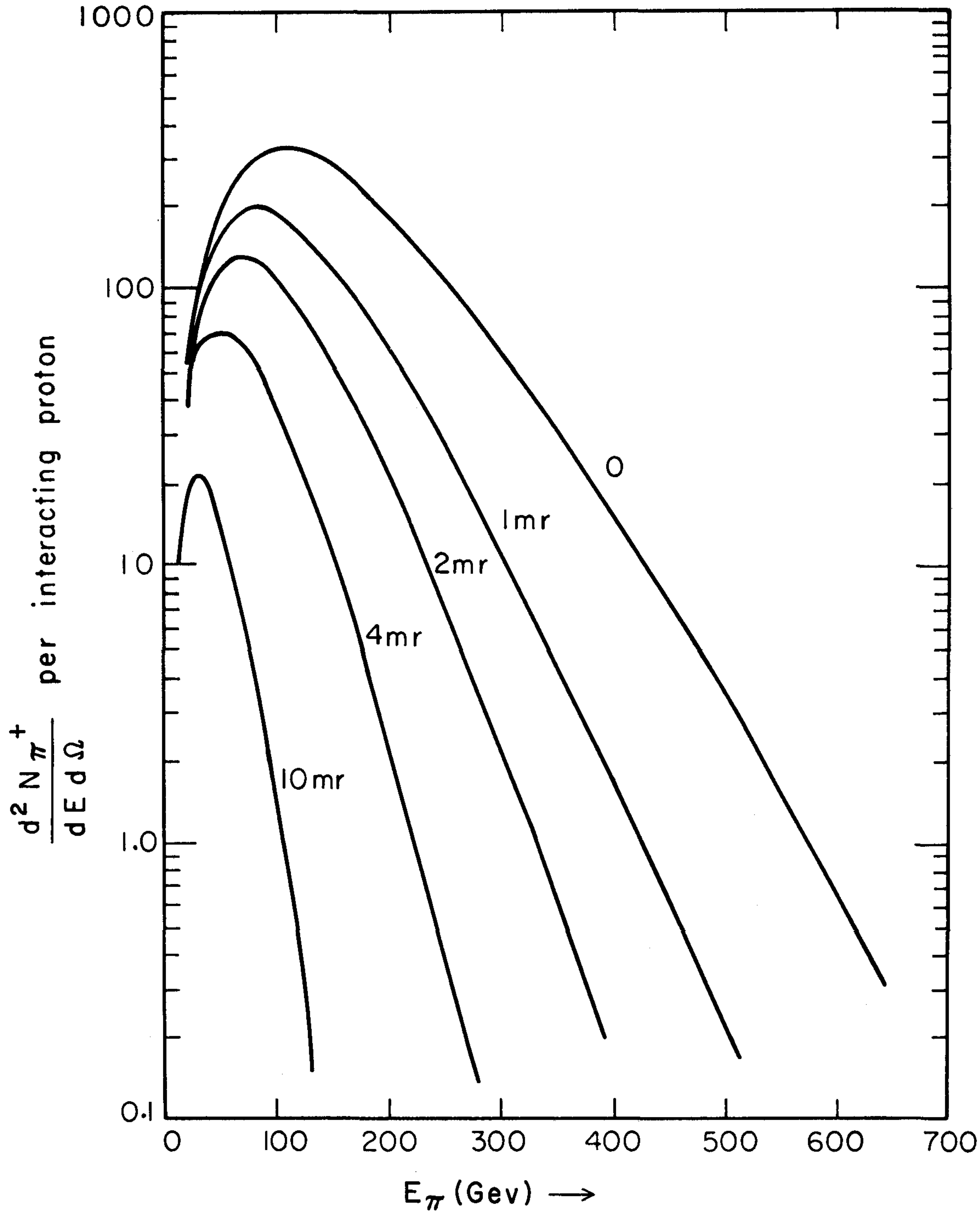

Fig. S28-12. 1000-Gev protons: pion fluxes (one sign)/sr/Gev/interacting proton.
$p_0 = 0.18$ Gev/c; $n = 7.23$; $T = 51.7$ Gev
Flux $= 0.229\, E^2 \exp\left[-E(.0194 + 5.55\,\Theta)\right]$.

Figure S28-13 shows the secondary proton spectrum derived from the Brookhaven flux measurements. The consistency between the results at different angles is best for a value $p_0 = 0.22$ Gev/c. For protons projected forwards in the c.m. system (that is, those of lab energy above 4 Gev), the intensity falls slowly with the lab energy; the same result will therefore apply in the c.m. system. If we assume that, on the average, 0.5 proton per collision is projected forward in the c.m. system then Fig. S28-13 indicates that, above 16 Gev, the spectrum cannot rise appreciably, and, most likely, will continue to fall slowly up to the maximum energy (30 Gev). Clearly, measurements of secondary proton fluxes at higher energy, and, if possible, at smaller angles, are needed to elucidate this point. As shown in the next section of this report, a proton momentum spectrum (c.m.) peaked at high values in fact gives a poor fit to the Brookhaven data.

Particle Spectra Calculated in the Rest Frame

By starting in the rest frame of the collision, or center-of-mass (c.m.) system, one makes use of the symmetry of the initial system of two colliding nucleons. The transverse and longitudinal momentum distributions are computed independently and tabulated in matrix form, where each matrix element (i, j) is the product of the probabilities for transverse momentum P_{1i} and for longitudinal momentum P_{2j}. The momenta P_{1i} and P_{2j} also transform independently into the lab system and determine the lab angle at which the particle appears. The computations are performed by an IBM 709 computer, which sums the probabilities corresponding to a given angular interval and presents, as a function of secondary momentum, the resulting number of particles per interacting proton per sr per Gev/c (lab).

Five conclusions drawn from experimental results with cosmic rays and 25-to 30-Gev accelerators form the underlying basis for this calculation; they have been mentioned above but can be restated here:

a. The average multiplicity $\langle n_s \rangle$ of the secondaries is slowly varying and may be taken as

$$\langle n_s \rangle \approx 6.5 \left(\frac{U_0}{25 \text{ Gev}}\right)^{1/4} \tag{5}$$

(including neutrals), where U_0 is the total lab energy of the incident proton.[1]

b. The average inelasticity K of the collision is about one-half; i.e.,

$$K = \frac{\text{Average energy (c.m.) given to particles created in the interaction}}{\text{Total energy available (c.m.)}} \approx \frac{1}{2} \tag{6}$$

This result does not depend strongly on the energy U_0.

c. The distribution of the transverse momentum P_1 of the secondaries is practically independent of the primary energy, the nature of the secondary particles, and, most important, the longitudinal momentum of the secondaries (Seminars 3, 10, and 11). This distribution is relativistically invariant and is well represented by the expression

$$n(P_1)\,dP_1 = A_1 P_1 e^{-A_2 P_1}\,dP_1 \left(0 \leq P_1 \leq 2 \text{ Gev}\right). \tag{7}$$

By integrating from zero to infinity, one finds the average value

$$\langle P_1 \rangle = 2/A_2 . \tag{8}$$

Empirically, $\langle P_1 \rangle \approx 0.4$ Gev. The coefficient A_1 is found by normalizing to one secondary, i.e.,

$$A_1 \int_0^\infty P_1 e^{-A_2 P_1}\,dP_1 = 1 = A_1/A_2^2 ,$$

so that (9)

$$A_1 = A_2^2 .$$

d. The longitudinal momentum P_2 (c.m.) depends on the nature of the particles and on the primary energy U_0. Inasmuch as the initial system is symmetric in the c.m. system, the longitudinal distribution of the secondaries should be mirror-symmetric with respect to a plane at

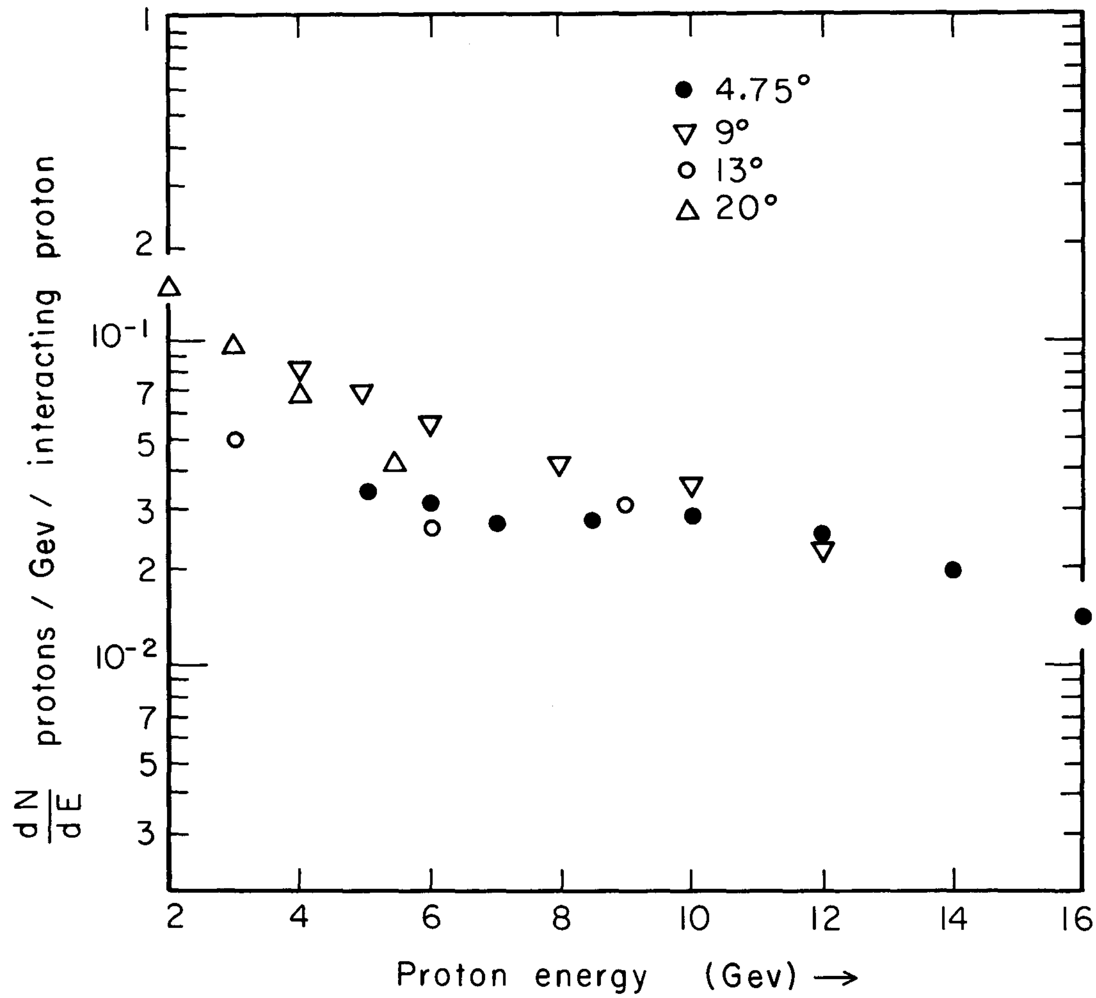

Fig. S28-13. Energy spectrum of protons from Al and Be targets bombarded with 30-Gev protons, computed from Brookhaven flux values.

rest in the c.m. system and perpendicular to the incident direction.

(i) The distribution of mesons and baryons created in the collision is peaked at small values of P_2 and can be described in the c.m. system by an exponential,

$$n\left(P_2\right) dP_2 = B_1 \exp\left(-B_2 \left|P_2\right|\right) dP_2 \quad \left(\text{for } -P_c \lessapprox P_2 \lessapprox P_c\right), \tag{10}$$

where P_c is the largest momentum possible in the c.m. system; integrating from zero to infinity, one finds

$$\left\langle \left|P_2\right| \right\rangle = 1/B_2 , \tag{11}$$

and normalizing to one secondary gives

$$B_1 = B_2/2 . \tag{12}$$

(ii) Since the nucleons start with the c.m. momentum P_c and give up some of it to the secondaries, the longitudinal momentum $\left(P_{2N}\right)$ spectrum of the nucleons is taken to be

$$n\ P_{2N}\ dP_{2N} = C_1 \exp\left(-C_2 \left|P_c - P_{2N}\right|\right) dP_{2N} \quad \left(\text{for } -P_c < P_{2N} < P_c\right). \tag{13}$$

Integrating from $-P_c$ to P_c, one finds, since $e^{2C_2 P_c} >> 1$,

$$\langle P_{2N} \rangle = P_c - 1/C_2 \, , \tag{14}$$

and, from the normalization to one emitted particle,

$$C_1 = C_2 \, . \tag{15}$$

To evaluate C_2, consider the inelasticity $K \approx \frac{1}{2}$. This says that half of all the (c.m.) energy goes to secondaries (mainly pions). The remaining half must be shared by the two nucleons, so that either nucleon may average one-fourth of the total energy. The total (c.m.) energy is the invariant

$$N = \sqrt{\mathcal{E}^2 - P^2} \, , \tag{16}$$

where $\mathcal{E} = U_0 + M = M(\gamma + 1)$ is the total lab energy $\left(\gamma = \frac{U_0}{M}\right)$, and $P = M\sqrt{\gamma^2 - 1}$ is the total lab momentum (that of the incident proton). Thus,

$$N = M\sqrt{2(\gamma + 1)} \, . \tag{17}$$

The Lorentz factor γ_c of the center of mass is given by

$$\gamma_c = 1/\sqrt{1 - \beta_c^2} \, , \tag{18}$$

where β_c is the velocity of the center of mass;

$$\beta_c = \frac{P}{\mathcal{E}} = \sqrt{\frac{\gamma^2 - 1}{(\gamma + 1)^2}} = \sqrt{\frac{\gamma - 1}{\gamma + 1}} \, . \tag{19}$$

Hence,

$$\gamma_c = \sqrt{\frac{\gamma + 1}{2}} \, ,$$

and, from Eq. ~~(13)~~ (17)

$$N = 2M\gamma_c \, . \tag{20}$$

If the emitted nucleon is to have on the average one-fourth of the total (c.m.) energy, then, from Eqs (16), (20)

$$\langle P_{2N} \rangle \approx M\gamma_c/2 \, . \tag{21}$$

Also, before the collision, the two nucleons share all the energy,

$$N = 2\sqrt{P_c^2 + M^2} \, ,$$

so that

$$P_c = M\sqrt{\gamma_c^2 - 1} = M\sqrt{\frac{\gamma - 1}{2}} \approx M\gamma_c \tag{22}$$

$$\text{for } \gamma_c >> 1.$$

Now C_2 can be evaluated from (14):

$$\frac{1}{C_2} = P_c - \langle P_{2N} \rangle = M\gamma_c/2 \, . \tag{23}$$

e. Finally, the mass spectrum of the secondaries seems not to change drastically above about 30 Gev.[1] Most of the secondaries are pions, and the fluxes of other secondaries can be evaluated by scaling down from the pion fluxes according to the ratios measured at 20 to 30 Gev.

The longitudinal momentum distribution of the secondaries involves a very delicate choice of shape. The exponential distribution Eq. (6) is suggested by the fact that all the momentum spectra produced by the CERN and Brookhaven accelerators at all angles have a tail well described by an exponential, up to momenta close to the maxima consistent with limited transverse momentum and the conservation of energy. Also cosmic-ray data[1] indicate that the exponential distribution remains valid up to energies of thousands of Gev.

The CERN and Brookhaven results can be used to evaluate the coefficient B_2 of the exponential decrease in Eq. (6). A fairly good agreement with the 30-Gev data results from the choice $B_2 = 2.4$ Gev^{-1}, i.e., $\langle |P_2| \rangle \approx$

0.4 Gev. To extrapolate to high energies, the relation postulated is

$$B_2 = 2.4\left(\frac{30\ \text{Gev}}{U_0}\right)^{1/4} . \qquad (24)$$

This choice is based on assumptions a and b together with energy conservation. The c.m. energy increases as $U_0^{1/2}$, from Eq. (13). The average number of secondaries increases as $U_0^{1/4}$. Since the average inelasticity K is constant, these secondaries must have an average energy proportional to $U_0^{1/2}/U_0^{1/4} = U_0^{1/4}$. In the extreme relativistic region, the longitudinal momentum is nearly equal to the total energy of the secondary pion, and Eq. (24) follows.

The program for the IBM 709 computer was prepared by Mr. Donald Zurlinden and requires the following input data: the rest mass μ (in Gev) of the emitted particle; the values of γ_c, A_1, A_2, B_1, and B_2; the starting and ending points and interval size for P_1, P_2, and P, and for the lab angle α. The computer forms

$$\text{Probability } 1 = A_1 P_1 e^{-A_2 P_1} \Delta P_1$$
$$\left(\text{for } 0 < P_1 < 2\ \text{Gev}\right)$$

and

$$\text{Probability } 2 = B_1 e^{-B_2 |P_2|} \Delta P_2$$
$$\left(\text{for } -P_c < P_2 < P_c\right) .$$

The computer evaluates the Joint Probability matrix (about 10^4 elements) in which

$$\text{Joint Probability} = \text{Prob. } 1 \times \text{Prob. } 2 . \qquad (25)$$

For each element of the matrix, characterized by the couple of values P_1 and P_2, the following are computed:

$$\bar{P} = \sqrt{P_1^2 + P_2^2} , \qquad (26)$$

$$\bar{\beta} = \bar{P}/\sqrt{\bar{P}^2 + \mu^2} \quad (\text{where } \mu = \text{rest mass of emitted particle}) , \qquad (27)$$

$$\tan\bar{\Theta} = P_1/P_2 \qquad (\text{c.m. system}) , \qquad (28)$$

$$\tan\alpha = \frac{1}{\gamma_c}\,\frac{\sin\bar{\Theta}}{\left(\cos\bar{\Theta} + \frac{\beta_c}{\bar{\beta}}\right)} \qquad (\text{lab angle}) , \qquad (29)$$

$$P = \frac{\gamma_c \bar{P}}{\bar{\beta}}\left[\left(\beta_c + \bar{\beta}\cos\bar{\Theta}\right)^2 + \left(\frac{\bar{\beta}}{\gamma_c}\sin\bar{\Theta}\right)^2\right]^{1/2} \qquad (30)$$

(lab momentum) .

The following final results are then evaluated: Average momentum in the c.m. system,

$$\left\langle\bar{P}\right\rangle = \Sigma(\bar{P} \times \text{Joint Probability}) ; \text{ and} \qquad (31)$$

Average lab momentum,

$$\left\langle P\right\rangle = \Sigma(P \times \text{Joint Probability}) . \qquad (32)$$

The computer searches its memory for momentum pairs falling within the specified angular range $\alpha_1 < \alpha < \alpha_2$ and tabulates the Joint-Probability sums versus P. Each entry represents

$$\frac{d^2\pi(\alpha)}{\Delta P\,\Delta\Omega} = \frac{\Sigma\left(P_i \times \text{Joint Probability}\right)}{2\pi\left(\cos\alpha_1 - \cos\alpha_2\right)} , \qquad (33)$$

with $\alpha_1 < \alpha < \alpha_2$ and $P < P_i < P + \Delta P$.

The flux of secondaries (e.g., π^+ mesons) produced by an interaction at the angle α (lab) is

$$\frac{n(\pi^+, \alpha)}{\frac{\text{Gev}}{c}\ \text{sr}} = \left\langle n(\pi^+)\right\rangle \frac{d^2\pi(\alpha)}{\Delta P\,\Delta\Omega} , \qquad (34)$$

where $\left\langle n(\pi^+)\right\rangle$ is the average number of π^+ mesons produced in one interaction. The fluxes of the other secondary particles are assumed to be proportional to that of the pions.

Notice that Eq. (34) must be used in order to interpret the tabulated spectra correctly. If they are tabulated in 1-Gev/c intervals, it is necessary only to multiply the ordinates by

$\langle n(\pi^+)\rangle$ to get the numbers of π^+ mesons per sr Gev/c. If, however, as is true at 300 Gev, they are tabulated in 10-Gev/c intervals, it is necessary to divide the ordinates by $\Delta P = 10$ Gev/c.

To evaluate the fluxes of nucleons emitted according to Eq. (13) the IBM data cards (the cards numbered 1 through 5 at the bottom of the program stack) are modified as follows: (a) insert $\mu = 0.938$ Gev for the proton mass instead of $\mu = 0.140$ Gev (for the pion mass) on card 1; (b) insert C_1 and C_2 $\left(C_1 = C_2 = 2/M\gamma_c \text{ Gev}^{-1}\right)$ in place of B_1 and B_2 on card 3; (c) punch a "1" in column 40 of card 3 to tell the computer to use Eq. (13) instead of Eq. (10) [This column must be left blank to compute pion fluxes by Eq. (10)] .

Results and Comments

The experimental data from the Brookhaven AGS were used to test the validity of the computed fluxes. First, the measured pion spectra from 30-Gev incident protons at lab angles 4.75°, 9°, 13°, and 20° were compared with the computed spectra as shown on Fig. S28-14. At this energy, the average multiplicity of pions of one sign is roughly 2, and the fraction of the circulating protons in the AGS that interact with the target is about 1/2. Since both the experimental points and the theoretical curve need to be multiplied by 2 to give fluxes per interaction, neither is changed. They simply are plotted without normalization. No distinction is made between π^+ and π^- fluxes, and nucleon-nucleon collisions are assumed. The agreement at the larger angles is sensitive to the choice of the transverse-momentum parameter A_2 , which is 6 Gev^{-1}, corresponding to an average transverse momentum of 0.33 Gev. The longitudinal-momentum parameter B_2 is also important, and is chosen to be 2.4 Gev^{-1} at 30 Gev. The values of B_1 and B_2 at all other energies U_0 are obtained from this one by the relation

$$B_1\left(U_0\right) = \left(\frac{30 \text{ Gev}}{U_0}\right)^{1/4} B_1(30 \text{ Gev}) \quad .$$

Figure S28-15 shows the comparison with Brookhaven data at 20 Gev. Here, the calculated ordinates are multiplied by $(20/30)^{1/4}$ to take into account the decrease in pion multiplicity with energy. The same thing is done at 10 Gev for Fig. S28-16. The agreement here is not expected to be good because the energy is low enough that small discrepancies in the c.m. momentum allowed a pion make obviously wrong results, such as pions with too much energy (lab).

Having fixed the values of A_1 and A_2 and the constant in B_1 and B_2, one may compute fluxes at higher energies. Figure S28-17 shows the resulting spectra at 0 to 5, 5 to 10, 10 to 15, and 15 to 20 milliradians for a 300-Gev accelerator. The units are the same as before (the average multiplicity of π^+ mesons is about 4), and this graph shows how rapidly the flux decreases as the angle increases. Sometimes it is more useful, for small angles, to know how many particles are included in a cone of a certain half angle like 1 mr, 3 mr, or 5 mr. To answer this question, take the ordinates of Fig. S28-18, which have the same units $\left(\text{sr}^{-1}\right)$ as always, and multiply by the number of steradians included in such a cone. This means multiplying by $2\pi\left(\cos\alpha_1 - \cos\alpha_2\right) = 2\pi\left(1 - \cos\alpha_2\right) \approx 2\pi\left(1 - 1 + \alpha_2^2/2\right) = \pi\alpha_2^2$. For $\Theta = 1$ mr, this is a factor $\pi \times 10^{-6}$, multiplying the fluxes.

Figures S28-19 and S28-20 show the corresponding results for 1000-Gev incident protons.

Figure S28-21 compares the calculated fluxes of emitted nucleons with those measured at Brookhaven. Although the shapes are reasonable at angles different from zero, the magnitudes are wrong by a factor of 4, since the target efficiency is about 50%, and there is no reason to say that two protons will be emitted in a proton-neutron collision, for example. The significance of the calculation at zero angle is very uncertain.

Comparison of the Two Methods

The two methods of estimating pion fluxes appear to be in good agreement, for energies sufficiently high ($p >> \gamma_c m_\pi c$) so that the particles projected backwards in the c.m. system do not contribute. This result must follow from these considerations.

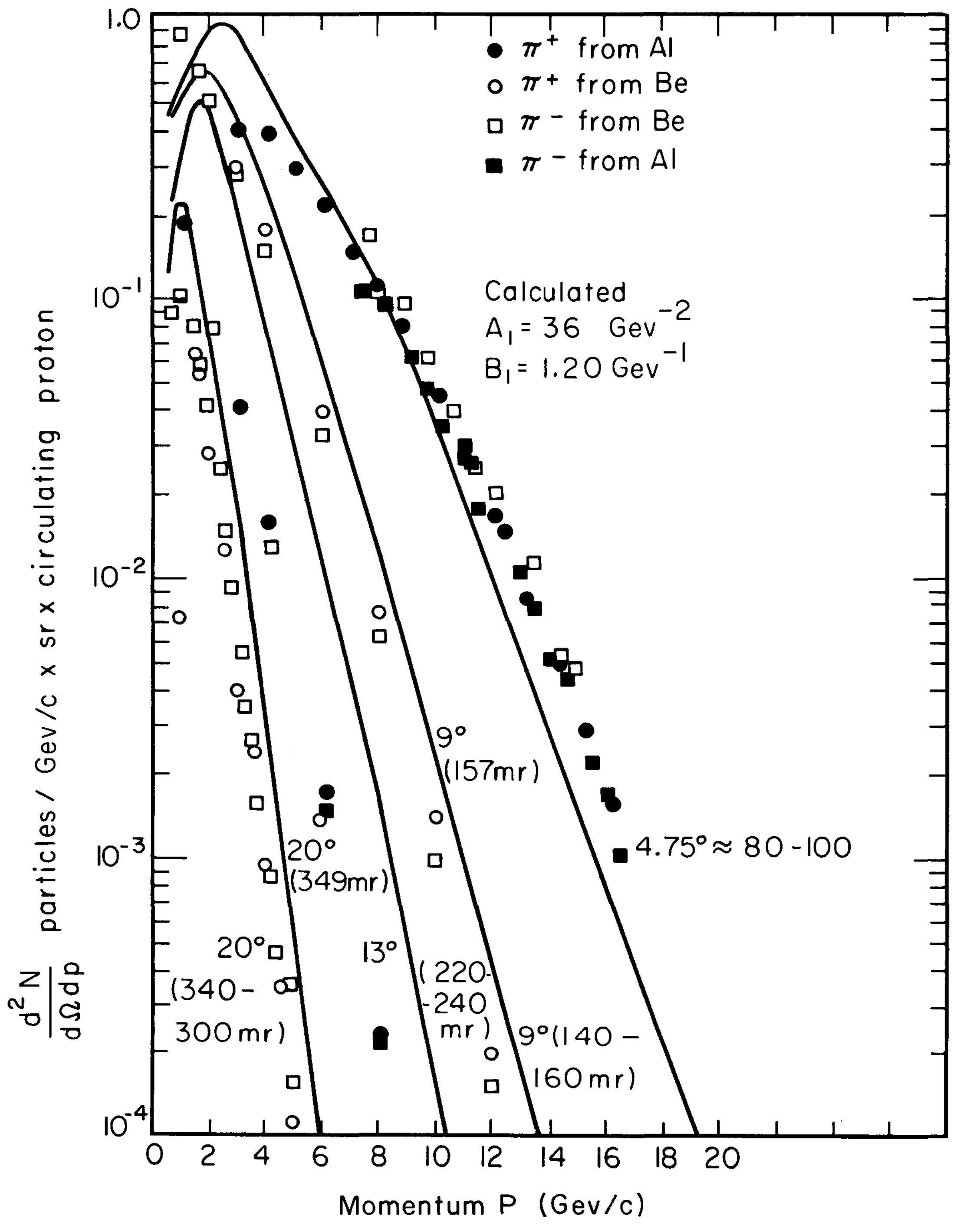

Fig. S28-14. 30-Gev AGS data (Yuan).

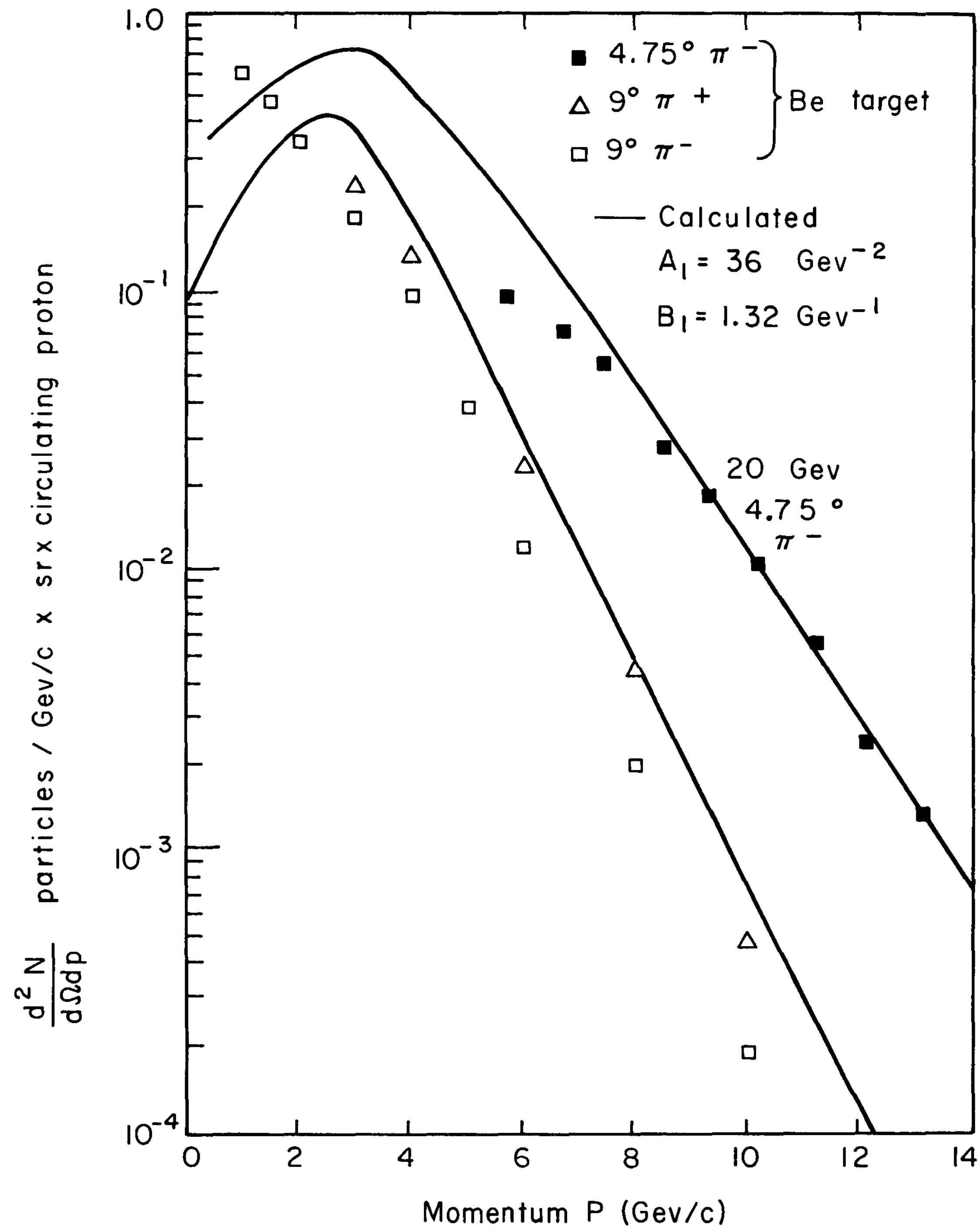

Fig. S28-15. Brookhaven AGS data (Yuan); 20 Gev.

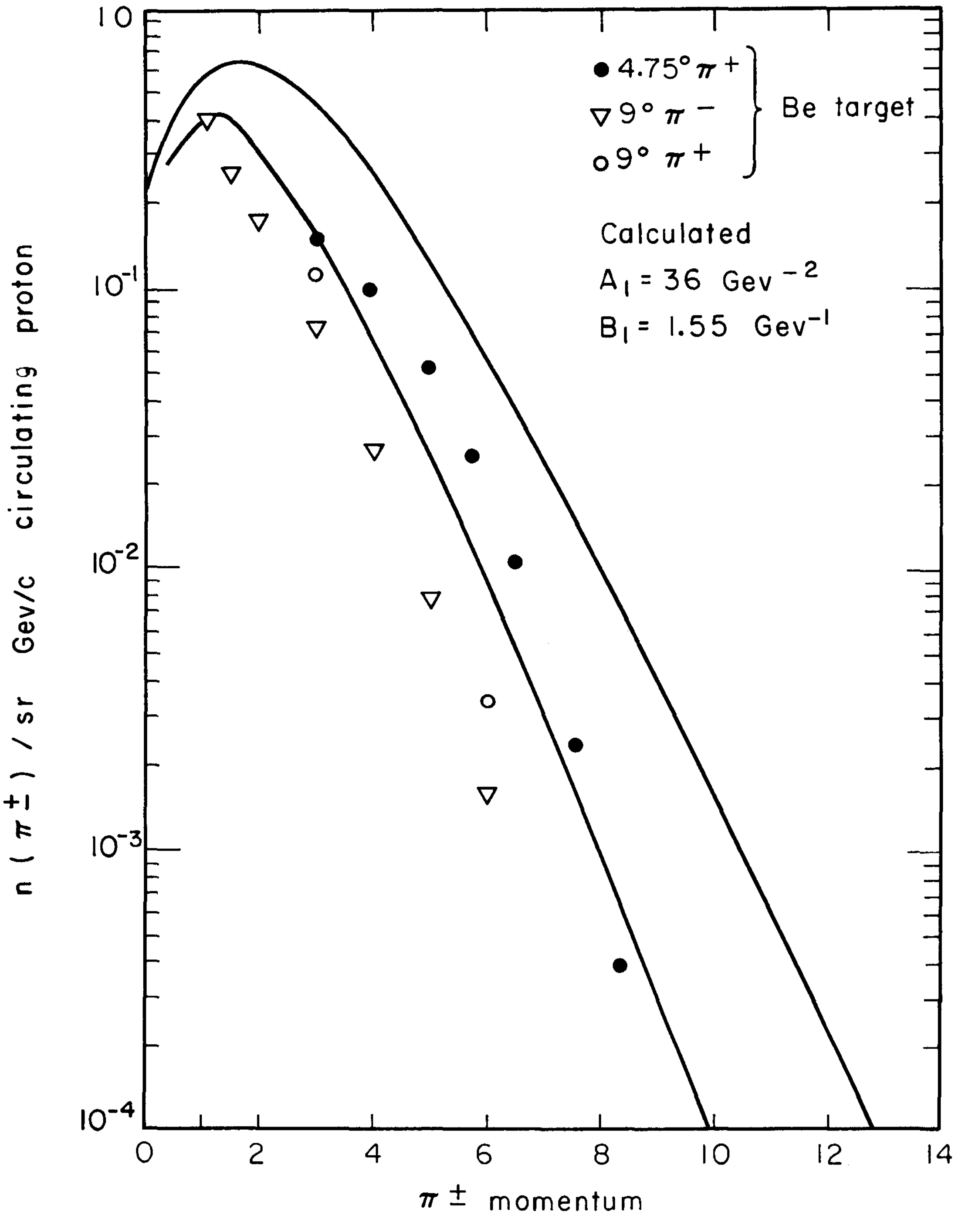

Fig. S28-16. Brookhaven 10-Gev data (Yuan).

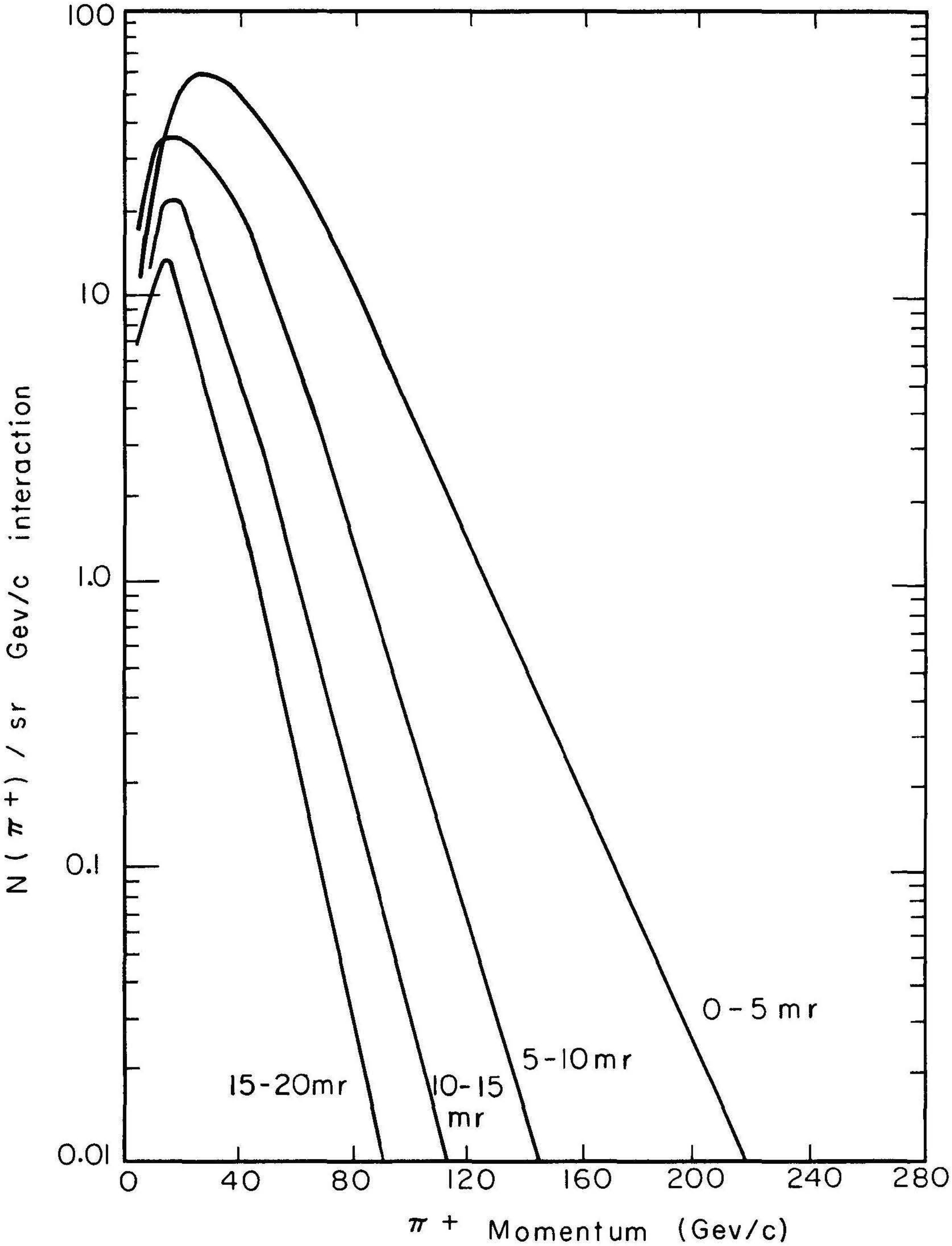

Fig. S28-17. 300-Gev π^+ (or π^-) spectra. $A_1 = 36$ Gev^{-2}
$B_1 = 0.70$ Gev^{-1}
$\langle n(\pi^+)\rangle \approx 4$

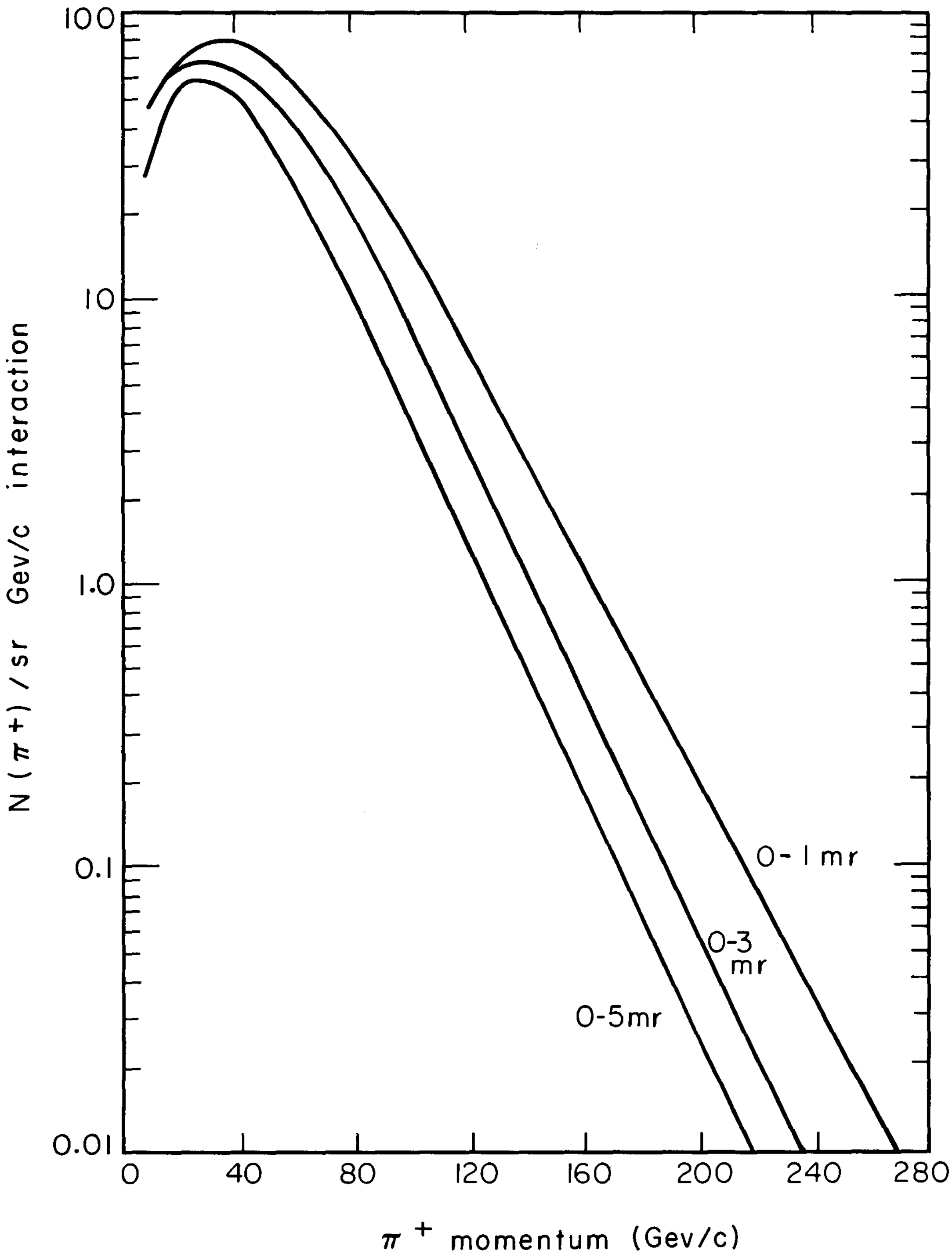

Fig. S28-18. 300-Gev π^+ (or π^-) spectra.

$A_1 = 36\ \text{Gev}^{-2}$
$B_1 = 0.70\ \text{Gev}^{-1}$
$\langle n(\pi^+) \rangle \approx 4$

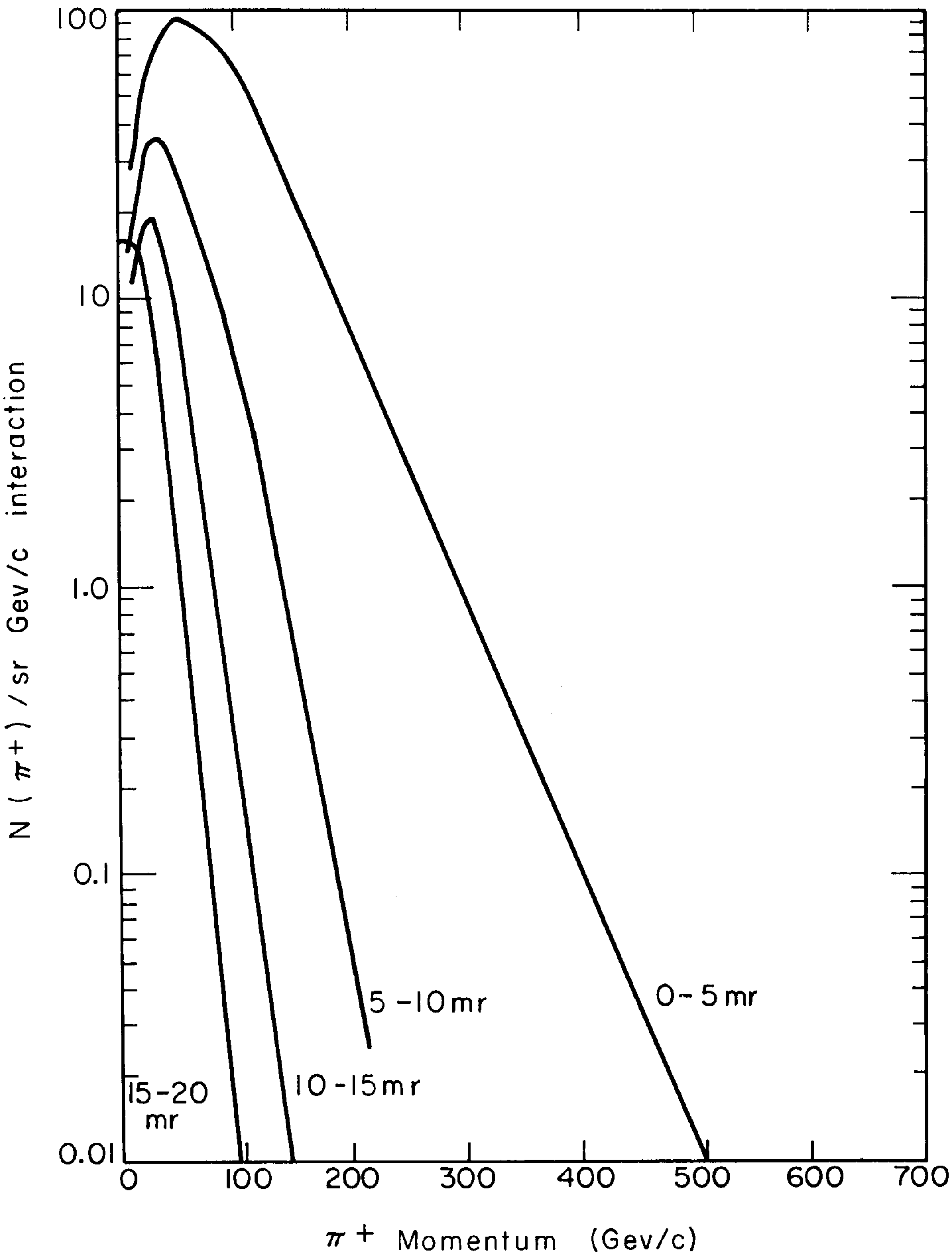

Fig. S28-19. 1000-Gev π^{+} (or π^{-}) spectra. $A_1 = 36\ \mathrm{Gev}^{-2}$
$B_1 = 0.50\ \mathrm{Gev}^{-1}$
$\langle n\,(\pi^{+})\rangle \approx 5$

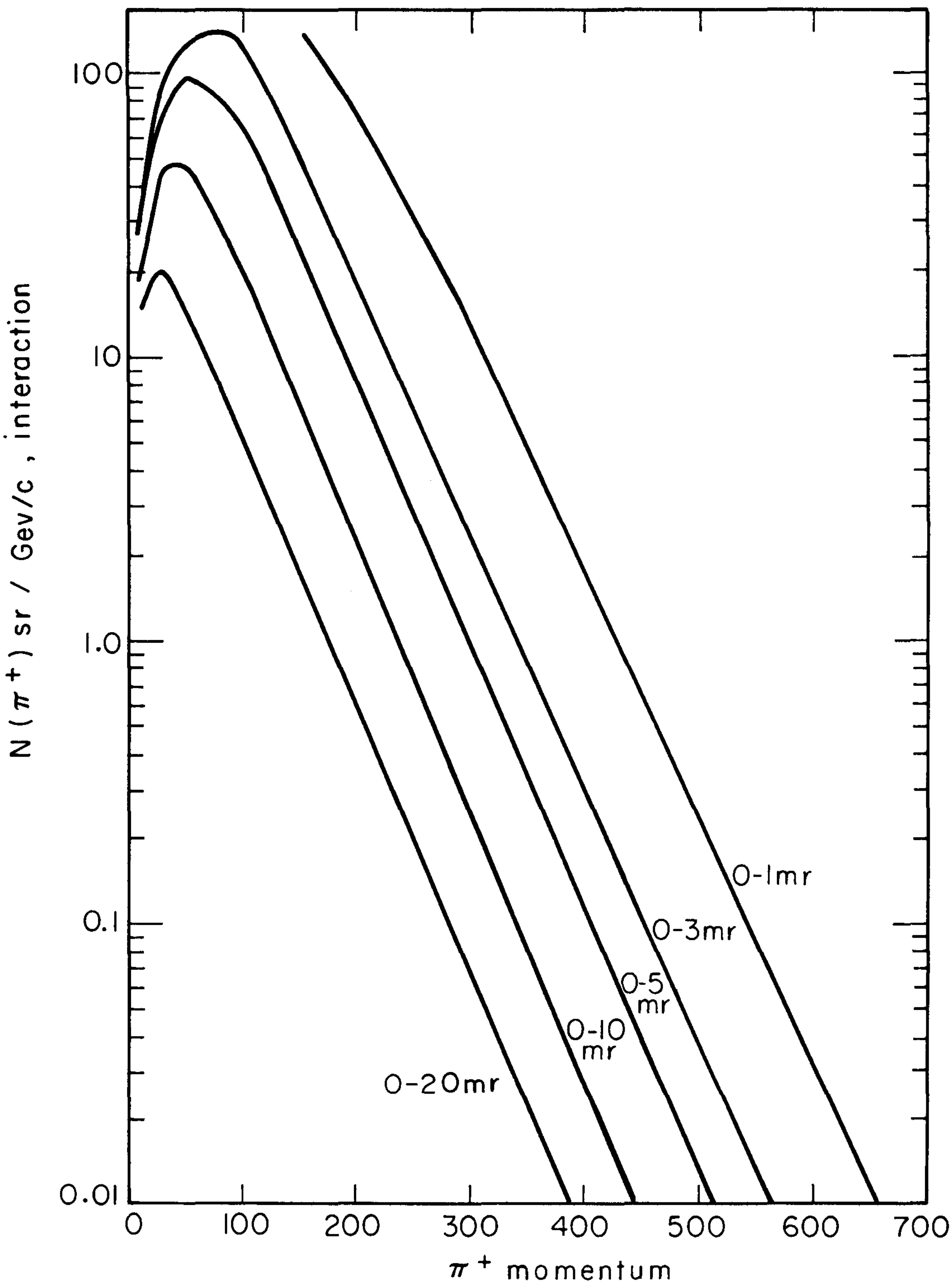

Fig. S28-20. 1000-Gev π^+ (or π^-) spectra. $A_1 = 36\ \text{Gev}^{-2}$
$B_1 = 0.50\ \text{Gev}^{-1}$
$\langle n\,(\pi^+)\rangle \approx 5$

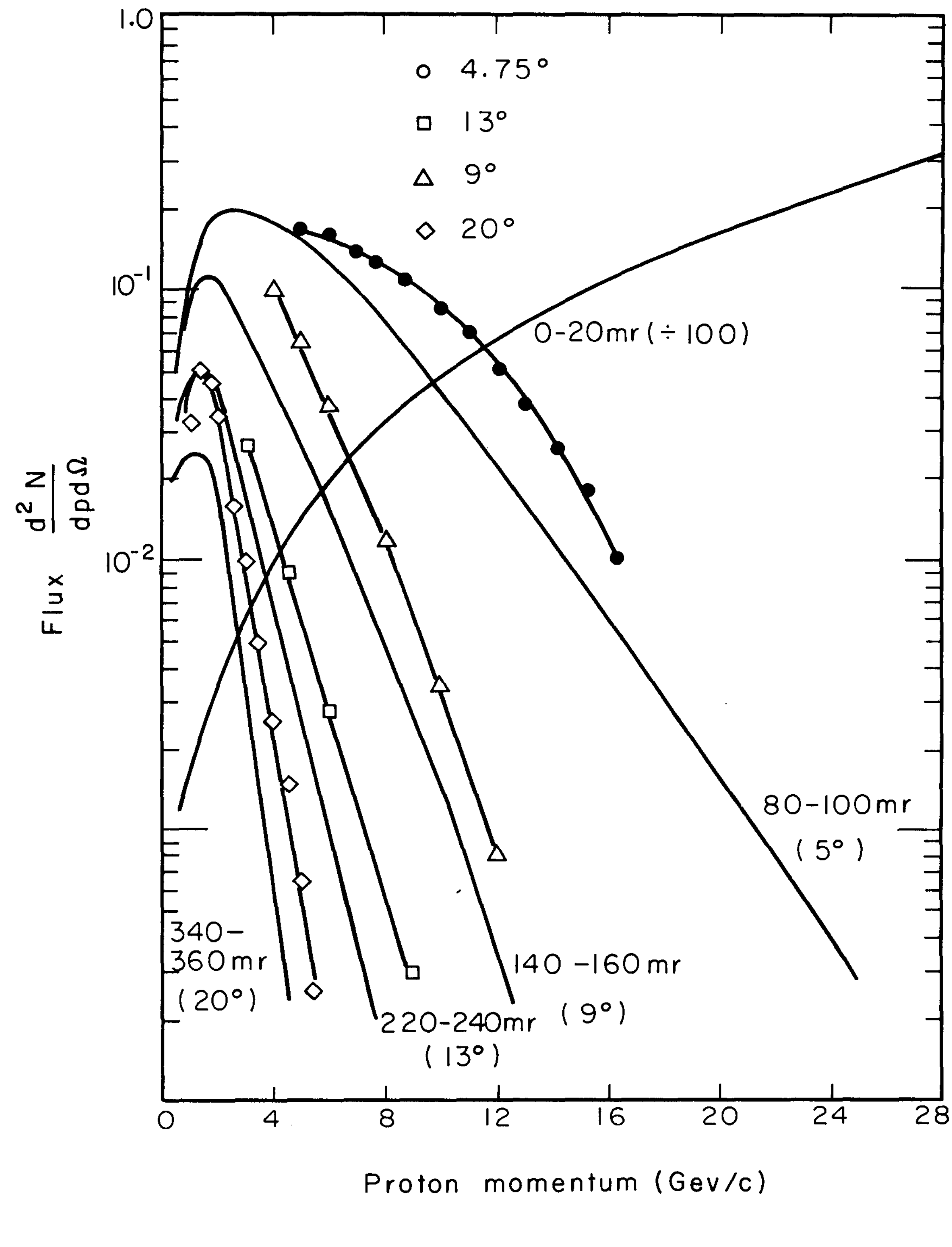

Fig. S28-21. 30-Gev AGS proton spectra. $A_1 = 36$ Gev^{-2}
$B_1 = B_2 = 0.5$ Gev^{-1}

The longitudinal momenta p_{11}^* (c.m.) and p_{11} (lab) are related by the Lorentz transformation

$$p_{11} = \gamma_c\left(p_{11}^* + \beta_c \gamma^*\right) ,$$

where the longitudinal momentum is expressed in units of $m_\pi c$. When p_{11}^* is positive (forward cone), we can set $\beta_c = 1$ (at $E_0 = 30$ Gev, for example, $\gamma_c \approx 4$ and $\beta_c = 0.97$). If $p_{11} \gg 2\gamma$, i.e., $p_{11} \gg 1$ Gev/c for $E_0 = 30$ Gev, both γ^* and p_{11}^* must be $\gg 1$ and nearly equal. In this case, one has

$$p_{11} \approx E \approx 2\,\gamma_c \cdot \gamma^* .$$

Thus, the lab energy and c.m. energy are proportional for forward-projected pions in the high-energy tail. The coefficient of the exponential distribution in p_{11}^* and that of the exponential distribution in E (the "temperature" T) should then be related by

$$T = 2\,\gamma_c / B\,(2) .$$

At $E_0 = 30$ Gev, $\gamma_c = 4.12$, B (2) was taken as 2.4, and this equation then gives T = 3.43 Gev, compared with the value 3.75 Gev actually used in the analytical method.

From the computer data one can obtain the mean lab momentum of the secondaries. For $E_0 = 1000$ Gev, one finds $(pc)_{av} = 26$ Gev, as compared with a T value of 51.7 Gev expected for this value of E_0 . The ratio $(pc)_{av}/T$ simply expresses the fact that the bulk of the lab energy is carried off by just half the pions — those projected forwards in the c.m. system — and the remainder obtain very little energy.

REPORTS

1. SUMMARY OF DISCUSSION OF PERIPHERAL COLLISION THEORY

(Amati, Chew, Frautschi, Goebel)

June 20 to July 7, 1961

Until recently, the standard approach to high-energy collisions has been through semiclassical "optical" and "statistical" models, which avoid a detailed specification of particle structure, so that their verification (or lack of verification) has not been relevant to the development of particle theory. Within the past year, however, a potentially quantitative framework for describing strong interactions at high as well as at low energies has begun to emerge from the combined properties of unitarity and analyticity of the S matrix. It is too soon to say how detailed and how reliable will be the high-energy theoretical predictions based on the S matrix, but it appears at the moment that the region of laboratory-system energies greater than about 100 Gev will be of major interest to the new theory.

Crudely speaking, the new approach divides each particle into "shells," the outermost of which — comprising the bulk of the "geometrical" cross section — is dominated by pions in a configuration controlled essentially by low-energy considerations. One expects, therefore, to make quantitative predictions about high-energy collisions of impact parameter approximately 10^{-13} cm, in terms of the low-energy interaction of pions with the incident as well as the final particles in question. There is abundant experimental evidence that such large-impact-parameter (low-momentum-transfer) collisions actually do predominate, so the "peripheral" approach should be capable of describing the majority of the strong-interaction phenomena to be observed. Collisions with small impact parameters ($<< 10^{-13}$ cm) will be difficult to predict theoretically, but also will be rare.

The S-matrix description of a large-impact-parameter (one-pion-exchange) collision of particle A with particle B can be discussed in terms of the diagram of Fig. R1-1.* "Clumps" of particles are emitted from the exchanged pion, the "outside" clumps A_1 and B_1 at the points of pion emission and absorption, but also "inside" clumps A_2, A_3 . . ., B_2, B_3 . . . at intermediate points. All possible numbers of clumps occur in each of the two groups, consistent with energy conservation, and the contents of each clump is restricted only by conservation laws. It appears likely, however, that the "mass" of each clump tends to be low—less than 1 Gev for clumps of zero baryon number and less than 2 Gev for clumps with baryon number equal to 1. This means that most of the time each clump contains no more than two particles.

It is to be expected that during the next few years detailed and quantitative calculations will be based on this picture, predicting total and elastic cross sections as well as the multiplicity and distribution of produced particles. The verification of such predictions will obviously be of importance, and it is expected that the most clear-cut predictions will apply to the "asymptotic" region, where low-energy irregularities have disappeared. The asymptotic region is, of course, not well defined, and develops gradually, but a factor-of-10 increase over existing accelerator energies will clearly be useful, since current CERN measurements show a substantial energy variation in some total cross sections as well as a difference between particle and antiparticle cross sections. Such effects are expected to die out "asymptotically."

---

* This is not the same as the description by Salzman, Drell, Pomeranchuk, et. al., although a connection between the two approaches can be made. The S-matrix approach is believed to be the more correct of the two.

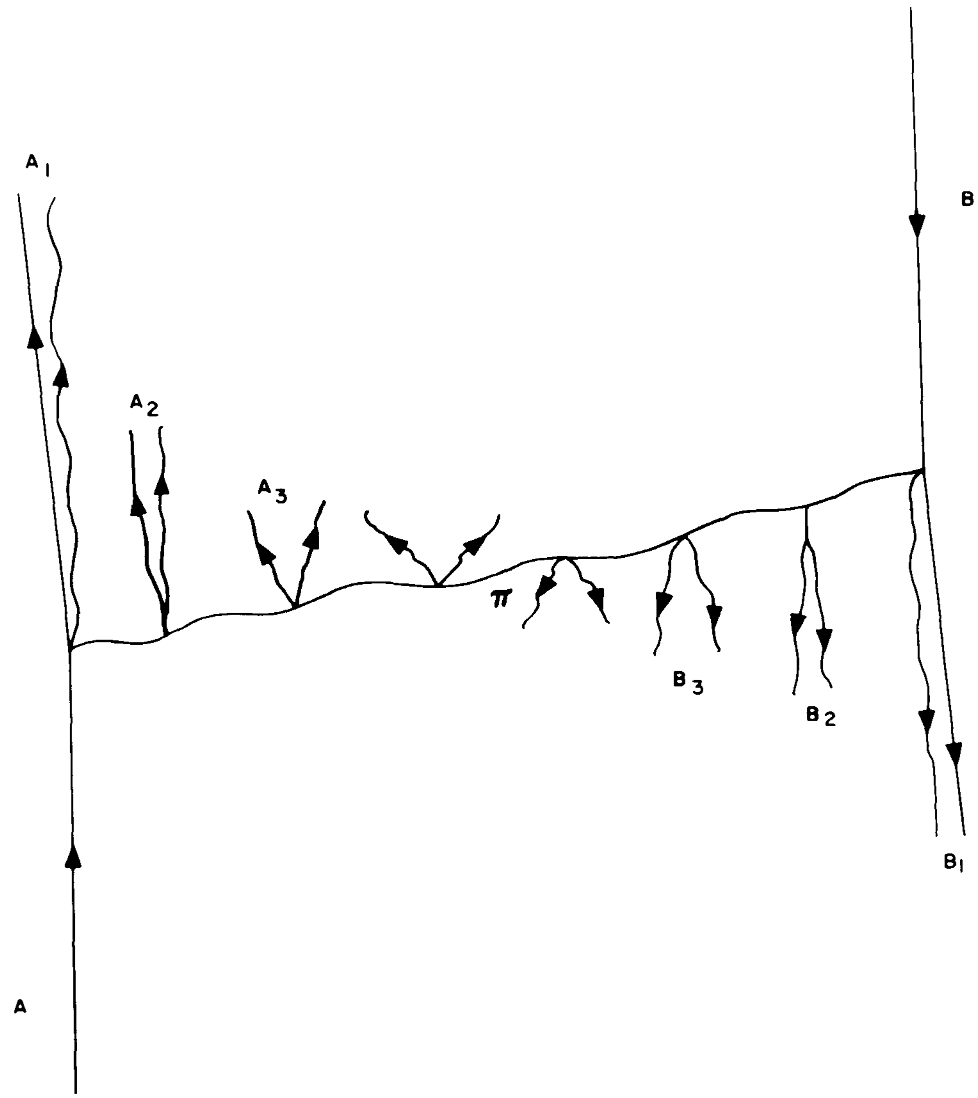

Fig. R1-1. One-pion exchange collision of particle A with particle B .

Although no reliable calculations on the basis of the analytically continued S matrix have yet been completed, we mention here some conjectured qualitative predictions, to illustrate the kind of experiments that may be desirable.

Elastic Scattering

It appears plausible that the combined requirements of unitarity and analyticity, although consistent with a constant limit for total cross sections, may require elastic cross sections to decrease logarithmically at high energy. Specifically, one expects, for large barycentric momentum k ,

$$\frac{1}{k^2} \frac{d\sigma_{el}}{d\Omega} = F(t)\, s^{2\left[\alpha(t) - 1\right]} , \qquad (1)$$

where s is the square of the total barycentric energy* and

$$t = -2k^2 (1 - \cos \Theta)$$

is the negative square of the momentum transfer. If the total cross section is constant, the optical theorem tells us, that we have $\alpha(0) = 1$,

* For nucleon-nucleon scattering, $s - 4M^2 = 4k^2 = 2M\,T_{lab}$. More generally, for $k >> M$, $4k^2 \approx s \approx 2\,ME_{lab}$.

but an analysis of Fig. R1-1 suggests that $\alpha(t)$ may be a slowly increasing function in the neighborhood of $t = 0$, i.e.,

$$2\left[\alpha(t) - 1\right] \approx \epsilon t, \qquad \text{for } \epsilon \geqslant 0 , \qquad (2)$$

for $-16m_\pi^2 \lessapprox t < 0$. The limitation on the range of t is basic, but we are including the bulk of the forward diffraction scattering. Substituting Eq. (2) into Eq. (1), we find

$$\frac{1}{k^2}\frac{d\sigma_{el}}{d\Omega} = \frac{1}{\pi}\frac{d\sigma_{el}}{dt} \approx F(t)\, e^{\epsilon t \ln s} , \qquad (3)$$

so that the width of the diffraction peak shrinks logarithmically with increasing s for $\epsilon \neq 0$, as does the overall elastic cross section. When the ratio of $\frac{d\sigma_{el}}{dt}$ is taken at two different values of s but at the same value of t, we find

$$\frac{\left(\frac{d\sigma_{el}}{dt}\right)_{s_1}}{\left(\frac{d\sigma_{el}}{dt}\right)_{s_2}} \approx \left(\frac{s_1}{s_2}\right)^{\epsilon t} , \qquad (4)$$

a formula that clearly shows the utility of an increase in lab energy by a factor of 10 in establishing the magnitude of ϵ when the latter is small.

Existing evidence from CERN (Cocconi et al.) indicates $\epsilon \lessapprox 1/50m_\pi^2$, a circumstance that is not surprising from a theoretical standpoint. As an illustration of the experimental problem, suppose that we have $\epsilon = 1/100\, m_\pi^2$, and we take $t = -10\, m_\pi^2$; then the elastic cross section varies as $(s_1/s_2)^{.1}$ and should change by a factor of approximately 1.3 in going from 30 to 300 Gev. It should be realized, of course, that $t = -10\, m_\pi^2$ means a momentum transfer of only approximately 1/2 Gev/c and thus a lab angle at 300 Gev of approximately 1/600 radian. Large angles will be interesting too, but not in connection with peripheral collisions.

Multiplicity

The implications of Fig. R1-1 for multiple production are not yet reliably known, but the picture suggests certain qualitative features, if the mass of each clump is on the average small and if the connecting pion line has a low momentum at all intermediate stages:

- Pion production will predominate at all energies and for all combinations of particles A and B .

- The transverse momentum will be of the order of magnitude of that internal to a clump and roughly independent of the total energy.

- The overall multiplicity should increase logarithmically, not as a power, once the average number becomes large.

- The "outside" clumps A_1 and B_1 will carry off a large fraction of the total energy and will maintain the directions of A and B , respectively. If A (or B) is a nucleon, then the clump A_1 (or B_1) must contain a nucleon and generally this nucleon will possess the bulk of the clump energy. There will often be, however, a pion accompanying the nucleon in the resonance state, with a good probability of carrying up to 40% of the clump energy.

Unfortunately, it is not easy to guess the distribution of longitudinal clump momentum, but it is plausible that there is a smooth gradation as one goes from the "outside" in, the clumps A_2, A_3 ... maintaining the direction of A with a diminishing tendency, while B_2, B_3 ... continue in the direction of B .

During the next few years, these guesses will almost certainly be supported and made quantitative by S-matrix theory, or revised and replaced by other predictions. The essential point is that there are a well-defined theory and a reasonably well-defined scheme of approximation to answer questions of this kind.

2. A PRELIMINARY STUDY OF ENRICHED HIGH-ENERGY ANTIPROTON BEAMS*

Gerson Goldhaber† and Sulamith Goldhaber‡

October 14, 1960

The relativistic rise in the energy loss has been successfully employed to sort particles of different masses, by comparing their relative ionization in low pressure argon-helium mixtures.[1] For the same momentum, pions have a larger energy loss, i.e., higher ionization than protons, which makes the discrimination between the two particles possible. The rise in the energy loss is mainly due to the additional interactions of the relativistically transformed electric field of the incident particle with distant atoms. The higher the $\beta\gamma$ of a particle, the more contributions to the energy loss come from distant interactions. In dense materials the electric field of the particle traversing the medium is shielded, and its longer-range interactions are therefore reduced. This effect, referred to as density effect, was first investigated by Fermi.[2] The density effect increases with increasing $\beta\gamma$ and suppresses the relativistic rise in the energy loss leading to a plateau in the dE/dx curve.

It has occurred to us that the difference in the total energy loss between pions and protons due to the relativistic rise can be utilized to obtain enriched antiproton beams for momenta of about 3 Gev/c up to about 10 Gev/c. If one passes a momentum selected beam of pions and protons through an absorber, the pions $(\beta_\pi\gamma_\pi \approx 7\beta_p\gamma_p)$ having lost more energy, will emerge with a lower momentum than the protons. The momenta distributions of the emerging particles will follow the Landau-Symon distributions, since the fractional energy losses are small for a reasonable absorber thickness. It should be noted, that the long asymmetric tail of the pions, arising from the statistical fluctuation in the energy loss, is towards low energies and does not overlap the proton distribution. This is an advantage of the present method over the absorber technique that has been employed for low-energy beams.[3,4] A further advantage is the fact that nearly the entire momentum spectrum of the μ mesons from $\pi-\mu$ decays falls below the initial pion momentum. The majority of the μ mesons will thus be bent away from the antiprotons in the final momentum analysis. Similarly, the electron component of the beam will be degraded to such an extent by the absorber that it will be completely swept out by the subsequent momentum analysis.

The principal elements for obtaining an enriched antiproton beam can be summarized by the following:

a. a magnet system of high dispersion leading to a focussed beam

b. a suitable absorber placed at the first focus. Pions will have lost more energy than protons and will emerge with lower momentum.

c. a second magnet which cancels the dispersion in the first system and thus gives two spatially separated foci for antiprotons and pions.

With such a system it may be possible to accept a momentum bite of $\Delta P/P \approx 1\%$. The problems to be solved are thus the choice of a suitable absorber and beam optics to satisfy the conditions of large dispersion and small image size.

---

* Reprinted with permission from Scientific Information Service at CERN.

† Ford Foundation Fellow at CERN, on sabbatical leave from the Physics Department, University of California, Berkeley, California.

‡ Ford Foundation Fellow at CERN, on leave from the Lawrence Radiation Laboratory, University of California, Berkeley, California.

The Absorber

To obtain the maximum difference in energy loss between pions and protons, absorbers of high Z and low density are best suited. A high-Z gas, such as xenon, at relatively low pressure would meet such a requirement. On the other hand, to minimize image broadening by multiple scattering, the absorber should be of low Z and concentrated at the focus which gives the requirement of low Z and high density. A compromise is obviously needed! We have investigated a number of substances trying to optimize the conditions of multiple scattering and density effect (see Table R2-I).

The separation of protons from pions is governed by their respective momentum distributions after having traversed x g/cm^2 of material. To obtain these distributions we evaluated the probable energy loss from

$$E_{prob} = \frac{2Cm_e c^2 x}{\beta^2}\left\{ \ln\left[\frac{4Cm_e^2 c^4}{1-\beta^2}\cdot\frac{x}{I^2(Z)}\right] - \beta^2 + j - \delta \right\}, \tag{1}$$

where C is considered the total "area" covered by the electrons contained in one gram;

$$C = \pi N \frac{Z}{A} r_e^2 \quad (r_e \text{ - radius of electron}),$$

$$= 0.15 \frac{Z}{A}\ \mathrm{cm}^2/\mathrm{g},$$

m_e = mass of electron,

I = 13 Z electron volts,

j is a parameter introduced by Symon[5] and expresses the extent to which the absorber deviated from a "very thin" one (Landau distribution),

δ is the Fermi density correction (evaluated according to Sternheimer[6]).

Equation (1) can be re-written in a more convenient form, separating the terms according to their physical significance:

$$E_{prob} = \frac{2Cm_e c^2 x}{\beta^2}\left[\ln \frac{2m_e c^2}{I^2(Z)} + \ln\frac{2Cm_e c^2 x}{\beta^2} + 2\ln\beta\gamma - \beta^2 + j - \delta \right]. \tag{2}$$

Since in the present separation scheme one deals with momenta rather than with energies, the relevant quantity is the probable momentum loss $P_{prob} = E_{prob}/\beta$. As can be seen from Eq. (2) the relativistic rise in the energy loss is governed by the $2\ln\beta\gamma$ term which is suppressed by δ, the density effect. The actual distributions of the momenta for pions and protons were next obtained by using the method outlined by Symon.[5]

Table R2-I illustrates the properties of a number of absorbers. Column 7 gives $\Delta P(\pi, \bar{p})$, the difference in the probable momentum loss of pions and protons. Column 8 lists that difference expressed as a percentage of the incident momentum. Values of the angular multiple scattering and values of $\langle y \rangle_{rms}$ which contribute to the fuzziness of the image are given in Column 9 and 10, respectively. Column 11 gives the absorber thickness expressed in terms of geometric mean free paths, x/λ_{geom}.

As can be seen from Table R2-I, high-pressure Xe is probably the best choice of absorber. Among the solids we find Cs, the highest-Z alkali metal, to give the largest difference in the probable momentum loss. This table is by no means exhaustive as far as optimizing the conditions of density effect and multiple scattering on one hand and cost and safety of handling on the other hand is concerned.

In Fig. R2-1 we present the density effect term, δ, as computed from data given by Sternheimer. The values for Xe and Pb were computed directly from Sternheimer's equations. The values for Cs were computed from Sn and Xe values taking proper account of the different electron densities. The two computations gave slightly different values for Cs and a mean of the two computations was used.

The present proposal hinges quite critically on $\delta_\pi - \delta_{\bar{p}}$ for any given momentum. A number of measurements of restricted ionization loss in

Table R2-I

Properties of Various Substances Suitable as Absorbers

(1) Substance	(2) Thickness (g/cm^2)	(3) Z	(4) A	(5) ρ (g/cm^3)	(6) Incident Momentum P_{inc} (Gev/c)	(7) $\Delta P(\pi, \bar{p})$ (Mev/c)	(8) $\frac{\Delta P(\pi, \bar{p})}{P_{inc}}$ (%)	(9) $\langle \theta \rangle$ rms (mrad)	(10) $\langle y \rangle$ rms (cm)	(11) x/λ_{geom}
Xe gas ($\approx$ 86 Atm)	100	54	130	0.50	6	18.0	0.30	8.7	1.00	0.75
Xe gas ($\approx$ 172.4 Atm)	100	54	130	1.00	6	16.3	0.27	8.7	0.50	0.75
Cs Metal	100	55	133	1.87	6	14.4	0.24	8.8	0.27	0.74
Cs Metal	150	55	133	1.87	6	23.0	0.38	10.8	0.50	1.11
NaI melted salt	100	11;53	23;127	3.67	6	11.3	0.19	5.9	0.09	0.99
NaI melted salt	150	11;53	23;127	3.67	6	19.0	0.32	7.4	0.18	1.49
Pb Metal	100	82	207	11.30	6	10.7	0.18	10.4	0.10	0.64
Pb Metal	150	82	207	11.30	6	17.8	0.30	12.7	0.19	0.94
Cs Metal	150	55	133	1.87	10	19.6	0.20	6.5	0.30	1.11
Cs Metal	150	55	133	1.87	4	18.9	0.47	16.2	0.75	1.11
Cs Metal	150	55	133	1.87	3	14.6	0.49	21.6	1.00	1.11

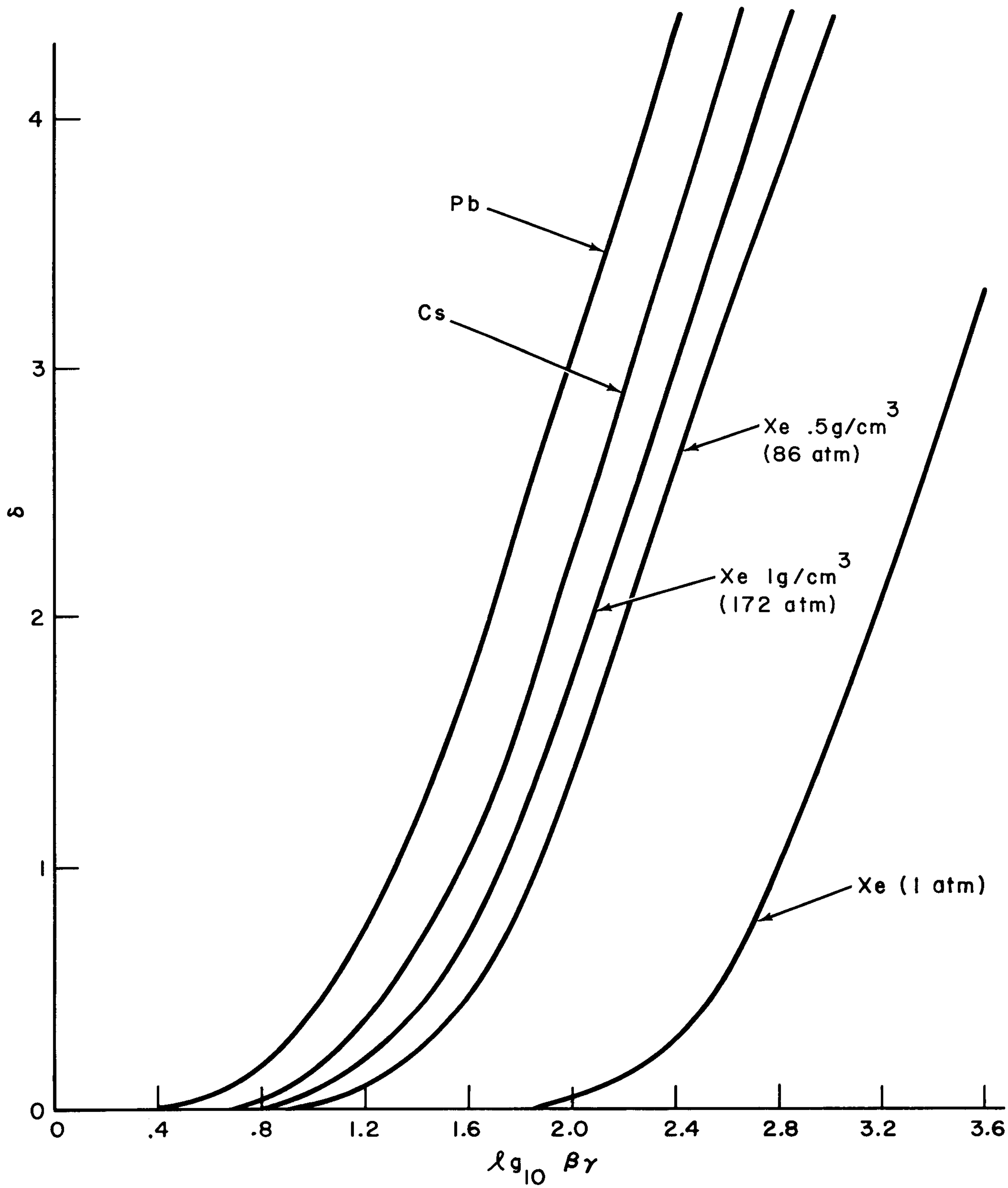

Fig. R2-1. Fermi density effect (according to Sternheimer). I = 13 Z ev .

dense materials such as emulsions[7] and bubble chambers[8] have been made. These measurements are in rough agreement with the computations, which makes the outlined separation scheme look promising. However, accurate measurements in the $\beta\gamma$ region of interest checking the theoretical predictions in detail are not available as yet.

In Fig. R2-2 we show the difference between the two most probable momenta $\Delta P(\pi, \bar{p})$ after traversing the absorber, as a function of the incident momentum. These values were computed for Cs of 100 g/cm^2 and 150 g/cm^2 respectively. In Fig. R2-3 $\Delta P(\pi, \bar{p})/P_{inc}$ is shown as a function of incident momentum. The momentum distributions of pions and antiprotons after traversing a Cs absorber of 100 g/cm^2 and 150 g/cm^2 are shown in Figs. R2-4 and -5. The figures were computed for an incident momentum of P_{inc} = 6 Gev/c. The curves are drawn for equal initial intensities of pions and antiprotons and are not corrected for (a) initial $\bar{p}/\pi$ ratio, (b) differences in the interaction cross sections of pions and antiprotons in the absorber, (c) multiple scattering effects in the absorber, and (d) finite image sizes. These effects will be discussed individually below.

Correction Effects

Initial $\bar{p}/\pi$ Ratio

Measurements at CERN indicate that the $\bar{p}/\pi^-$ ratio is of the order of 1% for the momentum region under consideration here.

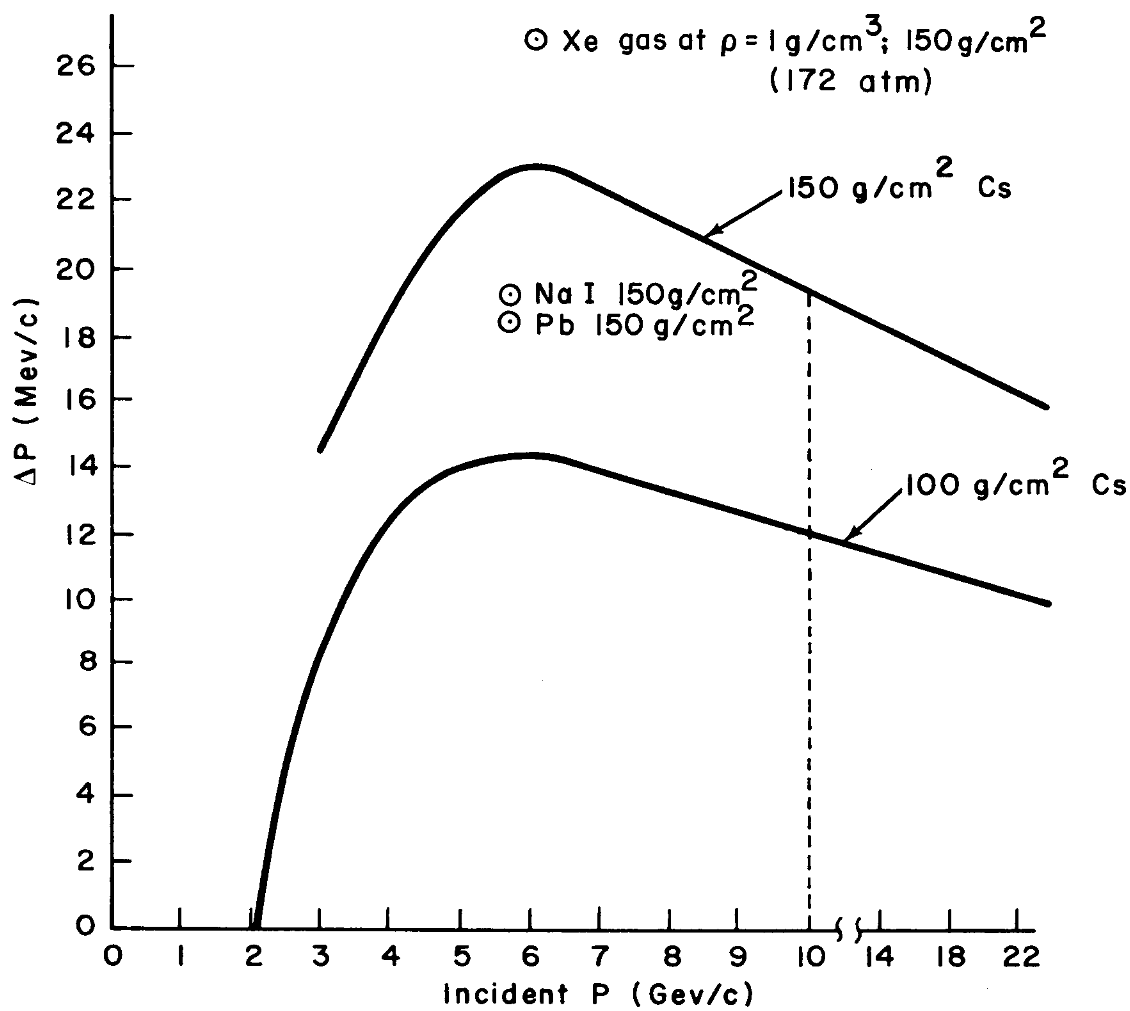

Fig. R2-2. Difference in probable momentum loss for pions and protons. I = 13 × Z .

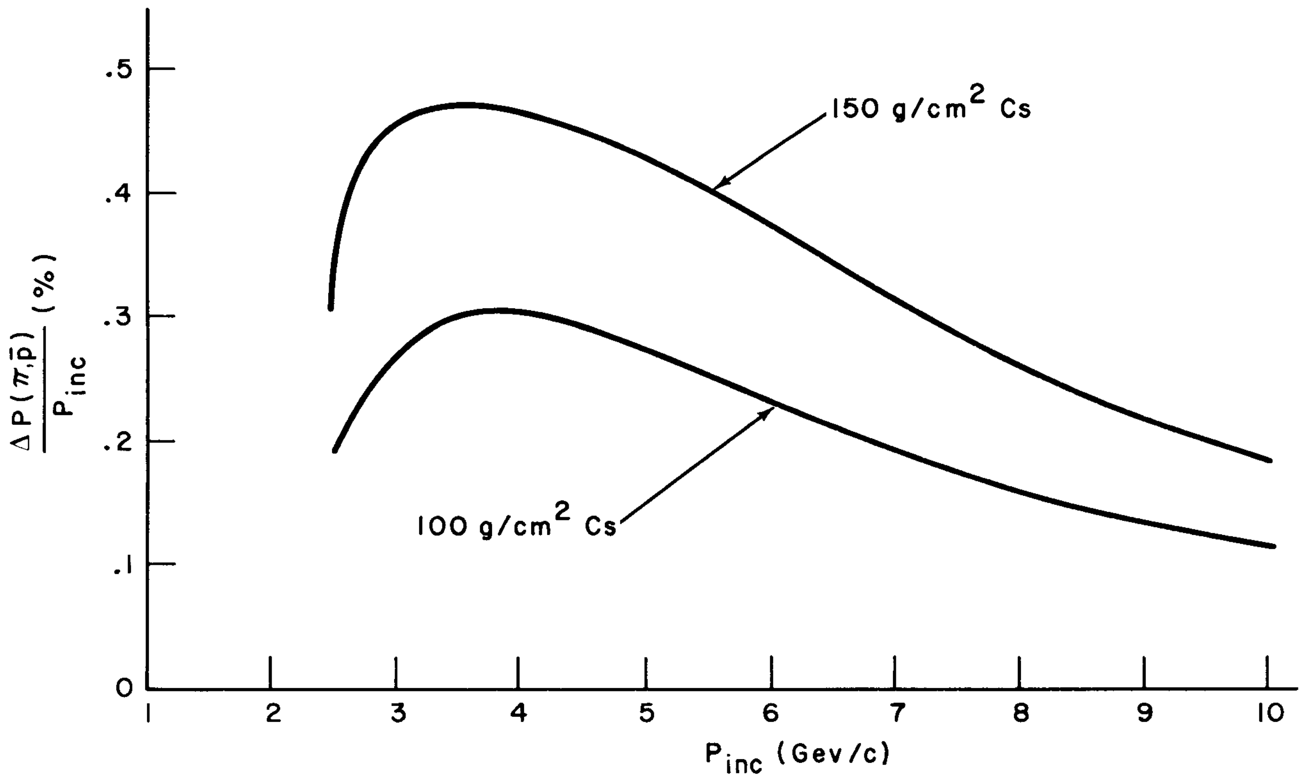

Fig. R2-3.

Interaction Cross Sections of $\bar{p}$ and π^-

An important consideration in the present scheme is the difference in the attenuation of the pion and antiproton beam by the absorber. The cross sections to be considered here are the total cross sections down to a scattering angle Θ_0, where Θ_0 is the aperture of the quadrupole lens following the absorber. The initial $\bar{p}/\pi$ ratio is thus changed by a factor

$$\exp\left[-x\left(\lambda_\pi - \lambda_{\bar{p}}\right)/\lambda_\pi\lambda_{\bar{p}}\right] ,$$

where λ_π and $\lambda_{\bar{p}}$ are the appropriate mean free paths for pions and antiprotons respectively.

Multiple Scattering

The effect of multiple scattering in the absorber is twofold:

a. The image broadening, given by

$$\langle y \rangle_{rms} = \frac{15}{p\beta}\,\frac{1}{\sqrt{3}}\,\sqrt{\frac{x}{x_0}}\;\frac{x}{\rho} ,$$

where x_0 is the radiation length of the material in g/cm^2. The computed values are listed in Table I, Column 10. If the center of the absorber is placed at the first focus, the effective image broadening gets reduced to $1/2\,\langle y \rangle_{rms}$. The image broadening limits the length of absorbers that can be used and renders long (> 2 meters) columns of relatively low-pressure gas impractical.

b. The beam loss by multiple scattering. All particles scattered by angles $> \Theta_0$ will miss the aperture of the quadrupole lens following the absorber and will contribute to the beam loss. The loss factor is

$$\left(1 - e^{-\Theta_0^2/\langle\Theta\rangle^2}\right).$$

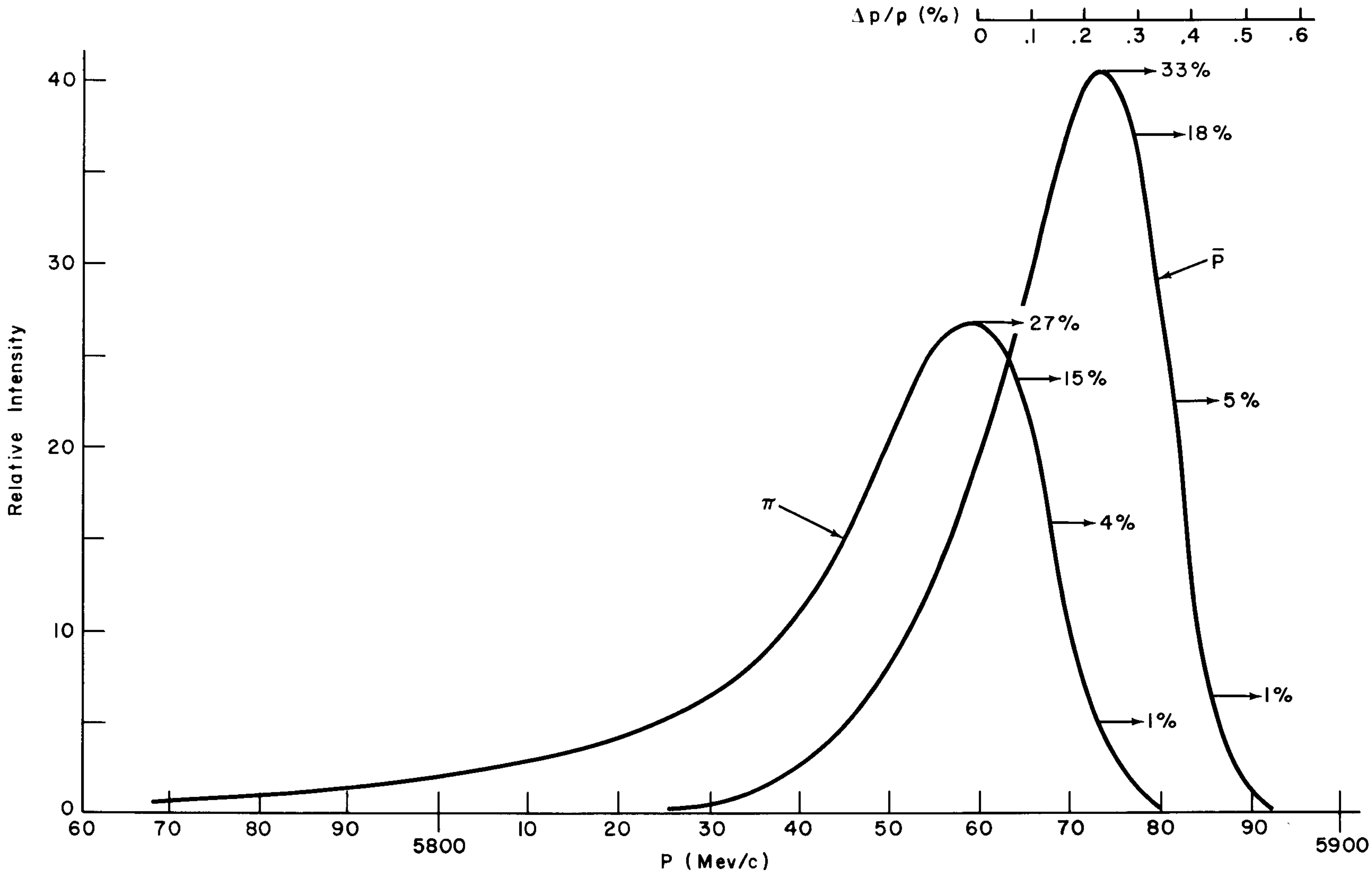

Fig. R2-4. Momentum distribution of π's and $\bar{p}$'s of 6 Gev/c initial momentum after traversing 100 g/cm^2 of Cs.

Multiple scattering introduces a small change in the original $\bar{p}/\pi$ ratio due to the differences in $\beta_{\bar{p}}$ and β_{π}. This change is, however, negligible.

Image Size

To compute the effect of the image size (including lens aberrations) and multiple scattering ($\langle y \rangle_{rms}$) on the final separation, it is best to express these quantities in terms of magnet dispersion. The image "spot" distribution and the Gaussian corresponding to the multiple scattering, $\Phi(y)$, can then be folded into the pion and proton momentum distribution. In Figs. R2-4 and -5 we have considered as an example a magnet dispersion of 0. 1% per cm. The $\Delta p/p$ scale shown in the figures can now be used as a "cm" scale which permits the folding of the above mentioned quantities.

Antiproton Transmission

Before final beam designs are complete, only crude estimates of the transmission of the separation system for antiprotons can be made.

The antiproton transmission $T_{\bar{p}}$ can be expressed by

$$T_{\bar{p}} = \left[1-e^{-\Theta_0^2/\langle\Theta\rangle^2} \right] \cdot e^{-x/\lambda_{\bar{p}}} \cdot q_{\bar{p}} \; .$$

The first two factors which are the loss due to multiple scattering and nuclear interaction, respectively, have been defined above. The factor $q_{\bar{p}}$ depends on the final choice of operating conditions. It represents the fraction of antiprotons which is permitted to pass the final collimator. Since the pion intensity drops rapidly as one moves towards the high-momentum edge of the antiproton distribution, reasonable operating conditions may be those at which the antiproton intensity is at 5% to 10% level (i. e., $q_{\bar{p}}$ = 0. 05 to 0. 1). Table R2-II lists optimistic and pessimistic values for the various parameters and gives the resulting transmission.

Estimates on the $\bar{p}/\pi$ Ratio

The final $\bar{p}/\pi$ ratio can be expressed by

$$\bar{p}/\pi = R$$

$$= R_0 T_{\bar{p}}/T_{\pi}$$

$$= R_0 \exp\left(-x \frac{\lambda_{\pi} - \lambda_{\bar{p}}}{\lambda_{\pi}\lambda_{\bar{p}}}\right) q_{\bar{p}}/q_{\pi} \quad ,$$

where R_0 is the initial $\bar{p}/\pi$ ratio, i. e., $R_0 \approx 0.01$. In what follows we make a crude estimate for R which will have to be modified when final beam designs and cross sections become available.

Assuming for the mean free paths $\lambda_{\pi} \approx 1.5\ \lambda_{\bar{p}}$ and $\lambda_{\bar{p}} \approx 1/3\,\lambda_{geom}$ we obtain

Table R2-II.

Transmission estimates for 150 g/cm^2 of Cs and P_{inc} = 6 Gev/c

Estimate	Quadrupole aperture Θ_0 mrad	Antiproton m.f.p. for $\sigma_{tot}(\Theta_0)$ $\lambda_{\bar{p}}$	Antiproton "acceptance level" $q_{\bar{p}}$	Transmission $T_{\bar{p}}$
"Optimistic"	10	$1/2\,\lambda_{geom}$	0. 10	6×10^{-3}
"Pessimistic"	5	$1/3\,\lambda_{geom}$	0. 05	0.3×10^{-3}

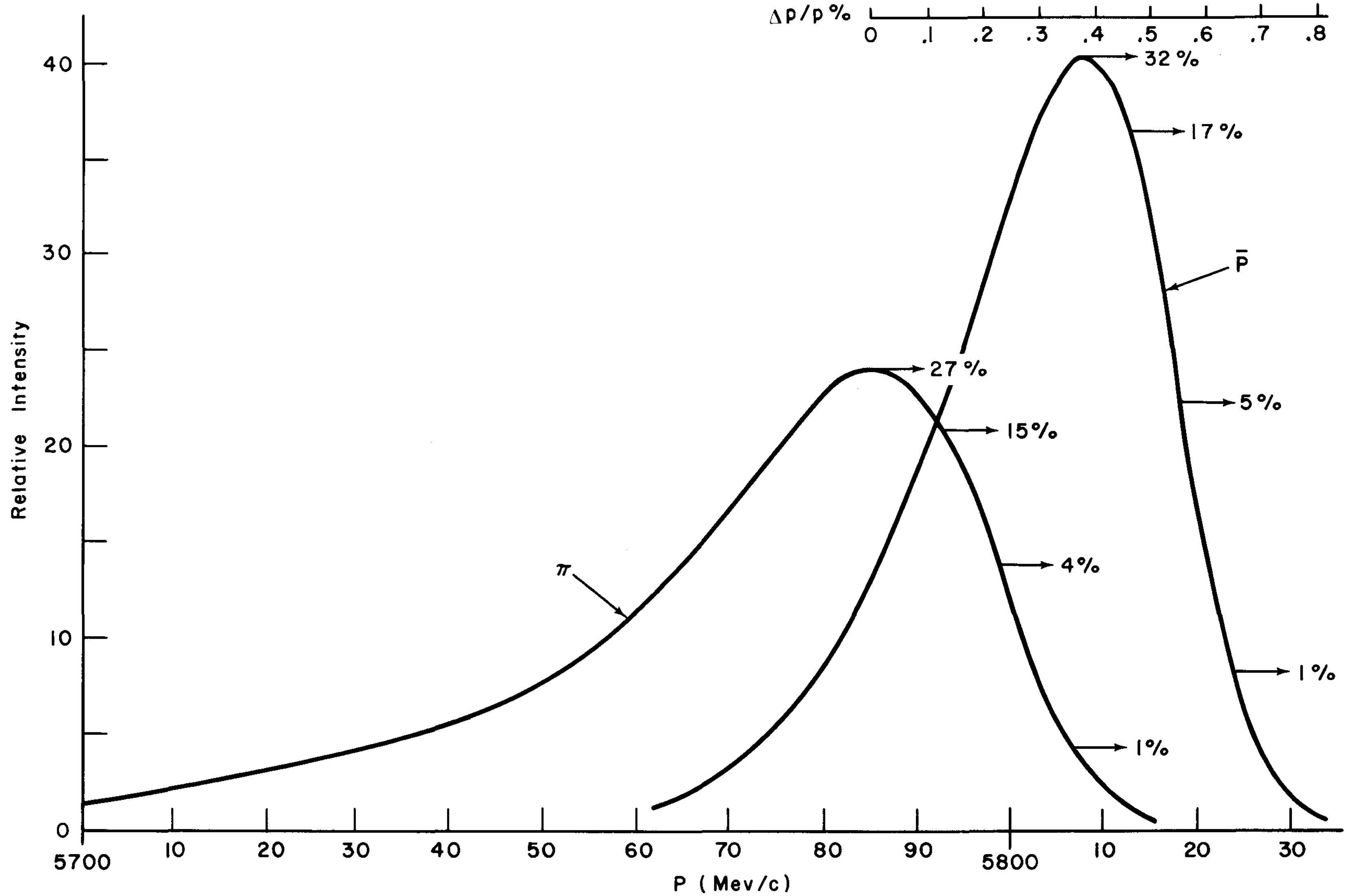

Fig. R2-5. Momentum distribution of π's and $\bar{p}$'s of 6 Gev/c initial momentum after traversing 150 g/cm^2 of Cs.

$$\exp\left(-x\,\frac{\lambda_{\pi}-\lambda_{\bar{p}}}{\lambda_{\pi}\lambda_{\bar{p}}}\right)\approx e^{-1}$$

for $x = 150\ g/cm^2$ of Cs. In order to evaluate the effect of the image size and multiple scattering on the momenta distributions shown in Figs. R2-4 and -5, we have numerically folded the former into the curves given (folded curves not shown in figures). An image size of 2 cm width at the first focus was assumed here. Under these conditions we find for $q_{\bar{p}}/q_{\pi} \approx 500$ to 2000, for $q_{\bar{p}} = 0.1$ and 0.05, respectively. We thus obtain for the estimated $\bar{p}/\pi$ ratio, $\bar{p}/\pi \approx 1.5{:}1$ and 8:1, respectively. More accurate calculations in co-operation with Dr. Montanet are now in progress.

It should be noted that the ratios quoted are still somewhat "idealized" since they

a. refer to the image at the first focus and therefore do not include aberrations in the second magnet system,

b. make no allowance for possible stray pions and muons scattered into the beam.

The Beam Optics

There is as yet no final beam design completed, although preliminary calculations by Mr. S. van der Meer indicate the feasibility of the requirements on the beam outlined here. The beam optics should be of comparable quality to that outlined by Mr. van der Meer for the case using electrostatic separators.[9]

Separated π^+ Beams

It is interesting to note that the proposed separation scheme can also be used as a means of separating π^+ mesons from protons in the momentum region of 2.5 to 10 Gev/c. Here one can utilize the long low-energy tail of the Landau-Symon distribution of the pions which extends much further than that of the protons to produce an effective separation scheme (see Figs. R2-4 and -5). In such a scheme the differences in probable energy loss between pions and protons become less important and simple absorbers such as $100\ g/cm^2$ Pb should be adequate. We estimate that the μ^+ contamination of a 3 Gev/c π^+ beam should be less than 10%.

Acknowledgement

We would like to take this opportunity to thank Mr.. S. van der Meer and Mr. B. de Raad for a number of helpful discussions. We also would like to express our appreciation for the hospitality offered to us at CERN.

References

1. See, for example, Hanson and Fretter, Phys. Rev. 118, 812 (1960)

2. E. Fermi, Phys. Rev. 56, 1242 (1939); 57, 485 (1940)

3. Chamberlain, Goldhaber, Jauneau, Kalogoropoulos, Segrè and Silberberg, Phys. Rev. 113, 1615 (1959)

4. Agnew, Elioff, Fowler, Lander, Powell, Segrè, Steiner, White, Wiegand and Ypsilantis, Phys. Rev. 118, 1371 (1960)

5. K. Symon, Thesis, Harvard (1948), available as a microfilm. Also described by B. Rossi - High Energy Particles (Prentice-Hall Inc., 1952), p. 32.

6. R. Sternheimer, Phys. Rev. 88, 851 (1952); 91, 256 (1953); 103, 511 (1956). The first two papers describe the calculations, but use an old value for I (I = 9.4 Z). The last one gives the relevant constants with the new value I = 13 Z which was used here.

7. See, for example, B. Jongejans, Nuovo Cimento 16, 625 (1960)

8. For example, B. Hahn and F. Hugentobler (preprint), to be published in Nuovo Cimento.

9. S. van der Meer, CERN 60-22 PS Division, 1st June 1960 (unpublished).

3. SOME THOUGHTS ON BEAM INTENSITY IN A 300-Gev SYNCHROTRON

Kjell Johnsen

August 7, 1961

I. Introduction

Essentially, two different injection methods have been proposed for a high-energy synchrotron. The two methods are (a) injection from a linac directly into the big machine, and (b) use of a booster synchrotron between the linac and the big synchrotron to inject a number of pulses given by the ratio of the radii of the two synchrotrons.

For method (a), a linac of several Gev is required. For method (b), the linac energy can be lower than for method (a) by more than an order of magnitude, but the booster must be a high-repetition-rate synchrotron.

Intensity will be governed by such things as the maximum current that can be obtained from a linac, space-charge limits of various parts of the system, and obtainable repetition rate. The gain one can hope for by multiturn injection must also be looked into.

It has been suggested that, if one made a 300-Gev synchrotron, it could be run at, let us say, 30 Gev with 10 times as high a repetition rate, thus gaining an order of magnitude in intensity at this low energy. If a booster is used for injection, it probably will be run at the maximum feasible repetition rate already under normal operation (approximately 25 pulses per sec), and, therefore, one can gain very little in intensity by reducing the energy of the big machine and increasing its repetition rate. It looks as though the maximum gain would be a factor of 3 in this case, assuming that normal operation is 1 sec increasing field, 1 sec decreasing field, and 1 sec filling time.

If one wants to use this method of increasing the intensity, it appears that one must use a linac for injection. This would mean that the linac would have to be made with a repetition rate of about 10 pulses per sec.

However, if the linac can be made with a high repetition rate one immediately asks the question whether or not one could take advantage of this to bring the full intensity thus gained up to full energy, not by higher repetition rate of the big machine, but by the stacking of 20 to 50 pulses before acceleration. It is the main purpose of this report to consider the feasibility of such a scheme and some of the restrictions this would impose on machine parameters.

In Table R3-I are listed the main machine parameters that I have used to obtain numerical results, and also the source of these parameters.

Some comparison with other injection schemes is made, but main consideration is given to intensity — in the end, other factors may be decisive in the choice of type of injector.

It is not unlikely that most of the intensity considerations in this report will be, in the end, irrelevant, as it may prove fairly easy to reach high enough intensities that contamination and other difficulties connected with the handling of the final beam will be the outstanding technical problems. What intensity limits such problems may impose will not be discussed in this report.

II. Stacking in the Synchrotron

The principle of the scheme we discuss is as follows: The synchrotron has a constant magnetic field for the whole injection period, which may be as long as 1 sec. A linac pulse is inflected into the synchrotron by a fast inflector that should be placed near the wall of the vacuum chamber and should occupy a small fraction of

Table R3-I

Machine parameters used in the report

A. 300-Gev synchrotron (mainly from Ref. 1):	
Mean radius R	1250 m
Radius of curvature r	824 m
Aperture	3.5 cm × 7 cm
No. of magnet periods	275
Betatron frequency Q	40.25
μ	0.92
Form factor F	≈1.57
dB/dt	15 kG/sec
Θ_s	60°
Acceleration time	1 sec
Repetition period	2 to 3 sec
Rotation time at velocity of light	26.2 μsec
B. 3-Gev linac (mainly from Refs. 2 and 3):	
Energy gradient of first part of linac	2 Mev/m
Energy gradient of latter part of linac	10 Mev/m
Θ_s	30°
Frequency in first part of linac	200 MHz
Frequency in latter part of linac	1000 MHz
Momentum spread $\Delta p/p$ at 2 Gev	$\pm 1 \times 10^{-3}$
Phase spread at 2 Gev	±3°
Emittance area at 50 Mev	$\pi \times 10^{-5}$ rad. m
γ at 3 Gev	4.2
β at 3 Gev	0.972

Table R3-I (Continued)

C. 10-Gev booster synchrotron (mainly from Ref. 4):

Mean radius R	50 m
Radius of curvature r	33 m
Aperture	5 cm × 12 cm
No. of magnet periods	35
Betatron frequency Q	5.25
μ	0.943
Form factor F	≈1.59
Injection energy	150 Mev
γ inj.	1.16
β inj.	0.508

the available aperture. The injected beam, which is coasting near the wall, should be picked up by an rf system and moved a little past the middle of the chamber, where it is released again. By this time, the system is ready to take another pulse from the linac. This pulse is also picked up by the rf and released in the same place as the first pulse, which, by the effect of the rf system bringing the second pulse, is moved slightly towards the inflector again. This process can continue until one has stacked a large enough number of pulses that the available space for the stack is occupied. This is not mainly determined by aperture requirements, but more by the momentum spread that can be handled by the accelerating system, as the whole stack has to be picked up and accelerated in the normal way after the desired number of linac pulses has been accumulated.

We assume that a separate rf system is used in the big ring to pick up and stack the bunches from the linac. To do this in the most efficient way with regard to dilution of phase space, this rf system should run at the same frequency as the initial part of the linac.

The following approximate expression for the momentum width of an rf bucket is valid for $\beta \approx 1$ and $\gamma << \gamma_{tr}$:

$$\frac{\Delta p}{p} \approx \pm 2 \sqrt{\frac{\gamma\, e\, U_a\, (\tan \Theta_s - \Theta_s)}{m_0 c^2 \; 2\pi\, M}} \quad . \tag{1}$$

In this formula eU_a is the energy gain per revolution, Θ_s is the phase stationary angle measured from the peak of the wave, and M is the ratio between the radio frequency and the rotation frequency.

It can be shown that the area of the bucket in p, Θ space is approximately

$$A_B \approx (\pi + k - 2)\, \Theta_s\, \Delta p \quad , \tag{2}$$

where $k\Theta_s$ is equal to the total phase width of the bucket; k is close to 3 for $\Theta_s < \pi/3$ but rises rather sharply after that to the value $k = 4$ at $\Theta_s = \pi/2$.

The theoretical stack width, Δp_s , we define by

$$2\pi\ \Delta p_s = N_s A_B \ ,$$

which gives

$$\Delta p_s \approx N_s \frac{\pi + k - 2}{2\pi} \Theta_s \Delta p \ , \qquad (3)$$

where N_s is the number of stacked pulses. From Eq. (1) the theoretical stack width can be written

$$\frac{\Delta p_s}{p} = N_s \frac{\pi + k - 2}{\pi} \sqrt{\gamma \frac{e U_a \Theta_s^2 (\tan \Theta_s - \Theta_s)}{2\pi M}} \ . \qquad (4)$$

We define stacking efficiency as the ratio of particles inside the theoretical stack width to the total number of particles contained in the stacked buckets. Computational results from CERN indicate that high stacking efficiency can be obtained with $N_s \gtrapprox 10$ and $\Theta_s \gtrapprox \pi/3$. (These computational results will be reported by Don Swenson from MURA at the Brookhaven Conference in September.) We can therefore consider the theoretical stack width as the practical stack width with a small fraction of the particles outside this width.

From Eq. (4) it is seen that one wants a small U_a , a small Θ_s , and a large M to get the maximum number of pulses into a given stack width. U_a is limited by the longest time one can permit for passing through the stack. With regard to Θ_s , the CERN computations were made only for $\Theta_s \gtrapprox \pi/3$, but they indicated a rapid deterioration of the stacking efficiency with decreasing Θ_s . Until further computational results are available, we limit ourselves to $\Theta_s = \pi/3$ when going through the stack. As already mentioned, the stacking frequency is given by the frequency of the first part of the linac, and M is therefore fixed by this choice. (However, if it should prove desirable, one could depart from this choice and stack with a harmonic of this frequency, let us say the same frequency as the latter part of the linac.)

Let us consider some practical figures for a possible stacking system: We assume that we would not like the stack to be wider than 1 cm, and that it is therefore only over 1 cm that the motion has to be slow, whereas it can be fast before that. We further assume, conservatively, that, all together, we have to move the beam 6 cm. We would like to do the whole process in, let us say 20 msec, of which we spend half on the first 5 cm and the other half on the last 1 cm. There must be an adiabatic transition between the two.

A. Moving the Beam the Last 1 cm

To move the beam 1 cm at an injection field corresponding to 3 Gev, it must be given an energy gain or loss of $\Delta E = 50$ Mev . (In calculating this, the parameters listed in Table R3-I have been used.) To do this in 10 msec, the energy gain per revolution is $eU_a = 136$ kev. As already stated, $\Theta_s \approx \pi/3$ is a reasonable choice. This gives $k \approx 3$, and the required rf voltage would be $U_m = 272$ kv.

The frequency of the first part of the linac is assumed to be 200 MHz, which gives the harmonic number $M = 5400$.

All these data, together with data from Table R3-I inserted into Eq. (1), give for the momentum width of the stacking bucket

$$\frac{\Delta p}{p} = \pm 2.2 \times 10^{-4} \ .$$

The theoretical stack width is [Eq. (3)]

$$\frac{\Delta p_s}{p} = 1.5 \times 10^{-4} N_s \ .$$

Let us assume that we want to stack 30 pulses, which could be done in less than 1 second. The theoretical stack width would then be

$$\frac{\Delta p_s}{p} = 4.6 \times 10^{-3} \ ,$$

and the horizontal space occupied by the theoretical stack width would be

$$\Delta R_s = 3.6 \times 10^{-3} \text{ m} \ .$$

B. Moving the Beam the First 5 cm

Since we want to spend the same time on the first 5 cm as on the last 1 cm, we need 5 times the acceleration, i.e., $eU_a = 680$ kev.

In this process, we are not concerned about stacking efficiency and we could run with a smaller phase-stationary angle, let us say $\pi/4$, which means that the rf voltage would be $U_m =$ 930 kv. The total phase width of this bucket would be nearly $3\pi/4$, and the momentum width is [from Eq. (1)]

$$\frac{\Delta p}{p} = \pm 2.8 \times 10^{-4} \quad .$$

The bunches injected from the linac must be within these limits. We shall return to this problem later.

C. Frequency Modulation

The 200-MHz rf system for the stacking process must be frequency-modulated. The total frequency swing needed is

$$\frac{\Delta f}{f} = \left[\left(\frac{\gamma_{tr}}{\gamma}\right)^2 - 1\right]\frac{\Delta R}{R} \approx 4.3 \times 10^{-3} \quad . \tag{5}$$

The frequency modulation must be 5 times as large during the first 10 msec as during the next 10 msec.

D. Transition between the Fast-Moving and Slow-Moving Region

In order to preserve phase space efficiently, the transition between the two regions should be smooth. This, however, is not very relevant, as the parameters for the stacking buckets are not determined by phase-space considerations, but rather by the time required to stack a sufficient number of pulses. This means that the transition between the regions, as the parameters have come out, need not be really adiabatic.

However, for efficient phase-space preservation, one should make the changeover adiabatically, and, therefore, one is interested in the phase oscillation frequency. This is lowest in the slow-moving bucket, and, thus, we consider only that. With the assumptions $\beta \approx 1$ and $\gamma \ll \gamma_{tr}$, the oscillation frequency is

$$f_\Theta \approx \frac{c}{2\pi R\gamma}\sqrt{\frac{M U_m \sin \Theta_s}{2\pi \gamma m_0 c^2/e}} \approx 2\text{kHz} \; , \tag{6}$$

which shows that it should not be difficult to make an adiabatic change in amplitude by a factor of about 3 and an adiabatic phase shift from $\pi/4$ to $\pi/3$, within, let us say, a few milliseconds, which is short compared with the total transfer time that we have considered.

III. The Main rf System for the Synchrotron

In order to capture the stacked particles efficiently, the total momentum width of the capturing bucket must be appreciably larger than the theoretical stack width—let us say, 4 times as large. This puts important restrictions on the main rf system—especially on its frequency.

The acceleration needed per revolution is

$$U_a = 2\pi R \cdot r\dot{B} \; . \tag{7}$$

This should be inserted into Eq. (1), which should then be compared with Eq. (4) after substituting the stacking parameters listed in Table R3-I. For Θ_s, we take $\pi/3$. This gives

$$eU_a = 9.7 \text{ Mev/rev} \; ,$$

$$U_m = 19.4 \text{ Mv} \; ,$$

$$\frac{\Delta p}{p} \approx \pm 0.138/\sqrt{M} \; .$$

Introducing the condition that the total momentum width of the bucket should be at least 4 times the theoretical stack width for 30 pulses, we get the following restriction on the harmonic number of the main rf system and its frequency:

$$M \leqslant 225 \; , \text{ and}$$

$$f \leqslant 8.6 \text{ MHz} \; .$$

This is a comfortable frequency for standard types of accelerating stations, but it excludes the use of any of the accelerating methods suggested in the frequency range above 100 MHz.

IV. Bunch Size of Injected Beam

It is necessary to consider the bunch size of the linac beam to see if it can be fitted into the buckets of the stacking system. Lloyd Smith has estimated (Ref. 3) the bunch size of a 2-Gev linac, assuming no increase due to irregularities. We scale his estimate to 3 Gev and get

$$\frac{\Delta p}{p} = \pm 9 \times 10^{-4} ,$$

$$\Delta\Theta = \pm 2.4° .$$

The stacking bucket that we considered in Section II.B could take only bunches with momentum width up to $\Delta p/p \approx \pm 2.8 \times 10^{-4}$. Consequently, the bunches arrived at here have too much energy spread by a factor of a little more than 3.

However, the bunches are very narrow in phase, and one can gain considerably by applying a "debunching" device. (One such method has been proposed by Teng in Brookhaven Internal Report LCT-3.) If the debunching device uses the same frequency as the latter part of the linac, one can debunch by a factor of at least 10 without difficulties due to nonlinearities. If one would, in the debunching device. go back to the same frequency as that of the input end of the linac, one could debunch much more.

Conservatively, we assume a debunching factor of 10, which gives, for the final bunch size,

$$\frac{\Delta p}{p} = \pm 0.9 \times 10^{-4} ,$$

$$\Theta = \pm 24° .$$

Remembering that the bunches in the ring will be picked up again by a system with a frequency equal to that of the first part of the linac, we have the phase width of the bunches, with regard to this system,

$$\Delta\Theta \approx \pm 5° .$$

In this way, we have obtained bunches that are considerably smaller than the stacking bucket. One has, in fact, a safety factor of about 3 in momentum spread and nearly 10 in phase spread. However, these safety factors will certainly be needed, as it will be very difficult to keep the linac parameters to sufficiently close tolerances to keep the increase factor smaller than this safety factor.

The bunch shape, as calculated above, does not quite match the stacking bucket. However, the mismatch is not bad, and there is very little point in trying to do better until more is known about expected linac performance.

V. Intensity Prospects

It is difficult to see at this stage what, in ten years' time, may limit the current in such a machine. Already, ion sources can give about 100-ma protons. Whether a large linac can handle such high currents reliably is still a somewhat open question.

However, with such high injection currents, space-charge problems start becoming serious even at such high injection energy as 3 Gev. We shall therefore consider this problem first.

The space-charge limit is given by

$$n_{sc} = \frac{8\pi\, m_0 c \beta^2 \gamma^3}{e^2 \sqrt{\mu/\epsilon}\,(b - \nu\gamma^2)} \, A\,\Delta Q , \qquad (8)$$

where n_{sc} is the total number of particles in the ring, A is the admittance—i.e., the area of the acceptance ellipse— ΔQ is the tolerable shift of the betatron oscillation frequency, b is the bunching factor, and ν is the neutralization factor—i.e., the degree to which the time-average electrostatic field is removed.

Two situations have to be considered: that in each individual pulse just after injection, and that a little after the stacking is finished and the main rf system has started rebunching the beam.

A. Space-Charge Limit of Injected Bunches

The bunches are only 10° wide as they enter the synchrotron (see Section IV), and the bunching factor is therefore $b = 36$. We assume that no neutralization has developed, i.e., $\nu = 0$. We further assume that the beam can be permitted to increase in size only to a diameter of 1.5 cm, which gives, for the admittance,

$$A = \pi \frac{Q a^2}{RF}$$

$$= 0.36 \times 10^{-5} \text{ rad m} , \qquad (9)$$

where a is the permissible beam radius and F the form factor.

The permissible ΔQ we take as 0.50. From Eq. (8), we now get

$$n_{sc} = 0.55 \times 10^{13} \text{ particles} .$$

This corresponds to an injection current of 30 ma with single-turn injection, which is certainly obtainable.

One way of increasing this space-charge limit would be to debunch the linac bunches more than assumed in the above calculation. One could thus gain a factor of 5 if the debunching section is run at 200 MHz.

B. Space-Charge Limits after Stacking and Rebunching

After the stacking, the bunches have intermingled and the bunching factor is nearly unity. However, in the rebunching, when acceleration starts, the bunching factor increases again. It is reasonable to assume a bunching factor $b = 4$.

Since we are no longer concerned about the beam's not coming into the fringing field of the inflector, we can tolerate a larger diameter of the beam. We therefore assume the tolerable beam diameter to be 3 cm, i.e., an acceptance four times as large as in the previous example.

If we still assume no neutralization, the space-charge limit of the stacked beam is

$$n_{sc} = 1.6 \times 10^{14} \text{ particles} .$$

If neutralization develops, this figure should be divided by $(1 - \frac{\nu}{b} \gamma^2)$. If we assume full neutralization, the space-charge limit is therefore

$$n_{sc} \approx 5 \times 10^{13} \text{ particles} .$$

This means that one could inject only about 10 space-charge-limited linac pulses to bring the intensity up to the neutralized space-charge limit. To make proper use of the possibilities that such a stacking process offers, one must remove neutralization by clearing fields.

But even with this extra complication, the space charge, and not the obtainable linac current, seems to be what limits the final intensity obtainable by this method, and the limit is about 1.6×10^{14} particles per pulse of the big machine—corresponding to about 0.5×10^{14} particles/sec.

An increase in vertical aperture by 1 cm would increase all these intensity figures by a factor of about 2.

There are still uncertainties about how serious space-charge effects really are, and, if it turns out, as the calculations above indicate, that the final intensity may be ultimately limited by space charge, these problems should be analyzed in more detail, both theoretically and experimentally if possible.

At lower energy, say 30 Gev, the rise time of the synchrotron could be reduced considerably. However, the stacking time stays unchanged. The obtainable mean intensity increase at 30 Gev is therefore greater than the above figures by only a factor of about 3, let us say to 1.5×10^{14} particles/sec.

VI. Comparison With Other Injection Methods

In this section, we briefly consider the intensity one can expect with other injection methods as compared with the method already outlined.

A. Ordinary Single-Turn Injection from a Linac

If we compare this case with the one considered in Section V.A, the main difference is that we can permit the beam to diverge to a larger diameter, owing to the different geometry of the inflector. It is reasonable to assume that the beam can be permitted to have a diameter of 3 cm, which would mean an admittance of

$$A = 1.4 \times 10^{-5} \text{ rad m} \quad ,$$

and the space-charge limit would be (with $b = 36$ as before)

$$n_{sc} = 2.2 \times 10^{13} \text{ particles} \quad ,$$

which, with 2-sec intervals between the pulses, would give an average intensity of about 10^{13} particles per sec up to full energy.

This intensity could, with this method, be reached by an injection current of about 130 ma.

It should be possible to increase the repetition rate of the big machine by a factor of ten (to 5 pulses per sec) by running it at 1/10 of its maximum energy. In this way, one should be able to get 10^{14} particles per sec at 30 Gev, which compares with 1.5×10^{14} particles per sec at 30 Gev or 0.5×10^{14} particles per sec at 300 Gev by the method of intermediate stacking.

B. Multiturn Injection from a Linac

We assume that we carefully inject the bunches between one another on successive turns. This, however, means that the space-charge limit is for each individual turn given by Eq. (8), which we rewrite

$$n_{sc} = C A_{beam} \tag{10}$$

where A_{beam} is the value to which we permit the emittance of each individual bunch to increase. Since there are about 40 betatron wave lengths around the machine, we assume that a possible diameter increase due to space charge has developed after less than one turn. This means that the maximum number of turns that one can hope to inject is A_{vc}/A_{beam}, where A_{vc} is the admittance of the vacuum chamber. If we assume that the efficiency of a multiturn-injection scheme is η, then the intensity one can obtain in this way is from Eq. (10)

$$n = \eta \frac{A_{vc}}{A_{beam}} n_{sc} = \eta C A_{vc} \; . \tag{11}$$

It should be remembered that, in calculating C, one must use the bunching factor of the individual turns, since this is where space charge is critical.

However, Formula (11) is exactly the same as the one we used for estimating the single-turn injection in the previous section with the modification η. This means that all limits are as obtained in that section, reduced by η, concerning which, the hope that it can be larger than 0.5 is very optimistic.

Multiturn injection would therefore be useful only if it is difficult to approach the space-charge limit for single-turn injection. One does not gain anything by the fact that the bunches can be injected between one another. The necessary debunching must be done before the beam enters the synchrotron, even with multiturn injection.

C. Multipulse Injection from a Synchrotron

The Cal-Tech proposal envisages injection into the big ring from a 10-Gev booster synchrotron. Since one injection from the booster would fill only a very small fraction of the big ring, it is planned to run the booster at a high repetition rate and fill the big ring azimuthally by a number of pulses, given by the ratio of the diameters of the two rings. We shall call this method azimuthal stacking. (This should not be confused with the stacking process described earlier in this report, which is based on a quite different principle.)

In the numerical examples, we shall assume booster parameters close to the ones listed in Cal-Tech Report CTSL-10 (Ref. 4), with the exception that we assume the injection into the booster to be at 150 Mev (Table R3-I).

If we assume that the beam diameter in the booster can be permitted to be 4 cm, we find the admittance [Eq. (9)]

$$A = 2.55 \times 10^{-5} \text{ rad m} \quad .$$

In calculating the space-charge limit, we assume a bunching factor of 4, no neutralization, and a permissible Q shift of 0.5. We then get [from Eq. (8)]

$$n_{sc} = 1.7 \times 10^{12} \ .$$

This space-charge limit could be reached by single-turn injection from a linac of 130 ma. Nothing can be gained by multiturn injection (see previous section).

The ratio between the diameters of the two rings is 25, which means that a maximum of 25 space-charge-limited booster pulses can be injected into the big machine. This gives

$$n = 4.2 \times 10^{13} \text{ particles.}$$

As in the case of intermediate stacking, we assume 3 sec between the pulses (which means that the booster must run at 25 pulses per sec) and the booster would therefore offer the possibility of 1.4×10^{13} particles per sec up to full energy. This is less by a factor of 3 to 4 than obtainable with intermediate stacking. No clearing fields would be needed.

VII. Conclusions

The results can be summed up as in the following table:

Intermediate Stacking

Intensity at 300 Gev ($\frac{1}{3}$/sec rep. rate)	0.5×10^{14} pulses/sec
Intensity at 30 Gev (1/sec rep. rate)	1.5×10^{14} pulses/sec
Linac current needed	30 ma
Linac repetition rate	30/sec

Ordinary Linac Injection

Intensity at 300 Gev ($\frac{1}{2}$/sec rep. rate)	10^{13} pulses/sec
Intensity at 30 Gev (5/sec rep. rate)	10^{14} pulses/sec
Linac current needed	130 ma (or very efficient multiturn injection)

Injection from Synchrotron Booster

Intensity at 300 Gev ($\frac{1}{3}$/sec rep. rate)	1.4×10^{13} pulses/sec
Intensity at 30 Gev (1/sec rep. rate)	4×10^{13} pulses/sec
Booster repetition rate	25/sec
Linac current needed	130 ma (or very efficient multiturn injection)

The scheme with linac injection and stacking seems to be the most promising method of obtaining extremely high beam intensities. It has the further advantage of requiring a rather modest current from the linac. The method does impose other severe requirements on the performance of the linac, however, especially with respect to energy spread — meeting these requirements may be one of the major problems in the project; another severe technical problem will be in the inflector.

Again, it should be emphasized that contamination, and other problems connected with the handling of the final beam, have not been studied. The fact that a beam intensity of 5×10^{13} particles per sec at 300 Gev corresponds to a beam power of 2.4 Mw is an indication of the magnitude of the problems. These difficulties may impose an upper limit on the intensity that is far below the maximum intensity otherwise obtainable. If this is so, the method of injection may no longer be governed by intensity considerations, but by what is the simplest technical solution. It is outside the scope of this report to try to evaluate this. All the methods considered in this report seem capable of giving at least 10^{13} particles/sec.

VIII. Acknowledgments

This work was done while the author was on leave of absence from CERN to take part in a design study for a 300-Gev proton synchrotron at the Lawrence Radiation Laboratory. The author would like to acknowledge the hospitality extended to him by the Lawrence Radiation Laboratory and the stimulating discussions he had with the staff of the Laboratory and the other participants of the HEPS group.

References

1. Smith, L., LRL Accelerator Planning Group Report LS-4 — Revised Parameter List, Dec. 1960.

2. Smith, L., LRL Accelerator Planning Group Report LS-1 — Beam Characteristics of a Linac Accelerator Injector, Nov. 1960.

3. Smith, L., LRL Accelerator Planning Group Report LS-3 — R. F. Tolerances and Focusing Requirements in a Near Relativistic Linac Accelerator, Nov. 1960.

4. Sands, M., Cal. Inst. of Tech. Synchrotron Laboratory Report CTSL-10 — A Proton Synchrotron for 300 Gev, Sept. 1960.

5. Teng, L. C., Brookhaven Accelerator Department Report LCT-3 — Phase Space Matching of Longitudinal (Phase) Oscillations Using the Injector as the Matching System, Apr. 1961.

4. NOTES ON MISCELLANEOUS EXPERIMENTAL TOPICS

Lawrence W. Jones*

August 25, 1961

This paper brings together several short, unrelated considerations by the author on experimental problems with a 300-Gev synchrotron.

Synchrotron Radiation as a Means of Particle Identification

In an attempt to explore all possible systems for identification of very-high-energy particles of the same momentum, numbers were put into the standard expressions for synchrotron radiation by high-energy particles in a magnetic field. This effect is generally regarded as negligible except for electrons; however, the very high energies now under consideration, together with the possibility of higher magnetic fields produced by superconductors, made a reinvestigation appear interesting. In fact, it turns out that the effect is not large enough to be useful even with the present parameters, but it comes close.

The radiated power by a charged particle is given (in mks units) by

$$\frac{dW}{dt} = \frac{e^2 a^2 \omega^4 \gamma^4}{6\pi\epsilon_0 C^3},$$

where $\omega = v/a$. From this, the energy radiated per unit path length, in ev/m, is

$$\frac{dW}{d\ell} = 9.6 \times 10^{-10} \frac{\gamma^4}{a^2} = 0.88 \times 10^{-12} \frac{B^2}{(pc)^2} \gamma^4,$$

where B is in gauss, pc in Mev, and a in meters. The spectrum of radiation is sharply peaked about a critical wavelength, λ_c, given by

$$\lambda_c = \frac{2}{3} \frac{a}{\gamma^3}.$$

If it is assumed that all the energy loss goes to quanta of this wavelength, the energy loss can be expressed as a number of quanta per meter :

$$\frac{dn_q}{d\ell} = 4.8 \times 10^{-3} \frac{\gamma}{a} = 1.5 \times 10^{-4} \frac{B}{m_0 c^2},$$

where B is in gauss and m_0c^2 is in Mev.

As numerical examples, consider particles of 100 Gev/c and 300 Gev/c momenta in a magnet of 200 kilogauss 10 meters long. The energy radiated, critical wavelength, and (approximate) numbers of quanta given off are tabulated in Table R4-1.

In conclusion, even collecting all the radiated quanta on an efficient photocathode (probably feasible) would give only marginal detection of π's and even poorer reliable detections of K's. A suprising result is that (to the extent of validity of this calculation) the number of quanta radiated is independent of γ, but depends only on the magnetic field and rest mass of the particles.

It might be noted that, in these high fields, an electron of 100 Gev loses most of its energy in 10 meters, so that synchrotron radiation can be effective in removing electrons from beams.

Effects of the Relativistic Rise in Ionization

The Goldhabers and others have discussed the possible utility of the relativistic rise of

* Permanent Address: Dept. of Physics, University of Michigan, Ann Arbor, Michigan.

Table R4-I.

Synchrotron radiation of particles in a 200-kilogauss magnet 10 meters long.

	Particle	W_{ev}	λc	n_q
100 Gev/c	μ	35	700 Å	3
	π	9	1900 Å	2
	K	0.06	9 μ	2/3
300 Gev/c	μ	320	80 Å	3
	π	76	230 Å	2
	K	0.5	1 μ	2/3

ionization as a means of distinguishing particles, and Yuan has built a xenon-filled scintillation counter for studying the feasibility of such schemes. This effect is utilized, e.g., in the gas proportional counter and the scintillation chamber.

Gas Proportional Counter

A gas-filled (argon-CO_2) proportional counter could be used (surprisingly) in a high-energy well-collimated beam in place of the gas scintillation counter. Consider a 3-meter-long gas proportional counter filled to 0.1 atmosphere with argon-CO_2. A minimum-ionizing particle passing through this counter would make about 2.5×10^4 ion pairs. By making the counter a coaxial transmission line parallel to the beam and terminated properly, the voltage pulse from the electron avalanches would arrive with a rise time due only to electron drift time dispersion and independent of the counter length. Thus, the 3-meter counter could, in principle, have a pulse rise time less than the 10-nanosecond transit time of the particle. Actually, since the electron mobility is only a few centimeters per μsec, the rise time would be generally limited by this effect. Thus, if a particle went through the counter at an angle of 10^{-4} radian, its distance from the central wire would vary by 0.3 mm, and the electron-collection time would vary by 10 nsec from one end of the counter to the other. However, the pulses of parallel particles would be large (using a short clipping line) compared with pulses of background (transverse) particles, even of high ionization, so that it might be unnecessary to use it in coincidence with other counters.

The possible advantage of this counter over a gas-scintillation counter in discriminating particles of different masses would lie in its greater energy-loss resolution owing to better statistics per unit mass of material traversed or particle energy lost. Thus, in gas scintillators, one would probably get one photoelectron per 1000 ev of particle energy loss, contrasted with one ion pair per 30 ev in the proportional counter.

Scintillation Chamber

Kerth and Keefe have described arrangements of spark chambers and magnets useful for studying elastic scattering at very high energies. The same general geometry could be used to study reactions of the types

$$\pi + N \rightarrow \begin{cases} 2\pi + N \\ 2K + N \\ \pi + K + Y, \text{ etc.,} \end{cases}$$

$$\pi + N \rightarrow \begin{cases} 3\pi + N \\ \pi + 2K + N, \text{ etc.} \end{cases}$$

Such diffraction production processes as discussed by Drell and others, and Coulomb production as discussed by Good and Walker, will be of interest at high energies. However, spark chambers do not give any information on the masses of the outgoing particles, so that, for example, π's and K's could not be distinguished. A scintillation chamber placed beyond the last reaction-products analyzing spark chamber would give information on track-ionization density. As a numerical example, we consider 40 g/cm^2 of NaI filamentary scintillator (5 in. long). For particles of 5 to 15 Gev/c momentum, the difference in average ionization between K's and π's is about 5%. For a 2% determination of ionization, about 3000 photoelectrons should be recorded, which is a conservative estimate for the figures above (sodium iodide produces about 10^5 photons per cm; filaments pipe 20% of the light to each end by total internal reflection; and good photocathodes convert 20% of the photons to photoelectrons). Image tubes of resolution adequate for such quantitative measurements do not yet exist, nor do filaments of sodium iodide. Both are feasible, however, and extrapolation of recent developments indicates that both will be available well ahead of the 300-Gev accelerator. The density effect in sodium iodide limits the usefulness of this technique to momenta below 15 to 25 Gev.

Such a terminal detector has other possible advantages: characteristic interactions (e.g., K^- interactions, $\bar{p}$ annihilations) in the sodium iodide would also serve to identify the particles, and neutral particles would be converted with possibly characteristic signatures.

The goal of the overall detection system would be to combine the sampling properties of a thin-plate spark chamber with the ionization and interaction-identification properties of a homogeneous medium--the scintillation chamber--while preserving the time resolution and postevent detection possible with both systems.

Neutrino Spark Chambers

Present neutrino experiments are aimed at detection of high-energy neutrino reactions. These first-generation experiments will probably be completed in a couple of years. More quantitative experiments will be required subsequently, and Perkins has shown how appropriately suited a 300-Gev synchrotron is for this purpose. Two second-generation neutrino detectors are suggested as indications of the scope of parameters possible; namely, an iron-plate magnetic-field chamber and a hydrogen-plate spark chamber.

An Iron-Plate Magnetic-Field Chamber

Consider a spark chamber made of iron plates, each 1 cm thick and 120 × 200 cm in area, with a 100 × 20-cm hole in the center. Two hundred plates would be stacked with 1-cm plate spacing to form a spark chamber, or chambers, with a total length of about 4 meters and weight of about 35 tons. By passing conductors through the central hole, all the plates could be magnetized at 10 to 20 kgauss (with the field in the plane of the plates) with only a few thousand ampere turns. The chamber geometry is indicated in Fig. R4-1. Thus a magnetic field would be applied to a considerable volume of detector with a minimum of cost or complexity.

The usefulness of the chamber would be in discriminating between μ mesons of different charges and in determining their momenta. In this, multiple scattering is the major limitation

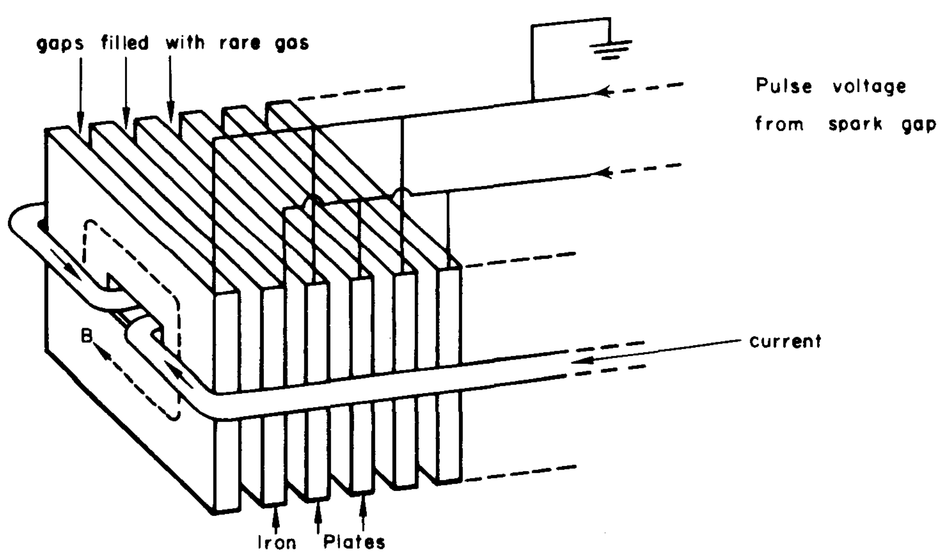

Fig. R4-1.

on momentum measurements. The ratio of apparent curvature due to multiple scattering, K_{sc}, to curvature due to magnetic field, K_H, is given by

$$\frac{K_{sc}}{K_H} = \frac{57}{H} \sqrt{\frac{1}{L X}} ,$$

where X is the radiation length and L the path length in cm, and H is the magnetic field in kgauss. In iron, X is about 1.7 cm or two plates. For a 1-meter track in a 15-kgauss field,

$$\frac{K_{sc}}{K_H} = 0.34 .$$

In 1 m of iron, a minimum-ionizing particle loses about 500 Mev, so that μ's and π's from interactions of neutrinos of a few Gev could be readily identified as to sign of charge, and measurements to within about 30% made on their momenta. Electron cascades would be observable with the same characteristics as in the Columbia spark chamber which has 1-in. aluminum plates.

A Hydrogen-Plate Spark Chamber

Ultimately, neutrino reactions should be studied in pure hydrogen, and preferably with a liquid hydrogen bubble chamber. However, very large chambers would be very difficult engineering undertakings. For example, the 1700-liter Shutt chamber contains only 0.12 metric ton of hydrogen, and the event rate would be low, even with the neutrino fluxes discussed for a 300-Gev synchrotron.

A spark chamber could be built of aluminum plates 0.010 in. thick made in the form of flat tanks 10 cm thick by 2 m square. These tanks, filled with liquid hydrogen, would be spaced 1 cm apart and the intervening gaps filled with helium gas for the sparking medium. Hydrogen would constitute 80% of the mass of each plate. Mechanical strength would be achieved by 0.020-in.-diameter aluminum wires welded on 10-cm centers between walls of the tanks. Occasional lucite spacers in the helium-filled gaps would assure uniform spacing over large dimensions.

Seventy such hydrogen "plates" (tanks) would then constitute a spark chamber containing 2 metric tons of liquid hydrogen with overall dimensions $2 \times 2 \times 8$ meters. The entire chamber, of course, would be in an evacuated container with appropriate cryogenic plumbing. The vacuum tank might resemble the tank of a horizontal Van de Graaff generator or linear accelerator. Mirrors in the form of thin louvers, one for each gap, could fold the images of the spark-chamber gaps so that little of the chamber area would be covered by radiation shielding. A simple thin lucite box would be adequate for separating the low-pressure helium-spark-chamber volume from the evacuated volume.

A magnetic field of 1000 gauss could be placed on the entire chamber by coils inside the cooled, evacuated volume. The steel vacuum tank would provide a return flux path for this low field, so that the required current would be about 2×10^5 ampere-turns. Cryogenic coil techniques, however, could make this relatively straightforward. The apparent curvature of tracks due to multiple scattering is 10% of that due to magnetic field for a 150-cm track in this field, so that more precise momentum measurements could be made than in the iron-plate chamber described above.

In both cases, scintillation counters could be placed between plates, as appropriate, for triggering by neutrino events (as described by Steinberger for the current Columbia chambers).

Colliding Beams

Continuing off the deep end, it seemed of interest to look at possible interaction rates of colliding beams of particles which could be obtained with storage rings operated in conjunction with a high-energy synchrotron. We assume the storage rings would have the same radius and aperture as the synchrotron, that the synchrotron beam could be transferred efficiently, that the vertical size of the beam at full energy is just the size of the vacuum tank times the factor (1/10) due to adiabatic damping from injection into the ring.

For beams intersecting at an angle α, the beam-beam interaction rate, in interactions per second for protons on protons, is given by

$$R = \frac{80\ I^2}{\alpha y}$$

where I is the circulating current in each beam in amperes, y is the vertical height of each beam, and the proton-proton interaction cross section is assumed to be 30 millibarns.

The circulating current (in amperes) is

$$I = Nf \times 1.6 \times 10^{-19} = \frac{N}{R} \times 2.5 \times 10^{-11} ,$$

where N is the number of protons, f is the frequency, and R is the ring radius (in feet).

Table R4-II summarizes reaction rates for three machines, assuming 1 to 3×10^{13} protons per pulse can be accelerated by the synchrotron, $y = (1/10)\ y_0$, and a beam-beam crossing angle α of 0.1 radian. Numbers are given for collision rates – assuming one accelerated beam bunch is transferred to each storage ring – and for the cases in which 100 and 1000 accelerated bunches are stacked in each storage ring.

Table R4-II.

Reaction rates for three possible storage rings

Synchrotron			Protons per pulse	Current	Colliding-beam reaction rate, R ($\alpha = 0.1$, $y = 0.1\ y_0$, $\sigma_{pp} = 30$ mb)		
Energy (Gev)	Radius (ft)	Vertical aperture y_0 (cm)			1 stack ($\times 10^2$)	100 stacks ($\times 10^6$)	1000 stacks ($\times 10^8$)
100	900	7	10^{13}	0.28	0.88	0.88	0.88
			3×10^{13}	0.84	7.8	7.8	7.8
200	1800	7	10^{13}	0.14	0.22	0.22	0.22
			3×10^{13}	0.42	2.0	2.0	2.0
300	2700	3, 5	10^{13}	0.09	0.18	0.18	0.18
			3×10^{13}	0.27	1.6	1.6	1.6

The numbers indicate that a reasonable interaction rate might be 10^7/sec.

Perhaps the relevance of these numbers is to suggest that consideration might be given to building a 200-Gev synchrotron plus storage rings rather than only a 300-Gev synchrotron for the same expenditure of time and effort, or at least to provide for expansion of an accelerator site to include storage rings at a later date. To emphasize this point, Table R4-III notes the lab and c.m. energies of the systems under consideration, including the energy of a proton incident on a stationary proton [E_{lab} (equivalent)] necessary to give the same c.m. energy as the colliding beams.

Table R4-III.

Center-of-mass and laboratory system equivalent energies.

Machine	E_{lab} (Gev)	$E_{c.m.}$ (Gev)	E_{lab} (equivalent) (Gev)
Synchrotron			
100 Gev	100	13.7	
200 Gev	200	19.4	
300 Gev	300	23.8	
Colliding beams			
100 Gev	100	200	21,000
200 Gev	200	400	85,000
300 Gev	300	600	190,000
1000 Gev	1000	2000	2,100,000 (2×10^{15} ev)

5. KINEMATICS OF 90-Gev p-p INTERACTIONS

Gerald R. Lynch

August 14, 1961

To facilitate the understanding of what accuracy could be achieved with bubble chamber measurements of interactions produced by particles with energies of about 100 Gev, I investigated the kinematics of proton-proton interactions for $\gamma_{cm} = 7$, which corresponds to a kinetic energy of 90 Gev for the incident proton. Figure R5-1 is a polar plot of the envelopes for pions and for protons coming from such collisions. Particles produced with the maximum energy of about 14 Gev (c.m.) appear at the edge of this cigar-shaped region; particles with smaller energies fall inside.

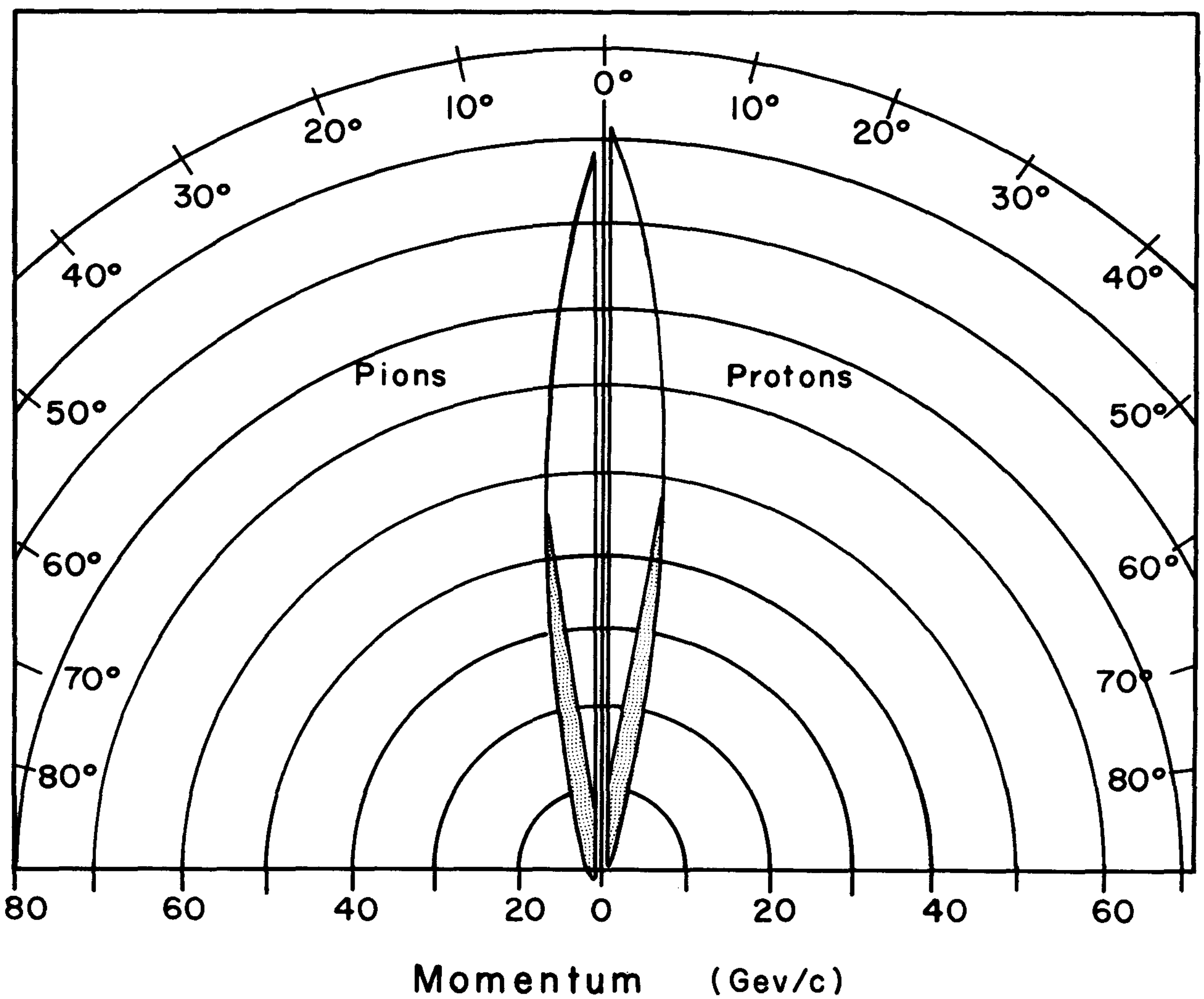

Fig. R5-1.

The two vertical lines are drawn where the transverse momentum is 1 Gev/c, a momentum which we have seen from cosmic-ray data is already in the tail of the transverse-momentum distribution. Thus most of the particles will be observed in the very narrow strip going up the center of the figure.

Because there must be forward-backward symmetry in proton-proton interactions, one can learn all one needs to know about these interactions from a study of only those particles which come out in the backward region in the center-of-mass system. Lines drawn at about 8° on Fig. R5-1 separate the particles that were produced in the forward hemisphere in the c.m. system from those produced in the backward region. Figure R5-2 is a magnification of the low-momentum region of Fig. R5-1. It shows that if one confines oneself to a study of particles emitted backward in the c.m. system all particles with a transverse momentum less than 1 Gev/c (those in the shaded region) have a lab momentum of less than 10 Gev/c, a momentum which can be measured with an accuracy of 5% with present-day bubble chamber techniques. Even particles with transverse momenta of 3 Gev/c will have lab momenta less than 25 Gev/c. This means that one can obtain quite accurate momentum and angular distributions for particles from proton-proton interactions.

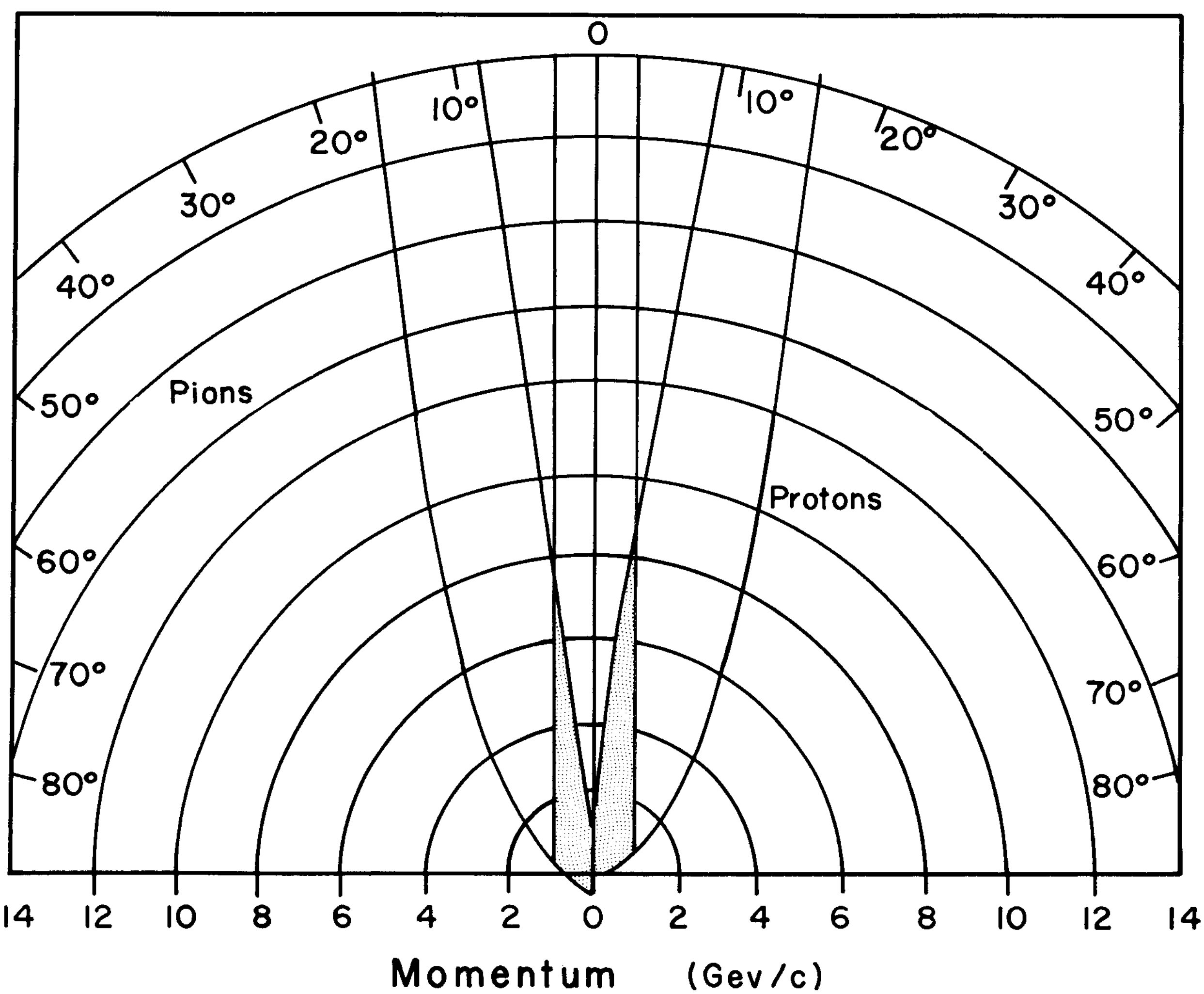

Fig. R5-2.

6. HIGH-ENERGY NEUTRINO BEAMS FROM A 300-Gev SYNCHROTRON

Donald H. Perkins *

July 31, 1961

Introduction

A very rough attempt is made to estimate the neutrino fluxes that could be obtained from a 300-Gev accelerator. It is assumed that, within the next year or so, qualitative experiments on neutrino interactions in the region of 1 Gev will have been successfully accomplished. The emphasis here, therefore, is on the possibility of quantitative experiments with larger neutrino fluxes at much higher energy (up to 50 Gev). It is believed that, with a pion flight path of the order of 400 to 1000 meters, the counting rate for neutrinos of energy 10 to 50 Gev would be of the order of 1 per hour per ton of detector, assuming an internal beam of 10^{12} protons/sec. Whether this rate is sufficient for quantitative experiments is doubtful. The production of neutrino beams with good momentum resolution over a wide energy range is discussed.

* Permanent Address: H. H. Wills Physics Laboratory, University of Bristol, Royal Fort, Bristol, England.

Pion Beam

First, we shall consider a pion beam of specific momentum 50 Gev/c. The achromatic-triplet bending magnet described in Kerth's report (Seminar 9, Part I) is run at a current such as to give a 3.3-mr deflection for the "neutral 0° beam" from the target T (Fig. R6-1). The 50-Gev/c negative secondary beam, coming off the target in the 0° forward direction, leaves magnet B with a 40-mr angular deflection and a lateral displacement of 35 cm from the internal proton beam. The negative beam is assumed to clear

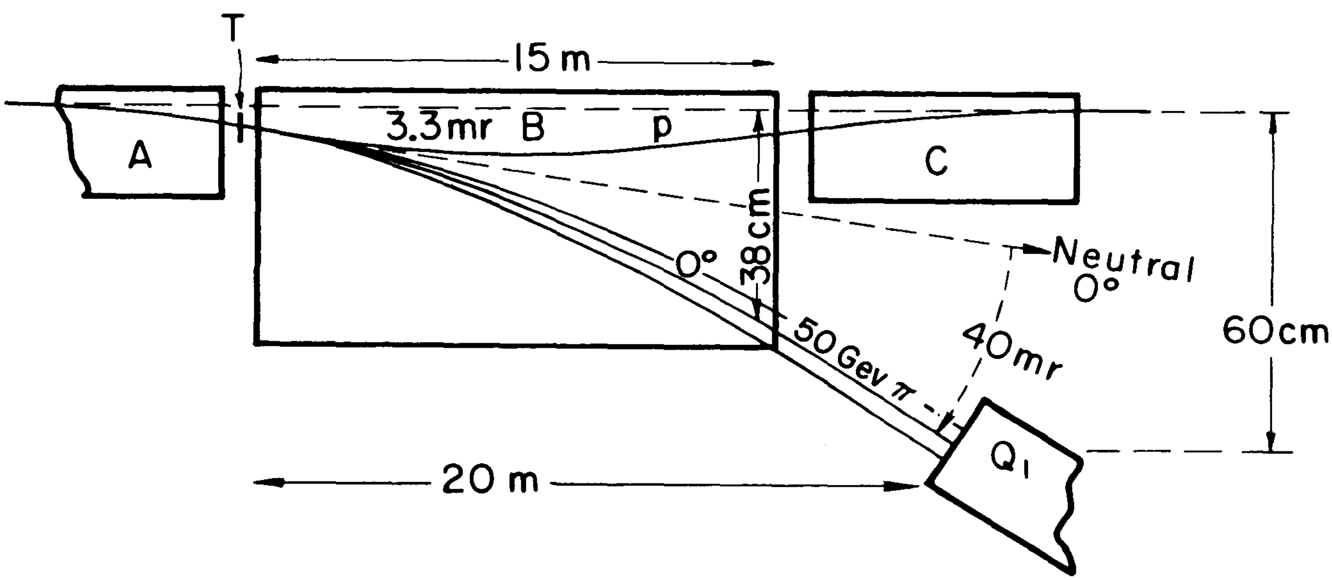

Fig. R6-1.

magnet C completely. Positive beams (giving neutrinos instead of antineutrinos) can be obtained by placing the target T ahead of magnet A and shaping B suitably.

The first focusing magnet Q_1 is located about 20 m from the target, so that the axis of Q_1 is laterally separated by 0.6 m from the internal beam. The aperture of Q_1 is assumed to be capable of accepting a secondary beam in a cone of 5-mr halfangle ($\Delta\Omega = 8 \times 10^{-5}$ sr), and focusing this in the plane of the second quadrupole Q_2.

The intensity and momentum spread of the negative beam has been estimated by assuming

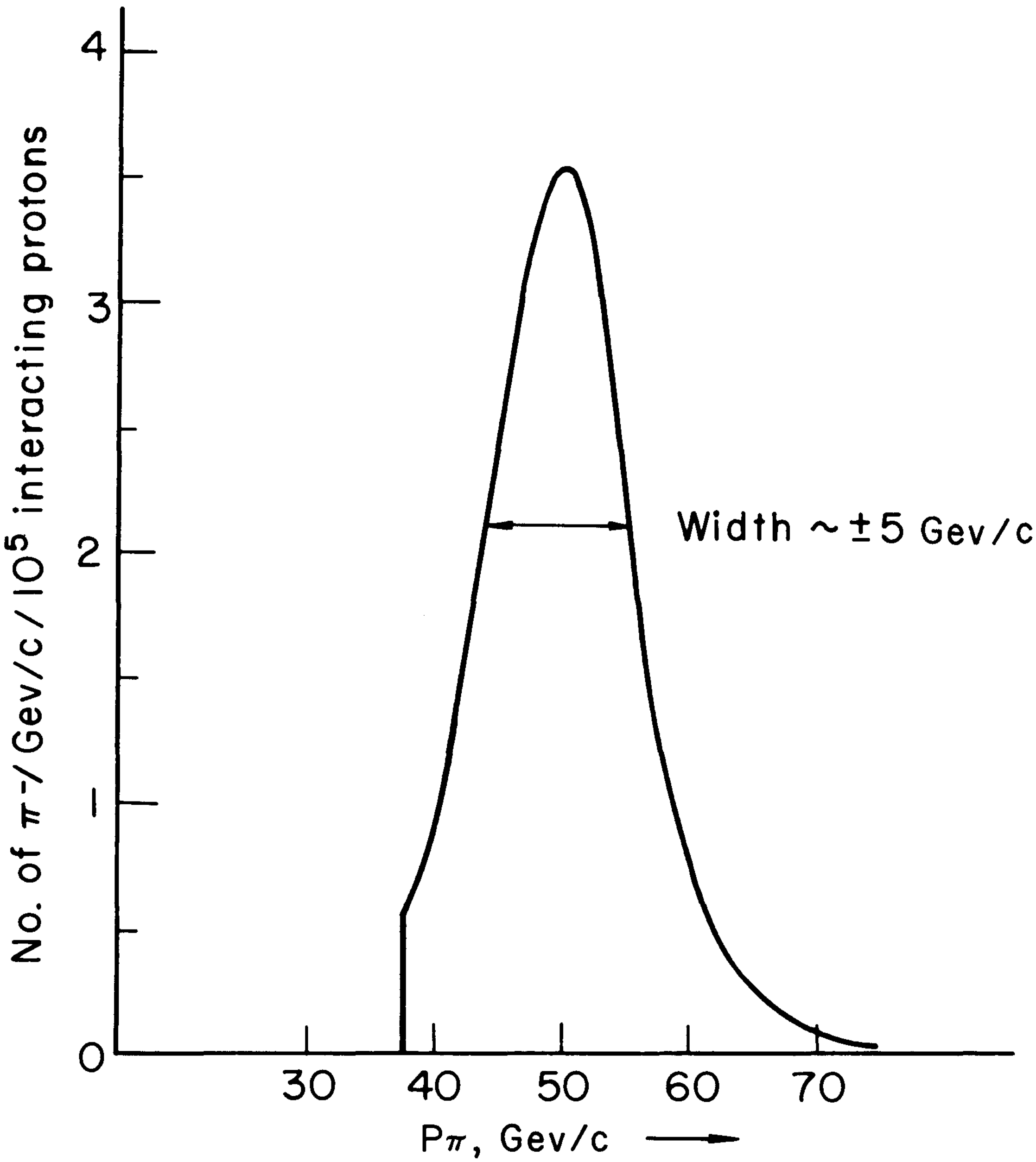

Fig. R6-2. Momentum dispersion of π^- beam.

that the source spectrum of pions is given by the formula (Report 7)

$$N_\pi(E,\alpha)\,dEd\alpha = \frac{n}{3T}\,e^{-E/T}\,\frac{E^2\alpha\,e^{-E\alpha/p_0c}}{(p_0c)^2}\,dEd\alpha, \tag{1}$$

where E is the pion energy, α is the angle of emission with respect to the proton beam, and $p_0 = 0.2$ Gev/c is the coefficient of the transverse momentum distribution. T is the pion temperature; extrapolating $T \propto$ (proton energy)$^{3/4}$ from the Brookhaven pion spectra, we obtain T = 22.5 Gev; n is the pion multiplicity, and, extrapolating $n \propto$ (proton energy)$^{1/4}$, we obtain

$$\frac{n}{3T} = 0.08 \;.$$

The momentum distribution of the negative beam is given in Fig. R6-2. For 10^{12} protons per sec striking the target, the beam contains a total of 3×10^{10} pions per sec, with a momentum of 50 ± 5 Gev/c. Approximately 40% of all the negative pions created in the target at the peak momentum (50 Gev/c) lie in the beam.

Q_1 is followed by a succession of quadrupole elements strung along the pion flight path to hold the beam divergence down to a cross section of mean radius $\lesssim 10$ cm over a distance of up to 0.5 km. If this path were in the open air, the mass traversed (approximately 100 g) would result in considerable losses by nuclear collisions. Further, Coulomb scattering would result in an rms angular deflection of 0.24 mr per 100 meters of path, and an rms lateral deflection of 1.4 cm over the same distance. These losses could be reduced by the use of helium bags; this would result in a fourfold decrease in Coulomb scattering, so that the beam could probably still be contained by the focusing lenses. The loss of particles from nuclear interactions would be less than 20%. If necessary, however, low-vacuum tubes could be employed. In what follows, we assume that losses by scattering and nuclear interactions can be ignored.

From the point of view of a neutrino beam, the only negative particles to consider are pions and kaons. As shown in a later section, the contribution of the latter is only about 5 to 10%. We shall be primarily concerned, therefore, with the π^- component of the beam.

Neutrino Beam

In the diagram (Fig. R6-3), EF is the pion flight path. Following F is a sweeping field serving to remove negative pions and muons —

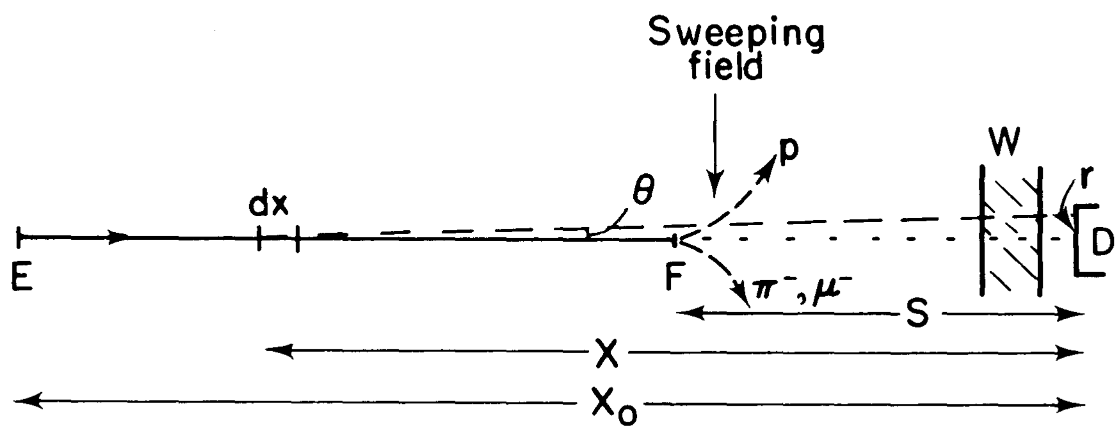

Fig. R6-3. EF represents the pion flight path. The sweeping field is assumed to remove all charged particles that would otherwise enter the detector D . The shielding wall W , about 30 m thick, is intended to remove γ rays, neutrons, K^0's, etc.

as well as protons, positive pions, etc., produced by interaction of the pions along the flight path. W is a shielding wall (about 30 m thick) to absorb γ rays, neutrons, and other neutral particles from the pion beam, as well as background due to particles outside the pion beam. D represents the neutrino detector.

The distances x_0, x, and s are in units of the pion decay length $\lambda = \gamma c \tau$. Here, γ is the value of E/mc^2 of the pions, τ is their mean lifetime. For 50-Gev pions, $\lambda = 2500$ m. For the present, we shall ignore the momentum spread of the pion beam, and treat γ as a constant. The radius r of the neutrino detector, assumed cylindrical with axis collinear with the pion beam, is measured in units of $c\tau = 7$ meters. In order to simplify the calculations, we assume that $rc\tau$ (about 70 cm, let us say) is large compared with the mean radius of the pion beam ($\leqslant 10$ cm, we hope).

The probability that a neutrino, originating in the interval dx, traverses the detector is simply

$$\frac{r^2}{r^2 + x^2} , \qquad (2)$$

under the valid assumptions $\gamma >> 1$ and $r << x\gamma$.

The total number of neutrinos N_ν, traversing the detector is then given by

$$P \equiv \frac{N_\nu}{N_\pi} = e^{-x_0} \int_s^{x_0} \frac{r^2 e^x}{\left(r^2 + x^2\right)} dx , \qquad (3)$$

where N_π is the number of pions at the starting point E (i.e., at Q_1). (Notice that, for a given detector of size r, P is independent of the pion momentum if x, x_0, and s are in units of $\lambda = \gamma c \tau$.)

Maximum Neutrino Flux

By numerical integration of Eq. (3), we can find under what conditions P is a maximum. Clearly, for any values of x_0 and r, P is greatest when $s = 0$. We consider this case first.

Figure R6-4 shows how P varies with x_0 for various choices of r. In considering what is the best value of r, we can assume, for example, a detector of a fixed mass or volume. If ℓ is the length of the detector, the number of neutrino interactions is proportional to

$$P(r)\,\ell \propto \frac{P(r)}{r^2} .$$

From the graph, we see that $P_{max}(r)$ rises somewhat more slowly than r. Hence, the maximum counting rate would be achieved for a long, thin detector, corresponding to the fact that the greatest neutrino flux is on the axis of the beam. However, there is no point in making r less than the radius of the pion beam itself. Further, the neutrino interactions may involve emission of secondaries at appreciable angles, and, if these are to remain inside the detector over a substantial fraction of its length, r must not be made too small. These considerations, and the fact that bubble or spark chambers cannot be made in completely arbitrary shapes, have led us to assume a minimum possible value of $r = 0.05$ (35-cm radius).

The rate R_ν of neutrino interactions in the detector, assumed to be a cylinder of radius r, is given by

$$R_\nu \approx \frac{2N_\pi}{10^{15}} M \frac{P(r)}{r^2} \left(\frac{2Z}{A}\right) , \qquad (4)$$

where N_π is the total number of pions in the original beam and M is the mass of the detector in tons. The neutrino-interaction cross section for a nucleus of charge Z has been taken as

$$\sigma = 10^{-38}\, Z\, cm^2 . \qquad (5)$$

The factor $2Z/A$ can be taken as unity for all elements above hydrogen.

As an example, consider the case $r = .05$ (35-cm detector radius); then $P_{max} = 0.05$ for a pion flight path $x_0 = 0.15$, or 370 meters. With $N_\pi = 3 \times 10^{10}$/sec as above, we obtain $R_\nu = \frac{1.2}{10^3}$ M/sec, or a rate of 1 per minute for a 15-ton detector. If made of pure lead, such a

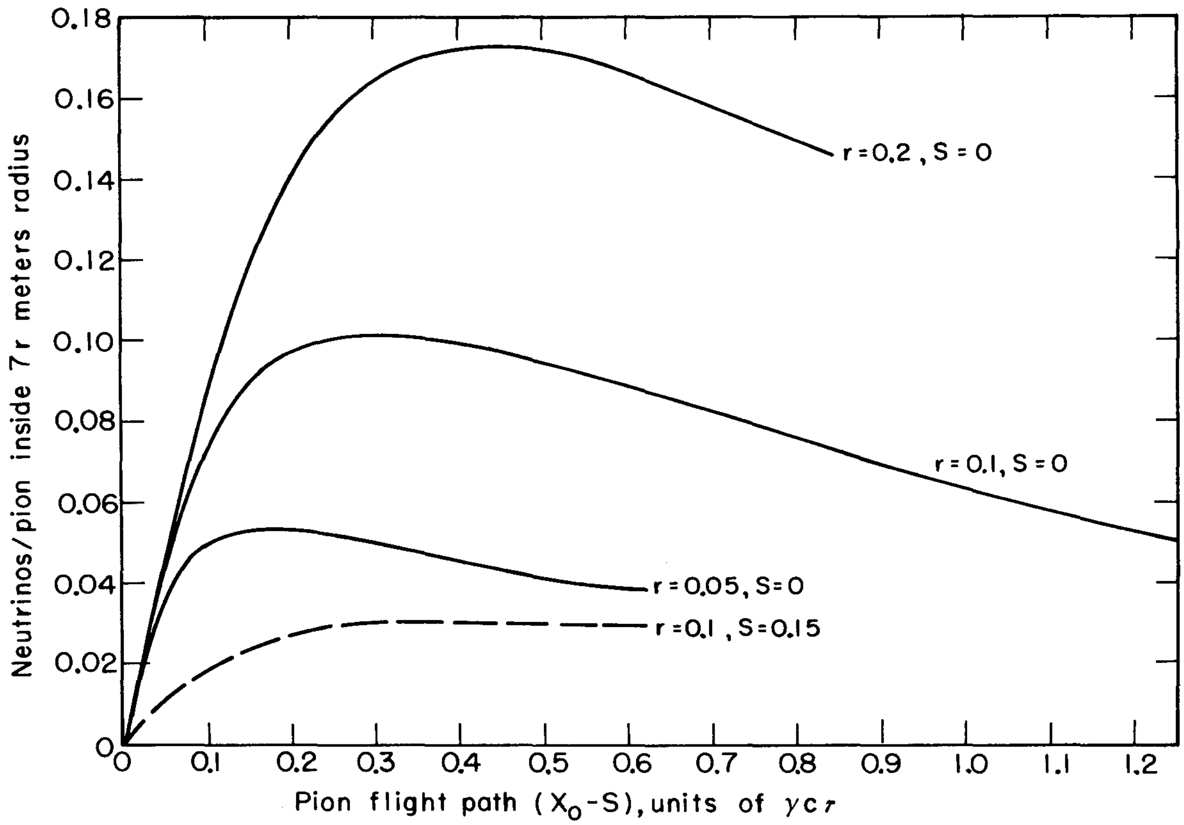

Fig. R6-4.

detector would be 3.5 m long. For a value of r = 0.1 , the rate for a given value of M would be reduced by 2, and the optimum flight path would be about doubled.

Neutrino Energy Spectrum

The energy E of a neutrino, emitted in the interval dx at angle Θ to the pion beam (Fig. R6-3), is

$$E = \epsilon E_{max} = \frac{1}{\left(1 + \gamma^2 \Theta^2\right)} E_{max} ,$$

where $E_{max} = 0.42 E_\pi$. If the neutrino is to traverse the detector, its minimum energy will be

$$E_{min} = \frac{x^2 E_{max}}{\left(r^2 + x^2\right)} .$$

The neutrino energy spectrum is then given by

$$N_\nu(\epsilon)\, d\epsilon = N_\pi \left[1 - e^{-(x_0 - s)}\right] d\epsilon$$

$$\text{for} \quad 1 > \epsilon > \frac{x_0^2}{\left(r^2 + x_0^2\right)}$$

$$N_\nu(\epsilon)\, d\epsilon = N_\pi\, e^{-x_0} \left(e^{x'} - e^{s}\right) d\epsilon \tag{6}$$

$$\text{for} \quad \frac{x_0^2}{\left(r^2 + x_0^2\right)} > \epsilon > \frac{s^2}{r^2 + s^2} ,$$

$$N_\nu(\epsilon)\, d\epsilon = 0 \quad \text{for} \quad \epsilon < \frac{s^2}{r^2 + s^2} ,$$

where

$$x' = r\sqrt{\frac{\epsilon}{1-\epsilon}} \ ,$$

and N_π is the initial number of beam pions.

The form of the neutrino energy spectrum is given in Fig. R6-5 for a few values of x_0, s, and r. For $s = 0$ — i. e., when the detector is placed at the end of the flight path — the spectrum has a long tail extending to zero energy. This tail can be largely removed (at a cost to intensity) by making s comparable to the flight path. The curve of P as a function of flight path $(x_0 - s)$ for such s values passes through a much flatter maximum than those for $s = 0$ (Fig. R6-4). As before, the maximum is in the region of $(x_0 - s) \approx 3r$, and has a magnitude given very roughly by

$$\frac{P(s)}{P(0)} \approx \left(1 - \epsilon_{co}\right) \ ,$$

where $\epsilon_{co} = s^2/\left(r^2 + s^2\right)$ is the cutoff value of ϵ. Thus, restriction of the neutrino momentum band to a value comparable to that of the pion beam — for example, $\epsilon_{co} = 0.8$ — would result in an approximately fourfold reduction in intensity. Some spectra for different values of s and ϵ_{co} are included in Fig. R6-5.

Contribution from K Mesons

Equations (1) and (2) hold also for the decay of K^- mesons in the K_{μ_2}, K_{μ_3}, and K_{e_3} modes, constituting approximately 60% of the total.

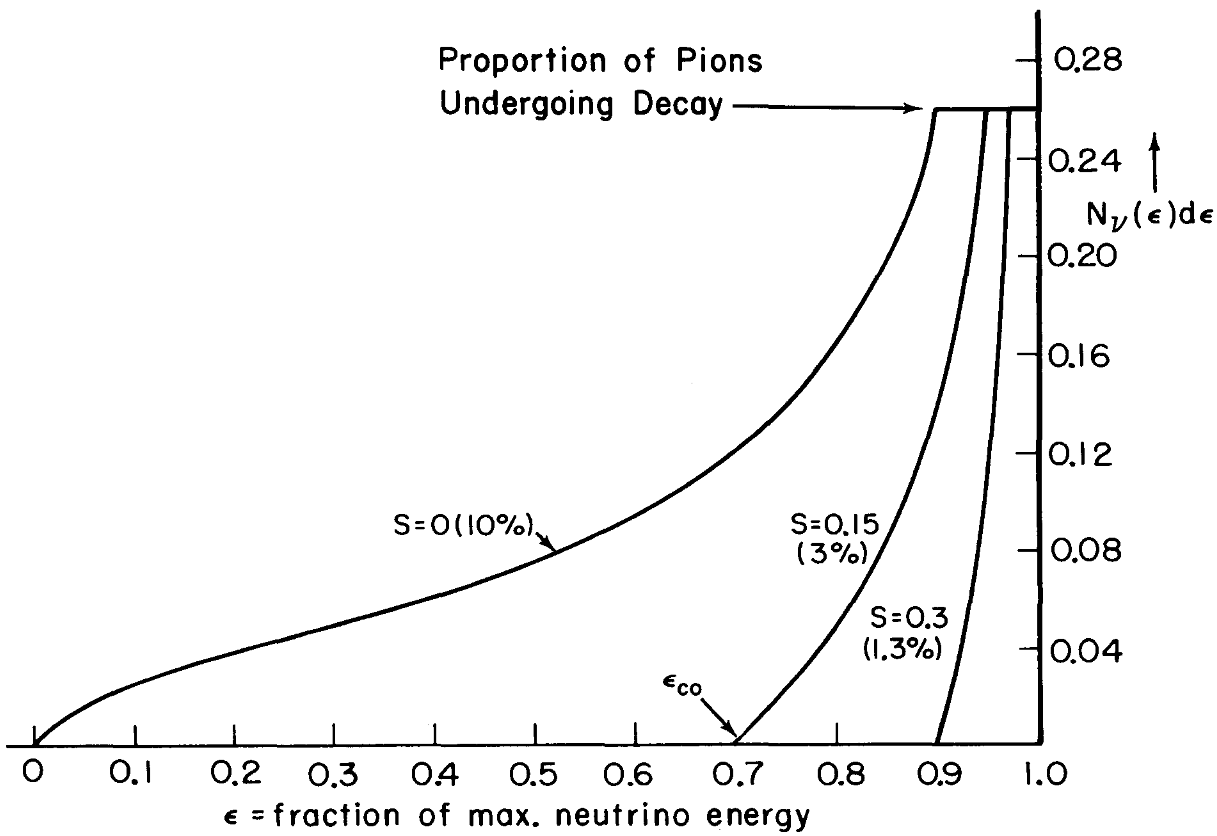

Fig. R6-5. Neutrino energy spectra for flight path $(x_0 - s) = 0.3\ \gamma c\tau$. Detector radius $r = 0.1$ (70 cm). The area under each curve is given as a percentage of the pion intensity.

(Neutrinos are also obtained through pionic decay modes of K^-, and the decay of these pions; since this involves a double decay process, we can neglect their contribution.) For a given flight path, the value of x_0 is increased over the value for pions by a factor

$$\frac{M_k \tau_\pi}{M_\pi \tau_k} \approx 7 \; ;$$

for a given detector radius, r is increased by a factor $\tau_\pi/\tau_k \approx 2$. Referring to the case $r_\pi = 0.05$ and $(x_0)_\pi = 0.15$ of Fig. R6-4, we see that the value of P for K mesons (at $r = 0.1$ and $x = 1.05$) is roughly equal to that for the pions. Since the number of K mesons in the original negative beam will be only about 10% of the number of pions, it follows that neutrinos from K decay will only contribute about 6% to the total. The neutrino momentum spectrum in K_{μ_2} decay extends from zero to 97% of the beam momentum, compared with the 42% in π decay. Again, the low-energy tail present for $s = 0$ can be removed by making s and r comparable.

Variation of the Pion Beam Momentum

The foregoing calculations have been made for a single value, 50 Gev/c, of the momentum of the pion beam. This particular momentum was chosen because it gave the maximum neutrino flux for a focusing system of angular aperture $\epsilon = 5$ mr. If the fractional momentum spread $(\Delta p/p)$ of the beam and of the aperture are both constant, the number of beam particles is proportional to

$$E\, e^{-E/T} \left[1 - \left(\frac{E\epsilon}{p_0 c} + 1 \right) e^{-E\epsilon/p_0 c} \right] ,$$

where E is the mean pion energy, and $\Delta\Omega = \pi\epsilon^2$ is the aperture in steradians. For $\epsilon = 5$ mr, $(\Delta\Omega = 8 \times 10^{-5}$ sr), $T = 22.5$ Gev and $p_0 c = 0.2$ Gev, this expression passes through a broad maximum at 50 Gev. The intensity is down by a factor 2 at $E = 24$ Gev and $E = 95$ Gev. For larger or smaller values of ϵ, the optimum E will be somewhat decreased or increased. These figures should not be taken too literally, as the above formula is only approximate, especially for $E \lessapprox T$. The essential feature that emerges is that the intensity does not depend very critically on the choice of E over quite a wide range. Figure R6-6 shows how the neutrino counting rate varies with energy, for a fixed 735-m flight path and a 70-cm detector radius ($r = 0.1$). The calculation was made for a value of $s = 0$; if momentum resolution is required, the value of s must be adjusted as previously described. For each pion momentum — chosen by adjusting the field in the bending magnets of Fig. R6-1 — the appropriate value of s must be chosen to give the required value of ϵ_{co}. For $\epsilon_{co} = 0.7$ ($s = 0.15$ at all energies) the neutrino flux would be reduced by a factor that increases slowly with energy — from 3 at $E_\nu = 20$ Gev to 4 at $E_\nu = 50$ Gev.

As might have been expected, if the maximum possible neutrino flux is desired, it would be necessary to use quadrupole lenses of much higher aperture and concentrate on pion beams of rather low energy (below 30 Gev). However, since a neutrino experiment is likely to be parasitic in nature, or at least a poor competitor with other experiments, a neutrino beam-transport system that essentially excludes all other negative beam experiments except those using very high momentum will scarcely be possible. It may be remarked that the 50-Gev beam described above already contains between 1 and 2% of all the negative particles produced in the target. With the three-magnet system of Fig. R6-1, it is difficult to see how one could improve the neutrino flux by more than one order of magnitude.

Conclusions

A 300-Gev synchrotron appears to offer reasonable possibilities for investigating neutrino interactions in the high-energy region. The optimum pion flight path is in the region of 0.5 to 1 km. In practice, the maximum flight path must be fixed in a single series of experiments, since the thick shielding wall (approximately 30 m) can be regarded as immovable. (The position of the sweeping magnet could, of course, be varied.) Momentum resolution can be varied by changing the position of the sweeping field or the detector, or both. With poor resolution ($s \approx 0$), the counting rates will be in the region of 1 per ton hour, for pion beam energies between 20 and 100 Gev.

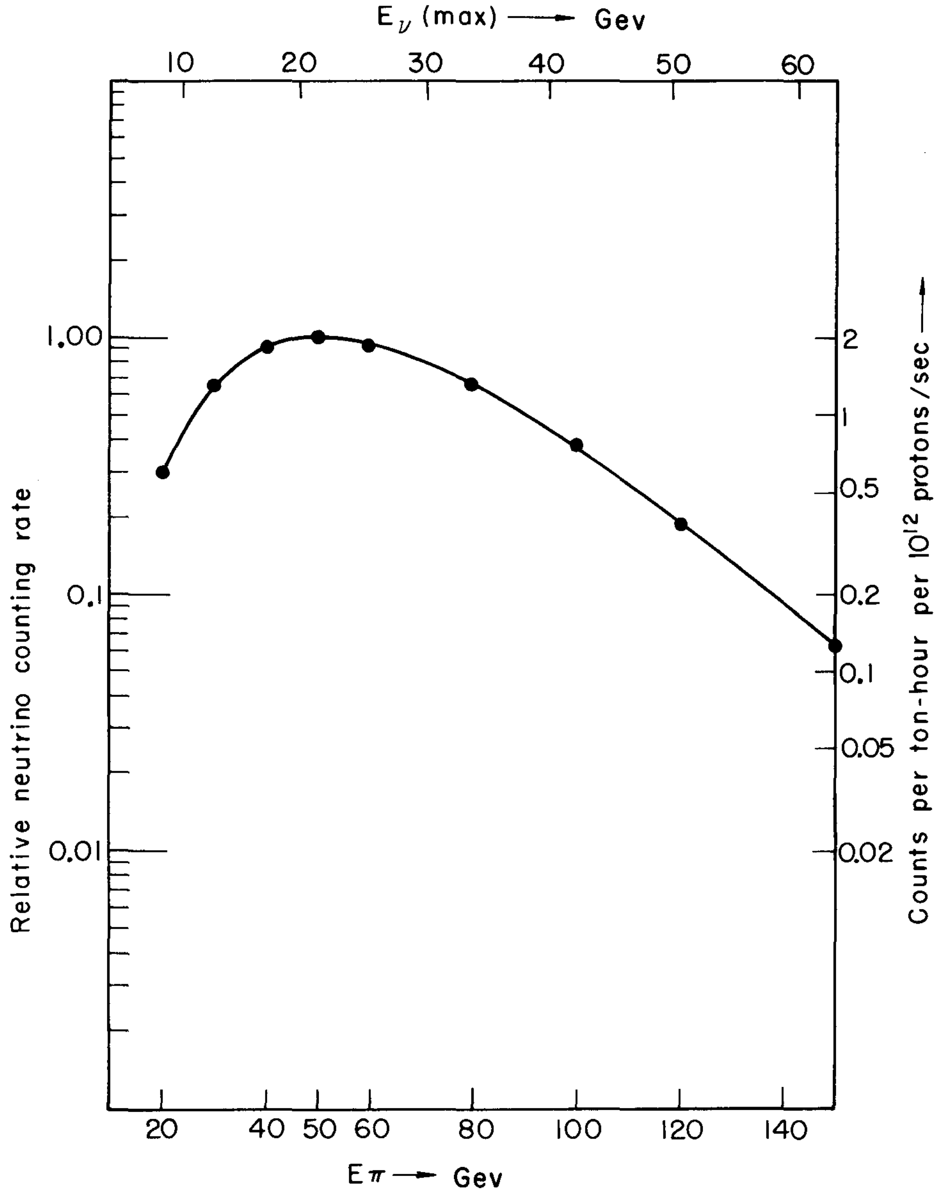

Fig. R6-6. Neutrino counting rates with poor resolution (s = 0), for a 70-cm detector radius and 750-m flight path (x_0 - s = 0.3). For ϵ_{co} = 0.7 ($\approx$ 10% momentum resolution) the counting rates will be down by a factor 3 to 4.

If a 10% neutrino-momentum resolution is required, the counting rate would be reduced to approximately 1/4. These figures assume a value of 10^{12} protons per sec striking the target.

The contribution of K mesons to the neutrino flux will certainly be small (not more than about 6%) at neutrino energies below 50 Gev. These K mesons will provide a neutrino "background" spectrum extending up to very high energy (greater than 100 Gev), which is unlikely to prove troublesome and would be difficult to eliminate without an elaborate system of gas-scintillator or Cerenkov tubes in anticoincidence.

One concludes that investigation of neutrino cross sections with energy up to 50 Gev will be relatively straightforward; detailed analysis of neutrino interactions, relying on counting rates well above 1 per ton hour, do not seem possible.

Acknowledgments

I am indebted to other members of the H. E. P. S. Group, in particular Dr. E. Courant and Dr. N. Dombey, for a number of stimulating and informative discussions.

7. OPTIMIZATION OF PION BEAMS FOR A HIGH-ENERGY ACCELERATOR

Donald H. Perkins*

August 29, 1961

The question to be answered is the following: Suppose one has a 300-Gev accelerator; what is the optimum energy at which it must run in order to achieve the most intense pion beam at a particular energy?

This question is most easily answered, first of all, by fitting a pion-production spectrum to the experimental data at CERN or Brookhaven energies. The assumption we make is that the probability of a pion's being produced with lab energy E and transverse momentum p_T is given by

$$f(E/T)\, d(E/T) \cdot g(p_T)\, dp_T \quad , \qquad (1)$$

where T is a parameter related to the mean pion energy. Equation (1) assumes that, for a given p_T value, pion spectra have the same shape at all proton energies.

The multiplicity of pions is

$$n = \iint f(E/T)\, \frac{1}{T}\, g(p_T)\, dp_T\, dE$$

$$= \int \frac{1}{T}\, f(E/T)\, dE \times \int g(p_T)\, dp_T \quad ,$$

since the values of p_T and E are independent.

Experimental data suggest that f and g have the forms

$$\frac{1}{T}\, f(E/T)\, dE = n \times \frac{1}{T} \exp(-E/T)\, dE \quad , \qquad (2)$$

and

$$g(p_T)\, dp_T = \frac{p_T}{p_0^2}\, e^{-p_T/p_0}\, dp_T \quad . \qquad (3)$$

Experimentally, $p_0 c \approx 0.2$ Gev, $T \propto E_0^{3/4}$ (E_0 = proton energy).

The flux of pions of energy E at angle Θ (lab) is then

$$\frac{d^2N}{dE\,d\Omega} = \frac{d^2N}{dE \times 2\pi \sin\Theta\, d\Theta}$$

$$= \frac{n}{Tp_0^2}\, e^{-E/T} \times \frac{p_T\, e^{-p_T/p_0}}{2\pi \sin\Theta}\, \frac{dp_T}{d\Theta} \quad .$$

At the energies considered ($E > 1$ Gev), it is a sufficiently good approximation to set $p_T c = E\Theta$ [i.e., $E \gg p_T c$ (≈ 0.2 Gev)] so that the flux is

$$\frac{d^2N(E,\Theta)}{dE\,d\Omega} = \frac{n}{2\pi p_0^2\, T}\, \frac{E^2}{c^2} \times e^{-E\left(1/T + \Theta/p_0 c\right)} \quad . \qquad (4)$$

Reverting to Eq. (2), we see

$$E_{av} = T \quad ,$$

$$nT = KE_0 \quad , \qquad (5)$$

where K = inelasticity, and

$$n_+ \approx n/3 \quad .$$

* Permanent Address: H. H. Wills Physics Laboratory, University of Bristol, Royal Fort, Bristol, England.

From Eq. (4) the photon flux, neglecting divergence of the γ's in π^0 decay (i.e., setting $m_\pi c << 2p_0$), is given by

$$\frac{d^2N_\gamma(E,\Theta)}{dEd\Omega} = \frac{n}{3\pi p_0^2 T\left(C/T + \Theta/p_0\right)^2}\left[E\left(1/T + \Theta/p_0 c\right) + 1\right] \times e^{-E\left(1/T + \Theta/p_0 c\right)}. \tag{5a}$$

Comparing Eq. (4) with Brookhaven results * for π^+ mesons from 30-Gev protons on an aluminum target, we find good agreement (for $p_0 = 0.20$ Gev/c) with the choice

$$T = 4.0 \text{ Gev} ,$$
$$\frac{n}{2\pi p_0^2 T} = 3.0 , \tag{6}$$

or $n = 3.0$ (pion multiplicity), and $K = 0.40$ (pion inelasticity); the last two figures being eminently reasonable.

Notice that the formula fails badly at very low energies (less than about 1 Gev), where our approximation (p_T)= $E\Theta$ and p_T and E independent) is no longer valid. Otherwise, the agreement is good enough to justify extrapolation of Eq. (4) to higher energies. For this purpose, we make the assumptions

K = constant for all E_0 (suggested by the cosmic-ray results), and

$$n \propto E_0^{1/4} . \tag{7}$$

Thus, we take

$$n = aE_0^{1/4} \; ; \; a = \frac{3}{(30)^{1/4}} = 1.28 \; ;$$

$$T = \frac{KE_0}{aE_0^{1/4}} = \frac{K}{a} E_0^{3/4} = 0.313 \; E_0^{3/4} \tag{8}$$
$$= bE_0^{3/4} .$$

Thus, at $\Theta = 0°$, the pion flux will be

$$F_\pi(0,E) = \frac{aE_0^{1/4}}{2\pi p_0^2 \cdot bE_0^{3/4}} E^2 e^{-E/bE_0^{3/4}} \tag{9}$$

$$= \frac{C_1}{E_0^{1/2}} E^2 e^{-E/bE_0^{3/4}} \tag{9a}$$

per interacting proton.

Let us now assume that the proton current is given by

$$i = \text{const} \cdot E_0^{-S} , \tag{10}$$

where E_0 is the proton energy at which the machine is run, and S is a constant of the order of unity. Thus, the flux/cm^2/sr/Gev/sec of pions varies with E_0 as

$$I \propto E^2 E_0^{-(1/2+S)} \exp\left(-E/bE_0^{3/4}\right) . \tag{11}$$

The maximum pion flux per sec is obtained then for $\frac{\partial I}{\partial E_0} = 0$, i.e., for

$$\frac{(S+1/2)}{E_0^{S+3/2}} = \frac{3E}{4bE_0^{3/4}} \times \frac{1}{E_0^{S+3/2}} ,$$

or
$$\left(E_0\right)_{opt}^{3/4} = \frac{3}{4b(S+1/2)} \times E . \tag{12}$$

With $S = 1$, Eq. (11) can be rewritten

$$\frac{I}{I_{max}} = e^2 \cdot \left(E_{opt}/E_0\right)^{3/2} \cdot e^{-2\left(E_{opt}/E_0\right)^{3/4}} , \tag{13}$$

* For comparison with the Brookhaven pion spectra and CERN photon spectra, see Seminar 28, Part II (Cocconi, Koester, Perkins).

where

$$b = 0.313 \quad ,$$

and

$$E_{opt} = (1.6\ E)^{4/3} \quad .$$

In Table R7-I, some values of E_0 correspond to $E_0 < E_\pi$, since we have assumed an exponential extending to infinity. The main conclusion to be drawn from this analysis is that there is little to gain by having a circulating beam with a widely variable energy. This conclusion is unlikely to be altered by errors in the simplifying assumptions made in computing the pion flux.

Table R7-I.

Variation in intensity of secondary pion beam with primary proton energy.

E_π = 10 Gev	E_π = 5 Gev	E_π = 25 Gev	E_π = 45 Gev
E_{opt} = 40 Gev	E_{opt} = 16 Gev	E_{opt} = 137 Gev	E_{opt} = 300 Gev

E_0/E_{opt}	I/I_{max}
0.25	0.21
0.50	0.89
1.0	1.0
2.0	0.8
3.0	0.59
5.0	0.36
10.0	0.16

8. ELECTROMAGNETIC PARTICLE SEPARATORS FOR A 100- TO 300-Gev ACCELERATOR

F. H. Schmidt*

July 14, 1961

The purpose of this note is to discuss crossed-field linear velocity selectors for use in secondary beams produced by a 100- to 300-Gev proton accelerator. No radically new ideas are presented, and the possibilities for separation of beams in the 100-Gev range remain difficult but not entirely hopeless. However, one or two proposals are made herein which, upon further study, may prove fruitful in the 25- to 100-Gev range. Electromagnetic separators are now used routinely at lower energies,[1] and Good[2] has discussed some problems in their use at higher energies.

General Considerations

It will be shown later that the required length of a separator is proportional to $E^{3/2}$, where E is the particle energy. Hence, for constant cross-sectional area, the solid angle subtended by the separator varies as $1/E^3$. Fortunately, nature has provided one partially compensating feature, viz, that the transverse momentum of secondary particles is apparently independent of the longitudinal momentum,[3] so that the fractional intensity of secondary particles increases in the forward direction. If the angular acceptance of the separator is very small, then the fractional intensity increases as E^2. The net fractional intensity through the separator is thus proportional to $1/E$ for constant fractional momentum acceptance.

The constancy of the transverse momentum of secondary particles alleviates the problem of focusing high-energy secondary beams by means of quadrupole magnets. The required length of a quadrupole system for constant solid angle is proportional to momentum (G. Cocconi, Seminar 3). However, the solid angle required for constant fractional intensity is proportional to $1/p^2$, so that the half-angle aperture varies as $1/p$. Thus, for constant field gradient, the length of magnet needed to focus the higher energies remains constant. It may be desirable to place quadrupole focusing systems between sections of a velocity selector, but there seems to be no great difficulty from these elements as the energy is increased.

The deflection for particles with unwanted masses is proportional to the electric field strength $\mathcal{E}$. It is easy to achieve the magnetic fields required to balance the maximum attainable $\mathcal{E}$ fields. Murray[1] has developed glass cathode surfaces which permit field strengths greater than 10^5 volts/cm for small gaps. In this study it is proposed to use very small gaps, and, in order to increase the transmission to a reasonable figure, multiple gaps are utilized.

From the above discussion, it is clear that the transmission by electromagnetic separators is small. On the other hand, the momentum acceptance for equal-mass particles can be made large. Accordingly, a possible scheme is proposed by which parallel beams of different momentum can be simultaneously directed into the separator.

The problem of field stabilization is severe for long separators. Some hope may be found in a system in which the ratio of electric and magnetic fields is stabilized; such a scheme may be facilitated if magnets composed of superconducting coils become available.[4]

Simple Crossed-Field Particle Separator

We consider a simple linear crossed-electric- and -magnetic-field velocity selector of length

* Permanent Address: Dept. of Physics, University of Washington, Seattle, Wash.

ℓ and conductor plate separation d. The plane of the conductors is perpendicular; their extent in the vertical plane is h. Singly charged particles whose velocity is v and total mass m then spend a time ℓ/v in the separator, and undergo a deflection

$$D = \frac{1}{2}\frac{e\,(\mathcal{E} - Bv)}{m}\left(\frac{\ell}{v}\right)^2 \qquad (1)$$

during the course of their traversal. B is the vertical magnetic field strength, and $\mathcal{E} = V/d$ is the horizontal electric field strength. Except where otherwise stated, mks units are used throughout. The deflection D is produced only in the velocity selector. It is assumed that this constitutes the major length of the apparatus and that any focusing magnets between sections of the selector, or after it, increase the resultant deflection by only a small fraction.

For particle separation, we are interested in the difference Δ_{21} between two deflections D_1 and D_2 produced by the selector when two beams of particles of rest mass m_{01} and m_{02} are sent into the selector. We assume that the selector is adjusted to transmit particles of mass m_{01}, momentum p, and total energy E. Two cases of interest arise: First, the energy of the entering particles is the same, and second, the momentum of the entering particles is the same; thus we have for the same energy

$$\Delta_{21} \approx \frac{1}{2}e\ell^2\frac{\mathcal{E}}{E}\left(\beta_2 - \beta_1\right), \qquad (2)$$

and for the same momentum

$$\Delta_{21} \approx \frac{1}{2}e\ell^2\frac{\mathcal{E}}{pc}\left(\beta_2 - \beta_1\right), \qquad (3)$$

where it has been assumed that $\beta_1 \approx \beta_2 \approx 1$.

For practical cases of high-energy beams, $pc \approx E$, so that there is very little distinction between Eqs. (2) and (3).

It is convenient to express the difference $\beta_2 - \beta_1$ in terms of the masses of the two particles. Equation (3) then becomes

$$\Delta_{21} \approx \frac{1}{4}e\ell^2\frac{\mathcal{E}}{pc}\frac{1}{\gamma_1^2}\left(1 - \frac{m_{02}^2}{m_{01}^2}\right), \qquad (4)$$

where $\gamma_1 = \left(1 - \beta_1^2\right)^{-1/2}$, and it has been assumed that γ_1 and γ_2 are large compared with one. Since $\gamma = E/E_0 + 1 \approx E/E_0$, and $pc \approx E$, we have $\Delta_{21} \propto \ell^2/E^3$. Hence, for constant Δ, $\ell \propto E^{3/2}$.

Table R8-I lists the values of the expression in parentheses in Eq. (4) for various particles. Particle 1 is the one for which the separator is adjusted.

Table R8-I

2 \ 1	μ	π	K	p
μ	0	0.42	0.955	0.987
π	-0.72	0	0.921	0.978
K	-21.00	-11.50	0	0.720
p	-76.00	-44.00	-2.560	0

It is also important to find the fractional momentum acceptance of the selector for particles of a single mass. If the selector is set for zero deflection at momentum p, then the deflection produced by a shift to momentum $p \pm \Delta p$ is given by

$$\delta = \frac{1}{2}e\ell^2\frac{\mathcal{E}}{pc}\times\frac{1}{\gamma^2}\times\frac{\Delta p}{p}. \qquad (5)$$

Clearly δ should be less than Δ_{21}.

Since $\gamma^2\,pc \approx E^3$, $\Delta p/p \propto E^3/\ell^2$ for constant δ. But we had $\ell \propto E^{3/2}$, so that $\Delta p/p \propto E^3/E^3 =$ constant.

Of great practical interest is the accuracy with which the $\mathcal{E}$ and B fields must be held constant. By differentiating Eq. (1) with respect to $\mathcal{E}$, or the ratio $B/\mathcal{E}$, one finds the deflection due to field variations.

$$\delta_f = \frac{1}{2}e\ell^2\frac{\mathcal{E}}{pc}\left(\frac{\Delta\mathcal{E}}{\mathcal{E}}\right)$$

or

$$\delta_f = \frac{1}{2}e\ell^2\frac{\mathcal{E}}{pc}\left[\frac{\Delta(B/\mathcal{E})}{B/\mathcal{E}}\right]. \qquad (6)$$

Numerical Considerations

Electric Field Strength

The first limiting practical consideration is the maximum achievable electric field. From Murray's work with glass cathodes,[1] we choose a gap $d = 0.1$ in. $= 2.5$ mm, which (see Fig. 3, Ref. 1) will permit a field of 5×10^7 volts/meter. (At $d = 1.0$ in., a field of 2×10^7 v/m seems reasonable.)

Magnetic Field Strength

For zero deflection $\mathcal{E} = B\beta c$, so that $B \approx 0.16$ weber/m^2 = 1.6 kgauss to "balance" the 5×10^7 v/m. Thus, no strain is placed upon the magnetic field requirements.

Separation of charged K particles from a K, π beam

With $d = 0.1$ in., $\mathcal{E} = 5 \times 10^5$ v/cm, Eq. (4) gives the following values:

p	ℓ	$\Delta_{\pi K}$
100 Gev/c	10^3 m	2.79 mm
25 Gev/c	125 m	2.79 mm

This deflection is already greater than the plate separation d, and hence is adequate for separation of the two beams. If the initial source of secondaries is a fine wire target, and very careful attention is paid to obtaining an achromatic focusing system at the exit of the separator, a separation of 1 mm may be adequate. The length is then reduced to $2.79^{-1/2} \times 10^3 = 600$ m for the 100-Gev/c case.

Obviously, a length of 10^3 meters is terrifying to contemplate, and among other frightening aspects, presents a severe alignment problem. However, if the selector were made in sections, and each aligned by passing a beam through it, the whole combination need not be precisely collinear.

The mean decay distance $\gamma\beta c\tau$ for charged K particles is approximately 750 meters at 100 Gev/c, and approximately 190 meters at 25 Gev/c. The 1-km length is thus not unreasonable to contemplate from this point of view.

$\mathcal{E}$ and B Field Stability

From Eq. (6), we can estimate the required $\mathcal{E}$ field stability if B is held constant. For $\ell = 10^3$ m, $\Delta\mathcal{E}/\mathcal{E} < 10^{-5}$; for $\ell = 125$ m, $\Delta\mathcal{E}/\mathcal{E} < 6 \times 10^{-4}$.

The required stability for $\ell = 10^3$ m is probably hopeless to achieve; that for $\ell = 125$ m is within present-day techniques. However, some hope derives from Eq. (6), which shows that only the ratio $\mathcal{E}/B$ need be held constant to the high degree of tolerances indicated. One might conceive of a system in which the magnet coils were placed in series electrically with the selector-plate voltage supply so that fluctuations could not affect the ratio.

This is a real possibility with superconducting magnet coils, for then resistance changes in the magnet coils cannot occur.

Consider, for example, a series circuit consisting of a precision resistor in series with the N-turn superconducting magnet coils. The required $\mathcal{E}$ field is derived from the Ri drop across the resistor. Then $\mathcal{E} \propto Ri$, and $B \propto Ni$, so the ratio $\mathcal{E}/B = R/N$. The scheme would require that N be large, and hence the coils would have a large inductance, but for steady operation this would introduce no difficulties.

Momentum Acceptance—Entrance Magnet

From Eq. (5), we can calculate the momentum acceptance of the 1000-m K-particle separator. For $\delta = 1.0$ mm, one obtains $\Delta p/p = 0.16$. This suggests that a scheme which permits parallel beams possessing a substantial momentum spread would be advantageous. Figure R8-1 illustrates one possible scheme by which to accomplish this. Three uniform-field magnets are placed in a long straight section[5] following a suggestion made by Kerth.[6] The first magnet and third magnet are one-half the length of the center magnet. Thus, the main proton beam is displaced just slightly from its normal path. A target at the entrance to the first magnet permits positive secondary beams to emerge,

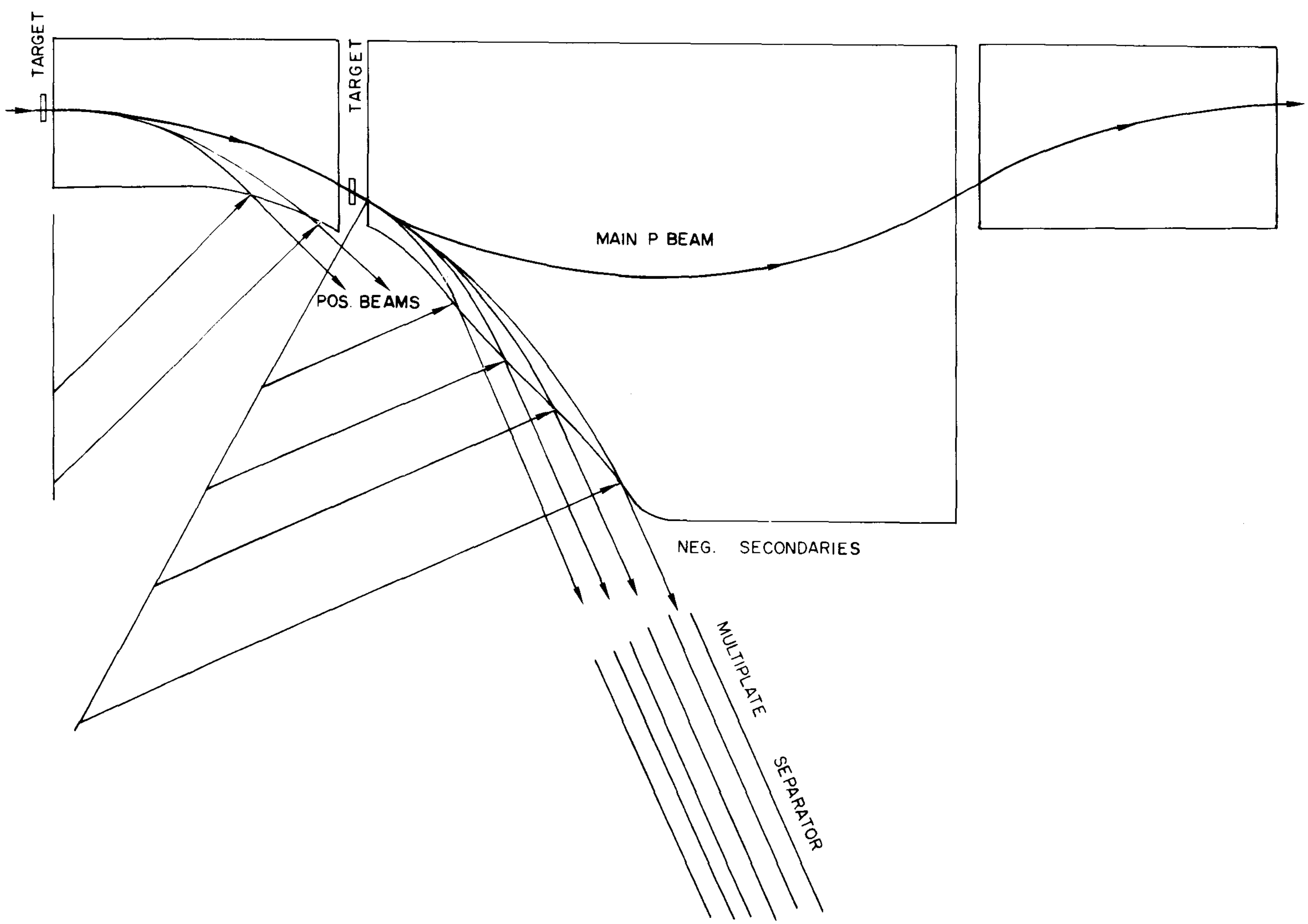
TARGET
TARGET
MAIN P BEAM
POS. BEAMS
NEG. SECONDARIES
MULTIPLATE SEPARATOR

Fig. R8-1.

whereas a target at the entrance to the second magnet permits negative beams to emerge. It is here proposed that the edges of these two magnets be shaped where the beams emerge in order to produce parallel beams of differing momenta. The scale of Fig. R8-1 is very greatly exaggerated in order to illustrate the method. Upon emerging from one or the other of the two magnets, the beams are permitted to enter the velocity selector.

Since the transmission of a very long selector with 0.1-in. plate separation d is very small, it is proposed to make a multiplate separator as shown in Fig. R8-1. The total voltage required for such a multiplate arrangement is about 250 kv.

The momentum spread produced by a magnet of the kind shown in Fig. R8-1 can be easily estimated. The relevant parameters are shown in Fig. R8-2, where S is the length of the magnet, and ϵ is the separation between two parallel beams which differ by Δp in momentum. The result is

$$\epsilon = \frac{1}{2}\frac{Be}{p}\frac{\Delta p}{p} S^2 \qquad (7)$$

for small angles of deviation.

A reasonable length for the center magnet of Fig. R8-1 is 10 meters. At a field of 20 kgauss, and $\epsilon = 0.1$ in. to match the proposed plate separation, $\Delta p/p = 0.8\%$ for 100-Gev/c K particles. Thus, a 10-plate selector would transmit an 8% momentum interval, which is only one-half that permitted by Eq. (5). At 25 Gev, $\Delta p/p = 0.2\%$, and a larger number of plates would be required to obtain an 8% momentum interval.

The angle through which a 200-Gev/c beam is deflected by this magnet is 3.4°. This is entirely adequate for insuring that the beam and apparatus clear any downstream obstructions.

Transmission and Beam Intensity

We are now in a position to calculate the solid angle of a selector and to estimate the separated beam intensity. If the vertical height of the selector plates is h, then the solid angle subtended by the far end of the instrument is $\Omega = hd/\ell^2$. A reasonable height is 20 cm, so $\Omega = 5 \times 10^{-10}$ sr per multiplate section for the 1000-m length.

The entrance angle in the vertical direction is small compared with the cone of maximum secondary beam intensity. Taking the transverse momentum of secondary particles equal to 0.4 Gev/c, we have the half-angle of the 200-Gev/c beam "cone" = 2 milliradians, whereas the vertical angle of the 1000-meter selector is 0.2 mrad.

We now estimate the expected beam intensity. Cocconi[7] has calculated the expected pion flux based upon a "two-fireball" theory. At 100 Gev/c, he obtains approximately 0.5 π^+ (or π^-) particles per Gev per sr per interaction at 0°; his corresponding number at 25 Gev is approximately 2.5. These numbers are, of course, subject to considerable fluctuations. The number of charged K particles expected is probably 10 to 20% of the pion flux.

If we take 10^{11} interactions per beam pulse (a rather conservative number, based upon multiple target traversals of a pulse beam of 10^{12} protons with 90% loss), a selector length of 10^3 m consisting of 10 stages with cross-sectional dimensions 2.54×20 cm, and a momentum

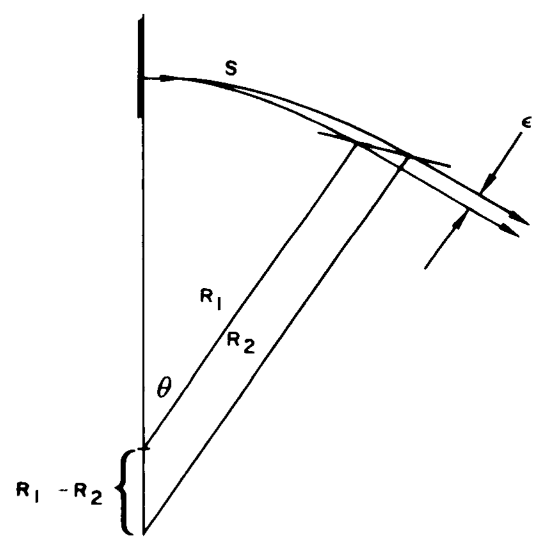

Fig. R8-2.

spread of 8%, we obtain 200 π's per pulse at 100 Gev emerging from the selector, or about 20 to 40 K's per pulse, not including an approximately 50% loss due to decay in flight.

The more optimistic selector length (600 m) would give fluxes about three times as high.

At 25 Gev, and a length of 125 m, the pion output goes up to 32,000/beam pulse (assuming Cocconi's flux for this energy), and thus about 3200 to 6400 K's/pulse.

Discussion

The predicted beam intensities at 100 Gev/c may be sufficient for many experiments. The technical difficulties in building a device 600 to 1000 meters long are admittedly great, but not necessarily beyond hope. Certainly the device would have to be built in sections, and each additional section would have to be aligned and calibrated. Between each section a good deal of shielding would be required in order to absorb the beam-produced radiations that are deflected into the plates.

At 25 Gev/c the situation is very much improved, and one would probably want to increase the gap spacing (and reduce the $\mathcal{E}$ field) in order to alleviate the alignment problem. All in all, it would seem that a 25-Gev/c separator is well within technical grasp by present-day techniques.

References

1. J. J. Murray, in Proceedings of an International Conference on Instrumentation for High-Energy Physics (Interscience Publishers, New York, 1961), p. 25.
2. Myron L. Good, ibid., p. 34.
3. S. Penner, Quadrupole Magnet Systems for Particles of Very Large Momenta, Report No. M-200-12, Stanford Summer Study Group, 1960.
4. T. G. Berlincourt et al., Phys. Rev. Letters 6, 671 (1961).
5. J. P. Blewett, Design Study for a 300- to 1000-Gev Accelerator, Preliminary Report, Brookhaven National Laboratory, 1961.
6. Leroy Kerth (Lawrence Radiation Laboratory), private communication.
7. Giuseppi Cocconi (Cornell University), private communication.

9. REPORT ON THE CAPABILITIES OF BUBBLE CHAMBERS IN ULTRA-HIGH-ENERGY EXPERIMENTS

George H. Trilling

August 30, 1961

Introduction

This report presents the results of some very simple calculations on the capabilities of bubble chambers for the study of the interactions of particles in the 100-Gev range. First of all, it should be pointed out, that for certain processes, owing to symmetry considerations, one can confine one's attention to relatively low-energy secondaries. Thus in proton-proton scattering, it is sufficient to look only at particles emitted backward in the center-of-mass system. A detailed report on the kinematics of high-energy proton-proton reactions is given in the accompanying report by Gerald R. Lynch (Report 5). In such situations, the ability to make precise measurements poses no great difficulties. On the other hand, where such simplifying principles do not apply, it will undoubtedly prove necessary to obtain quantitative information for the high-energy forward-emitted secondaries. It is therefore to these that we confine our attention here.

In order to obtain explicit numerical results, we consider the following specific situation. An incoming beam particle interacts at the center of a 2-m-long bubble chamber immersed in a 20-kgauss magnetic field. For simplicity, we measure just three points on every track, one in the middle and one at each end. We assume that the measurement of each point has an rms error of 50 μ in each coordinate direction perpendicular to the lens axis, and 250 μ in the direction of the lens axis. Finally, we consider only particles moving at small angles with respect to the beam direction. With these assumptions in mind, we can now give estimates of the feasibility of making reasonably precise measurements.

Momentum Precision

The fractional momentum measurement errors are summarized in Table R9-I. In this table, P is the particle momentum in Gev/c. The "long-lived" particles are assumed to travel 1 meter in the chamber, whereas the "short-lived" particles travel just one mean decay distance, provided this is less than 1 meter (the momentum limits in the table indicate when the mean decay distance is less than 1 meter).

Table R9-I

Fractional momentum errors

Measuring Errors	
Long-lived particles	0.0008 P
(track length = 1 m)	
Short-lived particles	
(track length = 1 decay length)	
Σ^+ (P < 50 Gev/c)	1.9/P
Σ^- (P < 25 Gev/c)	0.5/P
Ξ^- (P < 33 Gev/c)	1.0/P
Multiple-Scattering Errors	
(track length = 1 m)	
Hydrogen	0.009
Propane	0.027
Freon	0.086

Perhaps the best hope for improving this precision lies in the present investigations of the feasibility of using superconducting magnets to obtain fields considerably higher than 20 kgauss without the prohibitive cost increase expected with a conventional magnet design. The engineering difficulties which presently are still connected with the manufacture of long lengths of wire suitable for such magnets will very likely have been solved long before a 300-Gev accelerator can be completed, and one can guess that fields of 50 to 100 kgauss will be available, leading to a proportionate increase in the precision of momentum measurement.

Angular Precision

The necessity of good angular accuracy is made obvious by noting that a typical transverse momentum of 500 Mev/c in a 50-Gev/c particle implies an angle of 0.6°, which should be measurable with an error of only a small fraction of that value. Table R9-II shows the angular errors computed under the assumptions given in my introductory remarks. A few remarks on the various entries in this table are appropriate.

Charged-Particle Measurement Errors

The perhaps surprising fact that the errors in the two planes are the same in spite of the assumed stereo ratio of 5 comes about because in the plane perpendicular to the axis our three-point measurement must determine both curvature and direction, whereas in the plane of the axis the direction is the only unknown.

Multiple-Scattering Errors

A simple way of expressing these is to note that they imply a fixed transverse-momentum error dependent only on the chamber liquid and having the values

Hydrogen, 2 Mev/c

Propane, 6 Mev/c

Freon, 18 Mev/c.

Considered from this point of view, the multiple-scattering errors for all the above liquids are very small.

Λ^0

We have taken $P > 15$ Gev/c, which leads to a decay length greater than 100 cm, and have assumed that the Λ^0 decays 50 cm from the interaction point. The different errors in the two planes reflect just the stereo ratio.

Electron Pairs

For hydrogen and propane, we have taken the conversion point to be 50 cm from the interaction point. For freon, for which the conversion mean free path is only 14 cm, we have considered the conversion to take place 14 cm from the interaction point.

Particle Identification

Bubble Density

No significant rise in bubble density beyond the minimum value has been observed in hydrogen bubble chambers.[1] On the other hand, Hahn et al. have reported a rather substantial rise in freon.[2] Powell has preliminary data indicating a similar rise in his chamber when it is filled with a mixture of propane and freon.[3] A minimum track 1 m long has about 1500 bubbles, and hence the bubble density can be determined with a precision of about 3%. From Hahn's data, we find that at energies greater than about 20 Gev there is about 7% difference between protons and K's and about 9% difference between K's and π's. Thus, there seems to be reasonable indication that, indeed, particle identification by means of bubble counting may be feasible in chambers filled with propane-freon mixtures.

Perhaps a brief comment may be made here on the utility, or inutility, of studying high-energy interactions in a non-hydrogen chamber. Although the powerful technique of kinematic fitting, valuable in low-energy hydrogen chamber work, is not likely to be useful at ultrahigh energies, the hydrogen is still very superior in the respect that all interactions are known to involve free protons. On the other hand, in a propane-freon chamber, one can hope to use charge conservation for separating free-proton collisions with reasonable efficiency. As has been shown before, the multiple scattering, even

Table R9-II.

Angular errors

	Plane perpendicular to lens axis (deg)	Plane parallel to lens axis (deg)
Charged Particles		
Measurement error	0.015	0.015
Multiple scattering in:		
hydrogen	0.115/P	0.115/P
propane	0.35 /P	0.35 /P
freon	1.05 /P	1.05 /P
Λ^0		
(P > 15 Gev/c)	0.008	0.04
Electron pair		
hydrogen	0.008	0.04
propane	0.008	0.04
freon	0.03	0.15

in pure freon, does not preclude the possibility of making reasonably accurate momentum or angular measurements. Thus, in experiments in which particle identification by bubble counting or π^0 detection by gamma-ray conversion are important, a non-hydrogen chamber may be useful.

Delta Rays

We have not made a detailed study here of the usefulness of δ rays in identifying high-energy particles in hydrogen, and confine ourselves to very general remarks. The mean free path for producing δ rays (of sufficient energies to provide identification of the parent particle) increases with increments of energy. Hence, one can hope to use δ rays principally in a statistical way, in which actually only a small fraction of the observed particles are identified.

Furthermore, it is generally easier to identify a π meson than a K meson or a proton. This leads to the undesirable situation that one is identifying the frequent rather than the rarer components of the secondary particles, and hence one has great difficulty in obtaining even statistically the fractions of heavy, possibly rare, secondaries.

Decay in Flight of Strange Particles

Strange particles can be identified, in principle at least, by observation of their decays in the chamber. The mean decay lengths at 100 and 50 Gev are given for various particles in the first two columns of Table R9-III. The characteristic angles given in the last two columns are total opening angles for Λ and K^0, or the angle between π-secondary and parent particle for Ξ and $\Sigma^{\pm}$, obtained when the decay angle

Table R9-III

Properties of strange-particle decay.

	Mean decay length (m)		Characteristic angle (deg)	
	50 Gev	100 Gev	50 Gev	100 Gev
K^0	3.0	6.1	0.92	0.46
Λ^0	3.4	6.7	0.90	0.45
Σ^+	1.0	2.0	1.1	0.56
Σ^-	2.0	4.1	1.1	0.56
Ξ^-	1.5	2.9	1.1	0.53

in the rest system of the strange particle is 90°. It is clear that the angles are very small, but they can be measured with good accuracy if the precisions quoted in Table R9-III can be realized. Indeed, one will then be able to identify the particles by techniques similar to those employed in some of the early cosmic-ray studies of strange particles.

Additional Remarks and Conclusions

A factor which has been completely overlooked so far is the rather strong demand placed on resolution by the need to analyze a narrow cone of high-energy particles. It is clear that the precisions listed in Table R9-III cannot be realized if the various tracks are not adequately resolved. We can consider two limitations on resolution; namely, the optical system and the film. So far as the optical system is concerned, one would probably use a fairly wide-open lens to minimize the diffraction effect at the expense of depth of field. If the beam is designed to enter the chamber at a fixed depth, there is no need for a large depth of field to study the forward cone of particles. On the other hand, the film then becomes a limitation, unless the demagnification is considerably less than for present chambers, with the effect of greatly increasing film consumption. A possible alternative solution might be to use cylindrical lenses to provide much less demagnification in the transverse than in the beam direction. Such photographs would also be easier to scan in that small angles would be more readily visible.

In conclusion, the above analysis indicates that it is feasible to obtain accurate quantitative information from bubble chamber experiments at ultrahigh energies. However, it does require that the bubble chamber technique be developed to its limits. There are not many bubble chambers today that can fulfill the requirements for precision of coordinate location assumed in the calculations of this report, but there is no inherent limitation to prevent the attainment of these precisions.

References

1. Charles Peyrou, in Proceedings of an International Conference on Instrumentation for High-Energy Physics, 1960 (Interscience Publishers, Inc., New York, 1961), p. 157.

2. B. Hahn, E. Hugentobler, and F. Steinrisser, op. cit., p. 143.

3. Wilson M. Powell (Lawrence Radiation Laboratory), private communication.

10. HIGH-ENERGY PROTON LINEAR ACCELERATORS

William Walkinshaw

August 8, 1961

Introduction

In this paper, the basic design principles of a high-energy proton linear accelerator are reviewed. Particular emphasis is given to: (a) the effect of beam loading, (b) resonant vs traveling-wave systems, and (c) calibration and control systems for the accelerator. To some extent, these issues are closely related to one another and have considerable bearing on the overall conception of the accelerator. There is general agreement that a proton linear accelerator can be built. However, because it consists of many independent tanks, considerable care is required in controlling both the field amplitudes and phases of these tanks. The problem is analogous to beam control in an alternating-gradient synchrotron in which "phase lock" ensures the stability of the bunch, and "radial lock" controls the rate of acceleration.. Although it is unlikely that conditions are stringent in the linear accelerator, a careful computational study is required, particularly in the energy region from 200 Mev to 600 Mev. Above 200 Mev the Berkeley (Alvarez) waveguide becomes inefficient and has to be replaced by some other system. It is also desirable to increase the operating frequency at some point. In the design of the proposed Harwell 600-Mev system, it was intended to change from 200 Mc to 400 Mc at 50 Mev, and change the structure to a pillbox structure at between 150 and 200 Mev. At that time, it was thought necessary to continue a "quadrupole-drift-tube geometry" up to 600 Mev. This required a sufficiently large waveguide to house the drift tubes. Recently Lloyd Smith has suggested inserting quadrupole-lens focusing between sections of waveguide. This has the advantage of allowing greater freedom both in the choice of waveguide geometry and in frequency change. Final choice in this is dependent on a detailed assessment of the tolerances discussed earlier, and will have to follow a detailed computational study. Above 600 Mev, the problem of design becomes much easier and need not be discussed at any length here.

Effect of Beam Loading

Preinjectors are already capable of producing more than 50 ma of pulsed current at 500 kv. It is therefore necessary to consider what effects this may have on the radio-frequency fields. For a resonant cavity,

$$\frac{d}{dt}\,(\text{energy stored}) = -(\text{rf losses}) - (\text{beam losses}) + (\text{supplied power})\ , \text{ or}$$

$$\frac{Q}{\omega}\times\frac{d}{dt}\left(E^2\right) = -E^2 - \eta E I \cos\phi_s + P\eta/L\ , \tag{1}$$

where Q relates to the cavity, E is the peak accelerating field, η is the shunt impedance per unit length, P is the total power supplied, and L is the cavity length. There will also be reactive loading by the beam, but we shall assume that the cavity is servo-controlled to keep it in tune. (This may not prove possible with transients during the pulse.)

In the steady state, equating the right-hand side to zero gives

$$E = \frac{1}{2}\left[-\eta I \cos\phi_s + \left(\eta^2 I^2 \cos^2\phi_s + 4\,P\eta/L\right)^{\frac{1}{2}}\right]. \tag{2}$$

For no beam loading, the cavity field will be

$$E_{max} = \left(P\eta/L\right)^{1/2}\ . \tag{3}$$

When the beam is included, this gives

$$E/E_{max} = \frac{1}{2}\left[-x + \left(x^2 + 4\right)^{\frac{1}{2}}\right] , \qquad (4)$$

where

$$x = I \cos \phi_s / E_{max} \quad .$$

For example, for η = 40 MΩ/m, I = 100 ma, ϕ_s = 30°, and E_{max} = 2 Mev/m, x is 1.4 and Eq. (4) gives E/E_{max} = approx. 0.5. It is evident, therefore, that, with currents of this order, large variations in field level during the pulse are possible in the first tank of existing linacs.

Transient variation in the field is obtained by integration of Eq. (1) to give

$$-\frac{\omega t}{2Q} = \frac{R_1}{R_1 - R_2} \ln\left(E - R_1\right)$$

$$- \frac{R_2}{R_1 - R_2} \ln\left(E - R_2\right) , \qquad (5)$$

where

$$R_1 = \frac{1}{2}\left[-\eta I \cos \phi_s + \left(\eta^2 I^2 \cos^2 \phi_s + 4P\eta/L\right)^{\frac{1}{2}}\right]$$

and

$$R_2 = \frac{1}{2}\left[-\eta I \cos \phi_s - \left(\eta^2 I^2 \cos^2 \phi_s + 4P\eta/L\right)^{\frac{1}{2}}\right].$$

We have made no calculations of transient phenomena. It is clear, however, that smaller variations of field will occur if the beam is injected early in the pulse. One other solution—costly in power—is to decrease the shunt impedance of the waveguide. The peak field will be limited of course by breakdown limitations. Above 200 Mev, with a proposed accelerating gradient of 10 Mev/m, the effect of high current loading is not so severe. However, we shall see later that the high field gradient requires a strict control of field level, particularly in the region of 200 to 600 Mev.

For the resonant type of accelerator, there will be no spatial variation of fields, provided the tank is not too long. For the end-fed traveling-wave accelerator, on the other hand, beam loading increases the attenuation of the wave. Transient phenomena are less severe, but the field at entrance will have to be increased to maintain the same average acceleration. This will have to be taken into account in assessing breakdown limitations.

The formula for beam loading for the traveling-wave case is

$$E = - I\eta \cos \phi_s + \left(E_0 + I\eta \cos \phi_s\right) e^{-\alpha z} \quad . \qquad (6)$$

Without beam loading, the efficient length of the accelerator is given by $\alpha z = 1.2$.

Another possibility for the traveling-wave accelerator would be to design it to have constant field level along its length at the design current. For no current loading, there would then be a tendency for the field to increase away from the feeding end; unused power could then be fed into a load at the end.

Temperature Control

It is accepted that the whole of the accelerator is operated at the same frequency. We will now estimate the effect of temperature changes on individual tanks.

For a resonant system, the change in resonant frequency with temperature is

$$\frac{\Delta f}{f} = 1.7 \times 10^{-5} \text{ per °C for copper} \quad ,$$

and the consequent phase error is

$$\Delta \phi = \tan^{-1} Q\left(\frac{\Delta f}{f}\right) . \qquad (7)$$

That is, for $Q = 10^4$, the phase change per degree change in temperature is about 10°. This can be corrected with tuning plungers, and presents no serious problem.

For the traveling-wave system, the phase change at the end of the waveguide is

$$\Delta\phi = \frac{dk}{d\omega}\Delta\omega L$$

$$= \frac{c}{v_g}\frac{\Delta f}{f}\frac{2\pi L}{\lambda}$$

$$= 2Q\frac{\Delta f}{f}\cdot\alpha L \quad . \qquad (8)$$

If the phase error is measured from the middle of the section, then we see that, for $\alpha L = 1.0$, the phase error is the same as for the resonant case. In this case, however, tuning must take place smoothly along the whole length of the waveguide to prevent phase changes of the bunch with respect to the wave and also to avoid reflections in the power transmitted along the waveguide. This would demand a more elaborate tuning system than for the resonant case.

Care will also have to be taken in the design of the cooling system to prevent undue temperature changes along the length of an individual section for the traveling-wave case.

Before discussing the implications of the above effects, we summarize the basic formulae for beam dynamics. For a detailed account of this, the reader is referred to recent reports by Lloyd Smith and Lee Teng. The early Harwell proposal is contained in AERE T/M 112 (1954).

Phase Motion

The equation of phase motion (see Lloyd Smith LS-3) is

$$\frac{d}{dz}\left(m_0c^2\beta_s^3\gamma_s^3\frac{d\phi}{dz}\right) = \frac{eE2\pi}{\lambda}\left(\cos\phi - \cos\phi_s\right), \qquad (9)$$

where $E(z)$ is the peak field, ϕ is the phase of the particle and ϕ_s that of the synchronous particle, $\gamma_s = \left(1-\beta_s^2\right)^{-1/2}$, and β_s = phase velocity/velocity of light.

This equation applies equally to traveling-wave and resonant accelerators. The difference in energy of phase-oscillating particles from that of the synchronous particle is

$$\Delta\left(mc^2\right) = (2\pi)^{-1}\lambda\, m_0c^2\beta_s^3\gamma_s^3\, d\phi/dz \quad . \qquad (10)$$

The linear approximation to Eq. (9) is

$$\frac{d}{dz}\left(m_0c^2\beta_s^3\gamma_s^3\frac{d\Psi}{dz}\right) + \frac{eE2\pi}{\lambda}\sin\phi_s\cdot\Psi = 0 \;; \qquad (11)$$

with the adiabatic solution

$$\Psi \approx \left(\beta_s\gamma_s\right)^{-3/4}\left(E\sin\phi_s\right)^{-1/4}\sin\int\Omega\,dz \qquad (12)$$

$$\Delta\left(mc^2\right) \approx \left(\beta_s\gamma_s\right)^{3/4}\left(E\sin\phi_s\right)^{1/4}\cos\int\Omega\,dz\,, \qquad (13)$$

where the frequency of phase oscillation is

$$\Omega = \left(eE2\pi\sin\phi_s/\lambda\, m_0c^2\beta_s^3\gamma_s^3\right)^{\frac{1}{2}}\,, \qquad (14)$$

and the wavelength of phase oscillation is

$$\lambda_\phi = \left(\frac{2\pi\,\lambda m_0c^2\gamma_s^3\beta_s^3}{eE\sin\phi_s}\right)^{\frac{1}{2}} \quad . \qquad (15)$$

We shall be particularly concerned with the region around 200 Mev. From Lloyd Smith's graph, λ_ϕ = 10 meters at 200 Mev (E = 12 Mv/m, $\phi_s = 30°$ and a frequency of 1,000 Mc) . The amplitude of phase oscillation at the end of the 200-Mev section (E = 2 Mv/m, f = 200 Mc) is of the order of ±4°. If the frequency is changed to 1200 Mc at 200 Mev, the phase-oscillation amplitude will then be ±24°. This can be reduced by inserting a quarter-wave matching section with a field of

$$\frac{E_M}{E_1} = \sqrt{\frac{E_2}{E_1}\times\frac{\lambda_2}{\lambda_1}}\quad, \qquad (16)$$

where the suffixes refer to the regions before and after the frequency change. The phase amplitude is then given by

$$\Psi = \left(\frac{\lambda_1 E_2}{\lambda_2 E_1}\right)^{-1/4} \times 24°$$
$$= \pm 24° \left(6 \times 5\right)^{-1/4}$$
$$= \pm 10° \quad . \tag{17}$$

At 600 Mev this will have damped to ±6°. The tolerance on phase trapping at 200 Mev is therefore not severe.

Radial Motion

The equations of radial motion with periodic focusing can be represented (see, e.g., AERE, T/M 112, 1954) by

$$x = C\left(\frac{T_{12}}{\sin\mu}\right)^{1/2} \sin\left(\int \frac{\sin\mu}{T_{12}}\, d\Theta + \epsilon\right) , \tag{18}$$

$$m\dot{x} = C\left(-\frac{T_{21}}{\sin\mu}\right)^{1/2} \sin\left[\int \frac{\sin\mu}{T_{12}}\, d\Theta + \epsilon + \phi(\Theta)\right] , \tag{19}$$

where

$$\sin\phi = \sin\mu \cdot \left(-T_{12}\, T_{21}\right)^{-1/2} , \tag{20}$$

and

$$\int \frac{\sin\mu}{T_{12}}\, d\Theta = \mu \quad ,$$

when integrated over a period.

The T's are transfer matrices in momentum-configuration space. In this form, adiabatic variations of the parameter can be included. For example, for the simple case

$$\frac{d}{dt}(m\dot{x}) + Kx = 0 \quad , \tag{21}$$

$$x = \frac{C}{(mK)^{1/4}} \sin\left(\int\sqrt{\frac{K}{m}}\, dt + \epsilon\right) , \tag{22}$$

$$m\dot{x} = C\,(mK)^{1/4} \cos\left(\int\sqrt{\frac{K}{m}}\, dt + \epsilon\right) , \tag{23}$$

with conservation of the area $x \cdot m\dot{x}$.

For the general case, if x_0 denotes the maximum amplitude of radial oscillation, the conserved area is

$$\left(-T_{21}/T_{12}\right)^{1/2} x_0^2 = \text{const.} \tag{24}$$

We will now look at possible variations of focusing law along the linear accelerator.

In the section at less than 200 Mev, we assume quadrupoles housed in drift tubes. From 50 Mev to 200 Mev, for the accelerating gradients suggested, the effect of the radial defocusing radio-frequency field is small, and we shall ignore it at present. From detailed calculations (AERE T/M 112) for fixed aperture x_0. the maximum acceptance area occurs for a mode number close to $\pi/2$. The conserved area is then

$$x \cdot m\dot{x} = x_0^2\, m \cdot \frac{\pi e^{-\pi/2}}{2n\lambda/c} = \text{const} \quad , \tag{25}$$

where n is the number of drift-tube quadrupoles with the same polarity. This was taken as 2 in the Harwell, CERN, and Brookhaven 50-Mev linacs.

In Lloyd Smith's notation,

$$2n\lambda/c = L/\beta c \quad ;$$

$$\beta_{max} = \frac{L}{\beta c} \cdot \frac{e^{\pi/2}}{\pi} \quad .$$

For thin-lens focusing between sections,

$$\beta_{max} = L/\beta\, c \quad ;$$

for sinusoidal focusing,

$$\beta_{max} = \frac{L}{\beta\, c} \times \frac{2}{\pi} \quad .$$

For constant mode number and constant polarity number, n , the adiabatic variation of beam amplitude is

$$x_0 \approx \gamma^{-3/2} \quad . \tag{26}$$

The radial wavelength is proportional to drift-tube length, i.e.

$$L \propto \beta \quad . \tag{27}$$

The field gradient is given by

$$B' \propto \gamma/\beta \quad . \tag{28}$$

That is, to maintain this design, the field gradient will eventually increase above $\beta^2 = 0.5$.

The focusing conditions can, of course, be relaxed somewhat from the above conditions. If the smooth approximation is used and form factors are ignored, the following equations provide a rough estimate of the relationship between beam amplitude x_0, periodic length L, mode number μ , and field gradient B' (assuming constant ratio of quadrupole length to focusing length):

$$x \propto \left(LB'\right)^{-1/2} \quad , \tag{29}$$

$$\mu \propto \left(L^2 B'/p\right) \quad . \tag{30}$$

For example, if in the drift-tube section (< 200 Mev) we keep to fixed polarity number, then $L \propto \beta$. For constant beam amplitude, we have

$$B' \propto \beta^{-1} \tag{31}$$

and

$$\mu \propto \gamma^{-1} \quad . \tag{32}$$

For energies less than 200 Mev, this design is insignificantly different from that quoted above. The choice of adiabatic law for x will depend on beam quality, aperture considerations, and possible misalignments. For the present, we will assume constant beam amplitude. For a (+ + - -) system, the strength of quadrupole focusing required is roughly

$$\beta B' \approx 70 \times \frac{\text{pitch}}{\text{quad. length}} \text{ gauss/cm} \quad . \tag{33}$$

Except near injection, this is a very moderate focusing requirement, and it might prove desirable to change to a (+ -) system. If the radial wavelength is kept constant, then B' will increase by a factor of 2, L and μ will decrease by a factor of 2.

For $n = 2$, $\lambda = 150$ cm, and assuming a phase area of $\pi \times 10^{-3}$ cm rad gives

$$x_0 = \left[10^{-3} \times (0.3/0.63) \times 0.57 \times 4 \times 150 \times \frac{e^{\pi/2}}{\pi}\right]^{1/2} \text{cm} \approx 0.5 \text{ cm}. \tag{34}$$

Since we have assumed $\pi/2$ mode, the radial wavelength is

$$4 \times 2n\beta\lambda = 16 \times 0.57 \times 1.50 \text{ m}$$

$$= 14 \text{ m} \quad . \tag{35}$$

This is close to the radial wavelength (12 m) chosen by Lloyd Smith for entry into the accelerator above 200 Mev.

We shall now examine conditions for injection into the accelerator at 200 Mev. This is probably the most critical part of the design. Since the radio-frequency wavelength is decreased and the field level increased, the magnitude of rf defocusing is increased. The equation of radial motion in the accelerating section is

$$\frac{d}{dt}(m\dot{x}) - \frac{e\pi E \sin\phi_s}{\beta\gamma^2} x = 0 \quad . \tag{36}$$

From Lloyd Smith's analysis for lens focusing, we have

$$\cos\mu = \cosh\Omega t - \frac{t}{2F}\,\frac{\sinh\Omega t}{\Omega t} \quad , \tag{37}$$

where

$$\Omega^2 = \frac{e\pi E\sin\phi_s}{\lambda\beta\gamma^3 m_0} \,, \quad t = \frac{L}{\beta c} \,,$$

and F = focal length of lens.

If the focal length of the lens is chosen so that $\mu = \pi/2$ (at the design phase angle), computations indicate that particles at the peak of the wave (i.e., no rf defocusing) will have a mode number $\mu = \pi$ for $\Omega t = 2.0$ (at the design phase). From rough considerations of this type, we conclude that the radial motion will be strongly affected by the phase position of the bunch and phase oscillation unless $\Omega t << 1.0$.

For $\Omega t = 1.0$, a change in phase position of $\pm 10°$ from a design phase $\phi_s = 30°$ will produce about $\pm 10\%$ variation in μ . At 200 Mev, with f = 1200 Mc and $\phi_s = 30°$ and an accelerating gradient of 10 Mev/m, Ωt is 1.5 for a section length of 3 m. At 400 Mev Ωt has dropped to 0.8, while at 600 Mev it is about 0.5.

To complete this section, we now look at the tolerance on injection energy at 200 Mev. From the equation of phase motion, the amplitude of oscillation (of the bunch) induced by injection at the wrong momentum is

$$\Delta\left(mc^2\right) = \frac{\lambda}{2\pi} m_0 c^2 \beta_s^3 \gamma_s^3 \left[\frac{e E 2\pi \sin\phi_s}{\lambda \cdot m_0 c^2 \beta_s^3 \gamma_s^3}\right]^{1/2} \Psi_0 . \tag{39}$$

For the chosen injection at 200 Mev, this gives

$$\Delta\left(mc^2\right) = 9.38\,\Psi_0 \text{ Mev} . \tag{40}$$

That is, a $\pm 10°$ phase oscillation of the bunch will be induced by an error of about $\pm 1\%$ in injection energy; lower accelerating gradients will have tighter tolerances. To this must also be added the $\pm 10°$ amplitude of phase oscillation of the particles.

There is therefore a complication of tolerances at 200 Mev: (a) beam loading and its relation to shunt impedance and field strength; (b) rf defocusing and its relationship to wave length, field level, and section length; and (c) tolerance on phase position and amplitude of phase oscillations in relation to the rf defocusing.

Shorter section lengths than 3 m would impose severe tolerances on a traveling-wave system but could be used with a resonant system. We also feel that it is desirable to work at an intermediate frequency between 200 Mc and 1200 Mc in this region to completely remove radial and phase coupling. This would also demand a resonant rather than a traveling-wave system.

Calibration

In the light of the previous discussion, we can now discuss the problems of controlling many tanks in amplitude and phase.

To be specific, let us consider a resonant-type system which is essentially a continuation of the Harwell and CERN 50-Mev linacs. At present, each tank can be held accurately in phase and in field amplitude by servo controls. The choice of setting relative phases between tanks is arbitrary, and the position of the phase of the bunch is not known with any degree of accuracy. In a long accelerator with many tanks, a more positive method of setting phase and amplitude is required. At present no technique exists for measuring the phase position of the bunch relative to the rf; this would be a very valuable aid. It might then prove possible to use the beam itself to determine tank phase. This in itself is not sufficient, since it is also necessary to control the rate of acceleration either by choosing the phase position of the bunch or by adjusting the field level of individual tanks. In the alternating-gradient synchrotron, this control is related to the radial position of the beam, which provides a sensitive measure of particle momentum. In a linac machine, it would seem that an alternative method of measuring momentum is required.

Another possibility is to design the whole of the accelerator to have constant phase when operating under design conditions. This might be achieved in practice either by comparing phases between tanks and servo-controlling input phase, or by running a low-power resonant line along the whole length of the accelerator to act as a phase-datum line. If the tanks could all be held at the same phase, the problem remaining would be analogous to tank flattening, but is now determined by field level throughout the accelerator. In this connection, there is a need for information on the degree of phase variation with respect to the input feedline in existing linacs and how accurately this phase can be held with respect to a datum phase.

With resonant systems such as those just described, the spatial variation of the fields in individual tanks should not be affected by beam loading; there will, however, be time variation during the buildup of the pulse. Assuming the latter problem can be solved, this means that the calibration of the system (tank flattening) need not be repeated for different current loadings. With the traveling-wave system, a quick method of tank setting would have to be worked out, to cope with variation in beam loading.

To sum up, we feel it is essential to have some direct knowledge of the phase position and momentum of the beam. This can be used to monitor phase and amplitude control of the tanks, or, alternatively, to provide an automatic beam-control system. The choice of field level, waveguide system, and frequency, especially from 200 Mev to 600 Mev, will be greatly influenced by the degree of success that can be achieved.

Waveguide Structures

For high beam loading it would appear that high shunt impedance may not be the best criterion in the waveguide structure, but that high group velocity may be of greater importance. A structure having this property has been suggested by Chu (Stanford) and examined by Mohr.[1]

Waveguide loading can be produced by having periodic rods with alternate rods at right angles to each other. Drift tubes can also be included. A possible mode of operation could be with π - mode phase change between parallel rods.

1. Polytechnic Institute of Brooklyn: No. P1BMR1-892-61

Conclusions

It is concluded that:

- For high current loading (100 ma during the pulse), there are good reasons for preferring a resonant system throughout in a high-energy linac.
- Thought should be given to methods of calibration and control of many tanks, and to possible techniques for measuring the phase position and momentum of the accelerated bunch. In conjunction with this, a detailed computational study of tolerances on beam dynamics is required.
- High fields and high frequency at 200 Mev produce coupling between the radial motion and the phase motion, and impose tight tolerances on both field amplitude and phase. It may be desirable to work at a lower frequency than 1200 Mc, from 200 Mev to 600 Mev.

Acknowledgment

This work was done while the author was a member of the High-Energy Physics Study Group at the Lawrence Radiation Laboratory, on leave of absence from the Rutherford High Energy Laboratory, England. The author gratefully acknowledges the hospitality and stimulation received from members of the Laboratory staff and from other members of the Study Group.